

## INFORMATION TO USERS

The most advanced technology has been used to photograph and reproduce this manuscript from the microfilm master. UMI films the text directly from the original or copy submitted. Thus, some thesis and dissertation copies are in typewriter face, while others may be from any type of computer printer.

**The quality of this reproduction is dependent upon the quality of the copy submitted.** Broken or indistinct print, colored or poor quality illustrations and photographs, print bleedthrough, substandard margins, and improper alignment can adversely affect reproduction.

In the unlikely event that the author did not send UMI a complete manuscript and there are missing pages, these will be noted. Also, if unauthorized copyright material had to be removed, a note will indicate the deletion.

Oversize materials (e.g., maps, drawings, charts) are reproduced by sectioning the original, beginning at the upper left-hand corner and continuing from left to right in equal sections with small overlaps. Each original is also photographed in one exposure and is included in reduced form at the back of the book.

Photographs included in the original manuscript have been reproduced xerographically in this copy. Higher quality 6" x 9" black and white photographic prints are available for any photographs or illustrations appearing in this copy for an additional charge. Contact UMI directly to order.

# U·M·I

University Microfilms International  
A Bell & Howell Information Company  
300 North Zeeb Road, Ann Arbor, MI 48106-1346 USA  
313/761-4700 800/521-0600



**Order Number 9110780**

**Block and star polymers based on 2-substituted-2-oxazolines**

**Demopolis, Tom Nick, Ph.D.**

**Case Western Reserve University, 1990**

**Copyright ©1990 by Demopolis, Tom Nick. All rights reserved.**

**U·M·I**  
300 N. Zeeb Rd.  
Ann Arbor, MI 48106



BLOCK AND STAR POLYMERS BASED ON  
2-SUBSTITUTED-2-OXAZOLINES

by  
TOM NICK DEMOPOLIS

Submitted in partial fulfillment of the requirements  
for the Degree of Doctor of Philosophy

Thesis Advisors:

Dr. Irvin M. Krieger and Dr. Morton H. Litt

Department of Chemistry  
CASE WESTERN RESERVE UNIVERSITY  
August 1990

Copyright c (1990) by  
Tom Nick Demopolis

CASE WESTERN RESERVE UNIVERSITY

GRADUATE STUDIES

We hereby approve the thesis of

Tom Nick Demopolis

candidate for the Ph. D.

degree.\*

Signed:

*Jill Kofman*  
(Chairman)  
*Malcolm E. Kenney*  
*John W. Guerin*  
*William F. Lott*  
*W. M. Kelcey*

Date

5/9/90

\*We also certify that written approval has been obtained for any proprietary material contained therein.

I grant to Case Western Reserve University the right to use this work, irrespective of any copyright, for the University's own purposes without cost to the University or to its students, agents and employees. I further agree that the University may reproduce and provide single copies of the work, in any format other than in or from microforms, to the public for the cost of reproduction.

*at*  
*Tom Penfold*

---



# BLOCK AND STAR POLYMERS BASED ON 2-SUBSTITUTED-2-OXAZOLINES

Abstract

by

TOM NICK DEMOPOLIS

The objective of this research was to prepare star-block polymers which have potential surface activity. The basic method was ring-opening polymerization of 2-substituted oxazolines of differing polarities. In a preliminary phase, homo-, di- and tri- blocks were synthesized using a one-ended initiator. Triblocks were also prepared using several two-ended initiators, resulting in molecular weight distributions that were unacceptably broad. It was determined through a kinetic study that the reason for the broad distributions is that the initiation step is slower than the propagation step. The same problem was encountered when attempting to produce a three-armed star-block polymer starting with a trifunctional nosylate initiator.

For this reason, it was decided to abandon the "core-first" approach and to proceed with an "arms-first" approach, in which one-ended living poly(N-benzoyl ethyleneimine) chains are reacted with an anchoring moiety containing one or two primary amine groups. First the poly(N-benzoyl ethyleneimine) polymers were synthesized, and their molecular weight distributions characterized by Gel Permeation

Chromatography (GPC) and by Secondary Ion Mass Spectroscopy (TOF-SIMS). Using a monoamine anchor, it was found that one or two chains could be attached at will, depending upon the ratio of arms to anchors. Using a diamine anchor with a four-to-one arm to anchor ratio, a star-block polymer mixture was obtained in which the desired four-armed star predominated. Confirming GPC data are presented, accompanied by TOF-SIMS and  $^1\text{H}$  NMR spectra.

## TABLE OF CONTENTS

	Page
Abstract	ii
Chapter	
1 <b>General Introduction</b>	1
Block copolymers in surface-active applications	2
Living polymerization	3
Oxazolines	3
Factors affecting living polymerization	5
Diblock and triblock copolymers	6
Star-block copolymers	9
Synthetic Strategies towards star poly(N-acylethyleneimine)s	10
1. Core-first method	10
2. Arms-first method	12
Organization of the dissertation	15
References	17
2 <b>Synthesis and Characterization of 2-p-t-Octylphenyl-2-oxazoline Homo- and Di- Block Polymers</b>	19
a) Introduction	20
b) Experimental section	22
Materials	22
Instrumentation	22
Spinning-band	22
Oxidation apparatus	23
Cleaning of polymerization glassware	23
End-to-end distillation	24
Polymerization apparatus	27
Analytical instrumentation	27
2-p-t-octylphenyl-2-oxazoline synthesis	30
p-t-Octyltoluene, 2	30
p-t-Octylbenzoic acid, 3	32
p-t-Octylbenzoyl chloride, 4	34
N-Hydroxyethyl-p-t-octylbenzamide, 5	38
N-Chloroethyl-p-t-octylbenzamide, 6	38
2-p-t-Octylphenyl-2-oxazoline, 7	41
Experiment to test the purity of 7	45
Kinetics of O <sub>2</sub> homopolymerization	46

	Bulk homopolymerization of 7	48
	Characterization	49
	Block copolymerization using 7	
	and 2-ethyl-2-oxazoline, 10 as monomers	50
	Synthesis	50
	Further purification	52
	c) Results	53
	Monomer synthesis	53
	p-t-Octyltoluene, 2	53
	p-t-Octylbenzoic acid, 3	53
	2-p-t-octylphenyl-2-oxazoline, 7	54
	Living polymerization of	
	2-p-t-octylphenyl-2-oxazoline, 7	55
	1. Kinetics of 7 homopolymerization	55
	2. High molecular weight (O)	59
	3. Block copolymerization	65
	d) Summary	78
	References	79
<b>3</b>	<b>Core-first Approach to Star-Block Oxazolines</b>	
	1. p-t-Butylphenyl/Ethyl Oxazoline Triblock Polymers	81
	a) Introduction	82
	b) Experimental Section	84
	Cleaning	87
	P <sub>1</sub> (B <sub>10</sub> E <sub>40</sub> B <sub>10</sub> )	87
	I <sub>2a</sub> , I <sub>2b</sub> , I <sub>2c</sub> , and I <sub>3c</sub>	90
	P <sub>2a</sub> (B <sub>9.8</sub> E <sub>39.4</sub> B <sub>9.8</sub> ) and P <sub>2b</sub> (B <sub>8.7</sub> E <sub>38.4</sub> B <sub>8.7</sub> )	90
	P <sub>2c</sub> (B <sub>9.8</sub> E <sub>44</sub> B <sub>9.8</sub> )	91
	P <sub>3c</sub> (E <sub>39.1</sub> ) <sub>3</sub>	91
	P <sub>1</sub> (E <sub>20.9</sub> )	92
	c) Results	93
	One-ended initiation	93
	Two-ended initiation	95
	References	100
<b>4</b>	<b>Core-First Approach to Star-Block Oxazolines</b>	
	2. Initiation Kinetics	102
	a) Introduction	103
	b) Experimental	105
	Instrumentation	105
	2-Phenyl-2-oxazoline (PO)	105
	2-p-t-Butylphenyl-2-oxazoline	106
	2-p-Chlorophenyl-2-oxazoline,	
	and two-ended alkyl nosylate, 2	106
	9-Methylanthracene	106
	Acetonitrile	107

	Stoichiometric reaction of the dinosylate 2 with each of the three 2-oxazolines, 1	107
	Chromatography	108
	c) Results	108
	Polymerization of	
	2-(p-substituted)phenyl-2-oxazolines	108
	Kinetics of the Polymerization of 1 and 2	111
	The Runge-Kutta method	114
	Fitted values of $k_i$ and $k_p$	117
	Conclusions of the core-first method	124
	References	124
5	<b>Amine End-Capping of Poly(N-benzoyl ethyleneimine): An Arms-First Approach to Star-Block Oxazolines</b>	126
	a) Introduction	127
	b) Experimental	134
	Materials	134
	Instrumentation	134
	o-Dichlorobenzene	135
	N,N-Dimethylacetamide	135
	2-Phenyl-2-oxazoline	135
	Hexylamine, M	136
	Hexamethylenediamine, H stock solutions in o-DCB and DMAc	136
	Purification	137
	Kinetics of 2-phenyl-2-oxazoline (PO) polymerization in o-DCB to make (P) <sub>5.7</sub>	137
	P <sub>1.0</sub> /M reaction using (P) <sub>5.7</sub> in o-DCB at 108°C	138
	(PO) polymerization in DMAc at 117 and 127°C to synthesize (P) <sub>20.9</sub> and (P) <sub>49.2</sub>	139
	P <sub>1.0</sub> /M reaction using (P) <sub>4.8</sub> in o-DCB at 28°C and 117°C	139
	P <sub>0.5</sub> /M reaction using (P) <sub>10.2</sub> in o-DCB at 110°C	140
	Triisobutylamine, B	141
	Experiment to test that living (P) <sub>x</sub> does not react with B	141
	P <sub>3.5</sub> /H/B <sub>2.0</sub> reaction using (P) <sub>8.6</sub> in o-DCB at 121°C	142
	P <sub>4.0</sub> /H/B <sub>7.9</sub> reaction using (P) <sub>10.5</sub> in DMAc at 125°C	143
	P <sub>4.3</sub> /H/B <sub>8.8</sub> reaction using (P) <sub>10.0</sub> , and P <sub>2.1</sub> /H/B <sub>8.4</sub> using (P) <sub>10.2</sub> , in DMAc	144
	c) Results and Discussion	147
	Determination of the propagation rate constant, $k_p$ of PO in o-DCB and in DMAc	147
	Synthesis and characterization of (P) <sub>x</sub>	153

Time-of-Flight characterization of the polymers in the (P) <sub>x</sub> series	154
GPC characterization of the (P) <sub>x</sub> polymer series	167
Peak position calibration	172
Reactions of poly(N-benzoylethyleneimine)s, (P) <sub>x</sub> with hexylamine, <b>M</b>	172
Reactions of poly(N-benzoylethyleneimine)s, (P) <sub>x</sub> with hexamethylenediamine, <b>H</b>	181
Summary and conclusions	195
References	196

## Appendix

<b>A</b>	<b>Purification Procedure of Poly(N-benzoylethyleneimine)s, and their Amine-Terminated Products</b>	197
<b>B</b>	<b><sup>1</sup>H NMR and TOF-SIMS Spectral Analysis of Hexylamine-Treated Poly(N-benzoylethyleneimine)s</b>	203
	<sup>1</sup> H NMR characterization of (P) <sub>10-3</sub>	204
	Experiment (1a)	206
	Experiment (1b)	208
	Experiment (2)	208
	Experiment (3)	209
<b>C</b>	<b><sup>1</sup>H NMR and TOF-SIMS Spectral Analysis of Hexamethylenediamine-Treated Poly(N-benzoylethyleneimine)s</b>	225
	Experiment (4)	227
	Experiment (5)	229
	Experiment (6)	231
	Experiment (7)	231

<b>Bibliography</b>	243
---------------------	-----

*Στους γονείς μου  
Νίκο και Ντίνα Δημοπούλου  
για τα τόσα που έχουν κάνει για μένα*

*Και στον Γιώργη Μπουκασούρη  
Για την ατέλειωτη αγάπη, συμπαράσταση και αφοσίωσή σου*

## Acknowledgments

The author expresses deep appreciation for the invaluable advice of Professors Irvin M. Krieger and Morton H. Litt during the course of the research leading to this dissertation. Their consistent counsel and support throughout these years led to the success of this research, and to my developing love and devotion for Science.

Gratitude is expressed for a generous Fellowship Award offered by the Graduate Alumni of Chemistry for the period of 1986–1987.

Gratitude is also expressed to the Departments of Chemistry and Macromolecular Science, Case Western Reserve University.

Special appreciation is expressed to Mr. Gang–Feng Cai for his help in preparing the figures of this dissertation.

Last, but not least, I thank Dr. Claudio Sellitti for all his efforts and support. You have stood by me like a brother.



## **Chapter 1**

### **General Introduction**

### Block copolymers in surface-active applications.

Block copolymers have been extensively utilized in the recent years in many applications. Their ability to combine different chemical natures in the same structure makes them very attractive in applications that involve boundaries between materials of different properties<sup>1</sup>. Thus a block copolymer concentrates at the interface between the different materials due to the resemblance of each block to the chemical nature of the corresponding material. The result is a system with new properties. One can therefore use these polymers in a wide range of surface-active applications. A few examples are promoters of adhesion<sup>2</sup> or abhesion<sup>3</sup>, emulsifiers<sup>4</sup>, compatibilizing additives in polymeric blends<sup>5</sup> and antielectrostatic agents<sup>6</sup>.

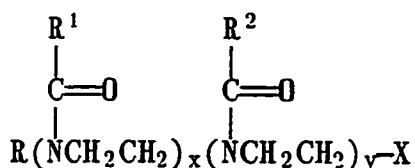
To achieve good properties using a small amount of a surface-active block copolymer one should prepare it in such a way that it will be very effective in covering the interface between the different materials. We then speak of a well-defined block copolymer as a prerequisite for achieving effective usage. A well-defined polymer is one that has a very narrow distribution of chain lengths for each block, as measured by the ratio of the weight average molecular weight ( $\bar{M}_w$ ) over the number average molecular weight ( $\bar{M}_n$ ). This ratio is called the polydispersity index (PDI) and reflects the molecular weight distribution (MWD). PDI values are greater than or equal to one; the smaller the PDI the better defined is the polymer.

### Living polymerization.

The best way to obtain well-defined polymers is to synthesize them through a living polymerization mechanism. By living we refer to a non terminating propagating species, with no chain transfer to solvent, monomer or any other species in the polymerization medium. However in addition to the above requirements for living polymerization, to achieve a monodisperse polymer there should also be fast initiation compared to propagation<sup>7</sup>.

### Oxazolines

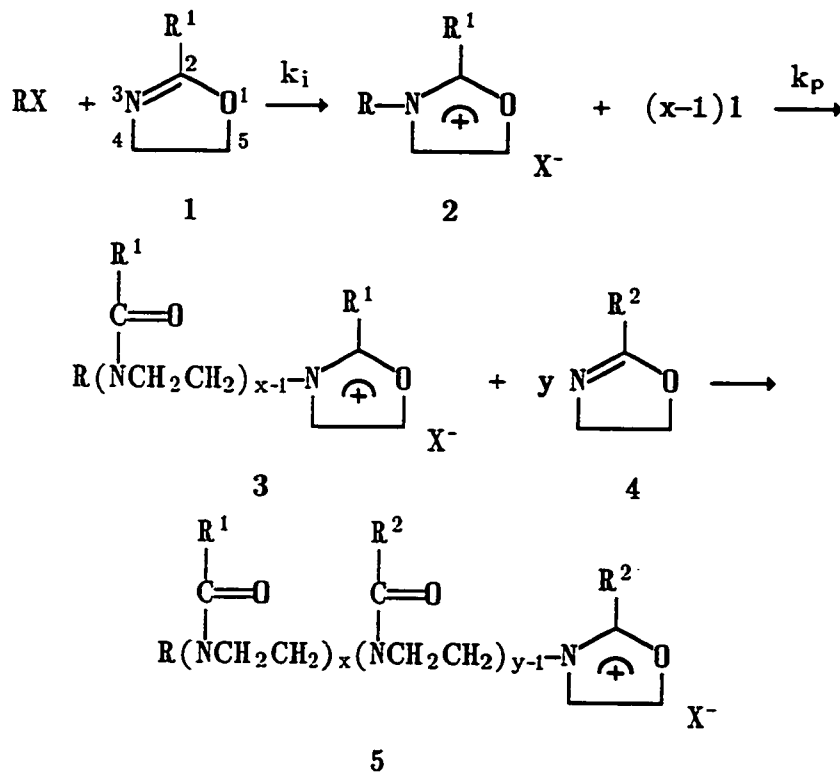
In this thesis we will concentrate exclusively on poly(N-acyl or aroylethyleneimine)s<sup>8</sup> as suitable, well-defined homo- and block copolymers.



These polymers have regular backbones; thus most are crystallizable<sup>9</sup>. Relatively facile synthesis of the monomers<sup>10</sup> permits production of a great variety of R-substituted polymers. Varying the R group allows production of blocks having specific properties. Thus one can engineer a block co-polymer to meet the specific requirements of a surface-active application by combining the properties of different blocks<sup>11</sup>.

Poly(N-acylethyleneimine)s are produced by living cationic ring-opening polymerization of 2-substituted oxazolines (Scheme 1.1):

Scheme 1.1



2-substituted oxazolines are about as basic as pyridine. Initiation occurs upon reaction of the monomer at N-3 with an electrophilic species, to produce an N-alkyl oxazolinium salt. This salt is stabilized through resonance of the positive charge between N-3 and O-1. Propagation then follows as monomer reacts with the oxazolinium ion at its C-5 position, leading to ring-opening isomerization of the latter, i.e. cleavage of the bond between C-5 and O-1. Concurrently a new oxazolinium salt is formed by alkylation of the attacking monomer. Consequently, at the end of monomer addition, one obtains a linear poly(N-acylethyleneimine)

containing a living oxazolinium cation end. One can utilize this living end to initiate polymerization of a second monomer. The final structure is thus a block copolymer.

#### Factors affecting living polymerization

A number of recent reviews on oxazoline polymerization can be found in the literature<sup>12</sup>. In preparing narrow molecular weight distribution oxazoline polymers, one has to be aware of a number of variables. Broadening of the MWD can result from chain transfer or termination.

With careful purification of all components of the system one avoids nucleophilic impurities from the monomer synthesis that terminate the living end, or electrophilic ones such as acids or CO<sub>2</sub> that compete with the initiator for monomer. To avoid chain transfer to solvent one employs a non-nucleophilic solvent<sup>13</sup>. Chain transfer to C-2 alkyl-substituted monomer can also occur if it has an  $\alpha$ -hydrogen<sup>14</sup> which can be abstracted from the oxazolinium end at elevated temperatures by unreacted monomer, thereby causing termination. The resultant polymer chain has an enamine terminal structure that can consequently react with another growing chain and repolymerize to give a new chain of double the initial length.

One must also use a suitable initiator to achieve monodispersity. A large number of initiators have been used to polymerize 2-substituted oxazolines<sup>15</sup>. These include covalent species like Lewis acids, or ionic ones, e.g. protic acids, with non-nucleophilic anions like p-toluenesulfonate (tosylate), p-nitrobenzenesulfonate (nosylate), and trifluoromethanesulfonate (triflate) as well as their esters. For initiators that give non-nucleophilic

anions the mechanism of polymerization is ionic, as shown in Scheme 1.1. The rate constant of initiation  $k_i$  is then influenced by the nucleophilicity of the monomer, while  $k_p$ , the rate constant of propagation, is determined by the polymerizability of the oxazolinium salt. One then speaks of a fast initiator when  $k_i$  is greater than or equal to  $k_p$ . For living polymerization with instantaneous initiation, the number average degree of polymerization  $\bar{X}_n$  is equal to the monomer-to-initiator molar ratio (M/I). The MWD of such a system is very narrow and is described by the Poisson distribution (Flory<sup>16</sup>) for which:

$$\bar{X}_w/\bar{X}_n \cong 1 + 1/\bar{X}_n$$

where  $\bar{X}_w/\bar{X}_n$  is equal to  $\bar{M}_w/\bar{M}_n$ .

#### Diblock and Triblock Copolymers

The question of the structure of a copolymer is an important one when looking at the effect on the desired properties for a particular application<sup>17</sup>. From a recent study in our group it was shown that amphipathic poly(N-acyl or aroylethyleneimine) type copolymers were very good emulsifiers<sup>20</sup>. Specifically, AB type diblock polymers of narrow polydispersity consisting of a hydrophobic block, poly(N-p(t-butyl)benzoylethyleneimine) (A), and a hydrophilic one, poly(N-propionylethyleneimine) (B) were synthesized. These polymers were used as surface-active agents to stabilize water-in-styrene (inverse) emulsions. Low-density microporous foams resulted after polymerization of

the styrene when the diblocks contained about equal weights of the two blocks. It was found that there was a maximum surfactant concentration for a given styrene/water ratio for which a stable inverse emulsion could be obtained. Higher surfactant concentrations yielded mixtures of solid inverse and liquid normal emulsions. Analysis of scanning electron micrographs (SEM) revealed that the mean diameter of the droplets, as well as the thickness of the separating wall,  $\Delta d$ , decreased with increasing surfactant concentration. Thus there is a minimum  $\Delta d$  below which the wall becomes mechanically weak and ruptures. Detailed investigation showed that the hydrophobic block A stands nearly normal to the styrene/water interface in a close-packed arrangement. Thus there is a monolayer of surfactant towards the oil phase. The stability of the wall between droplets is consequently influenced by the strength of this monolayer. This is well known in surfactant theory; the question of film rupture has been considered by various authors, e.g., Scheludko<sup>18</sup> and Vrij<sup>19</sup>.

A major factor influencing the strength of the interface is the geometry of the blocks that compose the surfactant molecule. We therefore decided to compare the emulsification properties between AB diblock and ABA triblock copolymers<sup>20-21</sup>. A series of triblocks was synthesized, as in the study mentioned above, with the same chemical structures for A and B. The weight ratio of A:B was maintained about 1:1, with each A having the same length as before and B about twice the previous length. These triblocks were then tested in styrene/water emulsions. As before, completely solid inverse emulsions resulted after polymerization of the styrene. Again, there was a maximum amount of surfactant that give

stable inverse emulsions, with higher amounts giving mixtures of inverse solid and normal liquid emulsions. However, for the same styrene volume fraction, the maximum surfactant concentration was larger for ABA triblocks than AB diblocks. Analysis of the completely dry solid foams by SEM revealed that ABA at this concentration gave a much smaller foam droplet size than did AB at its limiting amount. Moreover, the average wall thickness,  $\Delta d$ , of the foam formed using ABA was considerably smaller than that of AB. Similar analysis showed that the surfactant is positioned so that the A blocks close-pack to form a monolayer. We therefore suggested that ABA is located at the interface in a "hairpin" conformation. The long B block, anchored in the aqueous phase, bends almost  $180^\circ$ , thus permitting the A blocks to pack together in the oil phase.

These observations indicate that the triblock architecture is far superior to that of the diblock for surface-active applications. As Balazs and Lewandowski<sup>22</sup> point out, the presence of two adsorbing blocks per triblock molecule ensures that the polymer chains are more securely bound at the interface than only one adsorbing block, in the case of a diblock molecule. This inevitably leads to a stronger surfactant film adsorbed at the interface.

In order to benefit from the above mentioned advantages however, one has to keep in mind the need for well-defined structures. From the preliminary study on emulsification using triblock ABA copolymers, it was also shown that triblocks of high polydispersity were much poorer emulsifiers than triblocks of narrow MWD having similar molecular structure.



### Star-Block Copolymers

The implications of the comparison between di- and triblocks point toward new kinds of polymers that could be used for improved surface-active properties, namely star-block copolymers. These have a geometry in which three or more chains, each amphipathic, are chemically bound to a central core. The triblock can be considered to be a two-arm star-block.

Star polymers have previously been used in surfactant applications<sup>21</sup>. But why are they better than block copolymers of other geometries? A surface-active diblock molecule has only one block with which it can bind at the interface. A triblock molecule with two binding blocks gives stronger adsorption at the interface because the chains are more securely bound. This then favors monolayer formation because complete coverage of the interface is obtained more easily by adsorbing triblock chains than by diblocks. In the case of the star-block copolymer, there are three or more amphipathic chains bound to a single anchor, each possessing a binding block. Hence, a star-block polymer molecule contains more binding blocks that can simultaneously adsorb at the interface<sup>17</sup>. This can lead to stronger adsorption of the star molecule at the interface than of the triblock. As a result, monolayer coverage is favored even more. The result is a well-packed, tightly bound film of surfactant at the interface. This conclusion was also reached by Balazs and Lewandowski<sup>22</sup> who suggested branched or "dog-boned" amphiphilic structures for better surface adsorption.

In planning the synthesis of a well-defined star structure, one thinks

of oxazolines as a convenient route to tailor the blocks on each chain to the specific surface-active application. The versatility of the oxazoline synthesis as well as the improvement by the star geometry in stabilizing an interface then provides an attractive path to efficient application.

### Synthetic Strategies towards Star Poly(N-Acylethyleneimine)s

Consider a star oxazoline molecule with  $z$  branches ( $z \geq 3$ ). There are two ways to synthesize this structure:

1. Grow the chains out of a  $z$ -functional electrophilic core. We will refer to this as the core-first method.
2. Use a monofunctional initiator to synthesize the chain. Then react the living oxazolinium ends of the chains with a  $z$ -functional nucleophile. This path will be called the arms-first method.

We will next describe the factors that govern each synthetic strategy.

#### 1. Core-first Method

The two main components of this strategy are the polyinitiator ( $I_z$ ) and the substituted oxazoline monomer ( $M$ ) to be polymerized.

The goal is to make a narrow MWD star, i.e., one that contains  $z$  chain branches, each having a narrow distribution of monomer units. To generate such a structure successfully, it is necessary to compare the relative chemical reactivity of ( $M$ ) with each functional site of  $I_z$ .

Before we address the question of relative reactivities, however, we should mention a number of requirements that  $I_z$  should satisfy in order to be a good initiator. First it should be stable at storage temperatures, since decomposition may deactivate one or more initiator sites and cause undesired structures to be obtained.

Furthermore  $I_z$  must be soluble in the polymer mixture and stable at the temperatures of polymerization. This is necessary because to understand the kinetics of the reaction in solution one must know the M/I feed ratio, which determines the number of monomer units on each of the  $z$  branches. If the initiator is only partially dissolved, then this ratio is larger but unknown. As polymerization proceeds, the monomer will be completely consumed, but some initiator may dissolve or react at an unknown number of sites. Then the number of branches on the final star will be less than  $z$ , and the average degree of polymerization on each chain will not correspond to the initial  $[M]/[I]$  ratio.

Once the above requirements are satisfied, we can look into the question of reactivity. Each reactive site on  $I_z$  must react independently of the other  $(z-1)$  sites. Thus the reaction between an initiator site and M is not deactivated by nearby initiator sites already reacted.

The reaction rate ( $k_i$ ) between an active site of  $I_z$  and monomer must be greater than or equal to the rate of propagation ( $k_p$ ). Only then does each branch contain the number of monomer repeats specified by the M/I ratio. If  $k_i$  is less than  $k_p$  then some active sites will contain more monomer units than the specified feed ratio, while other sites may contain few or no monomers at all. The resultant polymer will then have a high

polydispersity and will be of unknown geometry.

$k_i$  is influenced by electronic effects arising from the reactivity of the active site towards the nucleophilic oxazoline, and by steric effects reflecting the ease with which the active center can "find" the nitrogen on the oxazoline ring. A major factor that contributes to the reactivity of the initiator is the ease of bond cleavage between the electrophilic center on the active site and its leaving group. This is usually governed by the lack of nucleophilicity of the produced counterion. For example, an alkyl triflate (ROTf) is  $10^4$  times more reactive in alkylation than the corresponding tosylate (ROTs)<sup>24</sup>.

## 2. Arms-first Method

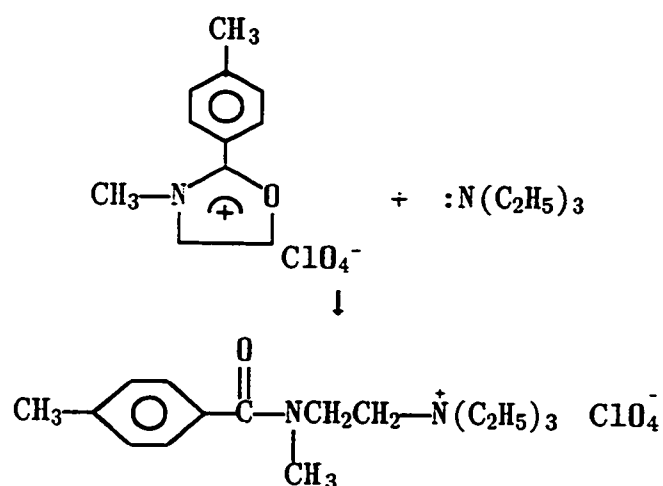
The principal components of this strategy are a polymer chain (P), containing a living oxazolinium cation end, and a multifunctional nucleophile which we will refer to as an anchor.

Nucleophilic end-capping of living cationic polymer chains has been known for a number of years now<sup>25</sup>. Only recently, however, have a number of studies appeared in the literature involving living poly(N-acylethyleneimine)s<sup>26</sup>. By end-capping, i.e. the reaction of the oxazolinium living-end with a nucleophile, one can introduce a suitable polymerizable group at the end of the chain that can initiate anionic or radical polymerization of a different monomer<sup>27</sup>. The functionalized polymer chain is hence called a macromonomer or macromer. For example, poly(2-methyl-2-oxazoline) macromer was derived by reacting the oxazolinium chain-ends of methyl tosylate-polymerized 2-methyl-2-oxazoline

with a nucleophilic amine containing a vinyl styrene group<sup>28</sup>. Graft poly(2-methyl-2-oxazoline-g-styrene) copolymers resulted when the vinyl group subsequently polymerized styrene.

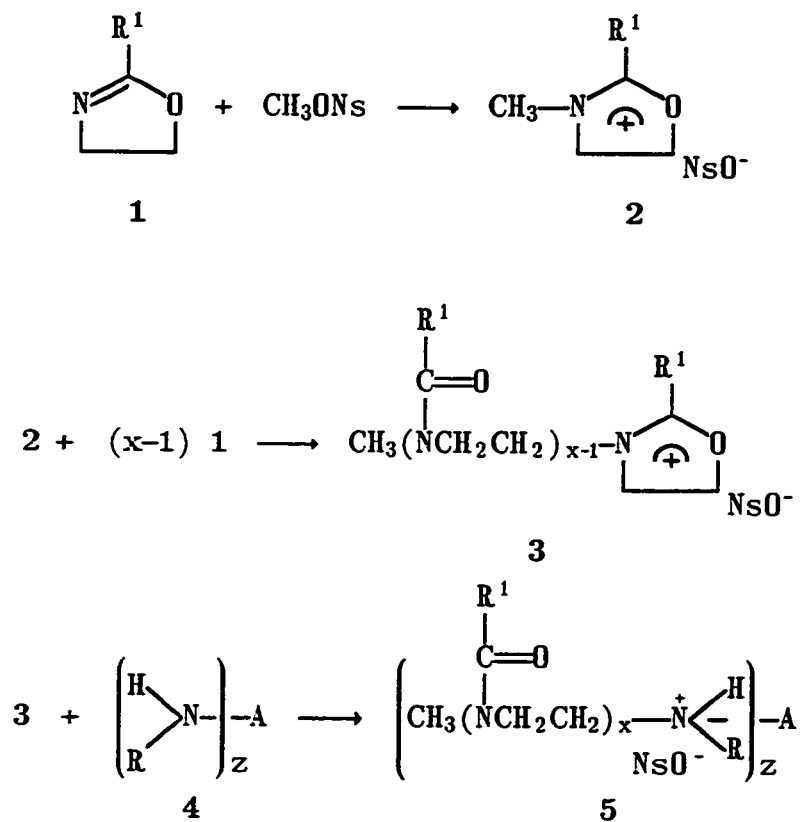
Swamikannu<sup>29</sup> reported in 1984 on the reaction between N-methyl-2-p-tolyloxazolinium perchlorate with triethylamine (Scheme 1.2). The amine induces ring-opening of the cation by attacking the C-5 position to produce an amine-terminated product.

Scheme 1.2

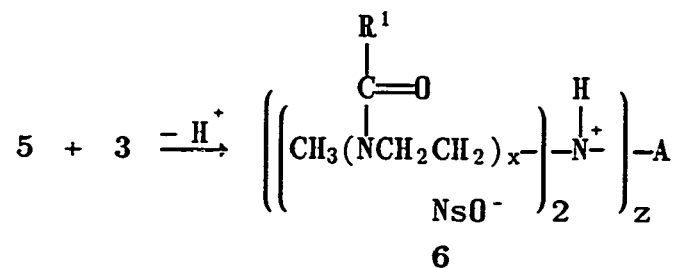


This work suggests that a star structure should result when a polyfunctional amine is reacted with a polymer chain possessing a living oxazolinium end (Scheme 1.3).

Scheme 1.3



If R = H then:



where  $\text{NsO}^-$  is nosylate.

Polyamine 4 is composed of a central core A and z amine units, each

of which can be primary ( $R = H$ ) or secondary ( $R \neq H$ ). The amine units can in principle also be tertiary. However, steric constraints will impede full reaction of **3** on all  $z$  sites (in this case  $z \geq 3$ ), as will be explained in Chapter 5. If the amine sites are primary, **5** can be deprotonated with a suitable agent, so **3** can further react with **5**, thus yielding two polymer chains per amine site.

### Organization of the Dissertation

The purpose of this work was to illuminate the path to the synthesis of well-defined star block poly(N-acylethyleneimine)s. In the course of this dissertation we describe the synthesis and characterization of di- and triblock copolymers made from 2-substituted oxazolines. Methods are devised to evaluate the two strategies of star synthesis: core-first vs. arms-first. Finally, star oxazoline polymers are synthesized and characterized. The work performed is reported in the following four chapters.

The second chapter of this dissertation deals with the synthesis of p-t-octylphenyl-2-oxazoline monomer and its homo- and copolymerization with ethyl-2-oxazoline to make diblock co-oligomers.

Then, in the third chapter, we report on the synthesis of triblocks using 2-p-t-butylphenyl-2-oxazoline and 2-ethyl-2-oxazoline. Several two-ended initiators are tested, and the resulting polydispersities compared to those obtained via the one-ended initiation, step-by-step approach. Also three-ended initiators are evaluated in a first attempt toward star oxazolines using the core-first method.

We then compare the strategies toward star synthesis. In the fourth chapter we report on the attempts to make a two-ended oxazolinium salt which is fast-initiating towards 2-ethyl-2-oxazoline polymerization. A long-alkyl-core, two-ended dnosylate ester is reacted with three 2-(p-substituted)phenyl-2-oxazolines; the reaction is followed by high pressure liquid chromatography (HPLC). A kinetic model is devised to explain the reaction mechanism. The resulting kinetic equations are optimized numerically to best-fit the experimental data. From the resulting best-fit  $k_i$  and  $k_p$  values, we show that the core-first method generates broad MWD polymers because of slow initiation vs. propagation.

Chapter 5 deals with the arms-first approach to star polymers. A series of Poisson molecular weight distribution poly(N-benzoyl ethyleneimine) polymers are synthesized and characterized. Living 2-phenyl-2-oxazolinium nosylate-ended polymer chains are reacted with two primary amines: a monofunctional (hexylamine) and a bifunctional (hexamethylenediamine). By controlling the molar stoichiometry between the polymer chains and hexylamine we achieve once- or twice-reacted adducts. Hexamethylenediamine generates mainly tetra-substituted star polymers under careful stoichiometric control and with the help of a proton scavenger. Appendix A deals with purification of the polymers produced in Chapter 5. In Appendices B and C we report on structure characterization of the hexylamine and hexamethylenediamine end-capped polymers respectively, using  $^1\text{H}$  NMR and Time-of-Flight Secondary Ion Mass Spectroscopy.



## References

1. (a) Riess, G.; Hurtrez, G.; Bahadur, P. In "*Block Copolymers*", *Encyclopedia of Polymer Science and Engineering*, 2nd ed.; John Wiley & Sons: New York, 1985; Vol. 2, pp 324-434. (b) *Dispersion Polymerization in Organic Media*; Barrett, K. E.; John Wiley & Sons: London, 1975. (c) Hancock, R. I. In *Surfactants*; Tadros, Th. F., Ed.; Academic: London, 1984; p 287.
2. Chujo, Y.; Ihara, E.; Ihara, H.; Saegusa, T. *Macromolecules* 1989, *22*, 2040.
3. (a) Cai, G.; Litt, M. H. *J. Polym. Sci., Polym. Chem.* 1989, *27*, 3603. (b) Cai, G.; Litt, M. H.; Krieger, I. M. In *Contemporary Topics in Polymer Science*; Albertson, B. M., Ed.; Plenum: New York, 1989; Vol. 6, in press.
4. Tadros, T. F.; Vincent, B. *J. Phys. Chem* 1980, *84*, 1575.
5. Lin, P.; Clash, C.; Pearce, E. M.; Kwei, T. K. *J. Pol. Sci., Polym. Phys. Ed.* 1988, *26*, 603-619.
6. Miyamoto, M.; Sano, Y.; Kobayashi, S.; Saegusa, T. *Eur. Polym. J.* 1983, *19*, 955.
7. Szwarc, M. In *Carbonion Living Polymers and Electron Transfer Processes*; John Wiley and Sons: New York, 1968.
8. First reported by: (a) Litt, M. H.; Levy, A., Belgian Patent 666,828, 1965. (b) Kagiya, T.; Narisawa, S.; Manabe, T.; Fukui, K. *J. Polym. Sci., B4* 1966, 441. (c) Tomalia, D. A.; Sheets, D. P. *J. Polym. Sci., A4* 1966, 2253. (d) Also see Reference 15.
9. Litt, M. H.; Rahl, F.; Roldan, L. G. *J. Polym. Sci., Part A-2* 1969, *7*, 463-473.
10. (a) Saegusa, T.; Kobayashi, S. *Encyclopedia of Polymer Science and Technology*, John Wiley & Sons: New York, 1976; Suppl. Vol. 1; pp 220-237. (b) Litt, M. H.; Chen, T. T.; Hsieh, B. R. *J. of Polym. Sci., Polym. Chem.* 1986, *24*, 3407-3422.
11. Miyamoto, M.; Aoi, K.; Saegusa, T. *Macromolecules* 1989, *22*, 3540.
12. Recent reviews and articles therein can be found in: (a) Kobayashi, S.; Saegusa, T. *Encyclopedia of Polymer Science and Engineering*; John Wiley & Sons: New York, 1986; pp 525-537. (b) Kobayashi, S.; Saegusa, T. *Ring-Opening Polymerization*; Elsevier Applied Science: Essex, England, 1984; pp 751-807.
13. Levy, A.; Litt, M. H. *J. Polym. Sci., A1* 1968, *6*, 63.

14. Litt, M. H.; Levy, A.; Herz, J. *J. Macromol. Sci. - Chem.*, **A9** 1975, 703.
15. Bassiri, T. G.; Levy, A.; Litt, M. H. *Polym. Lett.* 1967, **5**, 871. See also References 8 (b) and 13.
16. Flory, P. J. *J. Am. Chem. Soc.* 1940, **62**, 1561-1565.
17. Tadros, T. F. In *Polymer Colloids*; Buscall, R.; Corner, T.; Stageman, J. F., Eds.; Elsevier Applied Science: London and New York, 1985; p 107.
18. (a) Sheludko, A. *Proc. Kon. Ned. Akad. Ventensch.* 1962, **B56**, 87 (b) *Adv. Colloid Interface Sci.* 1967, **1**, 391. (c) Scheludko, A.; Maner, E. *Trans. Faraday Soc.* 1968, **64**, 1123.
19. Vrij, A. *Disc. Faraday Soc.* 1966, **42**, 23.
20. Litt, M. H.; Hsieh, B. R.; Krieger, I. M.; Chen, T. T.; Lu, H. L. *J. of Colloid and Int. Sci.* 1987, **115**, 312.
21. Hsieh, B. R.; Litt, M. H.; Demopolis, T. N.; Krieger, I. M. *Polym. Prepr., Am. Chem. Soc. Div. Polym. Chem.* 1986, **27(2)**, 122.
22. Balazs, A. C.; Lewandowski, S. *Macromolecules* 1990, **23**, 839.
23. Gia, H. B.; Jerome, R.; Teyssie, Ph. *Colloid Polym. Sci.* 1979, **257**, 1294.
24. (a) Ahmed, M. G.; Alder, R. W.; James, G. H.; Sinnott, M. L.; Whiting, M. C. *Chem. Commun.* 1968, 1533. (b) Hansen, R. L. *J. Org. Chem.* 1965, **30**, 4322. (c) Streitwieser, Jr. A.; Wilkins, C. L.; Kiehlmann, E. *J. Am. Chem. Soc.* 1968, **90**, 1598.
25. Plumb, J. B.; Atherton, J. H. In *Block Polymers*; Allport, D. C.; Janes, W. H., Eds.; Applied Science: London, 1973.
26. (a) Miyamoto, M.; Naka, K.; Tokumizu, M.; Saegusa, T. *Macromolecules* 1989, **22**, 1604. (b) Kobayashi, S.; Uyama, H.; Higuchi, N.; Saegusa, T. *Macromolecules* 1990, **23**, 54. (c) See also Reference 2.
27. (a) Kobayashi, S.; Saegusa, T. *Macromol. Chem., Suppl.* 1985, **12**, 11-24. (b) Ikeda, I.; Kurushima, Y.; Takashima, H.; Suzuki, K. *Pol. J.* 1988, **20**, 243-250. (c) Shulz, R. C.; Schwarzenbach, E. *Macromol. Chem., Macromol. Symp.* 1988, **13/14**, 495-505.
28. Kobayashi, S.; Kaku, M.; Sawada, S.; Saegusa, T. *Polym. Bull.* 1985, **13**, 447.
29. Swamikannu, A. X. Ph. D. Thesis, Case Western Reserve University, August 1984, p 145.

## Chapter 2

**Synthesis and Characterization of 2-p-t-Octylphenyl-2-oxazoline  
homo- and diblock polymers.**

### a) Introduction

2-Oxazolines can be used to make block copolymers containing segments of differing polarity. Critical surface tension  $\gamma_c$  is the the surface tension of a possibly hypothetical liquid which would just make a contact angle of  $0^0$  with a given solid.  $\gamma_c$  is taken as a measure of the wettability of the solid<sup>1</sup>. Thus non-wetting, low-energy surfaces are characterized by low  $\gamma_c$  values. The wettability of surfaces coated by organic films is controlled by the nature, molecular organization and packing of the outermost groups on the surface and is independent of the nature and arrangements of the underlying atoms and molecules. Litt<sup>2</sup> showed that cast films of block polymers composed of poly(N-lauroylethyleneimine) and poly(N-propionylethyleneimine) exhibited low-energy surfaces, as shown by low  $\gamma_c$  values. These values were very close to that of paraffin, whose surface consists of close-packed methyl groups. It was therefore concluded that the nonpolar segment of the polymer forms a close-packed methyl group surface, and that the backbone methylene and tertiary amide groups are not exposed at the interface<sup>3</sup>. Work was also done on the use of diblock co-oligomers prepared from 2-p-t-butylphenyl-2-oxazoline (hydrophobic segment) (B) and 2-ethyl-2-oxazoline (hydrophilic segment) (E) in water/styrene emulsion polymerization. It was shown<sup>4-5</sup> that B blocks close-pack normal to the water-oil interface, resulting in low interfacial energy monolayer formation. p-t-Butylphenyl side-chains come together so that the energy of interaction is minimized; hence a surface film of close-packed t-butyl groups forms. Results from the literature<sup>6</sup>

indicate that tertiary butyl groups tend to decrease the density as well as the surface tension of hydrophobic liquids. A surface film composed of close-packed *t*-butyl groups might prevent probes from penetrating into the tight structure. Hence the number of interactions that contribute to  $\gamma_c$  are decreased, thus suggesting that such a structure might have a lower critical surface energy compared to that of normal paraffin. This can lead to a "superparaffin" structure.  $\gamma_c$  values of cast B films were indeed found lower than that of polyethylene but slightly higher than  $\gamma_c$  of paraffin<sup>4</sup>.  $\gamma_c$  values higher than that of paraffin suggest higher than expected electronic and steric interactions due to interference from the side-chain phenyl groups.

To lower  $\gamma_c$  we decided to prepare block polymers consisting of a hydrophobic poly(*N*-*p*-*t*-octylbenzoyl ethyleneimine) (O) and a hydrophilic poly(*N*-propionylethyleneimine) (E) segment. If (O) crystallizes to create a close-packed *t*-octyl group surface then we expect much less interactions of the phenyl groups with a probe, since they are located deeper into the structure. Therefore  $\gamma_c$  might be lower than that of B films.

This chapter describes the synthesis and characterization of polymers made from 2-*p*-*tert*-octylphenyl-2-oxazoline (O). In the experimental section we first present the equipment and techniques of monomer and polymer synthesis, as well as analysis. We then specifically discuss the synthesis of monomer, followed by kinetics to determine the rate of propagation  $k_p$ , using methyl nosylate (CH<sub>3</sub>ONs) as initiator. Next we describe the synthesis and characterization of a high molecular weight (O) followed by the synthesis of a series of diblocks consisting of hydrophobic

(O) and hydrophilic (E) segments. The nomenclature to be used is  $O_xE_y$ , where x indicates the number of repeat units per (O) block and y the corresponding (E) repeat units. We then discuss the polymer characterization by gel permeation chromatography (GPC) and  $^1H$  NMR. Finally we summarize the results and draw conclusions.

### b) Experimental section

#### Materials:

All chemicals were obtained from Aldrich unless otherwise noted. Solvents were Fisher reagent grade and were usually utilized as received. Diisobutylene was 99% pure and used from the bottle. Methyl p-nitrobenzenesulfonate (MeONs) was Aldrich Gold Label (99+% purity) and was used as received. Recrystallization from a 35:75 acetone/hexanes mixture, after heating to the boiling point to dissolve, did not improve the 88-90°C mp. o-Dichlorobenzene was Fisher HPLC grade and was purified as described later in this section.

#### Instrumentation:

Spinning-band: Separations (see later Scheme 2.1) of high boiling compounds (reaction of 1 to make 2) were accomplished using a Perkin Elmer spinning band distillation column. This was one meter high, silver, vacuum-jacketed, and could run either under vacuum or at atmospheric pressure. The reaction mixture and a magnetic stirring bar were placed in

a special pot flask and heated via a hot plate/stirrer. The pot flask had a thermo-well and a vacuum joint that connected to the band. A needle valve inside the condenser controlled the reflux ratio (i. e. the ratio of condensing drops at the bottom of the condenser over the collected drops) to about four. According to the manufacturer the efficiency of the column could reach ca. 70 theoretical equivalent plates of separation at high reflux ratios. The temperature was monitored via a Keithley digital thermometer connected to thermocouples ( $\pm .1^{\circ}\text{C}$ ) both at the pot-flask well and the top of the column in another thermo-well. Vacuum was controlled with a needle-valve system attached just after the dry ice trap, and monitored with a differential pressure mercury gauge.

Oxidation apparatus: To carry out the oxidation of substrates with  $\text{KMnO}_4$  (shown in subsequent Scheme 2.1), we used a three-liter reaction vessel equipped with a three-neck removable top. A stirrer motor was connected to the flask through the middle opening via a rod; the rod reached the bottom of the flask with an attached two-inch paddle blade. A thermometer and water condenser were also fitted through the openings of the head. The temperature was controlled with a Variac potentiostat connected to a heating mantle, which covered most of the reaction vessel.

Cleaning of polymerization glassware: A very strict procedure was applied for cleaning of all solvent reservoirs and polymerization vessels. The glassware (including the glass stirrers, if any) were filled with cleaning solution (conc.  $\text{H}_2\text{SO}_4$  and Nochromix<sup>R</sup>) and left overnight. The flasks

were then rinsed with water, followed by washing with 10% ammonium hydroxide, distilled water and acetone. Finally they were dried in a 90–100°C oven and left there until they were used.

End-to-end distillation: Distillations of solvent (o-DCB) and liquid monomer (2-ethyl-2-oxazoline), as well as all polymerizations described in this dissertation, were carried out on a rack system that could be used either under high vacuum or nitrogen<sup>5</sup> (See Figure 2.1). This had six outlets, each containing a stopcock and #15 o-ring joint. All stopcocks had glass barrels and Teflon<sup>R</sup> plugs. The rack stopcocks were from Ace Glass while all the others were from J. Young. The liquid was placed in a round-bottomed flask that had a #15 o-ring joint; this was connected to an adapter (Figure 2.2 (b)), equipped with a stopcock located between two o-ring joints. o-DCB was stirred overnight with P<sub>2</sub>O<sub>5</sub> to remove water, and 2-ethyl-2-oxazoline with Na/benzophenone until the solution turned deep blue. The flask was then connected to the vacuum rack by connecting the other end of the adapter. The liquid was next frozen with liquid nitrogen, the adapter stopcock opened, and the system evacuated to  $9 \times 10^{-5}$  torr or better. The stopcock to the flask was then closed and the liquid nitrogen removed to allow thawing of the solid. The liquid was thus degassed of trapped air. This procedure was repeated twice more, then the degassed liquid was transferred by distillation under high vacuum directly into a clean reservoir, which was attached to the line and immersed in liquid nitrogen. Reservoirs (Figure 2.2 (a)) were composed of a cylindrical 50–60 mL round-bottomed flask and a stopcock



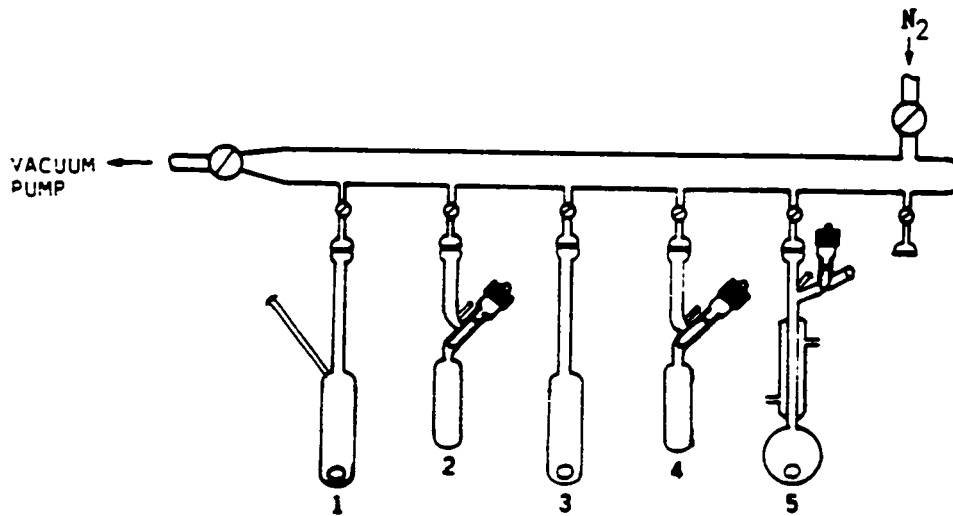


Figure 2.1. Schematic of polymerization apparatus.

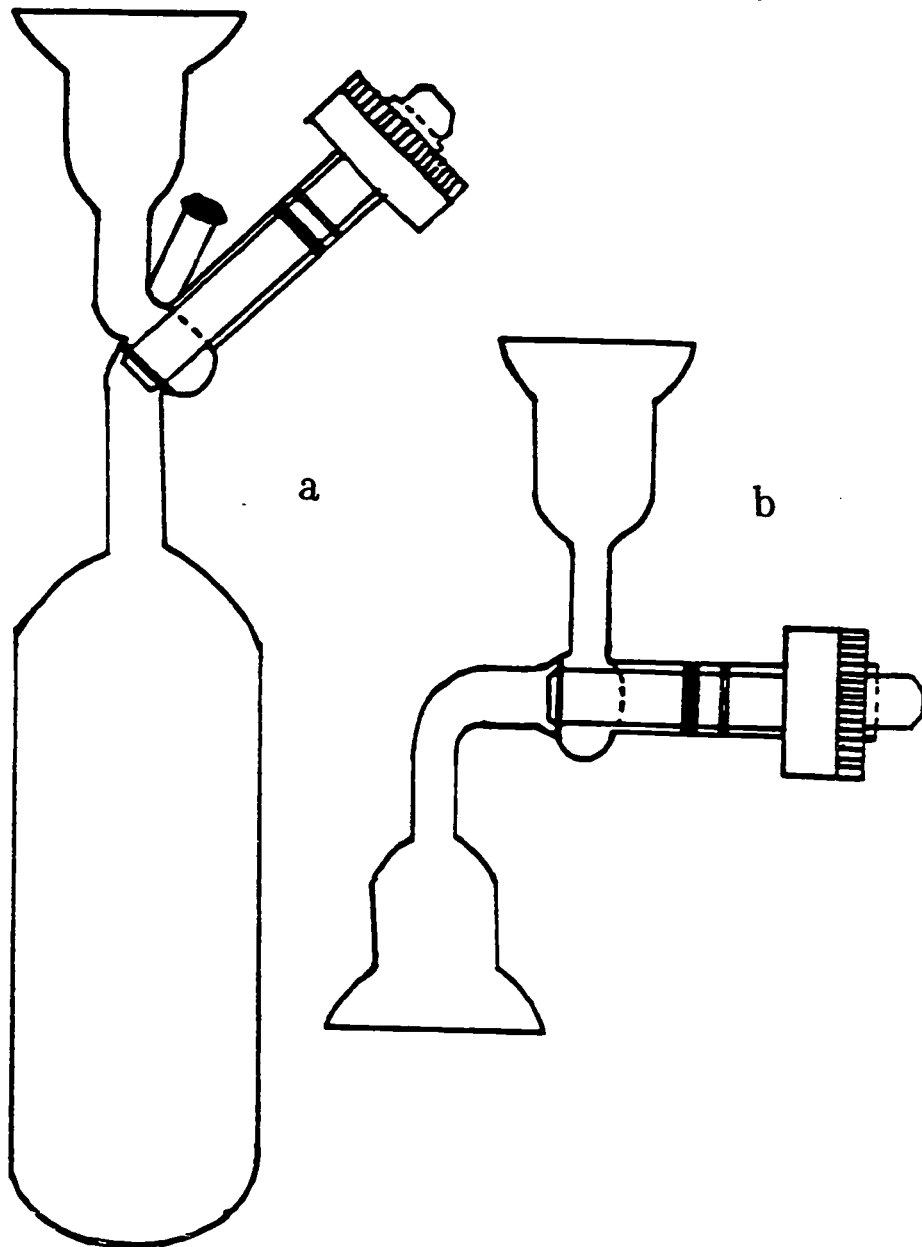


Figure 2.2. Distillation reservoir (a) and adapter (b).

which enabled the vessel to be connected to the rack through a second stopcock. The lower arm of the latter led to the vessel and the top to an o-ring joint. A rubber septum covered a stub on the top arm, adjacent to the stopcock plug, so that a long-syringe needle could fit through the stub and reach the bottom of the flask. The purified liquid was then isolated from the vacuum by closing the reservoir stopcock and opening the corresponding stopcock on the rack to the vacuum.

Polymerization Apparatus: The polymerization experiments described in this work were run in custom-made vessels, shown in Figure 2.3. These were composed of a 30–40 mL round-bottomed cylindrical compartment, connected to a 15-cm vertical tube with an o-ring joint at the top and an opening at the side, about 3 cm from the top. A condenser jacketed the vertical tube from the entrance of the side-tube until the entrance of the bubble. A stopcock was fitted so one arm led into the side of the tube while the other led to the side-opening, which was sealed by a rubber septum. Connection to the vacuum rack was made via the joint at the top of the vessel.

Analytical instrumentation: HPLC chromatograms were taken with an ISCO high pressure liquid chromatograph, equipped with a UV-detector at 254 nm. The instrument was equipped with two pumps so there was a capability to run either one solvent or a mixture of two. A C-18 reverse-phase nonpolar HPLC column was connected and typical runs were done at 1 mL/min, with one solvent being MeOH, the other usually distilled H<sub>2</sub>O.

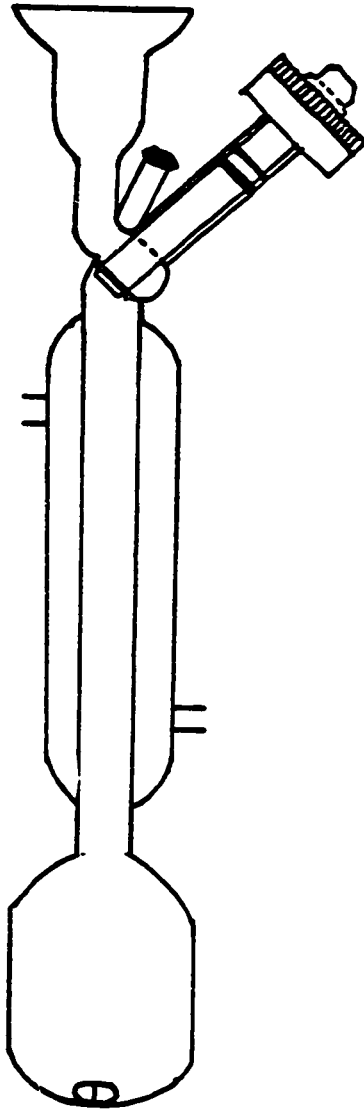


Figure 2.3. Polymerization reaction vessel.

All gel permeation chromatograms were done with a Waters GPC II instrument equipped with refractive index (RI) and Hewlett Packard UV detectors. RI signals were directed to and plotted on an analog chart recorder. The UV detector contained a multi-diode array which permitted storage of instantaneous UV spectra on a disk drive connected to an HP-85 computer. Signals, as well as UV spectra were plotted on a HP 1470 plotter. Up to eight signals could be recorded at a time, each resulting from subtraction of UV intensities of the instantaneous spectra of desired wavelength pairs. GPC samples were separated by passing through two Polymer Laboratories 300 mm GPC columns connected in series: a 500 Å, and a 10<sup>4</sup> Å pore size, with a molecular weight range of about 200–10<sup>6</sup>. The molecular weight versus elution volumes were calibrated using 17 narrow polydispersity polystyrene standards of known molecular weight after normalization to o-DCB internal standard. Runs were made with a flow rate of 1 mL/min THF.

<sup>1</sup>H NMR spectra were run either with an EM-360 (60 MHz) Varian, or a computerized Varian XL-200, 200 MHz Fourier transform NMR spectrometer. The solvent was CDCl<sub>3</sub> unless otherwise indicated. Tetramethylsilane (TMS) was used as reference.

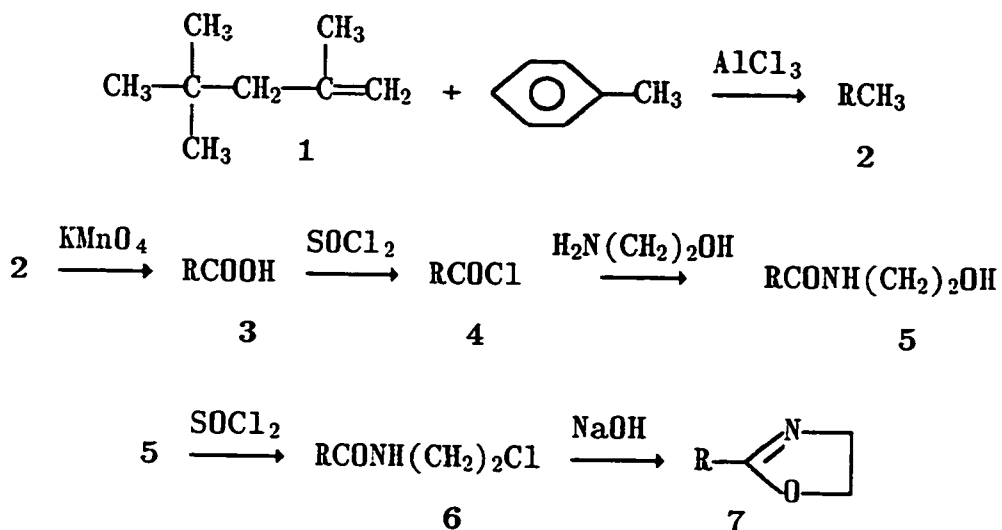
IR spectra were run on powders mixed with KBr and pressed to a disk and were taken on a Digilab FTS-14 Fourier transform infrared spectrometer connected to a VAX 780 computer. Frequencies are reported in cm<sup>-1</sup>.

Melting points were taken with a Thomas-Hoover capillary melting point apparatus and are uncorrected.

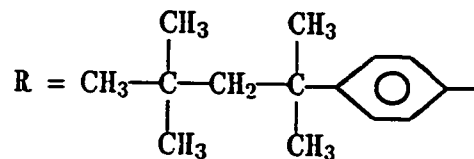
2-p-t-Octylphenyl-2-oxazoline Synthesis

The synthesis of this monomer was carried out as depicted in Scheme 2.2.

Scheme 2.2



where:



p-t-Octyltoluene, 2: Synthesis of **2** was done according to the method described by Sanford<sup>7</sup> on the preparation of t-octylbenzene from alkylation of benzene. 27 g (.20 mol) powdery AlCl<sub>3</sub> was added to a two-neck, round-bottomed flask, equipped with magnetic stirrer and thermometer, and immersed in a water bath. 71 mL nitrobenzene

(.69 mol) was added to dissolve the catalyst. To the resultant deep red solution was added 940 mL toluene (8.85 mol). 249 g (2.22 mol) (first weighed into a volumetric cylinder) of **1** and 105 mL toluene (.99 mol) were placed in a 500-mL addition funnel. The clear colorless solution was very carefully added dropwise with good stirring to the red  $\text{AlCl}_3$  solution over a period of sixty minutes while the temperature was kept between 24 and 30°C. Stirring was continued for ten more minutes after the addition was complete. To prevent rearrangements of **2**, the red solution was then quickly quenched by pouring it into a large excess of crushed ice/water. The resultant yellow slurry was then vigorously shaken until all color disappeared. Two layers resulted: a top organic and a lower aqueous phase. The slurry was transferred to a two-liter separation funnel and the aqueous layer removed. The organic layer was washed four times with an aqueous potassium bicarbonate solution, then dried by passing through an anhydrous sodium sulfate filter. The solution was then transferred to a rotary evaporator; some NaOH pellets were added to prevent possible rearrangement due to remaining acidic impurities. Excess toluene and some t-butyltoluene were then removed under vacuum. The resultant orange-red solution was transferred to a one-liter flask and attached to the spinning band column. A .25-torr vacuum was applied and the flask heated with stirring. A first low-boiling fraction was removed (mostly t-butyltoluene and nitrobenzene); then a colorless transparent middle fraction that weighed 254 g was collected at 80–85°C. Higher boiling polyoctylated compounds which distilled at temperatures equal to or higher than 85°C could be separated from the middle fraction according to the difference in refractive

index. **2** was then redistilled to give 198.5 g (.97 mol) (43.8% yield) by High Pressure Liquid Chromatography (HPLC) using MeOH as eluent solvent. 60 MHz  $^1\text{H}$  NMR of **2** is shown in Figure 2.4.

p-t-Octylbenzoic acid, 3: **3** was prepared from oxidation of **2** by  $\text{KMnO}_4$  in pyridine/ $\text{H}_2\text{O}$  according to a modified version of the method developed by Kovach<sup>8</sup> and Nightingale<sup>9</sup>. To 40.68 g (.20 mol) of **2**, poured into the reaction vessel, was added 300 mL (3.79 mol) pyridine. To the solution was gradually added 60 mL (3.33 mol) distilled water until cloudiness appeared. The mixture was heated with stirring to  $95^\circ\text{C}$  and an additional 10 mL of water was added. 120 g (.76 mol) of potassium permanganate was then added in two equal batches, the first as soon as the temperature reached  $90^\circ\text{C}$  and the second 35 min later. The solution turned purple as soon as the  $\text{KMnO}_4$  was added, and turned brown upon reaction. The exact point of the color change could not be determined because the very viscous slurry splashed all over the vessel and covered all sides with a muddy-brown precipitate. The slurry was subsequently stirred for 7 h to assure completion of the reaction. 55 mL hydrazine (1.73 mol) was then very slowly added dropwise to the brown slurry until a very light-brown colored fine powder developed. Extreme caution was taken in adding the hydrazine to the mixture, since hydrazine is a strong reducing agent and an exothermic reaction was observed upon addition of each drop, with concurrent evolution of nitrogen. 450 mL of conc. HCl (5.48 mol) was then added to lower the pH to zero. A small colorless organic phase formed on top of a large aqueous greenish one. A yellowish cheese-like



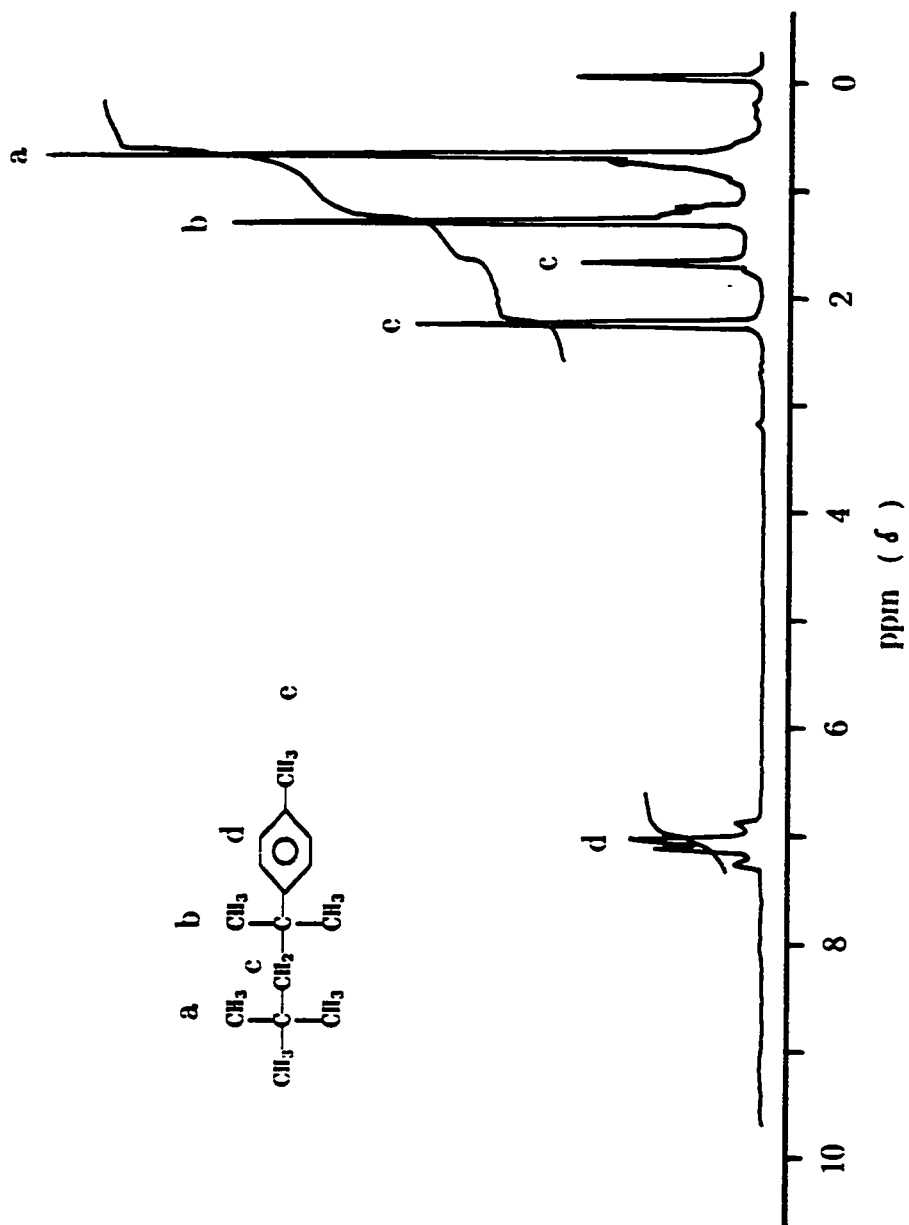


Figure 2.4. 60 MHz  $^1\text{H}$  NMR of t-octyl-toluene.

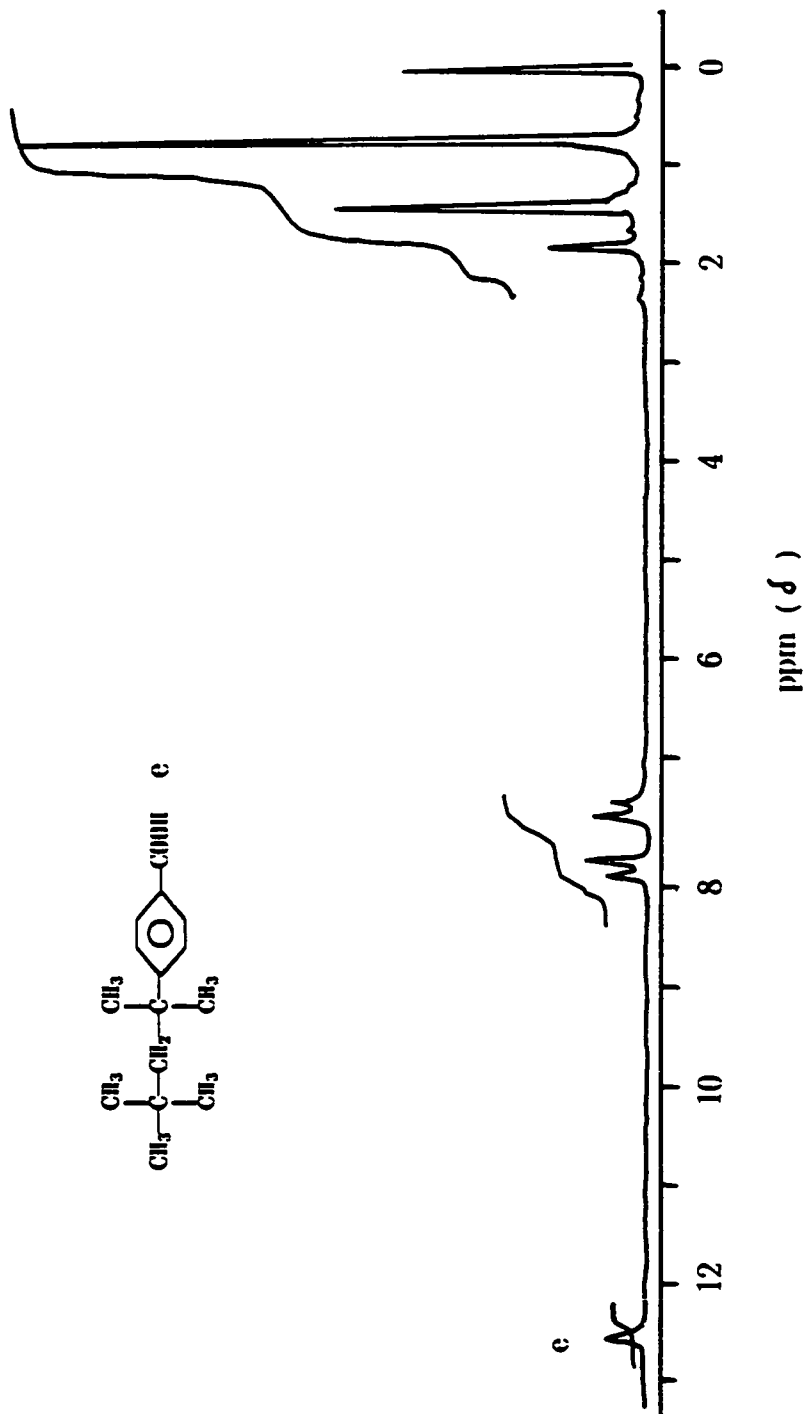
solid precipitated in the top layer upon standing. This was collected by decantation, and the aqueous layer was washed many times with  $\text{CHCl}_3$  to collect any left-over acid. The collected solid was dissolved in the combined organic phases, and passed through anhydrous sodium sulfate to remove water.  $\text{CHCl}_3$  was rotovaporated and the yellowish solid crystallized from hot isooctane on cooling to room temperature. 18 g (.08 mol) of white solid **3** was collected (38.5% yield). Shiny white crystals of **3** that melted at 154–155<sup>0</sup>C resulted from a second recrystallization from isooctane. <sup>1</sup>H NMR and FT-IR spectra are shown on Figures 2.5 and 2.6 respectively. <sup>1</sup>H NMR spectral assignments of **2**, **3**, **4**, **5**, and **7** are given in Table 2.1 with the Experimental Section.

FT-IR (KBr,  $\text{cm}^{-1}$ ):

3445, 3065, 2984, 2955, 2900, 2868, 2676, 2557, 1607, 1619, 1576, 1474, 1431, 1373, 1329, 1300, 1256, 1207, 1140, 1097, 1030, 966, 865, 850, 792, 719, 612, 574, 560, 516.

The subsequent steps of the synthesis of **7** were carried out for the most part without isolating intermediate products, according to a method in the literature<sup>5</sup>.

p-t-Octylbenzoyl chloride, 4: 34.75 g (.149 mol) of pure **3** was mixed with 32 mL (.44 mol) thionyl chloride in a one-neck round bottomed flask, equipped with water-cooled condenser and magnetic stirrer. The mixture was heated to reflux (79<sup>0</sup>C) to give a yellowish liquid. The solution was stirred at reflux for two hours; then excess  $\text{SOCl}_2$  was removed by rotovaporation to give a dark-yellow viscous liquid of **4**. A 60 MHz

Figure 2.5. 60 MHz  $^1\text{H}$  NMR of p-t-octylbenzoic acid.

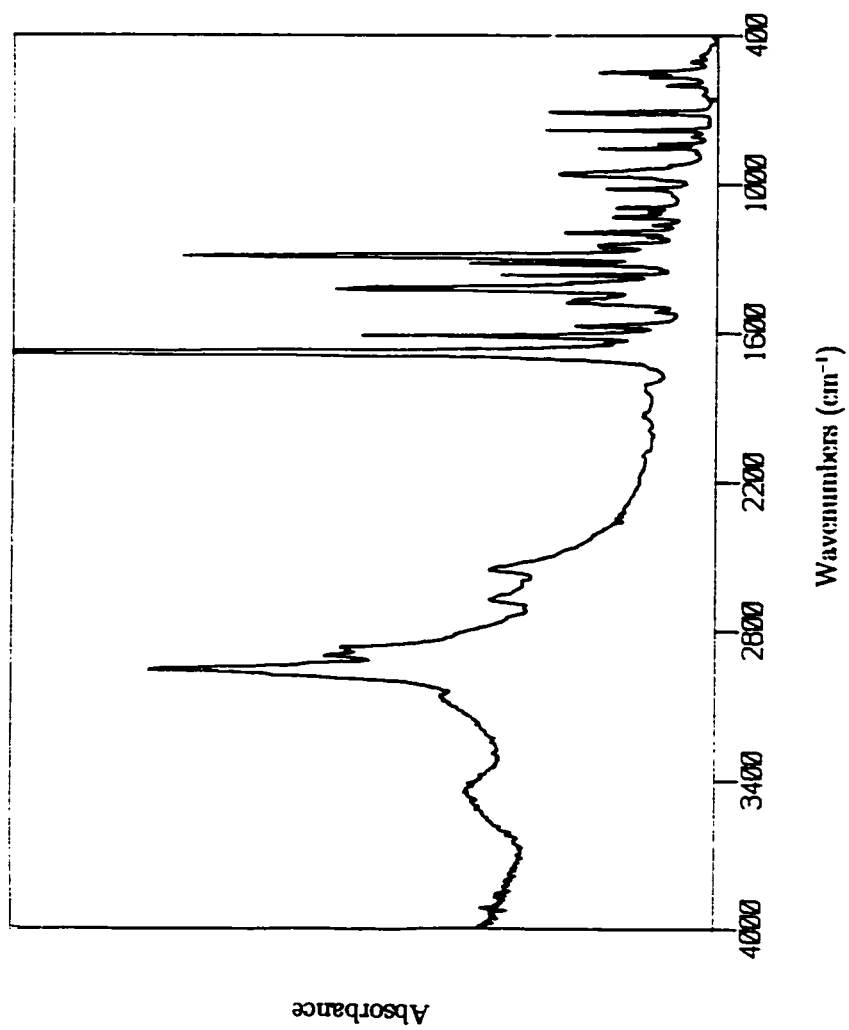
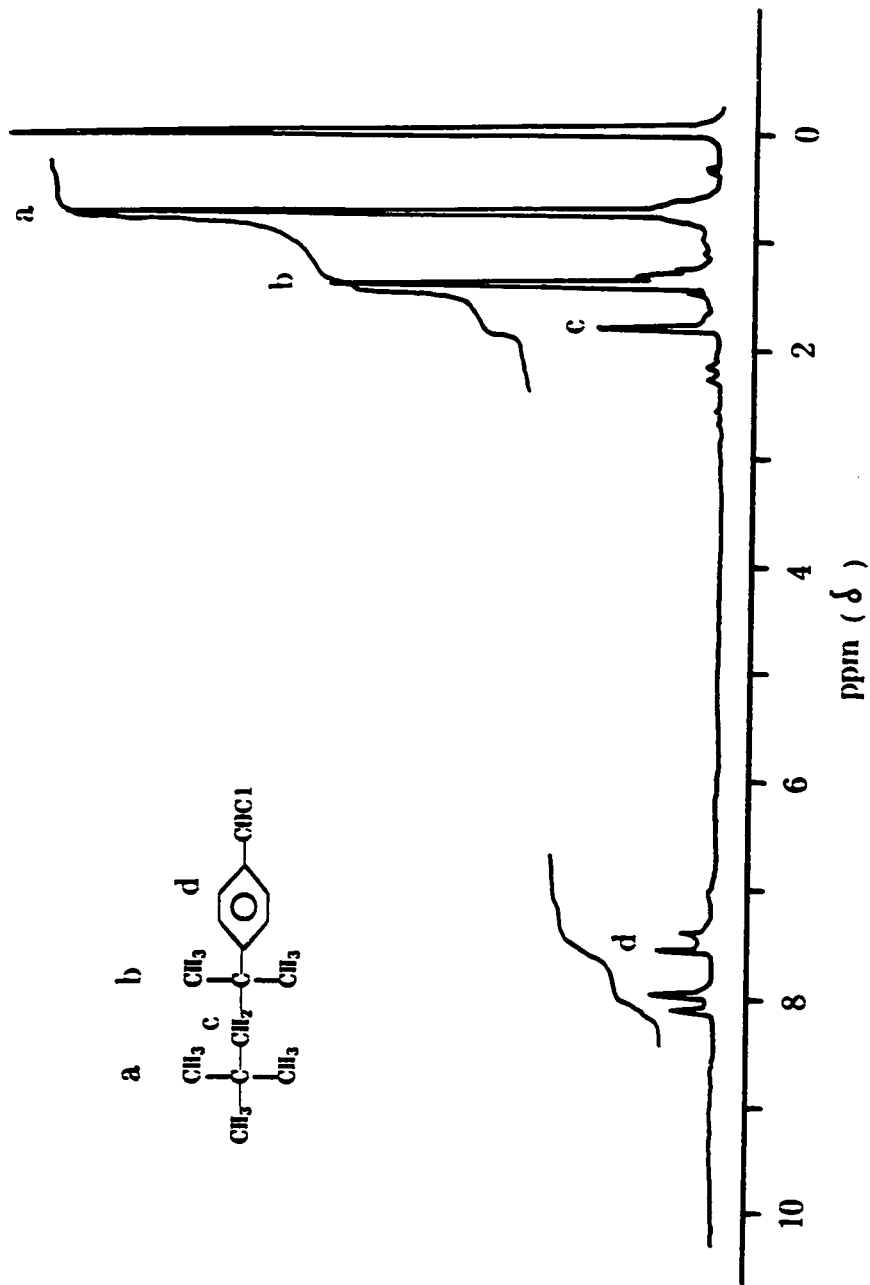


Figure 2.6. FT-IR of p-t-octylbenzoic acid.

Figure 2.7. 60 MHz <sup>1</sup>H NMR of *p*-*t*-octylbenzoyl chloride.

$^1\text{H}$  NMR spectrum of 4 is shown in Figure 2.7.

N-Hydroxyethyl-p-t-octylbenzamide, 5: 40 mL methylene chloride was added to the liquid 4 and the solution was added dropwise via an addition funnel with vigorous stirring to an ice/water-bath cooled solution of 20 mL distilled ethanolamine (.328 mol) in 160 mL  $\text{CH}_2\text{Cl}_2$ . The mol ratio of 4 to ethanolamine was thus 1:2.2. At the end of addition, the ice-water bath was removed and stirring continued for two more hours at room temperature (pH was basic). The solution was then filtered to remove the precipitated ethanolamine hydrochloride. A small amount of the solution was removed and evaporated. The solid was recrystallized from isooctane/toluene to give 5, a white crystalline solid that melted at 93–95 $^\circ\text{C}$ .  $^1\text{H}$  NMR and IR spectra are shown in Figures 2.8 and 2.9 respectively.

FT-IR (KBr,  $\text{cm}^{-1}$ ):

3358, 2960, 2906, 2876 1641, 1624, 1561, 1520, 1483, 1408 ,1376, 1353, 1324, 1264, 1218, 1175, 1105, 1085, 1028, 913, 864, 832, 789, 740, 674, 581.

N-Chloroethyl-p-t-octylbenzamide, 6: The methylene chloride solution of 5 was transferred to a round bottomed flask equipped with a magnetic stirrer and thermometer, and chilled to 0 $^\circ\text{C}$  with an ice-water bath. 13 mL  $\text{SOCl}_2$  (.178 mol) was then gradually added dropwise via an addition funnel for a 5/ $\text{SOCl}_2$  mol ratio of 1:1.2. The ice bath was then removed and the solution refluxed for 2 h. The white powdery solid formed during reflux (ethanolamine hydrochloride salt) was filtered after

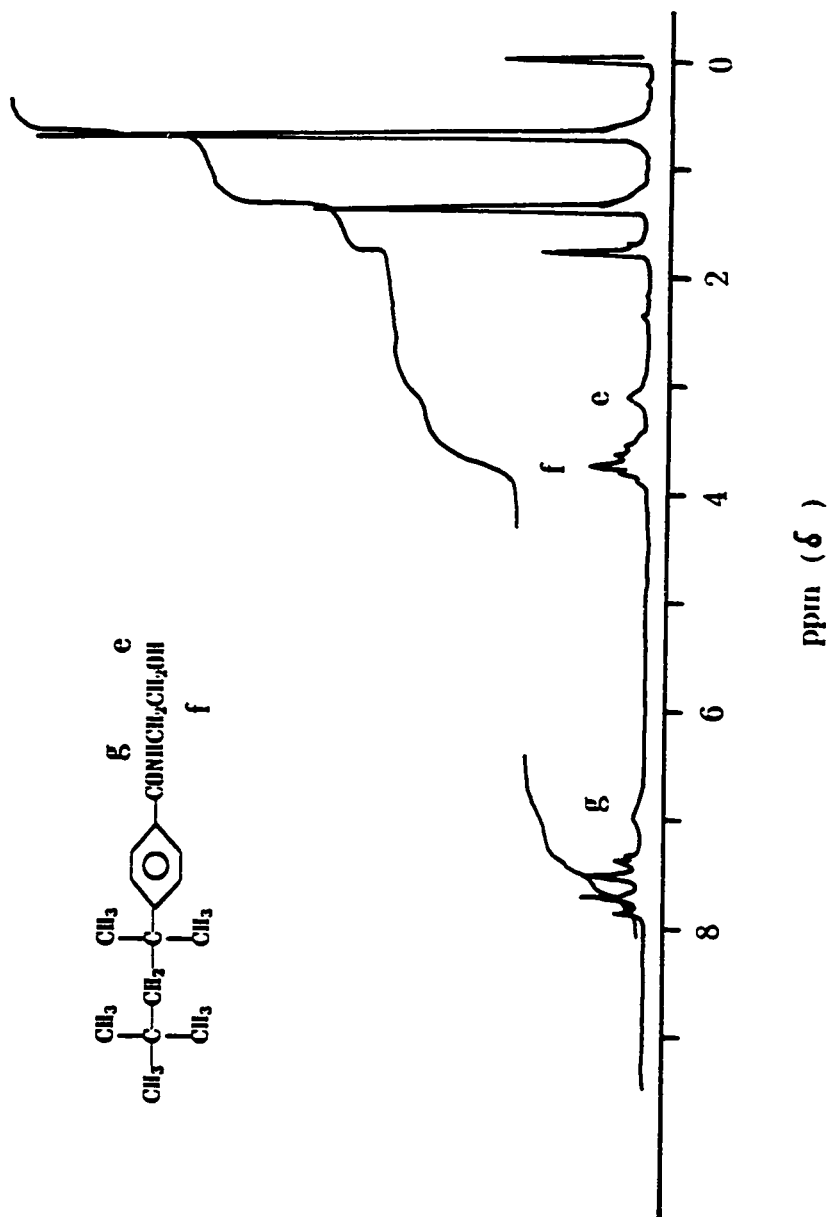


Figure 2.8. 60 MHz of N-hydroxyethyl p-t-octylbenzamide.

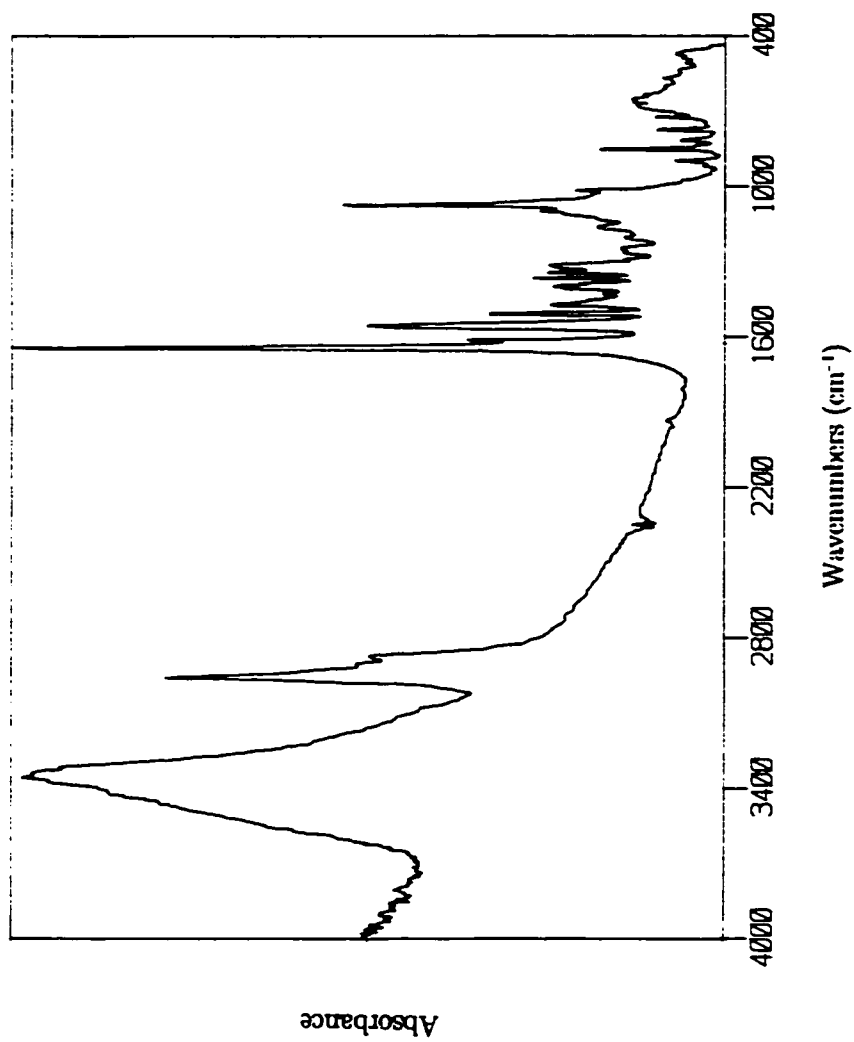


Figure 2.9. FT-IR of N-hydroxyethyl p-t-octylbenzamide.



cooling to room temperature. Excess  $\text{SOCl}_2$  and  $\text{CH}_2\text{Cl}_2$  were rotovaporated leaving a light brown solid **6** on the flask walls. A small amount of the solid was sublimed to give white crystals of mp  $76\text{--}77^\circ\text{C}$ .

2-p-t-Octylphenyl-2-oxazoline, 7: To 38.44 g (0.148 mol) of **6** in one-neck round-bottomed flask was added 700 mL of isopropanol. A magnetic stirring bar and condenser were added and the mixture heated to reflux. The solid dissolved at reflux temperature ( $80^\circ\text{C}$ ), giving a clear brown solution, and then 6.53 g (0.163 mol) NaOH pellets was added for a 1.1:1 mol ratio of NaOH/**6**. A white sodium chloride powder precipitated in the flask as soon as the base was added. The mixture continued to reflux for 30 min and a check showed the pH to be 8 at the end. The solution was taken to the refrigerator to help precipitate all the NaCl and later suction-filtered. Isopropanol was then removed in vacuo, leaving a yellowish solid of **7**. **7** was then dissolved into 200 mL of toluene and quickly passed through a short alumina column (20 g neutral alumina, activity III), packed with sea sand, to remove any polar impurities. 1.2 L of toluene was then passed through the column to elute the oxazoline. The toluene solutions were then rotovaporated giving 34.35 g of white solid **7**. This was then sublimed twice to give 33.25 g (.128 mol) of shiny-white needles of **7**. The overall yield from **3** was thus 86.5% and the purity was greater than 99% by HPLC. **3** was then dissolved in hot isooctane and crystallized at  $-18^\circ\text{C}$ , giving shiny-white needles that melted at  $80\text{--}81^\circ\text{C}$ . 26 g of **7** was collected from two crystallization crops.  $^1\text{H}$  NMR and IR spectra are shown in Figures 2.10 and 2.11.

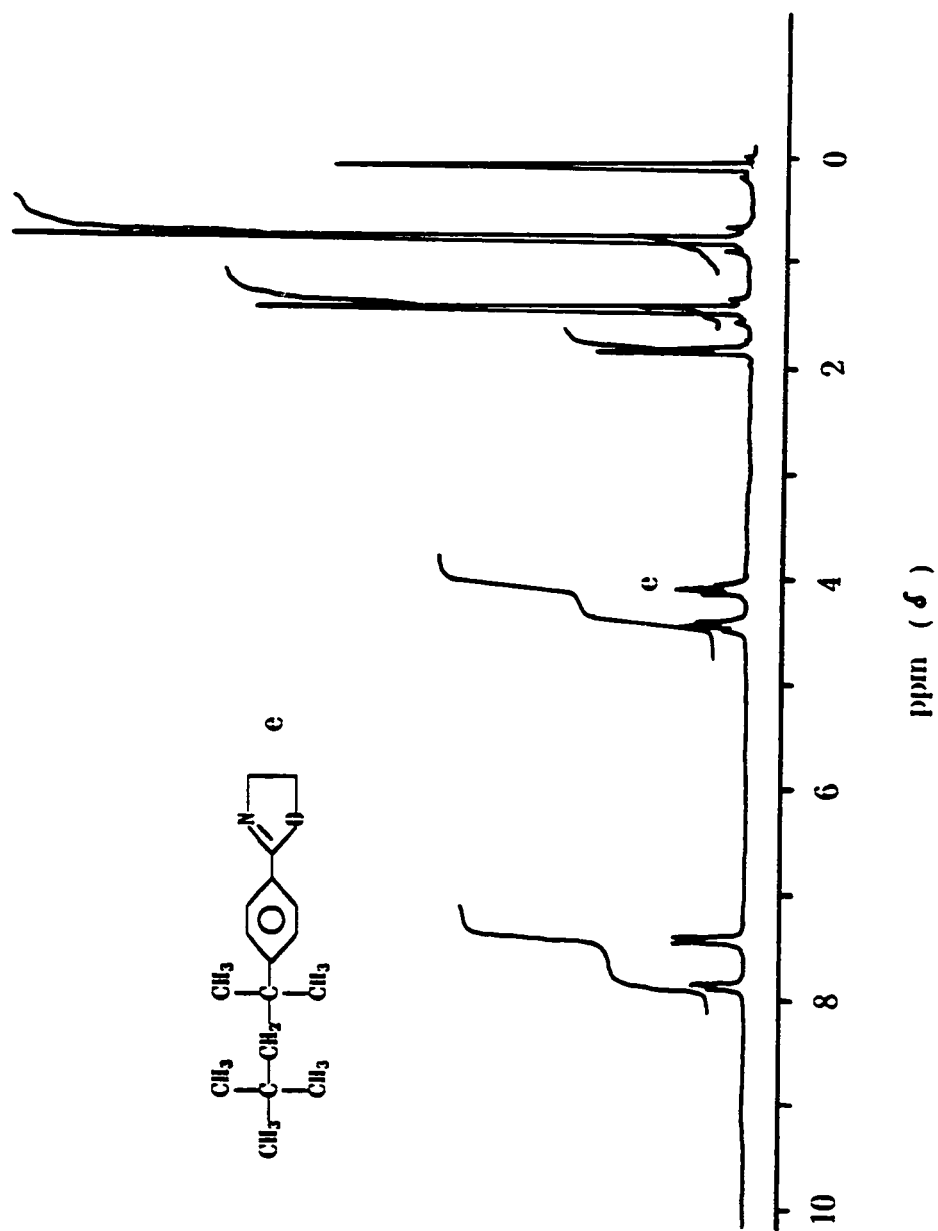


Figure 2.10. 200 MHz <sup>1</sup>H NMR of 2-p-t-octylphenyl-2-oxazoline.

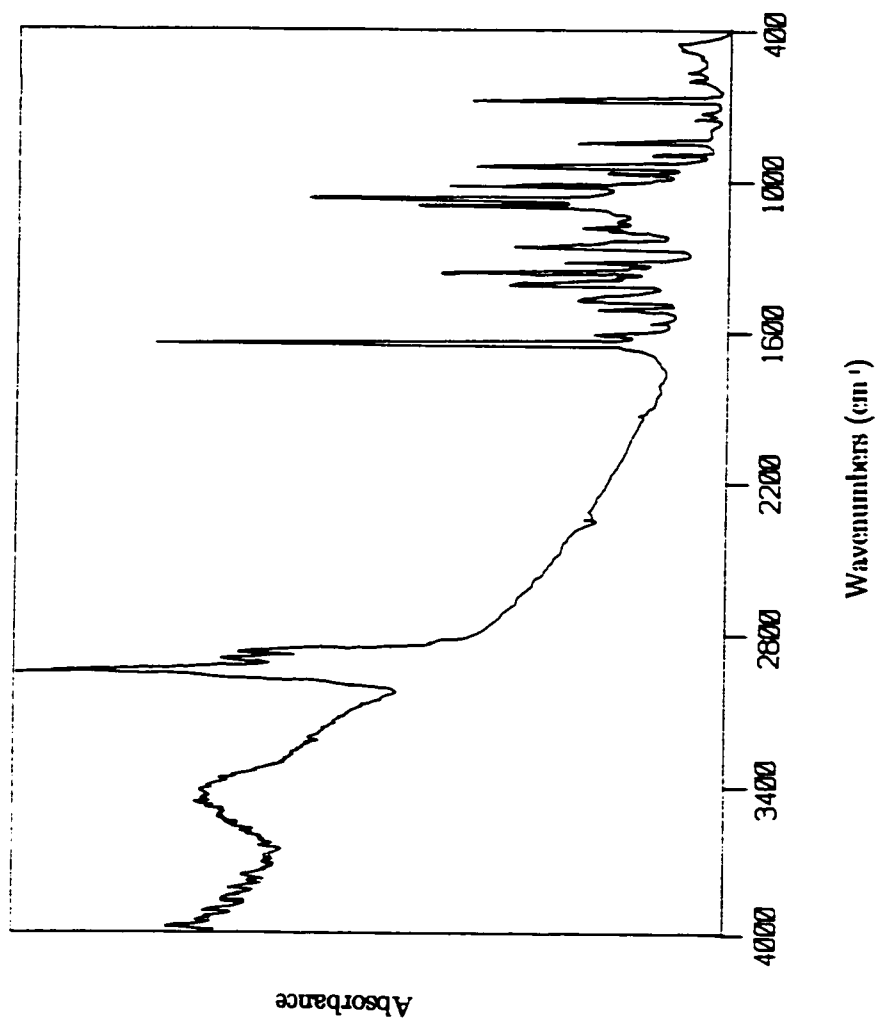


Figure 2.11. FT-IR of 2-p-t-octylphenyl-2-oxazoline.

FT-IR (KBr,  $\text{cm}^{-1}$ ):

3453, 2963, 2900, 2877, 1650, 1607, 1509, 1466, 1405, 1362, 1322, 1258, 1206, 1160, 1091, 1062, 1019, 962, 941, 890, 838, 746, 674, 596, 561.

A summary of the  $^1\text{H}$  NMR peak assignments of 2, 3, 4, and 7 is given in Table 2.1.

Table 2.1.  $^1\text{H}$  NMR spectral assignments of 2, 3, and 4


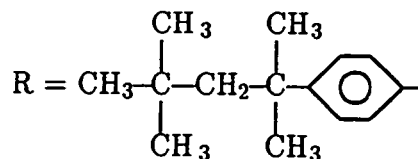
Structure	60 MHz $^1\text{H}$ NMR ( $\delta$ , ppm)
R-CH <sub>3</sub> (2)	$0.68$ (s, 9H, $\begin{array}{c} \text{CH}_3 \\   \\ -\text{C}-\text{CH}_3 \\   \\ \text{CH}_3 \end{array}$ ), $1.30$ (s, 6H, $\begin{array}{c} \text{CH}_3 \\   \\ -\text{C}-\text{CH}_2- \\   \\ \text{CH}_3 \end{array}$ ), $1.67$ (s, 2H, -C $1.23$ (s, 3H,  -CH <sub>3</sub> ), $6.83$ - $7.30$ (4 aromatic protons)
$\begin{array}{c} \text{O} \\    \\ \text{R}-\text{C}-\text{O}-\text{H} \end{array}$ (3)	$0.74$ (s, 9H, $\begin{array}{c} \text{CH}_3 \\   \\ -\text{C}-\text{CH}_3 \\   \\ \text{CH}_3 \end{array}$ ), $1.35$ (s, 6H, $\begin{array}{c} \text{CH}_3 \\   \\ -\text{C}-\text{CH}_2- \\   \\ \text{CH}_3 \end{array}$ ), $1.85$ (s, 2H, - $7.30$ - $7.95$ (4 aromatic protons), $12.5$ (s, 1H, $\begin{array}{c} \text{O} \\    \\ -\text{C}-\text{OH} \end{array}$ )
$\begin{array}{c} \text{O} \\    \\ \text{R}-\text{C}-\text{Cl} \end{array}$ (4)	$0.73$ (s, 9H, $\begin{array}{c} \text{CH}_3 \\   \\ -\text{C}-\text{CH}_3 \\   \\ \text{CH}_3 \end{array}$ ), $1.34$ (s, 6H, $\begin{array}{c} \text{CH}_3 \\   \\ -\text{C}-\text{CH}_2- \\   \\ \text{CH}_3 \end{array}$ ), $1.83$ (s, 2H, - $7.35$ - $8.10$ (4 aromatic protons)

Table 2.1 (Continued).  $^1\text{H}$  NMR spectral assignments of 5 and 7

$\begin{array}{c} \text{O} \\ \parallel \\ \text{R}-\text{C}-\text{NCH}_2-\text{CH}_2-\text{OH} \\   \\ \text{H} \end{array} \quad (5)$	$0.71 \text{ (s, 9H, } \begin{array}{c} \text{CH}_3 \\   \\ -\text{C}-\text{CH}_3 \\   \\ \text{CH}_3 \end{array}), 1.32 \text{ (s, 6H, } \begin{array}{c} \text{CH}_3 \\   \\ -\text{C}-\text{CH}_2- \\   \\ \text{CH}_3 \end{array}), 1.81 \text{ (s, 2H, -}$ $3.10 \text{ (s, 1H, -OH), } 3.40\text{--}3.93 \text{ (m, 4H, -N-CH}_2\text{-CH}_2\text{-O-),}$ $6.95 \text{ (br, 1H, } \begin{array}{c} \text{O} \\ \parallel \\ -\text{C}-\text{N-} \\   \\ \text{H} \end{array}), 7.30\text{--}7.92 \text{ (4 aromatic protons)}$
$\begin{array}{c} \text{R}-\text{C}=\text{N}-\text{CH}_2 \\   \\ \text{O}-\text{CH}_2 \end{array} \quad (7)$	$0.71 \text{ (s, 9H, } \begin{array}{c} \text{CH}_3 \\   \\ -\text{C}-\text{CH}_3 \\   \\ \text{CH}_3 \end{array}), 1.32 \text{ (s, 6H, } \begin{array}{c} \text{CH}_3 \\   \\ -\text{C}-\text{CH}_2- \\   \\ \text{CH}_3 \end{array}), 1.82 \text{ (s, 2H, -}$ $4.12 \text{ (t, 2H, } \begin{array}{c} \text{CH}_2 \\   \\ \text{C}=\text{N}-\text{CH}_2 \\   \\ \text{O}-\text{CH}_2 \end{array}), 4.50 \text{ (t, 2H, } \begin{array}{c} \text{CH}_2 \\   \\ \text{C}=\text{N}-\text{CH}_2 \\   \\ \text{O}-\text{CH}_2 \end{array}),$ $7.35\text{--}7.95 \text{ (4 aromatic protons)}$



Experiment to test the purity of 7: Before we polymerized 7 we carried out the following experiment to show that it was free of electrophilic impurities. A small quantity (.2 g) of pure 7 (greater than 99.5% by HPLC) was loaded into a polymerization ampoule and attached via an o-ring joint to a high vacuum system. The system was then evacuated to  $9 \times 10^{-5}$  torr and the ampoule sealed with a flame torch.

The sealed tube was then transferred to a preheated 130°C oil bath and left for 20 h. The colorless, transparent melt turned light yellow by the end of the experiment. The ampoule was then removed and cracked open. A white solid crystallized quickly upon standing at room temperature. This was dissolved in  $\text{CDCl}_3$  and taken to the  $^1\text{H}$  NMR spectrometer. The resulting spectrum was identical to the one of pure 7 shown in Figure 2.10. A blow-up of the region between  $\delta$  3.0 and 8.5 ppm revealed no trace of oxazolinium ring protons at  $\delta$  4.2 – 5.3 ppm ( $\text{A}_2\text{B}_2$ , 4H). Also, no polymer backbone protons appeared at  $\delta$  3.5 ppm proving that no polymerization occurred. These results therefore show that monomer 7 was free from electrophilic impurities. Therefore we proceeded with polymerization of 7.

Kinetics of  $\text{O}_{20}$  homopolymerization:  $\text{O}_{20}$  homopolymer was synthesized in the following manner: 0.0839 g (0.3863 mmol)  $\text{CH}_3\text{ONs}$  was loaded in a polymerization vessel equipped with magnetic stirrer. Also, 2.00 g (7.72 mmol) of 7 was placed in the first unit of the apparatus of Figure 2.1. The two vessels were attached to the high vacuum line and evacuated overnight to  $8 \times 10^{-5}$  torr with some stirring of the solids to help remove trapped air. A graduated syringe of suitable volume, fitted with a 12-in #18-stainless-steel needle, previously cleaned with several acetone rinses, was then removed from the 90°C oven. While the syringe and needle were cooling, the vacuum stopcock on the rack was closed and the stopcock to the nitrogen opened. The system was thus purged to a positive pressure of nitrogen, which had previously been passed through a long powdery  $\text{P}_2\text{O}_5$ -column. The o-DCB reservoir stopcock was then

opened; the long syringe-needle was pushed through the stub's septum and 5 mL of distilled o-DCB was removed. The liquid was then delivered near the bottom of the polymerization vessel, by passing the needle through the side-arm septum and down the vertical tube. The mass of transferred liquid was found by difference by weighing the syringe before and after delivery. A mechanical stirrer was used to dissolve the solids in the reaction vessel at room temperature, and the clear solution was quickly immersed in a preheated oil-bath on a hot plate/stirrer and stirred for the desired time to make homopolymer (O). The vacuum system was then purged with nitrogen and added via a long-needle syringe to the vessel of 7 through the rubber septum under positive pressure. 10 mL o-DCB was syringed into the MeONs flask and stirred to dissolve the solid. 7 was dissolved by a heat gun and the transparent colorless solution was retrieved with a fresh syringe and transferred to the polymerization flask. The calculated initiator concentration is then calculated to be 0.0227 M with an estimated total volume of 17.0 mL. The colorless solution was then quickly immersed in a 120°C oil-bath and stirred to polymerize 7. Aliquots of 0.8 mL were syringed after 0.37, 0.70, 1.13, 2.00, 2.78, 4.33 and 6.67 hours. Stirring was stopped after 24 hours. The aliquots were diluted with tetrahydrofuran (THF) and analyzed by GPC-RI. The polymer, monomer and solvent peaks were kept on scale by changing the attenuation of the RI recorder at chosen times (we were unable to scale all the peaks with the UV detector). Then the polymer and monomer areas were photocopied, cut, and weighed. The relative areas of monomer and polymer after scaling to the pertinent attenuation were used to calculate the monomer

conversions.

Bulk homopolymerization of 7: 0.050 g ( $2.30 \times 10^{-4}$  mol)  $\text{CH}_3\text{ONs}$  was loaded in a 50-mL volumetric flask and the flask filled with filtered acetonitrile to the mark. One mL ( $4.60 \times 10^{-6}$  mol) was transferred via a 1-mL pipet from the stock solution that resulted after the initiator dissolved, and placed in a cylindrical flask with an o-ring-joint neck, as shown in unit 3 of the apparatus in Figure 2.1. The flask was then connected to the vacuum line and the acetonitrile was removed under vacuo. The flask was then removed, 6.00 g of 7 ( $2.32 \times 10^{-2}$  mole) was placed in the tube for a 5,000:1  $[\text{M}]/[\text{I}]$  ratio, and a constriction made in the flask's neck using flame. The flask was then evacuated to  $4 \times 10^{-5}$  torr and the constriction sealed by heating with the torch. The tube was then placed in a  $140\text{-}^\circ\text{C}$  ethylene glycol bath and left to polymerize. A transparent light-yellow liquid resulted after melt that became viscous (like honey) within 6 h. The color gradually turned to a darker yellow and after ca. 24 h the material was a solid mass. The flask was then removed from the bath and opened. The transparent yellow solid did not crack upon cooling to room temperature indicating a high molecular weight material. The polymer was then fractionated according to the following procedure. 6 g of the homopolymer was dissolved in toluene and poured into an extraction thimble. A heat gun evaporated the solvent from the sides of the thimble leaving some shiny fibers of presumably the low molecular weight fraction, that appeared birefringent under an optical microscope. The thimble was then placed in a Soxhlet extractor which was



connected to a 250-mL round-bottomed flask containing 150 mL of isooctane and a condenser. The isooctane was then refluxed for 22 h and a small quantity of low-molecular weight oligomers was extracted into the flask, leaving the bulk of the polymer intact. A yellowish gummy solid precipitated from the isooctane upon cooling to room temperature. The solvent was then evaporated; a brown liquid was obtained after drying in a vacuum oven at 120°C and 0.25 torr, 0.67 g (11.2%). The yellow polymer remaining in the extraction thimble, insoluble in isooctane, was dissolved in boiling toluene, collected, and the toluene removed to give 3.8 g (63.3% of 7) of a yellow solid. Homopolymer (O) was soluble in THF, o-DCB, toluene and high-boiling hydrocarbon solvents like xylenes. It was not soluble in CH<sub>2</sub>Cl<sub>2</sub>, CHCl<sub>3</sub>, CH<sub>3</sub>CN, or acetone. Attempts to precipitate into stirring MeOH or hexanes resulted in gum formation.

Characterization: Sixteen different molecular weight polystyrene standards of narrow MWD were used to calibrate the columns and the peak elution volumes normalized to that of o-DCB internal standard. The elution volumes were then plotted versus logM. A calibration equation resulted from fitting the elution volume to a 5th degree polynomial using the MW as dependent variable.

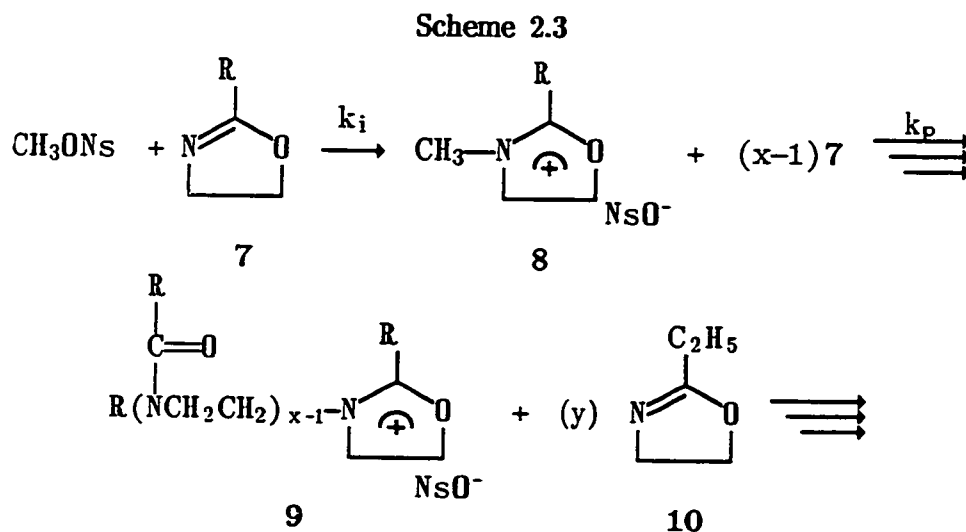
Viscosity measurements were taken using a 50-mL Ubbelohde viscometer immersed in a thermostatted 30°C (±.1°C) water bath. Run times of pure filtered solvent were taken, then the instrument dried. The experiment was repeated with 2, 1.333, 1.0, .8 and .666 g/dL solutions of the high mol wt fractionated homopolymer (O) in toluene. The specific

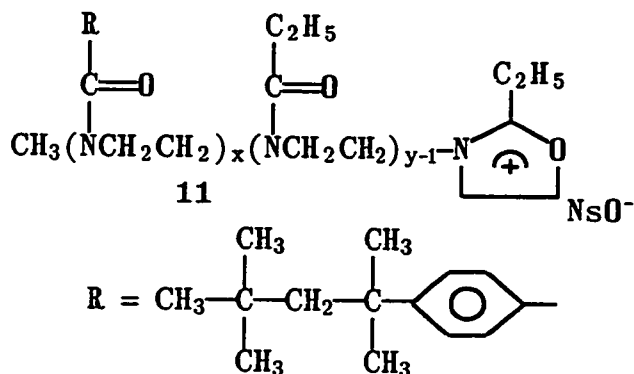
viscosity  $\eta_{sp}$  was calculated from  $(t-t_0)/t_0$ , where  $t$  and  $t_0$  are the run times of sample and solvent respectively. Relative viscosity  $\eta_r$  resulted from  $\eta_{sp}/c$ , where  $c$  is the concentration in g/dL. Also, inherent viscosity  $\eta_{inh}$  was calculated from  $(\ln(t/t_0))/c$ .  $\eta_r$  and  $\eta_{inh}$  were then plotted versus  $c$ , and the two plots best-fitted by linear regression so that both lines met at  $c=0$ . This point was used as the intrinsic viscosity  $[\eta]$ .

Differential scanning calorimetry (DSC) thermograms were obtained from a computerized Perkin Elmer DSC-7 instrument. Typical DSC runs were done at 20°C/min. Optical microscopy observations were done using a Jena microscope, connected to a Mettler FP-82 hot stage.

### Block Copolymerization Using 7 and 2-Ethyl-2-oxazoline 10 as Monomers

Synthesis: A series of diblock polymers was synthesized according to the route depicted in Scheme 2.3.





The diblock copolymers of the series were made in a similar way. Thus we will describe the synthesis of only one polymer and refer to this for the others. In this example, 2 g of **7** ( $7.72 \times 10^{-3}$  mol) and 0.1398 g MeONs ( $6.44 \times 10^{-4}$  mol) were loaded in a polymerization vessel, shown in Figure 2.3, then evacuated overnight to  $5 \times 10^{-5}$  torr). The system was then flushed with nitrogen and 5 mL distilled *o*-DCB was syringed into the flask. The solids were dissolved by stirring, and a 135–140°C oil-bath was quickly raised to cover the flask. GPC analysis of a retrieved aliquot after 65 min verified full reaction of monomer; no unreacted monomer was detected. The solution of **9** was then cooled to 110–115°C and 2.31 g ( $2.33 \times 10^{-2}$  mol) of distilled ethyl-2-oxazoline **10** was injected into the flask. After sixty more minutes of stirring the flask was removed from the rack and the solution pipetted into 200 mL of vigorously stirring hexanes. The resulting precipitated white powder of **11** was collected by suction-filtering, and redissolved in 10 mL  $\text{CHCl}_3$ . The polymer was reprecipitated into hexanes, and the fine powder dried overnight in a vacuum oven at 55°C. The ratio of  $[\eta]/[I]$  is equal to 12 and that of  $[\eta]/[I]$  is 36, thus the assigned formula for the block polymer is  $\text{O}_{12}\text{E}_{36}$ .

Further Purification: 0.7 g of precipitated O<sub>12</sub>E<sub>36</sub> was dissolved in about 10 mL ethanol, and 20% solution of KOH in EtOH was added until the pH reached 13–14. The solution was stirred for a short while with mild heating; a cloudy precipitate formed, then 30% aq. HCl was added to lower the pH to 3–4 in order to neutralize excess base. The cloudy precipitate was removed by filtration and the polymer solution rotovaporated to remove ethanol and ethanol/water azeotropes. To the resultant slurry was added 10 mL CHCl<sub>3</sub> to extract the polymer. The cloudy solution was filtered to remove salts, then slowly pipetted into 200 mL stirring hexanes. The precipitated O<sub>12</sub>E<sub>36</sub> was collected and dried in a vacuum oven.

### c) Results

#### Monomer Synthesis

##### p-t-Octyltoluene, 2

2 was synthesized from alkylation of benzene by modifying a method given in the literature<sup>7</sup>. 2,4,4-trimethyl-1-pentene 1 was first reacted with a large excess of toluene in the presence of AlCl<sub>3</sub> catalyst to produce 2. From many trials we found the reaction temperature 25<sup>0</sup>C for an optimum yield of 43.8%. The moderate yield is due to the formation of side products upon direct octylation of toluene. Conditions were optimized to minimize on one hand rearrangement of 2 in the presence of the acid catalyst to give low-boiling p-t-butyltoluene, and on the other polyalkylation, affording high-boiling di-p-t-octyltoluene and other polymer contaminants.

##### p-t-Octylbenzoic acid, 3

3 was made by a relatively low-yield oxidation step from 2, the difficulty being in separating 3 from the slurry of swollen MnO<sub>2</sub>, resulting from reduction of the large excess of KMnO<sub>4</sub>. The reason for the difficulty is probably that 3 emulsifies between the aqueous and organic phase due to the nature of the nonpolar t-octylphenyl and polar carboxyl group. To separate 3 from the swollen MnO<sub>2</sub> we reduced the latter to a water-soluble Mn<sup>2+</sup> salt using hydrazine, a powerful reducing agent. Other methods of separation, for example centrifugation and extraction of the organic phase

by  $\text{CHCl}_3$ , failed to give pure **3** in reasonably good yield. An alternate method to prepare **3** was attempted using oxidation of **2** with  $\text{O}_2$  in glacial acetic acid, catalyzed by cobalt acetate bromide<sup>10</sup>; however, the yield of **3** was only 9%. The mixture was a green oil indicating the presence of aldehydes that result from incomplete oxidation.

#### 2-p-t-Octylphenyl-2-oxazoline, 7

The synthetic route from **2** to **7** was based on a method, developed in our group<sup>5</sup> to prepare 2-substituted oxazolines. Although there are other methods to make oxazoline from acid in fewer steps, we chose this one in particular because of the following reasons: All four steps are conveniently done in one pot to give a high total yield, with no purification of the intermediates **4**, **5** and **6** required. A very high purity oxazoline monomer can be obtained with relatively simple purification. The oxazoline must be completely free of impurities because even traces of side products from the synthesis can lead to side reactions upon polymerization that broaden the MWD and lower the obtained  $\bar{X}_n$  below that calculated from the  $[\text{M}]/[\text{I}]$  feed ratio. For example, remaining hydroxyethylamide **5** in the polymerization mixture can terminate the oxazolinium ends. Other synthetic routes, e.g., treatment of the hydroxyethyl amide **5** with conc.  $\text{H}_2\text{SO}_4$  followed by neutralization by base, have been reported to introduce impurities into the oxazoline. These impurities are difficult to remove by purification and give color that ranges from yellow to deep orange to the final polymer.

Living Polymerization of 2-p-t-Octylphenyl-2-oxazoline, 7

In the following section we demonstrate the synthesis of homo- and diblock polymers using 7 and 2-ethyl-2-oxazoline as monomers (see Scheme 2.3).

1. Kinetics of 7 homopolymerization

In order to polymerize 7 properly, and produce a well-defined 8 containing a living oxazolinium-end, it is necessary to first study the kinetics of the polymerization. This experiment accomplishes two goals:

a) To prove that we obtain a narrow-MWD living polymer by homopolymerization of 7, and that monomer disappears by first-order kinetics as predicted from the proposed polymerization mechanism.

b) To calculate  $k_p$ , the rate constant of monomer propagation.  $k_p$  is then used to calculate the required time for complete monomer consumption, at the desired initiator concentration and temperature. 10 is added to the reaction mixture at the calculated time; further polymerization onto the living end of 9 subsequently gives block polymer 11, which has the desired composition  $O_xE_y$ .  $k_p$  reflects the polymerizability of the produced oxazolinium cation 8. We consider  $k_p$  to be the same for different non-nucleophilic counterions.

We chose methyl nosylate as the initiator for the following reasons. Previous work in our group and other laboratories has demonstrated that narrow MWD polymers are synthesized with a number of 2-substituted oxazolines using strong-acid ester initiators. For these  $k_i$ , the initiation

rate constant, is higher than  $k_p$ ; hence the polydispersity is described by the Poisson function. High  $k_i$  values indicate fast alkylation due to the non-nucleophilic nature of the nosylate leaving-group. Methyl tosylate, nosylate and triflate are in a group of strong-acid esters. They are classified in terms of their decreasing nucleophilicity as  $\text{TsO}^- > \text{NsO}^- > \text{TfO}^-$ . Methyl triflate should give the fastest alkylation because it has the least nucleophilic anion of the three. However, we chose methyl nosylate as the most convenient because it is very stable on storage, while methyl triflate can decompose upon standing and must be used as soon as prepared.

*o*-Dichlorobenzene was used as a polymerization solvent for the largest part of this thesis. It is a non-nucleophilic, relatively nonpolar solvent ( $\epsilon = 9.8$ ), in which both methyl nosylate and the polymers are soluble. Moreover, the high boiling temperature (170°C) of *o*-DCB permits carrying out polymerizations in a wide temperature-range.  $k_p$  is enhanced by increasing the temperature. Thus, by using *o*-DCB one can achieve a high conversion of monomer in a shorter time period at an elevated temperature than at the reflux temperature of a lower-boiling point solvent (e. g. in acetonitrile, bp 82°C).

To measure  $k_p$ , we polymerized **7**, using methyl nosylate in *o*-DCB at 120°C to make a homopolymer with an  $[\text{M}]/[\text{I}]$  ratio of 20 ( $\text{O}_{20}$ ). A low initiator concentration ( $[\text{I}]$  0.0227 M) permitted a long-enough time period to follow the disappearance of **7** and concurrent appearance of polymer (see Figure 2.12). The sum of the monomer and polymer areas is equal to that of the initial monomer area  $[\text{M}]_0$ . Thus the conversion of monomer can be



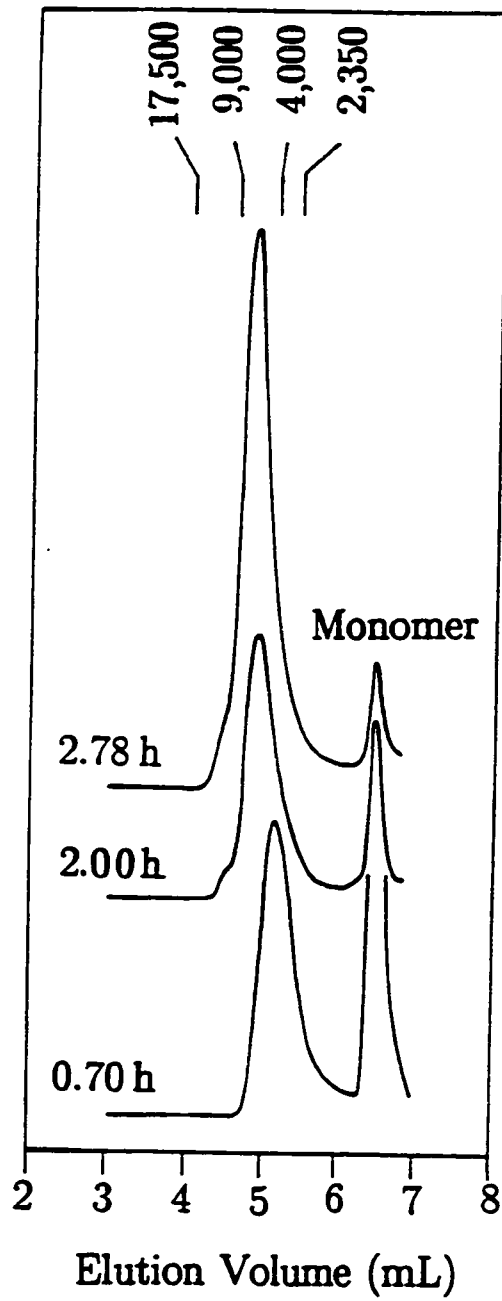


Figure 2.12. GPC profiles at different reaction times of 2-p-t-octylphenyl-2-oxazoline polymerization using an  $[M]/[I]$  of 20.

followed as the ratio of the area of unreacted monomer to the sum of areas of monomer plus polymer, that is  $[M]/[M]_0$ .  $k_p$  is averaged over the initial stage of reaction (governed by  $k_i$  to make 8) and the later stages of more monomer addition on 8. The rate of monomer consumption is given as follows<sup>12</sup>:

$$R_p = -d[M]/dt = k_p[P^*][M] \quad (1)$$

where  $[P^*]$  is the concentration of the propagating oxazolinium species. For fast initiation  $[P^*]$  is equal to  $[I]$ , hence integration of (1) yields:

$$-\ln[M]/[M]_0 = k_p[I]\Delta t \quad (2)$$

By dividing the left part of (2) by  $[I]$  and plotting against  $\Delta t$  we can thus obtain  $k_p$ . Table 2.2 shows the experimental values of  $[M]/[M]_0$  and results from the above calculations.

Table 2.2. First-Order Calculations of the Polymerization of 7 at 120°C in o-DCB Using an M/I ratio of 20 of 0.0227 mol/L MeONs

$\Delta T \times 10^{-3}$ (s)	M/M <sub>0</sub>	$-\ln(M/M_0)$	$-\ln(M/M_0)/I$ (1/mol)
0	1	0	0
1.32	0.895	0.111	4.89
2.52	0.565	0.564	24.84
2.52	0.562	0.576	25.39
7.20	0.199	1.614	71.10
10.02	0.101	2.293	101.0

Figure 2.13 shows the plot of  $-\ln([M]/[M]_0)$  versus  $\Delta t$ . A straight line is obtained proving the first-order kinetics mechanism.  $k_p$  is 0.0100 L/(mol.s) from the slope of the straight line.

## 2. High Molecular Weight (O)

7 was polymerized in bulk using a 5,000:1  $[M]/[I]$  of methyl nosylate in order to characterize high molecular weight poly(N-p-t-octylbenzoylethyleneimine) (O). The GPC-UV (254 nm) profile of the fractionated high molecular weight (O) is shown in Figure 2.14. The MWD was calculated from the shown profile using a comparative method<sup>13</sup> relating peak width  $W$ , and polydispersity  $d$ :

$$(W_1)^2/\log d_1 = (W_2)^2/\log d_2 \quad (3)$$

where  $W_1$  and  $W_2$  are the peak widths of polystyrene standard and polymer (O) respectively, and  $d_1$  and  $d_2$  are the corresponding polydispersities. The peak width of (O) was compared to that of a polystyrene standard of molecular weight  $1.67 \times 10^5$  and polydispersity  $d_1$  1.04. The value thus calculated for  $d_2$  of (O) was 1.26 after substituting 0.43 mL for  $W_1$  and 1.04 mL for  $W_2$  into Equation (3) for the peak widths at half-height of polystyrene and (O) respectively. The molecular weight of (O) was estimated from a peak position calibration curve relating elution volume of narrow MWD polystyrene standards to the log of MW. The MW value found at the peak position was  $2.27 \times 10^5$ .

Viscosity measurements of (O) were done in toluene at  $30.0 \pm 0.1^\circ\text{C}$ . The intrinsic viscosity  $[\eta]$  is by definition<sup>14</sup> equal to:

$$[\eta] = (\eta_{sp}/c)_{c=0} = [(\ln \eta_r)/c]_{c=0} \quad (4)$$

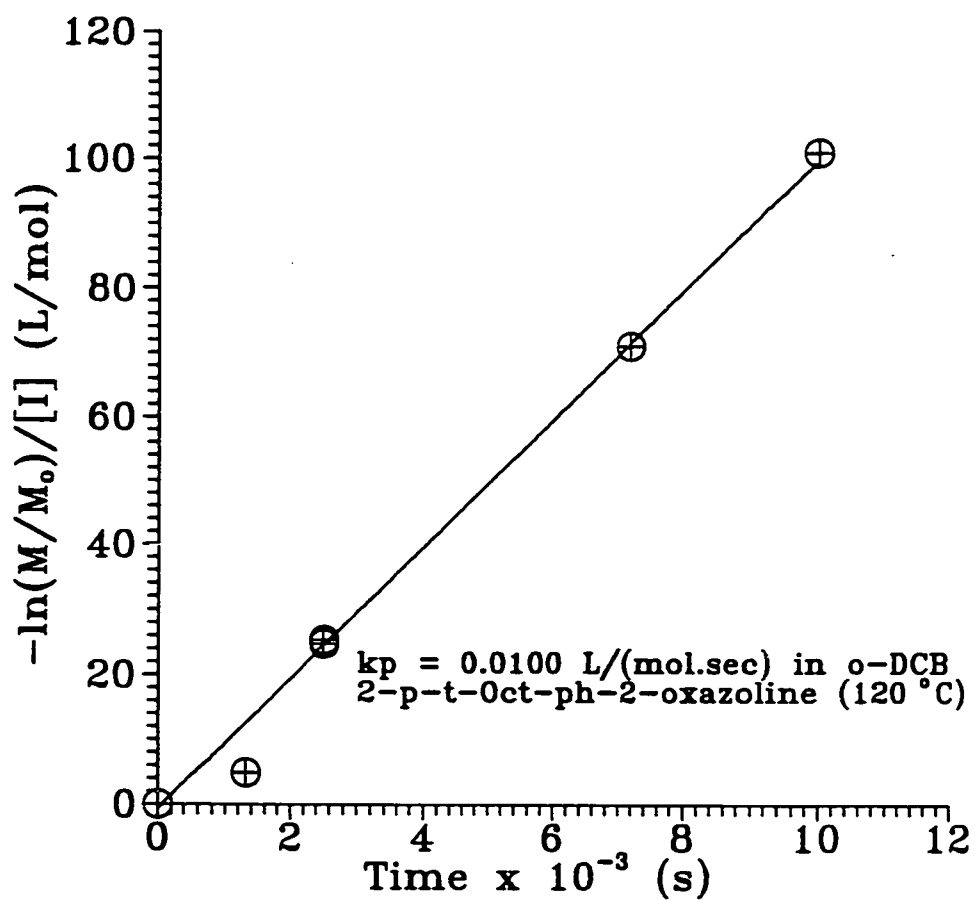


Figure 2.13. First-order plot to follow the time disappearance of 2-p-t-octylphenyl-2-oxazoline in o-DCB at 120°C using an  $[I]$  of 0.0227 mol/L.

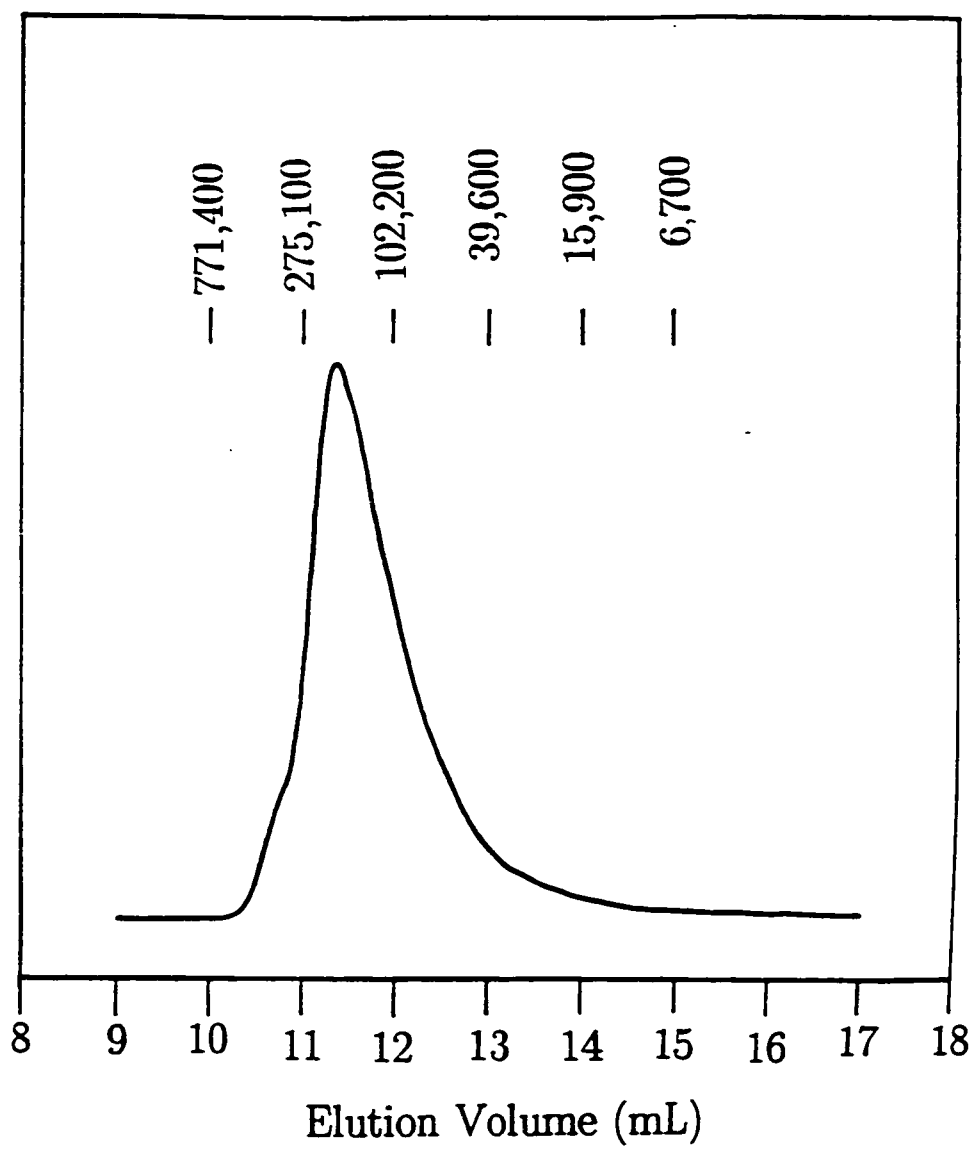


Figure 2.14. GPC-UV (254 nm) profile of high molecular weight (O) homopolymer after fractionation.

The left part of equation (4) is equal to the limiting relative viscosity  $\eta_r$  and the right to the limiting inherent viscosity  $\eta_{inh}$ . Figure 2.15 shows a plot of  $\eta_{sp}/c$  and  $\ln \eta_r$  at different concentrations.  $[\eta]$  was found 0.32 dL/g from extrapolation of the two straight lines to  $c=0$ .

A DSC thermogram of the fractionated high molecular weight (O) is shown in Figure 2.16. A glass transition temperature  $T_g$  is evident from the second order transition at about 108°C, with a calculated specific heat value ( $\Delta c_p$ ) of 0.30 J/(g°C). The absence of both an exotherm (crystallization) and endotherm (melting) peaks on the thermogram indicate that the polymer is amorphous. Also, annealing at 180°C for 75 h produced no crystallization. Optical microscopy confirmed the DSC analysis. Although the annealed polymer showed some birefringence under cross-polarized light, heating with a hot-stage under an optical microscope did not show any morphological changes below or above the  $T_g$ . Some flow was observed at about 220°C but it was not possible to clearly distinguish a melting point because the sample decomposed at the same temperature.

### 3. Block copolymerization

A series of  $O_xE_y$  copolymers was synthesized using monomers 7 and 10 to make the two blocks. Table 2.3 shows the ratios of the two blocks of the polymers in the  $O_xE_y$  series.

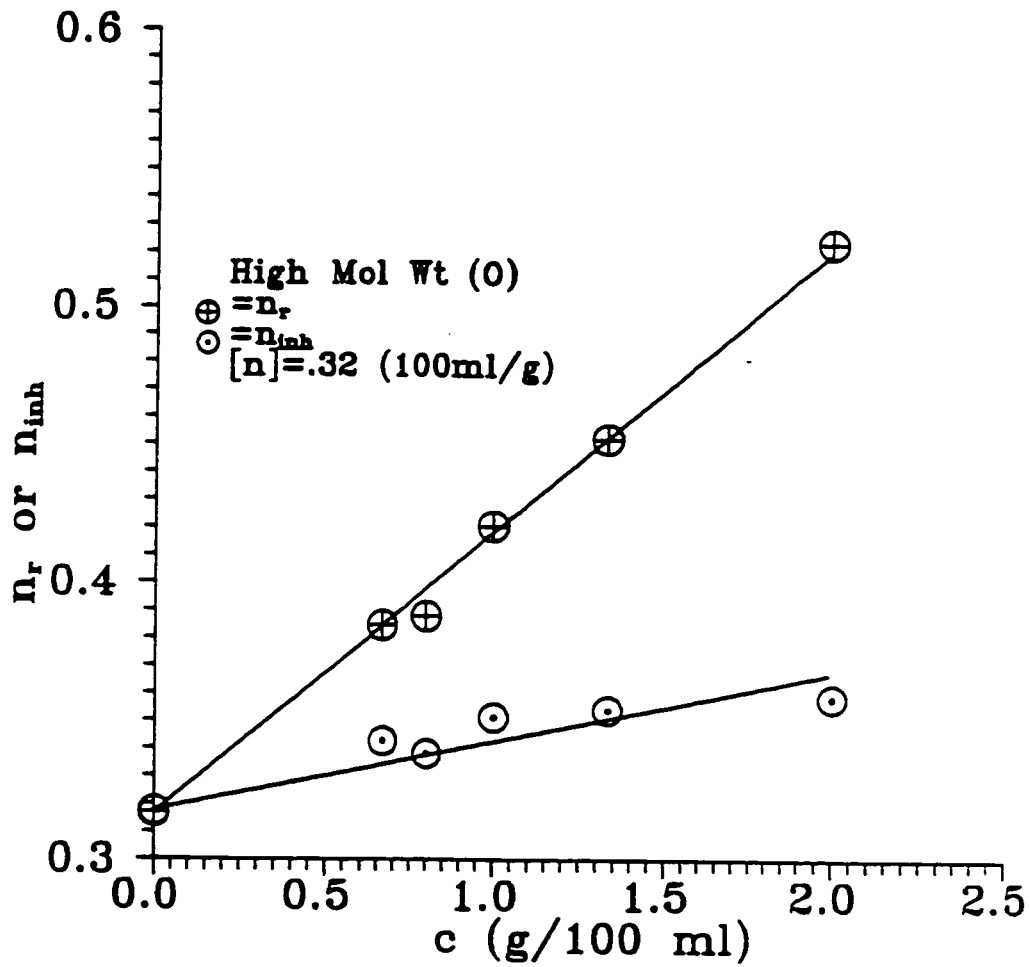


Figure 2.15.  $\eta_r$  and  $\eta_{inh}$  viscosities vs. concentration to calculate the intrinsic viscosity  $[\eta]$  of fractionated high molecular weight (O) in toluene.

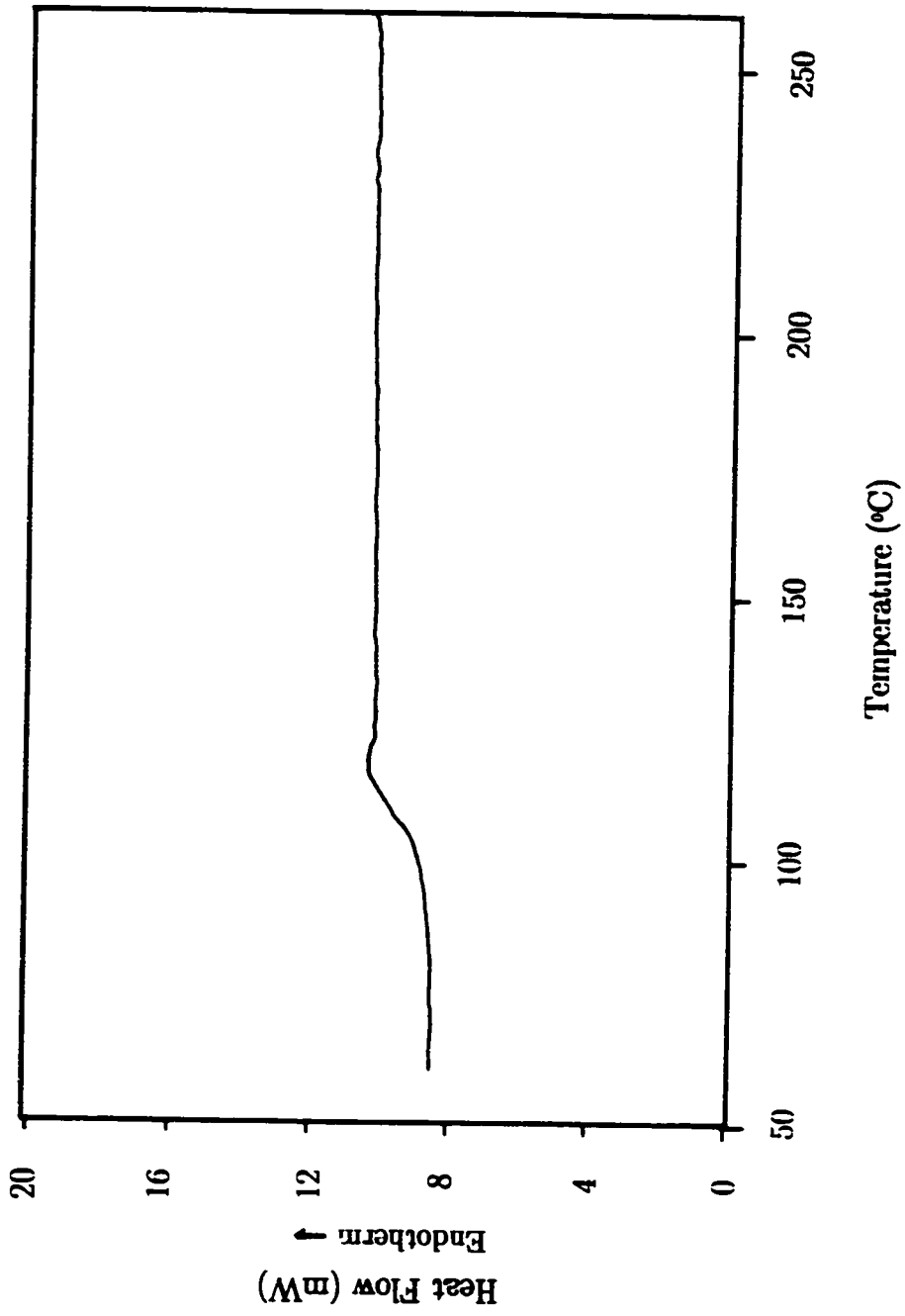


Figure 2.16. DSC thermogram of fractionated high molecular weight homopolymer (O).



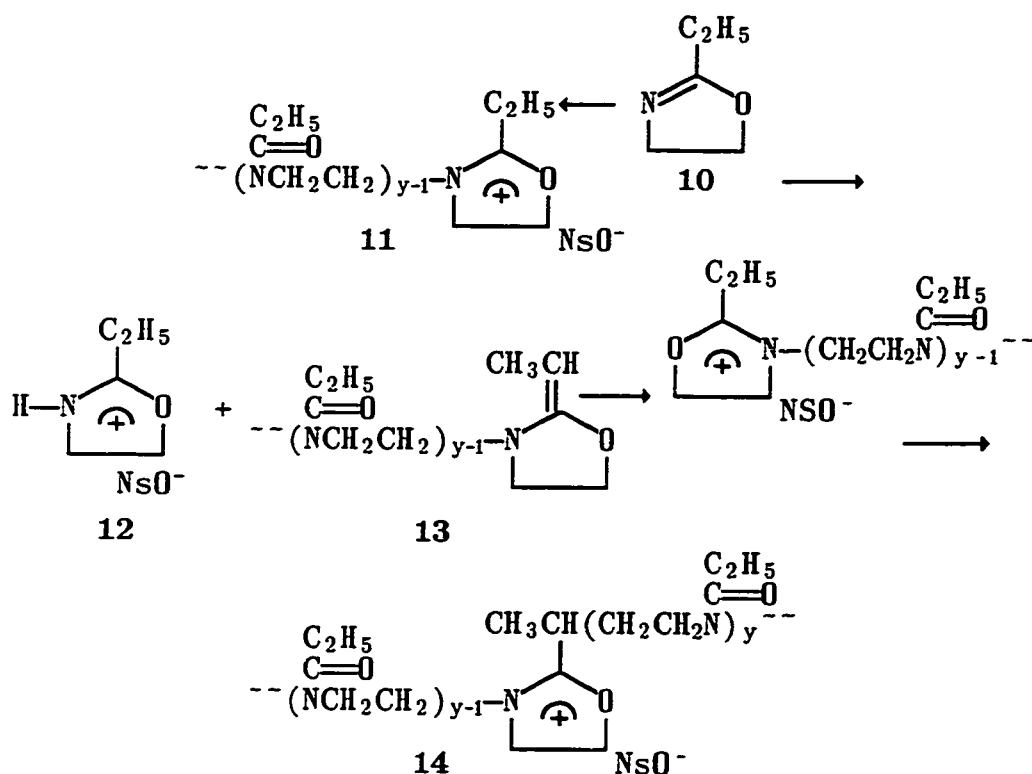
Table 2.3. Lengths of the O (x) and E (y) blocks of the O<sub>x</sub>E<sub>y</sub> series

#	O <sub>x</sub> E <sub>y</sub>
1	O <sub>7</sub> E <sub>17</sub>
2	O <sub>7</sub> E <sub>37</sub>
3	O <sub>10</sub> E <sub>40</sub>
4	O <sub>10</sub> E <sub>41</sub>
5	O <sub>12</sub> E <sub>36</sub>
6	O <sub>15</sub> E <sub>37</sub>
7	O <sub>15</sub> E <sub>50</sub>
8	O <sub>15</sub> E <sub>79</sub>

The first block was prepared by polymerizing **7** using methyl nosylate initiator in order to make homopolymer **9**, as shown in Scheme 2.3. **10** was then initiated by the living oxazolinium end of **9**, and polymerized to make block copolymer **11**. The number of repeats *x* in the first block was defined by the initial [M]/[I] ratio, while the length *y* of the second block was controlled by the weight ratio of **10** to **7**. **7** was reacted in *o*-DCB at temperatures ranging from 115–135°C and for time periods estimated from equation (2).  $\Delta t$  was calculated from  $k_p$  (0.0100 L/(mol.s) at 120°C) and [I] to give an estimated 99% conversion of **7**. To prove complete reaction of **7** we analyzed an aliquot of the reaction mixture and checked for

unreacted monomer. The temperature was lowered to 95–110°C before addition of 10 to prevent broadening of the MWD by possible chain termination and repolymerization reactions<sup>15</sup>. At high temperatures chain transfer to monomer might occur by reaction of 10 with an  $\alpha$ -hydrogen on the ethyl side-chain of 11 to produce 12. Repolymerization can also happen by reaction of the double bond on the enamine structure 13 with another chain to make 14, as shown in Scheme 2.4:

Scheme 2.4



Three diblock polymers, namely  $O_{10}E_{41}$ ,  $O_{12}E_{36}$  and  $O_{15}E_{50}$ , were analyzed by  $^1H$  NMR (see Figures 2.17–2.19) to compare the molar ratio of the two blocks to that by the experimental stoichiometry. Table 2.4 gives the peak assignments of the spectra in Figures 2.17–2.19.

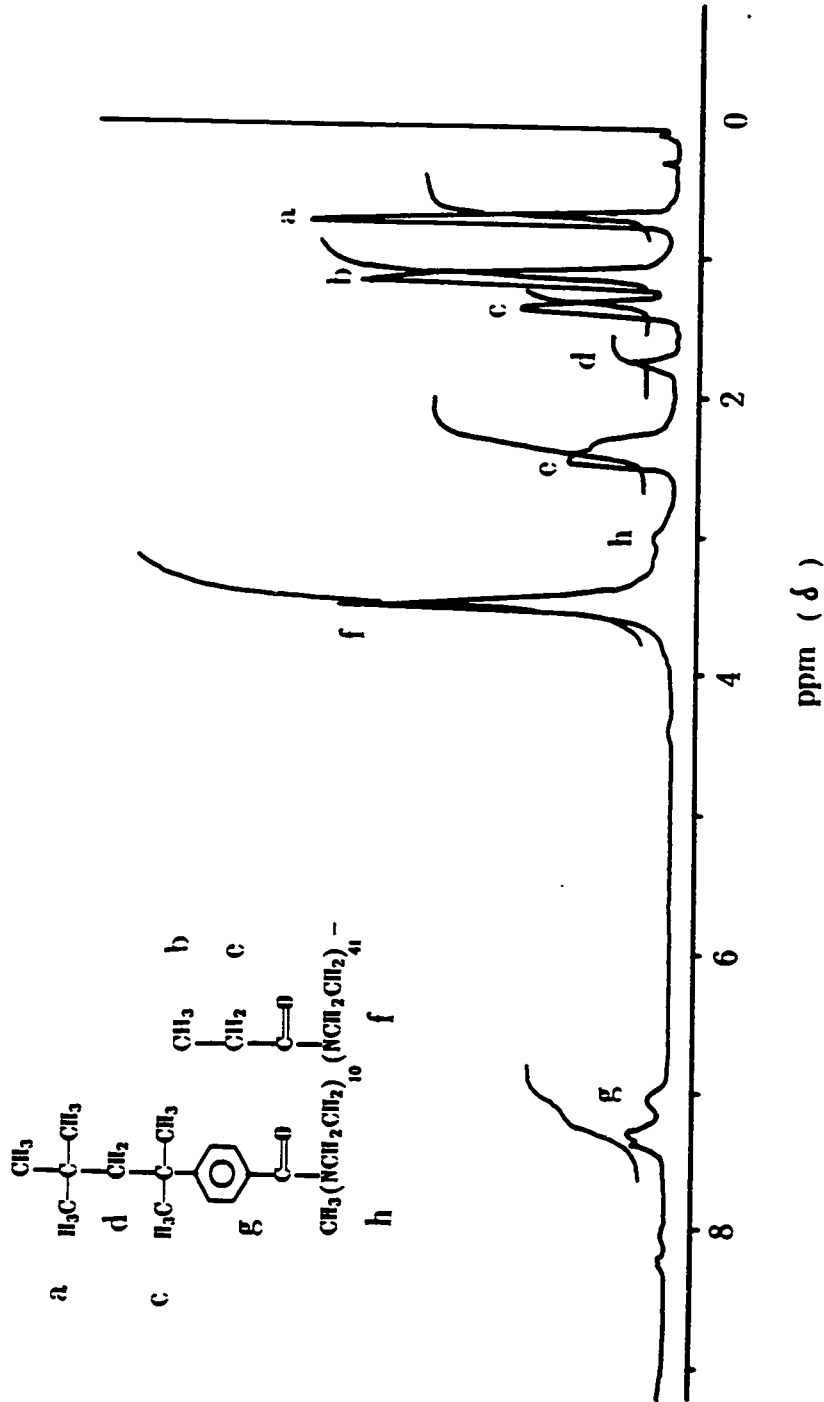


Figure 2.17. 200 MHz  $^1H$  NMR spectrum of  $O_{10}E_{41}$  as precipitated.

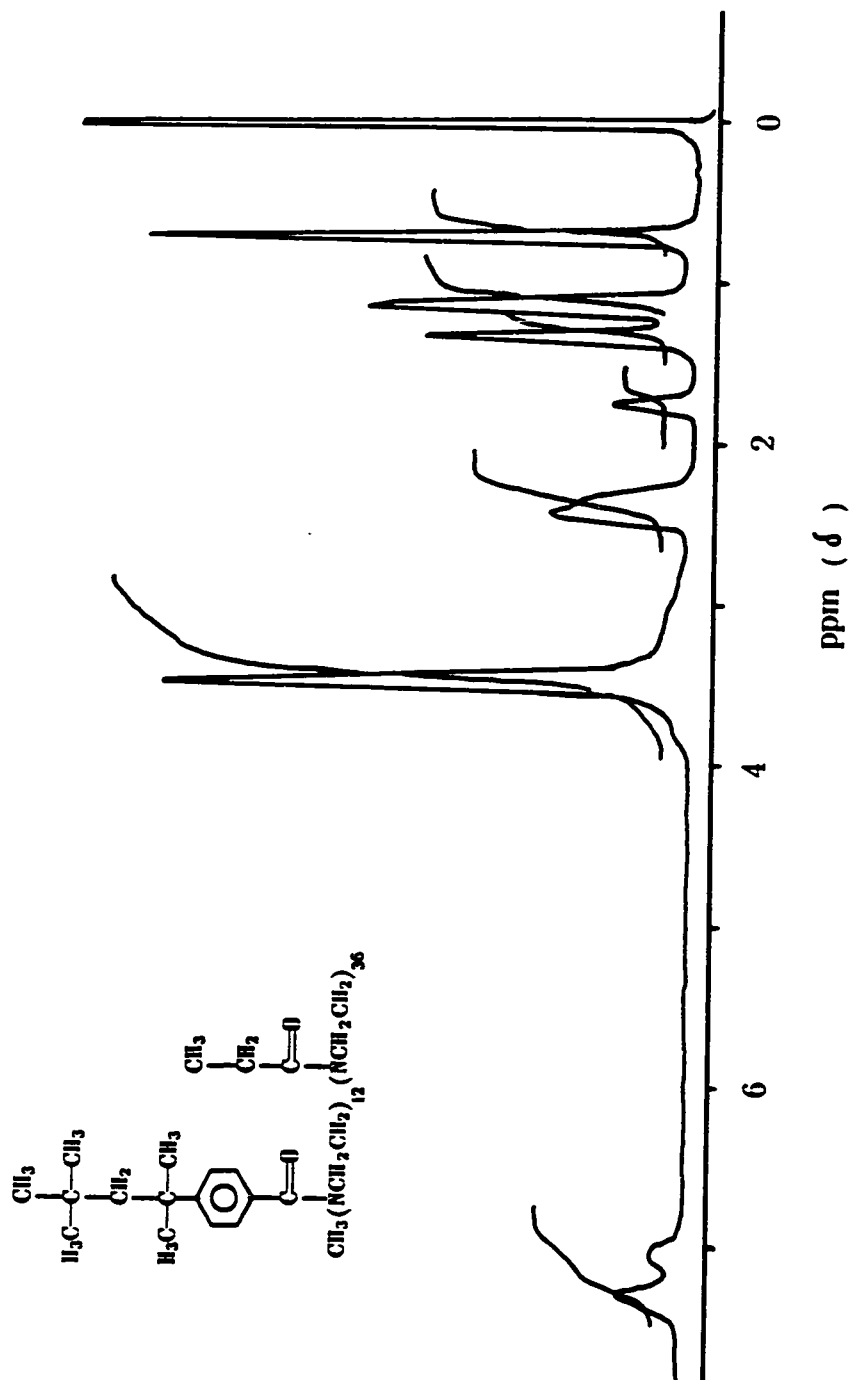


Figure 2.18. 200 MHz  $^1H$  NMR spectrum of  $O_{12}E_{36}$  as precipitated.

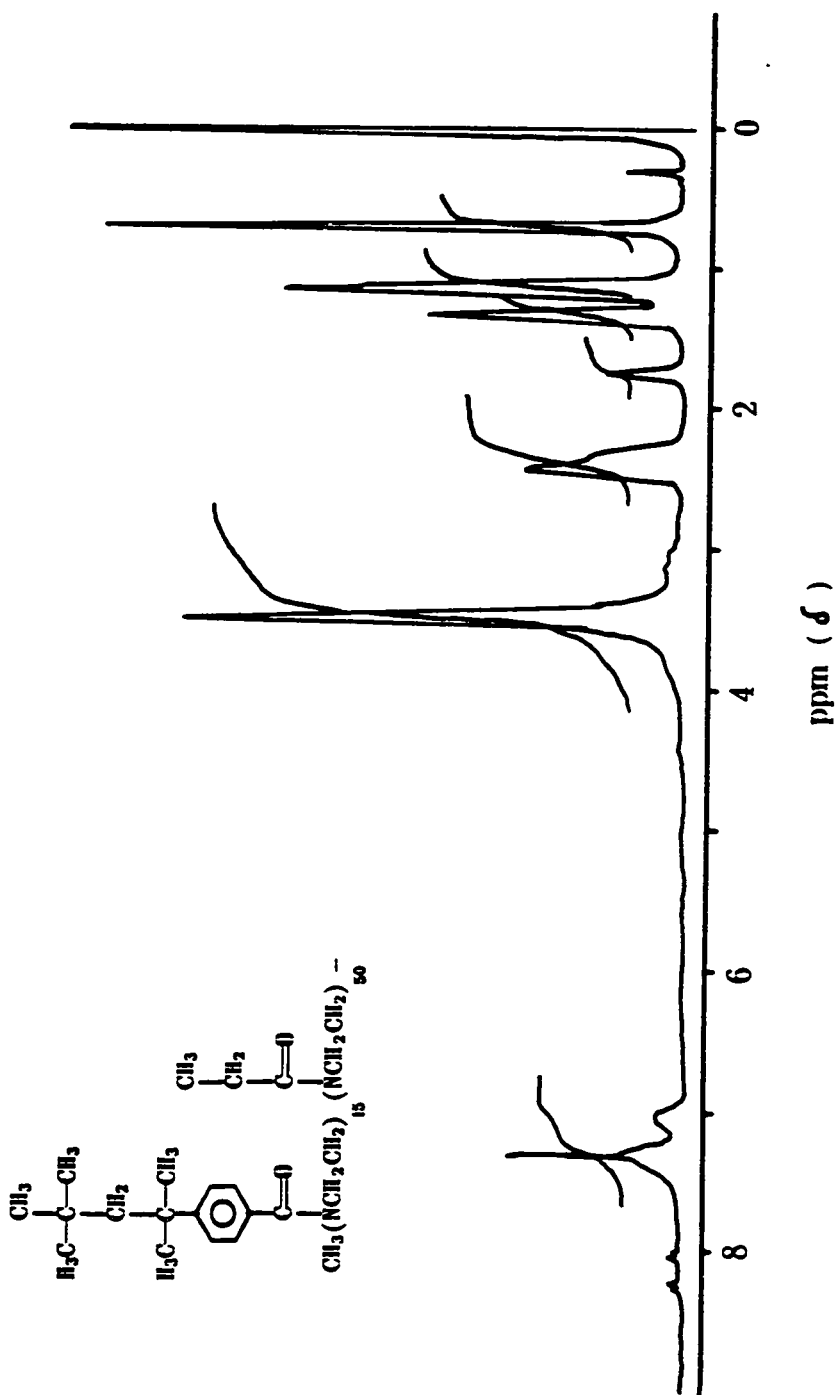
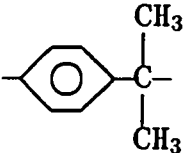
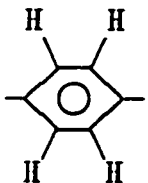


Figure 2.19. 200 MHz  $^1\text{H}$  NMR spectrum of O<sub>15</sub>E<sub>50</sub> as precipitated.

Table 2.4. Chemical shifts ( $\delta$ , ppm) and areas of the peaks of O<sub>10</sub>E<sub>41</sub>, O<sub>12</sub>E<sub>36</sub>, and O<sub>15</sub>E<sub>50</sub>, from the corresponding 200 MHz <sup>1</sup>H NMR spectra

No.	Group	Chemical Shift (ppm)	O <sub>10</sub> E <sub>41</sub>	O <sub>12</sub> E <sub>36</sub>	O <sub>15</sub> E <sub>50</sub>
a	$\begin{array}{c} \text{CH}_3 \\   \\ -\text{C}-\text{CH}_3 \\   \\ \text{CH}_3 \end{array}$	0.76	29.5	32.0	25.5
b	$\begin{array}{c} \text{O} \\    \\ -\text{C}-\text{CH}_2-\text{CH}_3 \end{array}$	1.16	43.5	32.0	27.7
c	$\begin{array}{c} \text{CH}_3 \\   \\ \text{---} \text{C} \text{---} \\   \\ \text{CH}_3 \end{array}$ 	1.38	15.5	20.0	16.5
d	$\begin{array}{c}   \quad   \\ -\text{C}-\text{CH}_2-\text{C}- \\   \quad   \end{array}$	1.75	5.2	5.2	5.5
e	$\begin{array}{c} \text{O} \\    \\ -\text{C}-\text{CH}_2- \end{array}$	2.20–2.55	28.6	26.0	22.0
f	$\begin{array}{c}   \\ -\text{N}-\text{CH}_2-\text{CH}_2- \end{array}$	3.52	67.5	74.0	54.0
g		7.05–7.48	15.0	16.0	11.5
h	$\begin{array}{c} \text{CH}_3-\text{N}- \\   \end{array}$	3.00	—	—	—

The molar ratios of the two blocks can be obtained from the integrated areas under the peaks of each block; for example, from the areas of a and b (divided by the corresponding H's in each group) we get the molar ratios given in Table 2.5.

Table 2.5. Block ratios for O<sub>10</sub>E<sub>41</sub>, O<sub>12</sub>E<sub>36</sub>, and O<sub>15</sub>E<sub>50</sub> from the peak areas under a and b of Table 2.3.

O/E Ratio	O <sub>10</sub> E <sub>41</sub>	O <sub>12</sub> E <sub>36</sub>	O <sub>15</sub> E <sub>50</sub>
From a/b	10.0:44.2	12.0:36.0	15.0:48.9
Theoretical	10:41	12:36	15:50

To check the diblock distributions in the series we used both the RI and UV detectors. The precipitated dried polymers exhibited peaks which were skewed towards high elution volumes and shapes that were dependent on the sample concentration. In some cases the profiles were multimodal, with long tailing at high elution volumes, extending well after the end of the columns, as shown in Figure 2.20 for O<sub>10</sub>E<sub>41</sub>. The skewed distributions and greater elution volumes observed with these polymers are characteristic of adsorption of polar substances on the column substrate, and have been reported previously by Cunliffe<sup>16</sup> and others<sup>17</sup>. The interaction might be between ionic groups like oxazolinium ends, or nosylate counterions, with

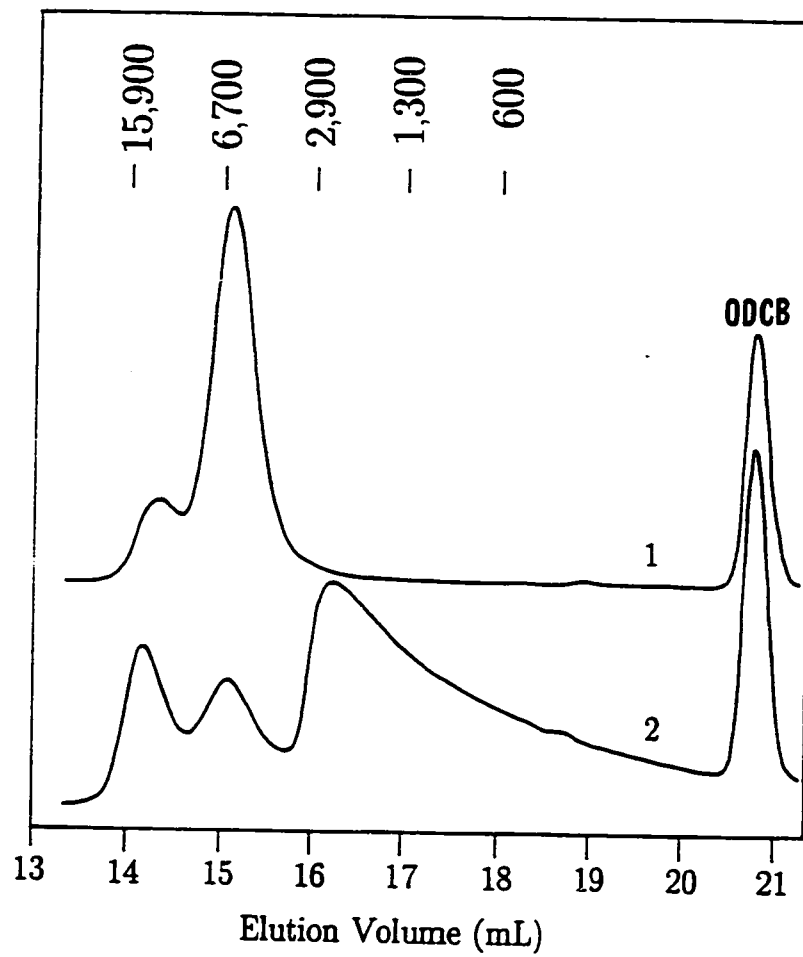
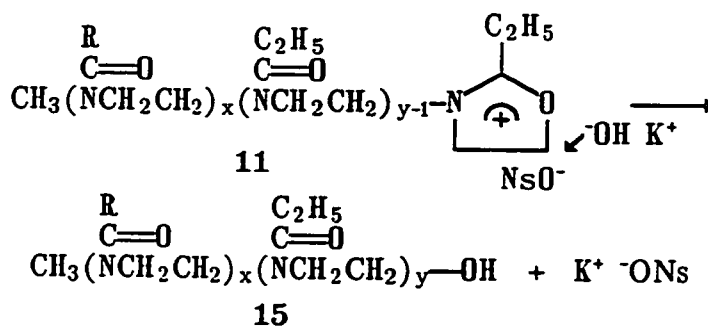


Figure 2.20. GPC column-effects of  $O_{10}E_{41}$  before (lower profile) and after (higher profile) purification.



polar sites on the column substrate. Cunliffe concluded that the leading polymer in the advancing front will become attached to the more strongly adsorbing sites and suffer greater delay in elution. Over the full length of the column this would remove the leading wing of the normal elution profile and increase the average time spent on the column. Molecules remaining adsorbed after the main polymer has passed will contribute to the extended tail of the profile. Higher concentrations of polymer cause even more severe trailing due to the abundance of ionic sites. An oxazolinium cation is considered to be hydrolyzed during precipitation of the polymer solution by ring-opening to generate structure 15, shown in Scheme 2.5. However, the GPC column-effects indicate that some of the oxazolinium cations and their associated nosylate counterions remain after precipitation into hexanes. We therefore decided to neutralize the polymers and remove the nosylate salts in order to eliminate the column effects. A pH 13-17 ethanolic potassium hydroxide solution was used to neutralize the polymer.

Scheme 2.5



Attack of  $\text{OH}^-$  can occur at C-5, as shown in Scheme 2.5, or at C-2<sup>18-19</sup>.

The second reaction is kinetically controlled; thus the product of that reaction rearranges to the thermodynamically favored 15. Nevertheless, the polymer was heated for a short while at pH 14 to ascertain that it rearranged to 15. The UV trace (254 nm), shown at the top of Figure 2.20, shows the purified polymer profile of  $O_{10}E_{41}$ , after removal of most of the salts. The peak is symmetrical, and has moved to a lower elution volume than before treatment with base. Trailing is barely noticeable on the high elution volume side, and the shape was the independent of sample concentration. It must be noted that attempts to treat a 2-phenyl-2-oxazolinium nosylate-ended polymer (see Appendix A) by dissolving the polymer in  $CHCl_3$  and shaking the solution with an aqueous potassium hydroxide solution did not eliminate the GPC salt-effects. However, this was accomplished when the base was in the same phase as the polymer. Therefore we used ethanol (or methanol) where both polymer and potassium hydroxide are readily soluble.

Figure 2.21 shows the GPC-UV (254 nm) profiles of the purified  $O_xE_y$  diblock polymers. Polystyrene MW's are shown at the top of the figure and should be used only to show the relative differences of MW between the  $O_xE_y$  polymer series. The profiles had the same shapes by the RI and UV detectors. Figure 2.22 of purified  $O_{10}E_{41}$  demonstrates the similarity of the traces by the two detectors. All profiles show very narrow molecular weight distributions. Most show a small peak on the low elution volume side of the peak, which is probably due to some repolymerization (Scheme 2.4) from chain transferred ethyl-oxazolinium ended chains.

Figure 2.23 shows a plot of the log of the molecular weights

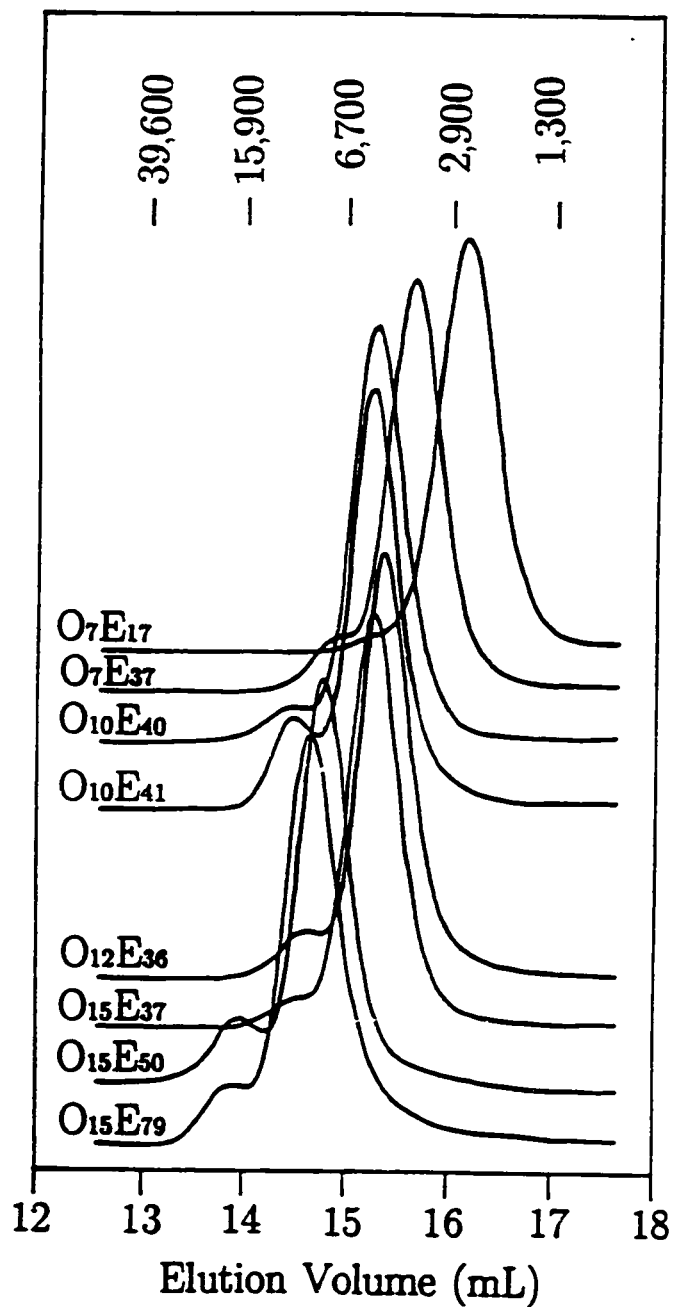


Figure 2.21. GPC-UV (254 nm) profiles of the purified diblock polymers in the series  $O_xE_y$ .

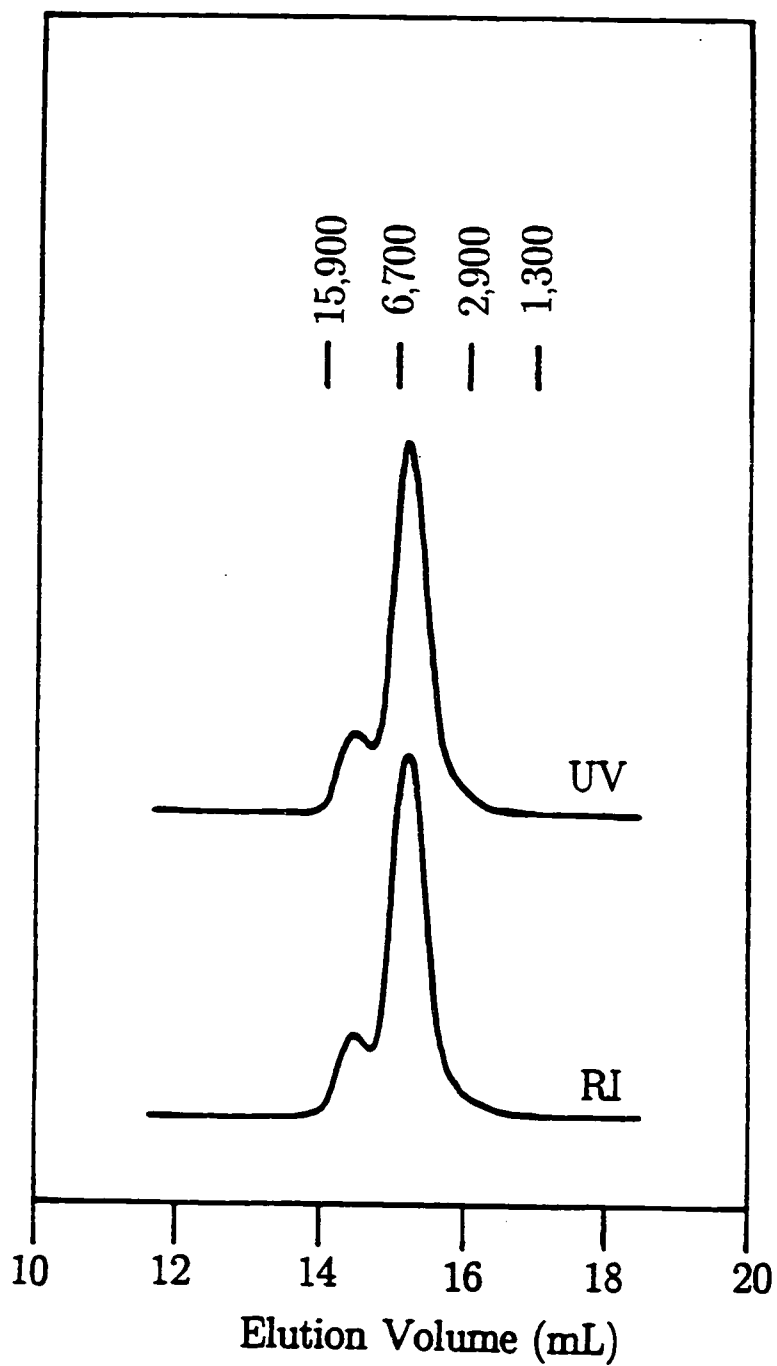


Figure 2.22. Comparison of GPC-RI and GPC-UV profiles of purified  $O_{10}E_{41}$ .

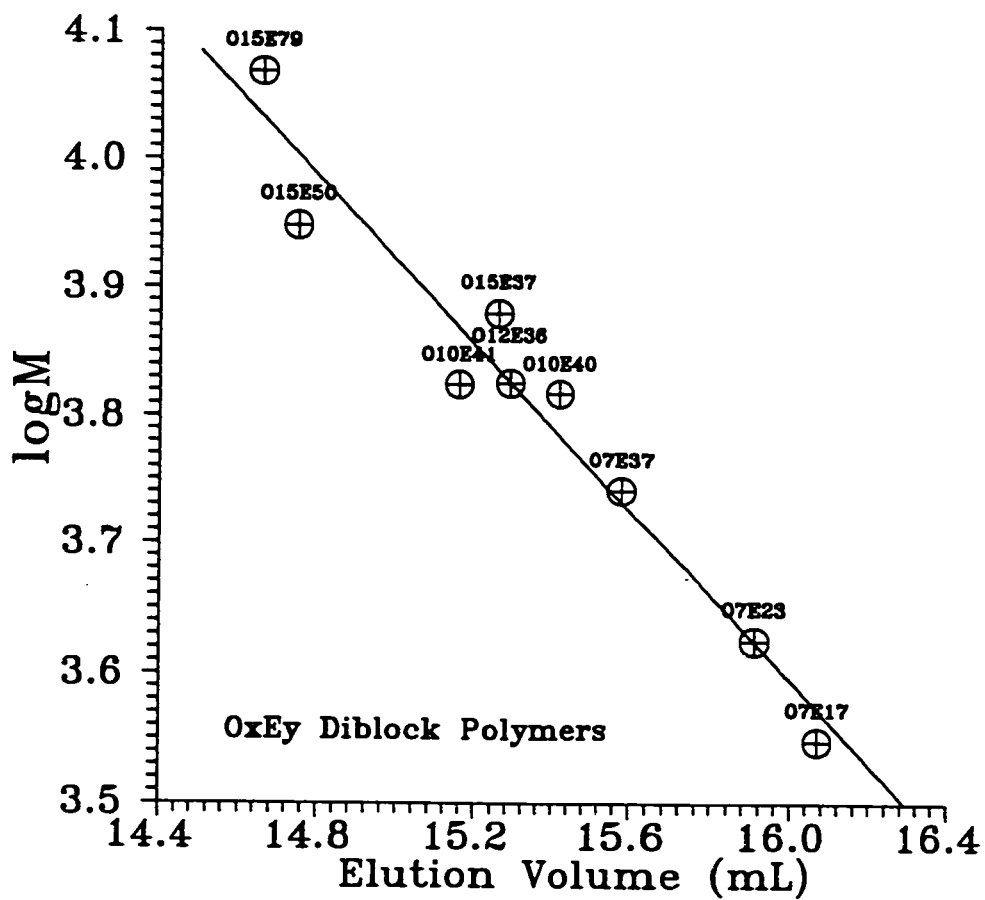


Figure 2.23. Plot of  $\log M$  from the  $[M]/[I]$  ratios of the blocks vs. elution volume for the  $O_xE_y$  polymer series.

calculated from the  $[M]/[I]$  ratios of each block of the  $O_xE_y$  series versus their elution volumes at the peak positions. Despite the differences in the structures of O and E blocks and the different block lengths, the points appear to fall on a straight line.

#### d) Summary

2-p-t-Octylphenyl-2-oxazoline **7** was made in six synthetic steps. The first two steps involved the synthesis of p-t-octylbenzoic acid **3** in 16.9% yield. In the next four steps **3** was converted into **7** in an overall yield of 86.5%.

Polymerization kinetics showed that the propagation rate constant of 2-p-t-octylphenyl-2-oxazoline at 120°C in o-DCB using methyl nosylate initiator was 0.0100 L/(mol.s). This rate constant was used to estimate the required reaction times for 99% conversion of **7** before addition and polymerization of 2-ethyl-2-oxazoline to make  $O_xE_y$  block copolymers.

A high molecular weight (O) homopolymer resulted after bulk reaction of **7** using a high  $[M]/[I]$  ratio of methyl nosylate. Fractionated (O) was amorphous and its glass transition temperature was 108°C. Bulk annealing did not induce crystallization. The molecular weight by GPC was found 227,000 using a polystyrene peak position calibration curve. The intrinsic viscosity  $[\eta]$  was 0.32 dL/g at 30.0°C in toluene.

A series of narrow molecular weight distribution block copolymers was made using (O) and (E) blocks. The mol ratio from  $^1\text{H}$  NMR spectral analysis of the two blocks was the same within experimental error to the

experimental  $[M]/[I]$  ratios. GPC column-effects due to the presence of salts were eliminated by treating the polymers with a pH 13–14 ethanolic potassium hydroxide solution.

### References

1. Zisman, W. A. In *Relation to the Equilibrium Contact Angle to Liquid and Solid Constitution*; Gould, R. F., Ed.; Advances in Chemistry 43; American Chemical Society: Washington, DC, 1964; p 20.
2. Litt, M. H.; Matsuda, T. In *Advances in Chemistry*; Platzner, N., Ed.; American Chemical Society: Washington, D. C., 1975; ACS Series No. 142; p 320.
3. Litt, M. H.; Herz, J. J. *Colloid Int. Sci.* 1969, 31, 248.
4. Litt, M. H.; Chen, T. T.; Hsieh, B. R. *J. Polym. Sci., Part A, Polym. Chem.* 1986, 24, 3407.
5. Litt, M. H.; Hsieh, B. R.; Krieger, I. M.; Chen, T. T.; Lu, H. L. *J. Colloid Int. Sci.* 1987, 115, 312.
6. Gallant, R. W. *Physical Properties of Hydrocarbons*; Gulf: Houston, 1968.
7. Sanford, R. A.; Kovach, S. M.; Friedman, B. S. *Ind. Eng. Chem.* 1959, 51, 1455.
8. Kovach, S. M.; Friedman, B. S. *J. Am. Chem. Soc.* 1953, 75, 6326.
9. Nightingale, D.; James, J. R. *J. Am. Chem. Soc.* 1944, 66, 154.
10. Hay, A. S.; Blanchard, H. S. *Can. J. Chem.* 1965, 43, 1306.
11. Wiley, R. H.; Bennett, Jr., L. L. *Chem. Rev.* 1949, 44, 447.
12. Matsuda, T. *Polymerization Reactions of Nitrogen-Containing Heterocyclic Compounds*; Ph. D. thesis; Kyoto University, 1972; p 100.
13. Williams, T.; Udagawa, Y.; Keller, A.; Ward, I. M. *J. Polym. Sci., A-2* 1970, 8, 35.
14. Billmeyer, Jr., F. W. *Textbook of Polymer Science, 3rd ed.*; John Wiley and Sons: New York, 1984; p 208.
15. Litt, M. H.; Levy, A.; Herz, J. J. *Macromol. Sci. - Chem., A9* 1975, 703.

16. Cunliffe, A. V.; Hartley, D. B.; Kingston, S. B.; Richards, D. H.; Thompson, D. *Polymer* 1981, 22, 101.
17. Ambler, M. R. *J. Polym. Sci. (Polym. Lett.)* 1976, 14, 683.
18. Fry, E. M. *J. Org. Chem.* 1950, 15, 802.
19. Goldberg, A. A.; Kelly, W. *J. Chem. Soc.* 1948, 1919.



## Chapter 3

### Core-first Approach to Star-Block Oxazolines

1. *p*-*t*-Butylphenyl/Ethyl Oxazoline Triblock Polymers

### a) Introduction

Beginning with the present chapter we will address the question of the paths to obtain monodisperse star-block copolymers using 2-oxazoline ring-opening polymerization.

One way to make a star-block copolymer is to begin with an initiator containing  $z$  ( $z \geq 3$ ) electrophilic centers,  $I_z$ . With this method, each site initiates polymerization of a first monomer to make the first block; then the second monomer adds to the oxazolinium chain-ends to produce the desired star-block structure.

To obtain a well-defined star-block polymer it is necessary to meet two requirements: a) a non-nucleophilic solvent in which both monomer and polymer are soluble, and b) an initiator,  $I_z$ , which is:

1. Stable upon heating to the polymerization temperature.
2. Completely soluble in the initial mixture so that we have the desired  $[M]/[I]$  ratio.
3. Alkylates an oxazoline as fast as or faster than reaction of the latter with the oxazolinium salt.

The requirement for the solvent is met by *o*-DCB, in which most monomers and polymers are readily soluble. We decided to evaluate different electrophilic initiator cores in terms of their ability to produce well-defined structures in order to define the requirements for the initiator. The simplest block copolymer geometry to test different core initiators on is the triblock; that is a structure which contains a central block between two end-blocks. A triblock polymer results from the core-first method

when a two-ended electrophile first polymerizes one monomer, then the second monomer is added and polymerized on the living oxazolinium-ends of the first block. Work in our group<sup>1-2</sup> has shown that narrow MWD diblocks result when methyl nosylate, a one-ended initiator, polymerizes 2-p-t-butylphenyl-2-oxazoline to make block (B), then 2-ethyl-2-oxazoline is added and polymerized on the resulting living chain to produce block (E). This sequential monomer addition can be extended by the incorporation of another (B) block on the diblock living-end, hence resulting in a well-defined BEB triblock structure<sup>3-5</sup>. The triblock geometry therefore provides a good model for comparison between the polydispersities of triblocks made by one-ended initiation to those synthesized via the core-first, two-ended initiation method.

We chose alkyl dinosylate esters as suitable two-ended initiators. If the alkyl chain between the nosylate ends is long enough then each end will react independently of the other. Moreover, nosylate esters are stable upon standing and should react faster with oxazolines than tosylates. Alkyl ditosylate initiators were tested before on 2-substituted oxazolines and found to give broad molecular weight distribution polymers<sup>6</sup>. This is due to their slow alkylation of the oxazoline compared to its propagation. Two-ended alkyl triflates on the other hand initiate oxazolines rapidly and the resulting two-ended polymers are nearly monodisperse<sup>7</sup>. However, these initiators are less readily available than tosylates or nosylates, and tend to decompose upon standing.

In this section we describe the synthesis of triblocks of the type  $B_xE_yB_x$  where  $x$  and  $y$  denote the number of monomer repeat units in

blocks B and E respectively. These are prepared in two ways (see Figure 3.1): by the sequential one-ended initiator method, and by the core-first method using several two-ended nosylate esters. Triblock copolymers made by the two methods are studied by GPC to compare the molecular weight distributions. Triblocks made by one-ended initiation are named  $P_1$ , for example  $P_1(B_{10}E_{40}B_{10})$ . Triblocks made by two-ended alkyl nosylates are named  $P_{2x}$ , where  $x$  denotes the specific core between the nosylate ends. For example,  $P_{2b}(B_{10}E_{40}B_{10})$  is made by first polymerizing (EO) with a  $[M]/[I]$  ratio of 20 per nosylate end using as the initiator 1,6-hexamethylene dinosylate ( $I_{2b}$ ). A three-arm star polymer is made using a three-ended nosylate initiator ( $I_{3c}$ ). The resulting polymer is named  $P_{3c}$ .

#### b) Experimental Section

p-t-Butylbenzoic acid was purchased from Aldrich (99%) and used as received.  $SOCl_2$  was Aldrich Gold Label (99+%), ethanolamine was distilled before use. Neutral alumina (activity III) was prepared from neutral alumina (activity I) by addition of water. 2-Ethyl-2-oxazoline was distilled on the high vacuum line, as described in Chapter 2, from blue Na/benzophenone. GPC analysis was done on the instrument described in Chapter 2, which was equipped with an IBM SEC gel permeation chromatography column (500 Å) that had a molecular weight range from  $2 \times 10^2$  to  $2 \times 10^4$ . The peak elution volumes were related to molecular weight using a peak position calibration curve based on known MWD and

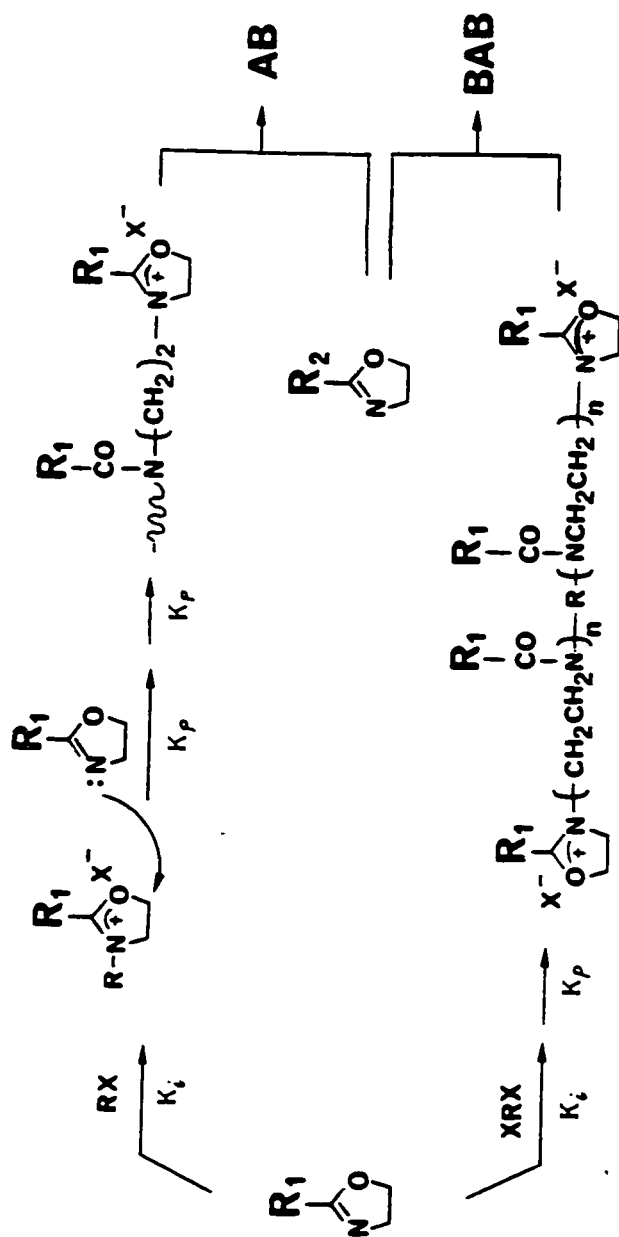


Figure 3.1. Synthetic paths towards a triblock structure. The top route shows one-ended initiation ( $R^1 = p$ -*t*-butylphenyl,  $R^2 = \text{ethyl}$ ) while the lower shows two-ended initiation ( $R^1 = \text{ethyl}$ ,  $R^2 = t$ -butylphenyl).

molecular weight polystyrene standards. THF was eluted through the column at 1 mL/min. The reported GPC profiles were taken using the refractive index detector.  $^1\text{H}$  NMR spectra were taken on a Varian XL-200 200 MHz Fourier Transform spectrometer.

The synthesis of 2-p-t-butylphenyl-2-oxazoline (TBO) was done according to a method developed in our group<sup>1</sup>. Thus, 250 g p-t-butylbenzoic acid (1.40 mol) and 300 mL (1.55 mol)  $\text{SOCl}_2$  was refluxed for 2 h. After cooling, the excess  $\text{SOCl}_2$  was evaporated off to give 252 g (1.28 mol) of the acid chloride. 100 g (0.508 mol) of this in 100 mL  $\text{CH}_2\text{Cl}_2$  was gradually added to 70 mL (1.15)  $\text{NH}_2\text{CH}_2\text{CH}_2\text{OH}$  in 400 mL with stirring (1:2.2 ratio). The mixture was stirred at room temperature for 2 h and the precipitate suction-filtered and washed with  $\text{CH}_2\text{Cl}_2$ . The filtrate was transferred into a 1 liter round-bottomed flask, cooled to  $0^\circ\text{C}$ , and 50 mL (0.32 mol) of  $\text{SOCl}_2$  was gradually added to the filtrate with stirring. The resulting mixture was refluxed for 2 h and concentrated in vacuo. 2.2 g  $\text{NaOH}$  ( $5.5 \times 10^{-2}$  mol) was added to 12 g ( $5.0 \times 10^{-2}$  mol) of the resulting chloroethylamide in 200 mL boiling 2-propanol. The mixture was refluxed for 30 min; then the solution was rotavaporated to remove the 2-propanol. The resulting white powder of oxazoline was then dissolved in toluene and quickly passing through a short alumina column. One liter of toluene was then also passed through the column, and the solutions collected and rotavaporated to remove the toluene. The yellowish powdery solid of TBO was then sublimed followed by recrystallization from hexane at room temperature to give 13.60 g ( $6.70 \times 10^{-2}$  mol) of shiny white crystals of TBO (mp after drying

78–79°C). The purity was found to be over 99% by  $^1\text{H}$  NMR and HPLC.

Cleaning: Polymerization glassware were cleaned as described in Chapter 2.

$P_1(\text{B}_{10}\text{E}_{40}\text{B}_{10})$ : All triblocks in the  $P_1(\text{B}_{10}\text{E}_y\text{B}_{10})$  series were made in the same way. We will therefore describe the procedure for only  $y = 40$ . 5 g ( $2.46 \times 10^{-2}$  mol) of TBO and 0.535 g ( $2.46 \times 10^{-3}$  mol) of  $\text{CH}_3\text{ONs}$  were placed in a polymerization reaction flask (see Figure 2.3, Chapter 2), which was connected to the high vacuum rack (Figure 2.1, Chapter 2) and evacuated until  $7 \times 10^{-5}$  torr. An additional 5 g ( $2.46 \times 10^{-2}$  mol) of TBO was placed in another vessel (unit 1 in Figure 2.1) which was simultaneously evacuated. The system was then purged with nitrogen; 15.0 and 5.0 mL of distilled *o*-DCB were next syringed into the reaction and secondary monomer flask respectively. After the solids were dissolved by stirring at room temperature, the polymerization flask was quickly immersed in a preheated 120°C oil-bath, and the clear yellowish solution stirred for 90 min. Then 9.56 g ( $9.66 \times 10^{-2}$  mol) of 2-ethyl-2-oxazoline (EO) was syringed into the polymer solution which was stirred for another 90 min. The TBO in the second flask was then dissolved in the *o*-DCB by heating and the colorless clear solution transferred to the polymerization vessel which was stirred for another 100 min at 120°C. The product  $P_1$  has average composition  $\text{B}_{10}\text{E}_{39.3}\text{B}_{10}$ , based on the relative amounts of monomer and initiator used in the reaction. Thus, the designation is  $P_1(\text{B}_{10}\text{E}_{39.3}\text{B}_{10})$ . GPC of the solution showed no trace of unreacted TBO. The light-yellow solution was precipitated into stirring hexanes, filtered and

the precipitate was dried in a vacuum oven until constant weight. A  $^1\text{H}$  NMR spectrum of the polymer is shown in Figure 3.2. Table 3.1 shows the peak assignments and integrated areas of the different groups.

**Table 3.1 Peak assignments and integrated areas from the  $^1\text{H}$  NMR spectrum of  $\text{P}_1(\text{B}_{10}\text{E}_{39.3}\text{B}_{10})$**

	Group	Chemical Shift (ppm)	Area	Area/H
a	$\begin{array}{c} \text{CH}_3 \\   \\ -\text{C}-\text{CH}_3 \\   \\ \text{CH}_3 \end{array}$	1.24	101	11.3
b	$\begin{array}{c} \text{H} \quad \text{H} \\ \diagdown \quad \diagup \\ \text{C}_6\text{H}_4 \\ \diagup \quad \diagdown \\ \text{H} \quad \text{H} \end{array}$	7.05–7.48	45	11.2
c	$\begin{array}{c}   \\ -\text{N}-\text{CH}_2-\text{CH}_2- \end{array}$	3.52	151	—
d	$\begin{array}{c} \text{O} \\    \\ -\text{C}-\text{CH}_2- \end{array}$	2.20–2.55	43	21.5
e	$\begin{array}{c} \text{O} \\    \\ -\text{C}-\text{CH}_2-\text{CH}_3 \end{array}$	1.16	61	20.3

When the area/H of from the groups in each block is averaged, we get 11.2/H for the B block and 20.9/H for the E block. Therefore the ratio of B/E is 0.536 or 20/37.3, compared to 20/39.3 from the



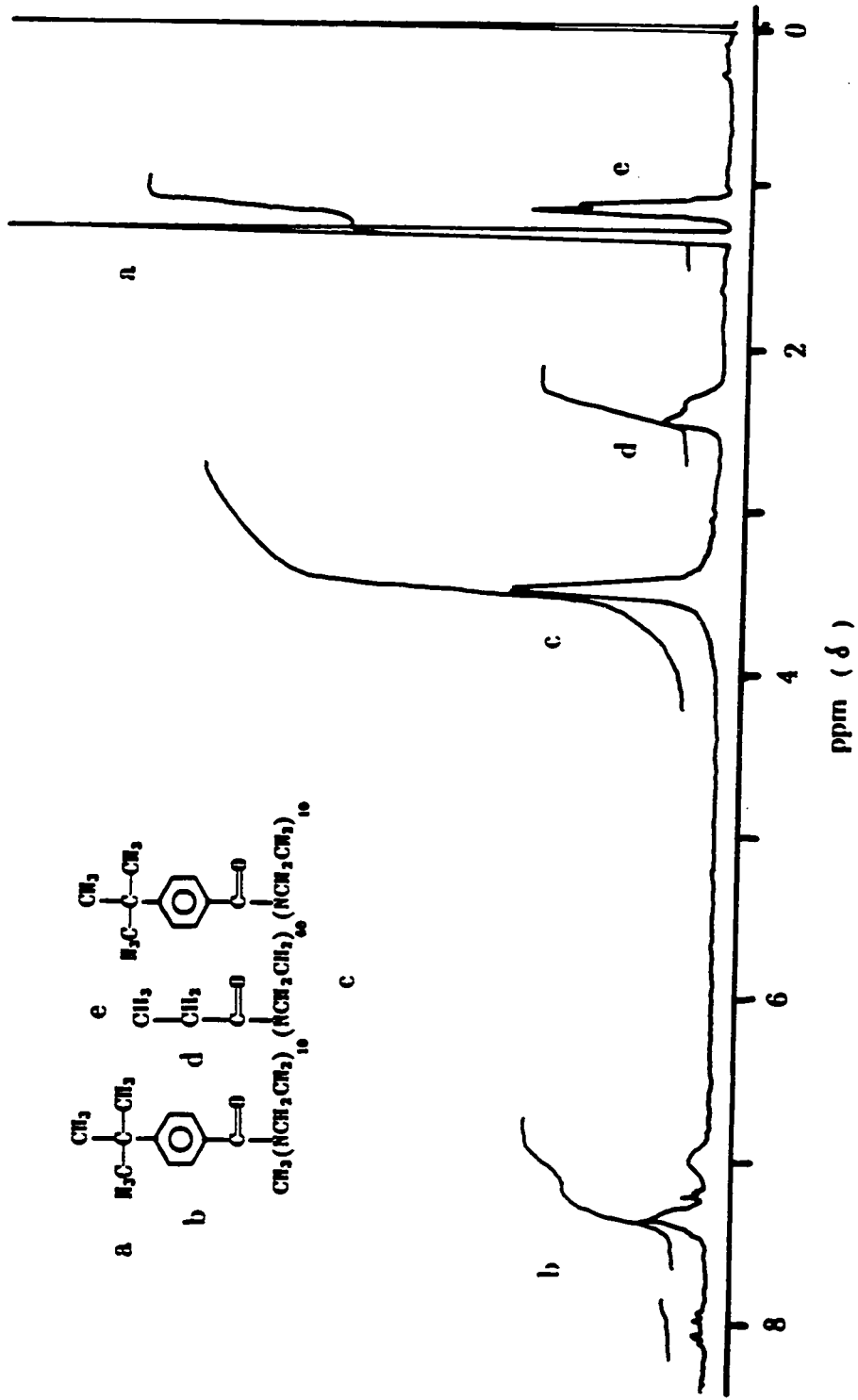


Figure 3.2. 200 MHz  $^1\text{H}$  NMR spectrum of  $\text{P}_1(\text{B}_{10}\text{E}_{40}\text{B}_{10})$ .

experimental molar ratio.

I<sub>2a</sub>, I<sub>2b</sub> and I<sub>2c</sub> and I<sub>3c</sub>: These initiators were synthesized by other members in our group. 1,3-Propylene dinosylate (I<sub>2a</sub>)<sup>8</sup>, 1,6-hexamethylene dinosylate (I<sub>2b</sub>)<sup>8</sup>, and 1,4-(NsO(CH<sub>2</sub>)<sub>6</sub>OCH<sub>2</sub>)<sub>2</sub>φ<sup>9</sup> (I<sub>2c</sub>) melted at 200–201, 171–172, and 104–105°C respectively. The structure of I<sub>3c</sub> was 1,3,5-(NsO(CH<sub>2</sub>)<sub>6</sub>OCH<sub>2</sub>)<sub>3</sub>φ with a mp at about room temperature. The purity of I<sub>3c</sub> was checked by <sup>1</sup>H NMR and HPLC and found to be greater than 95%.

P<sub>2a</sub>(B<sub>9.8</sub>E<sub>39.4</sub>B<sub>9.8</sub>) and P<sub>2b</sub>(B<sub>8.7</sub>E<sub>38.4</sub>B<sub>8.7</sub>): I<sub>2a</sub> (.2286 g, 5.123 x 10<sup>-4</sup> mol) and I<sub>2b</sub> (.2500 g, 5.123 x 10<sup>-4</sup> mol) were placed in polymerization flasks and attached to the high vacuum rack. TBO (4.00 g, 1.97 x 10<sup>-2</sup> mol) was loaded into a separate flask (unit 1 of Figure 2.1, Chapter 2). All three units were evacuated to 9 x 10<sup>-5</sup> torr. The system was then purged with positive pressure dry nitrogen and 8.0 and 12.0 mL distilled o-DCB were syringed in the TBO flask and each of the two reaction vessels respectively. The I<sub>a</sub> vessel was immersed in a 120–125°C oil-bath and a cloudy solution resulted. I<sub>b</sub> dissolved completely within 2–3 min of immersion in a 125–130°C oil-bath. TBO dissolved in o-DCB when the flask was heated with a heat gun. 2.00 (2.02 x 10<sup>-2</sup> mol) and 1.95 g (1.97 x 10<sup>-2</sup> mol) EO were then syringed into the solutions of I<sub>a</sub> and I<sub>b</sub> for [M]/[I] ratios of 39.4 and 38.4 respectively. I<sub>2a</sub> dissolved very quickly, and both clear yellowish solutions were stirred for 30 min. Aliquots of P<sub>2a</sub>(E<sub>39.4</sub>) and P<sub>2b</sub>(E<sub>38.4</sub>) were then taken and analyzed by GPC. 7.42 and

6.54 g of the TBO solution were then injected into the polymerization flasks. The formulas calculated, using 1.300 for d(o-DCB) at 20°C, were  $P_{2a}(B_{8.9}E_{39.4}B_{8.9})$  and  $P_{2b}(B_{8.7}E_{38.4}B_{8.7})$ . The clear solutions were stirred for another 60 min and precipitated by gradually adding the solution to stirring hexanes.

$P_{2c}(B_{9.8}E_{44}B_{9.8})$ : 0.5366 g ( $7.58 \times 10^{-4}$  mol) of  $I_{2c}$  and 3 g ( $1.48 \times 10^{-2}$  mol) of TBO were placed in a reaction and secondary monomer vessel respectively, and both evacuated to  $8 \times 10^{-5}$  torr. 14.0 and 3.0 mL o-DCB were then syringed into the reaction and TBO flasks. TBO was dissolved by heating the flask. The initiator was stirred in o-DCB at room temperature; most dissolved but some remained undissolved. 3.30 g ( $3.33 \times 10^{-2}$  mol) of EO was then injected into the stirred solution of  $I_{2c}$  ( $[M]/[I] = 44.0$ ) and the reaction vessel was immersed in a 120°C oil-bath. The solids dissolved completely at about 60°C during warm-up. After 90 min, an aliquot was analyzed by GPC, and the TBO solution was injected into the solution (calculated ratio  $P_{2c}(B_{9.8}E_{44}B_{9.8})$ ). After four additional hours of stirring at 120°C the solution was cooled and precipitated into 300 mL of vigorously stirring hexanes.

$P_{3c}(E_{39.1})_3$ :  $I_{3c}$  was removed from a refrigerator (4°C) and .2477 g ( $2.52 \times 10^{-4}$  mol) was quickly loaded into a reaction vessel. 3.00 g ( $2.04 \times 10^{-2}$  mol) of TBO was also placed in a separate monomer flask. Both units were evacuated overnight until  $10^{-4}$  torr, and the system was

purged with dry nitrogen. 15.0 and 5.0 mL *o*-DCB were injected into the reaction and monomer vessels respectively. 2.93 g ( $2.96 \times 10^{-2}$  mol) of EO was then syringed into the reaction vessel for an  $[M]/[I]$  ratio of 39.1 per active end, and the mixture was stirred at room temperature to dissolve all solids; a yellowish transparent solution resulted. The reaction flask was then immersed in a stirred oil-bath which was then gradually heated to 120°C. Aliquots of the homopolymer were taken at 45 and 90 min after EO injection. At that point the warmed TBO solution, was injected into the reaction vessel and stirred for another 4.5 h. We will report only on the GPC-RI profile of this E homopolymer because the block polymer's molecular size exceeded the upper limit of our column.

P<sub>1</sub>(E<sub>20.9</sub>): .5500 g CH<sub>3</sub>ONs ( $2.532 \times 10^{-3}$  mol) in a reaction vessel was evacuated overnight until  $7 \times 10^{-5}$  torr. The pump was then isolated from the vacuum rack and about 15 mL *o*-DCB was directly distilled under vacuum into the reaction flask from P<sub>2</sub>O<sub>5</sub>-dried solvent. The mixture was then stirred at room temperature to dissolve the initiator and 5.24 g ( $5.29 \times 10^{-2}$ ) of EO was distilled under vacuum into the polymerization flask from Na/benzophenone, as described in the end-to-end distillation section in Chapter 2. The exact weight of EO was found by weighing the Na/benzophenone unit before and after distillation. The system was then purged with nitrogen and the reaction flask immersed in a 95°C oil bath. P<sub>1</sub>(20.9) resulted after stirring the mixture for about an hour.

### c) Results

#### One-ended initiation

A series of  $P_1(B_xE_yB_x)$  triblock polymers was synthesized using methyl nosylate as initiator and sequential addition of TBO, EO, and once again TBO to make the three blocks. For reasons of comparison  $x$  was kept 10 while  $y$  varied from 27 to 62. Figure 3.3 shows the GPC profiles of the precipitated polymers. For comparison we have included the profile of  $P_1(B_{10}E_{22})$ , which was one of the narrow MWD diblock cooligomers made from a previous study in our laboratory<sup>2</sup>. The widths at half peak-height,  $(w)_{1/2}$  can be taken as a measure of the MWD breadth. A Polystyrene standard of MW 4000 and MWD 1.04 gave  $(w)_{1/2}$  0.3 mL. The profiles of the triblock polymers shown in Figure 3.3 have  $(w)_{1/2}$  of ranging from 0.3 – 0.35 mL, while the breadth of the diblock control is 0.30 mL. Therefore, when methyl nosylate is used as initiator the triblock polymers obtained by the step-by-step approach do not have higher polydispersities than those of diblocks. This is due to the strong alkylating nature of methyl nosylate which gives a high initiation rate constant,  $k_i$  compared to the propagation rate constant of TBO,  $k_p$ .

Another observation from Figure 3.3 is that as  $y$  increases a high molecular weight peak appears at the edge of the main peak. The intensity of this peak seems to be largest at  $y = 62$  and minimal at  $y = 27$ . The peak might be due to a small degree of chain transfer and repolymerization of EO. This phenomenon has been known to occur at high temperatures and  $[M]/[I]$  ratios for alkyl-2-oxazolines that possess an

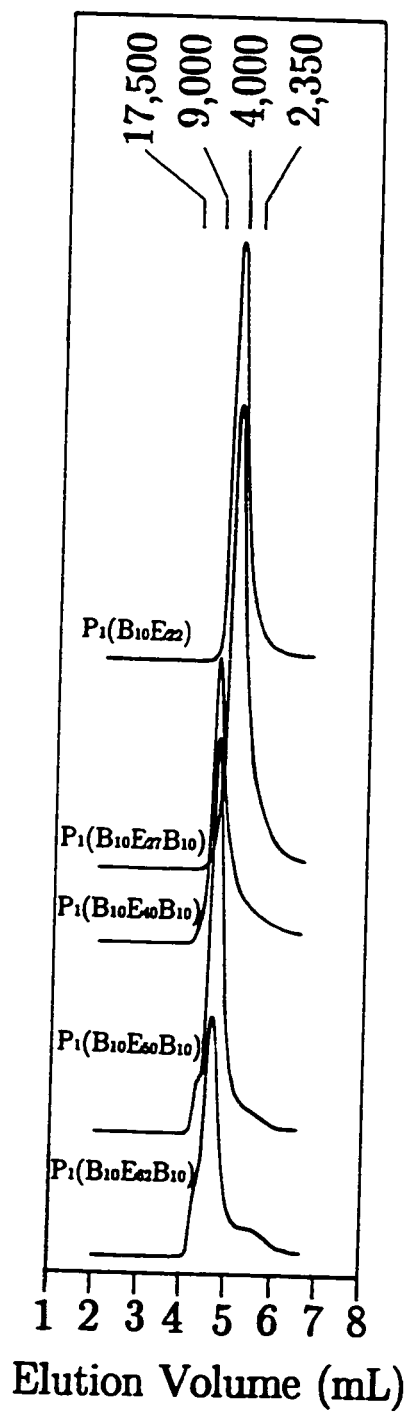
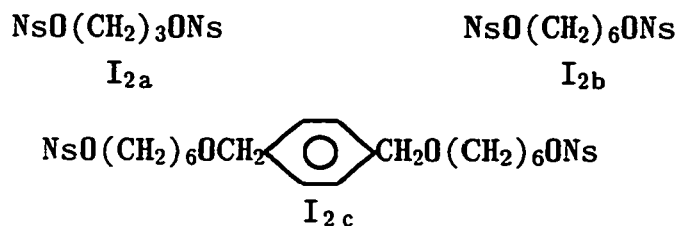


Figure 3.3. GPC-RI profiles of different E length  $P_1(B_{10}E_yB_{10})$  triblocks and one diblock.

$\alpha$ -hydrogen on the side chain (see Scheme 2.4, Chapter 2).

### Two-ended initiation

The polydispersities of obtained polymers using three two-ended alkyl nosylate initiators were compared. Their structures are shown below:



$\text{I}_{2a}$  and  $\text{I}_{2b}$  were high-melting and soluble in *o*-DCB only at temperatures above  $100^\circ\text{C}$ . We studied the structure  $\text{I}_{2c}$  because the ether groups lower the mp so that the dinosylate is readily soluble at room temperature. Also, benzyl nosylates should be better alkylating agents than alkyl nosylates. For reasons of comparison we maintained the ratio of B/E approximately the same. Thus, we chose the  $\text{P}_{2x}(\text{B}_{10}\text{E}_{40}\text{B}_{10})$  stoichiometry and compared the polymer profiles to that of  $\text{P}_1(\text{B}_{10}\text{E}_{40}\text{B}_{10})$ , run at about the same date in order to have the same column characteristics. Figure 3.4 shows the profiles made from the three initiators and that of  $\text{P}_1(\text{B}_{10}\text{E}_{40}\text{B}_{10})$ . The MWD's of the polymers in Figure 3.4 were calculated using a comparative method relating peak width  $W$ , and polydispersity  $d$ , as already described in Chapter 2:

$$(W_1)^2/\log d_1 = (W_2)^2/\log d_2$$

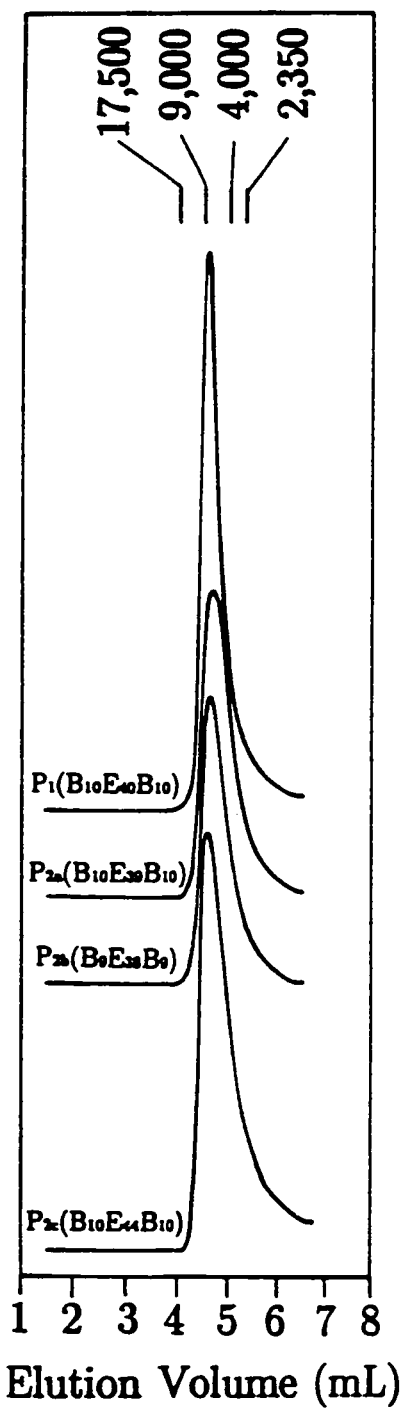


Figure 3.4. GPC-RI profiles of  $P_{2x}(B_{10}E_{40}B_{10})$  triblocks using different two-ended initiators.



where  $W_1$  and  $W_2$  are the peak widths of polystyrene standard and polymer respectively, and  $d_1$  and  $d_2$  are the corresponding polydispersities. The peak widths were compared to that of polystyrene standard of molecular weight 4,000 and polydispersity  $d_1$  1.04. Table 3.2 summarizes the calculated polydispersities based on the comparative method.

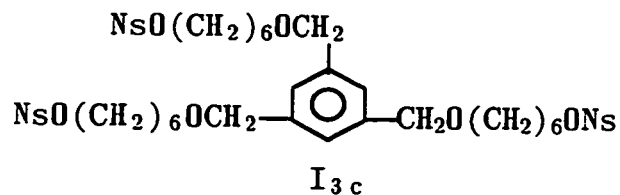
**Table 3.2** Calculated polydispersities of  $B_{10}E_xB_{10}$  triblocks obtained from one-, two-ended initiation

$B_{10}E_yB_{10}$	$\bar{X}_w/\bar{X}_n$
$P_1(B_{10}E_{40}B_{10})$	1.05
$P_{2a}(B_{10}E_{39}B_{10})$	1.12
$P_{2b}(B_9E_{38}B_9)$	1.08
$P_{2c}(B_{10}E_{44}B_{10})$	1.13

From Table 3.2 we note that the polydispersities of the triblocks made from two-ended initiators were higher than of the triblock made from the one-ended sequential method.

The broader polydispersities of the polymers from the three initiators compared to that of polymer from one-ended methyl nosylate indicate that these compounds initiate EO slower than its propagation. To prove this we compared the polydispersities of (E) homopolymers made using one-, two- and three-ended nosylate ester initiation. For one-ended initiation we

used a  $P_1(E_{20})$  homopolymer made from MeONs. For two-ended initiation we used the E homopolymers of the previously described triblocks made from  $I_{2a}$ ,  $I_{2b}$  and  $I_{2c}$ . Finally, for three-ended initiation we made a  $P_{3c}(E_{39})_3$  homopolymer using  $I_{3c}$  of the structure shown below:



The GPC profiles, shown in Figure 3.5 show much broader peaks than that of the  $P_1(E_{20})$  standard.

Table 3.3 summarizes the calculated polydispersities of the E homopolymers.

**Table 3.3** Calculated polydispersities of E homopolymers made from one-, two-, and three-ended nosylate ester initiators

E	$\bar{X}_w/\bar{X}_n$
$P_1(E_{20})$	1.05
$P_{2a}(E_{20})_2$	1.13
$P_{2b}(E_{20})_2$	1.13
$P_{2c}(E_{22})_2$	1.10
$P_{3c}(E_{39})_3$	1.11

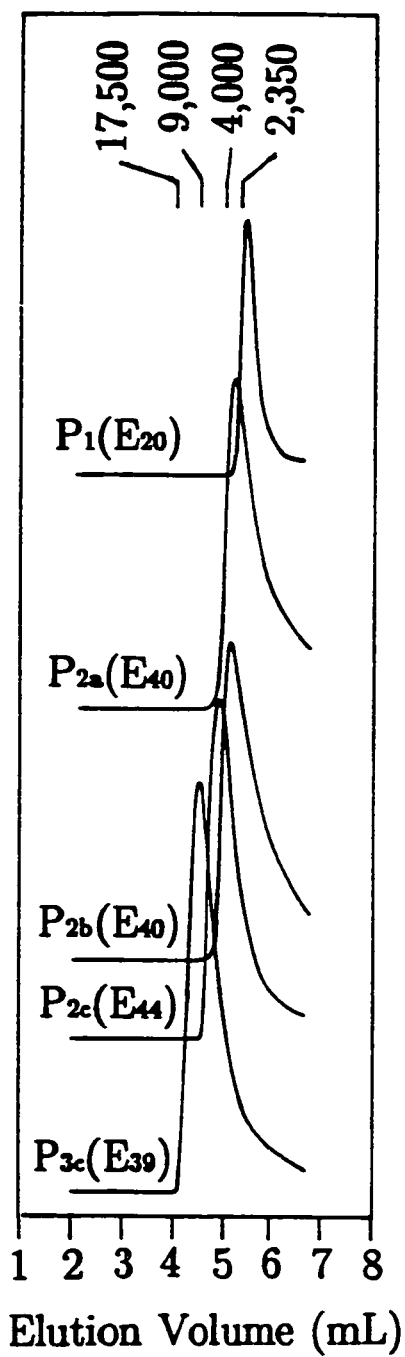


Figure 3.5. GPC-RI profiles of E homopolymers made by one-, two-, and three-ended initiators.

From Table 3.3 we note that the MWD of  $P_1(E_{20})$  made from methyl nosylate is much narrower than the rest of the series. Therefore, this shows that alkylation by two- and three-ended nosylates is slow for EO compared to its propagation rate.

In order to increase the alkylation rate we show in Chapter 4 the attempts to produce a fast-initiating two-ended substance. From the resulting kinetic study we assess the validity of the hypothesis of slow initiation compared to propagation by calculating the  $k_p/k_i$  ratios for three systems.

## References

1. Litt, M. H.; Chen, T. T.; Hsieh, B. R. *J. Polym. Sci., Part A, Polym. Chem.* 1986, *24*, 3407.
2. Litt, M. H.; Hsieh, B. R.; Krieger, I. M.; Chen, T. T.; Lu, H. L. *J. Colloid Int. Sci.* 1987, *115*, 312.
3. Hsieh, B. R.; Litt, M. H.; Demopolis, T. N.; Krieger, I. M. *Polym. Prepr., Am. Chem. Soc. Div. Polym. Chem.* 1986, *27(2)*, 122.
4. Kobayashi, S.; Igarashi, T.; Moriuchi, Y.; Saegusa, T. *Macromolecules* 1986, *19*, 535.
5. Kobayashi, S.; Iijima, S.; Igarashi, T.; Saegusa, T. *Macromolecules* 1987, *20*, 1729.
6. (a) Percec, V. *Polym. Bull* 1981, *5*, 643. (b) Saegusa, T.; Ikeda, H. *Macromolecules* 1973, *6*, 805. (c) Litt, M. H.; Swamikannu, X. In *Ring-Opening Polymerization*; Mc Grath, J. E., Ed.; ACS Symposium Series 286; American Chemical Society: Washington, DC, 1985; p231.
7. Swamikannu, A. X. Ph. D. thesis; Case Western Reserve University; 1984; p 150.
8. Hsieh, B. R.; Litt, M. H. Unpublished work.
9. Cai, G. F.; Litt, M. H. In preparation for publication.

## Chapter 4

### Core-first Approach to Star-Block Oxazolines

#### 2. Initiation Kinetics

a) Introduction

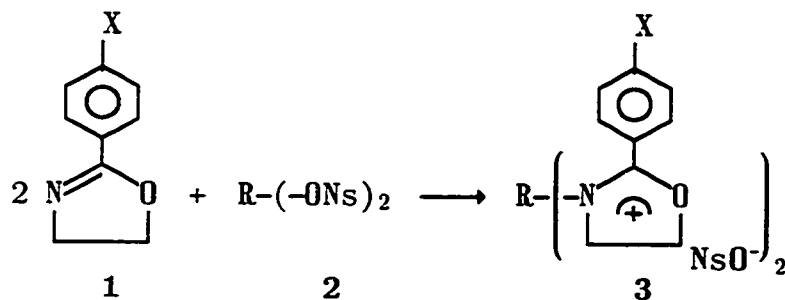
The goal of the core-first method is to obtain a polyfunctional initiator that will produce oxazoline star-block copolymers of narrow molecular weight distribution. The blocks to be constructed will use 2-ethyl-2-oxazoline (EO) to make the central segments, and 2-p-t-butylphenyl-2-oxazoline to make the outer segments. The work shown in Chapter 3 demonstrated that two- and three-ended long alkyl chain nosylates produce broad MWD polymers when used as initiators for EO. We believe this is because of slow initiation compared to the propagation rate of EO.

According to Saegusa et al<sup>1</sup>, N-methyl-2-phenyl-2-oxazolinium tosylate reacts more than twice as fast with 2-methyl-2-oxazoline as does N-methyl-2-methyl-2-oxazolinium tosylate; that is, its  $k_p$  is twice as large. Therefore, a rate enhancement should result if a two-ended N-alkyl-2-phenyl-2-oxazolinium nosylate initiates polymerization of EO instead of its precursor two-ended alkyl-nosylate ester. A study on the reaction between methyl tosylate and three p-substituted phenyl-2-oxazolines<sup>2</sup> indicated that the rate of N-methylation,  $k_i$ , is controlled by the nucleophilicity of the oxazoline,  $\text{CH}_3\text{O}^- > \text{H}^- > \text{Cl}^-$ . Also, the authors concluded that the rate determining step is predominantly the ring-opening of the oxazolinium end. Thus,  $k_p$  values range in the order  $\text{Cl}^- > \text{H}^- > \text{CH}_3\text{O}^-$  for the three oxazolines. However, the ordering of  $k_i$  and  $k_p$  for the same oxazolines might be different if a methylene-ended bulky initiator is used, because of both electronic and

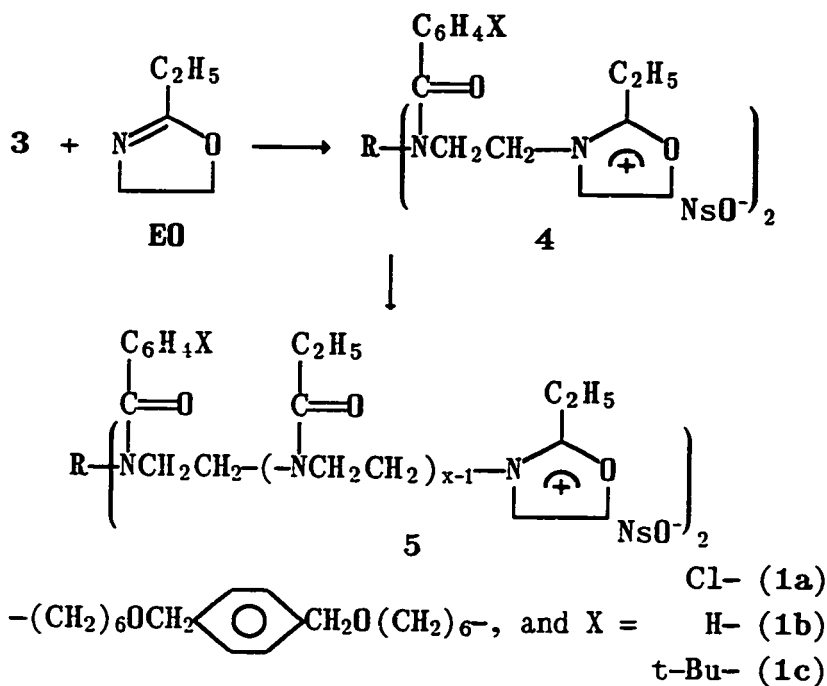
steric differences.

In this chapter we discuss the reaction of a two-ended long-chain nosylate, **2**, with each of three 2-p(substituted)phenyl-2-oxazolines, **1**, the substituents being Cl-, H-, and t-bu- (see Scheme 4.1). The goal of this work was to isolate the two-ended oxazolinium salt, **3**, and react it with EO. **3** should react faster with EO than its precursor nosylate-ester, **2**; therefore the resultant polymer **5** should have a sharply defined MWD. In order to understand the mechanism of the reaction between the different oxazolines and the dinosylate, and to determine the relative ordering of  $k_i$  and  $k_p$  we undertook a kinetics experiment. Aliquots of the reaction mixtures of **1** and **2** were analyzed as a function of time by high pressure liquid chromatography (HPLC), and the reaction analyzed kinetically to determine  $k_i$  and  $k_p$ .

Scheme 4.1







### b) Experimental

**Instrumentation:** HPLC chromatograms were taken on an ISCO Model 2300 High Pressure Liquid Chromatograph, equipped with a UV detector Model UA-5 operating at 254 nm, and interfaced to an Apple IIe computer. The column used was a C-18, nonpolar HPLC column. The data were digitized, and the areas under each peak integrated by an HPLC analysis program (Chromatochart<sup>R</sup>).

**2-Phenyl-2-oxazoline (PO):** A mixture of benzonitrile (23.79 g, .2103 mol) with 2-aminoethanol (13.95 g, .2287 mol) was stirred for about 26 h at 120–145°C with 1.27 g of Cd(OAc)<sub>2</sub> (benzoylnitrile/cadmium acetate ratio, 1:0.026 molar ratio), according to the literature<sup>3</sup>. The resulting brown

slurry was then transferred to a distillation flask, some KOH pellets were added and the flask connected to spinning band distillation column, described in Chapter 2. A forerun was removed at 60–69<sup>0</sup>C and .10–.11 torr, then PO was collected at 73<sup>0</sup>C and the same pressure. The column was then rinsed with CHCl<sub>3</sub>, and PO was redistilled at 75<sup>0</sup>C and 0.1 torr to give a transparent colorless liquid that crystallized in a refrigerator at –18<sup>0</sup>C, and remained solid on warming to room temperature. The yield was 17.41 g (56%). PO purity was over 99% by <sup>1</sup>H NMR and HPLC.

2-p-t-Butylphenyl-2-oxazoline: TBO was prepared from p-t-butylbenzoic acid, described in Chapter 3.

2-p-Chlorophenyl-2-oxazoline, and two-ended alkyl nosylate 2: These were furnished by G. Cai. The oxazoline was prepared according to the literature<sup>4,5</sup>, and the nosylate was made according to a method to be published<sup>6</sup>.

9-Methylanthracene: Reagent grade 9-methyl anthracene was dissolved in a 95/5 volume ratio of hexane/ethylacetate and passed through a silica-gel column. Several fractions were collected by eluting with the hexane/EtOAc solution, and analyzed by HPLC to determine the purity. The fractions containing the compound were combined and rotavaporated to remove the solvents. Orange shiny crystals were obtained after drying in a vacuum oven.

Acetonitrile: The following drying procedure for  $\text{CH}_3\text{CN}$  is based on a recommended purification and drying method<sup>7</sup>. .98 g of a 1% aqueous KOH solution was added to 300 mL  $\text{CH}_3\text{CN}$  which was then refluxed for 4 h. The  $\text{CH}_3\text{CN}$  was fractionally distilled and the middle fraction collected and stirred overnight with  $\text{CaH}_2$ . The slurry was filtered, stirred with  $\text{P}_2\text{O}_5$ , and redistilled. The collected higher boiling fraction was then stirred overnight in a vacuum ampoule with  $\text{P}_2\text{O}_5$ , then distilled using the high vacuum rack into a clean solvent reservoir (see Figures 2.1 and 2.2, Chapter 2).

Stoichiometric reaction of the dinosylate with each of the three 2-oxazolines: In each of three polymerization vessels (Figure 2.3, Chapter 2) was loaded 0.2400 g  $\text{NsO}(\text{CH}_2)_6\text{OCH}_2\phi\text{CH}_2\text{O}(\text{CH}_2)_6\text{ONs}$  ( $3.388 \times 10^{-4}$  mol) and 0.0112 g of 9-methylanthracene ( $5.83 \times 10^{-5}$  mol). To reaction vessel 1 was then added 0.1376 g 2-p-t-butylphenyl-2-oxazoline ( $6.778 \times 10^{-4}$  mol), to reaction vessel 2 0.1230 g 2-p-chlorophenyl-2-oxazoline ( $6.777 \times 10^{-4}$  mol), and to reaction vessel 3 0.0996 g 2-phenyl-2-oxazoline ( $6.776 \times 10^{-4}$  mol). The vessels were equipped with glass-covered magnetic stirrers, placed on a high-vacuum rack (Figure 2.1, Chap. 1), and evacuated overnight to  $3 \times 10^{-5}$  torr. The system was then purged with positive-pressure dry  $\text{N}_2$ , and 2.90 mL dried  $\text{CH}_3\text{CN}$  was transferred into reaction vessel 1 via a 5-mL syringe, 2.92 mL into 2, and 2.94 mL into 3. The dinosylate concentration was thus ca. 0.103 M in all three units. The resulting slurries were dissolved by stirring at room temperature to give transparent

yellow solutions. The vessels were immersed in preheated oil-baths immersed after turning on the cold water to the units' condensers; the solutions quickly reached reflux temperature (bp  $\text{CH}_3\text{CN}$   $82^\circ\text{C}$ ). Aliquots of the reaction mixtures were retrieved periodically, and analyzed by HPLC. The solutions were stirred for a total of 73 h.

Chromatography: The reaction aliquots were diluted with methanol and injected into the HPLC. The samples were chromatographed with MeOH at 1 mL/min purging rate. The concentration of 9-methylanthracene (standard) was chosen so that the initial mixture gave peaks for nosylate, oxazoline, and standard that were comparable in intensity. As the reaction proceeded, the unreacted dinosylate and oxazoline peaks decreased and product peaks (low retention times, polar) increased. To maintain all peaks on scale during the run, we switched the detector attenuation in a blank region of the chromatogram, then used the appropriate scale factor to determine the integrated areas.

Analysis: Numerical calculations were done with an IBM-AT computer by running a program written in Pascal.

### c) Results

#### Polymerization of 2-(p-substituted)phenyl-2-oxazolines

Three para-substituted phenyl oxazolines (1a-c) were prepared. A long-alkyl chain dinosylate 2 was reacted with equivalent amounts of each

of 1a-c (Scheme 4.1). The reaction was run in acetonitrile at 82°C using 9-methyl anthracene as internal standard (IS). Aliquots of the reaction mixture were taken at different times, and analyzed by HPLC using UV detection at 254 nm. Figure 4.1 shows the HPLC chromatograms of the reaction mixture of 1a after a few seconds of injection, and after most of the oxazoline had reacted (24.5 h). The peaks assignments in the figure are given as follows: 269 s 9-methylanthracene, 186 s remaining 1a, 141 s remaining dinosylate ester, and 93 s N-alkyl oxazolinium salt products. Also, there is a small peak at 160 s due to an unknown impurity. At longer reaction times when more than 90% of the oxazolines had reacted, another small peak was evident at about 180 s, the size of which did not decrease with time. The peaks due to unreacted dinosylate and oxazoline are distinct and do not overlap with anything. However, we obtain overlapping peaks for once- and twice-reacted nosylate, as well as for salts containing an indeterminate number of oxazoline units. In order to determine the concentrations of unreacted nosylate and oxazoline, we used an internal standard (IS) in the reaction mixture. (IS) should be a substance that is inert towards all reagents and solvents, and which would be detected at a retention time away from all other peaks. We chose 9-methyl anthracene among many compounds, because it is inert towards nosylates, oxazolines and acetonitrile, and its non-polar nature causes its peak to appear at longer retention times than anything else. Hence, the concentrations of unreacted oxazoline and dinosylate can be found by normalization of the corresponding integrated areas to the area of (IS).

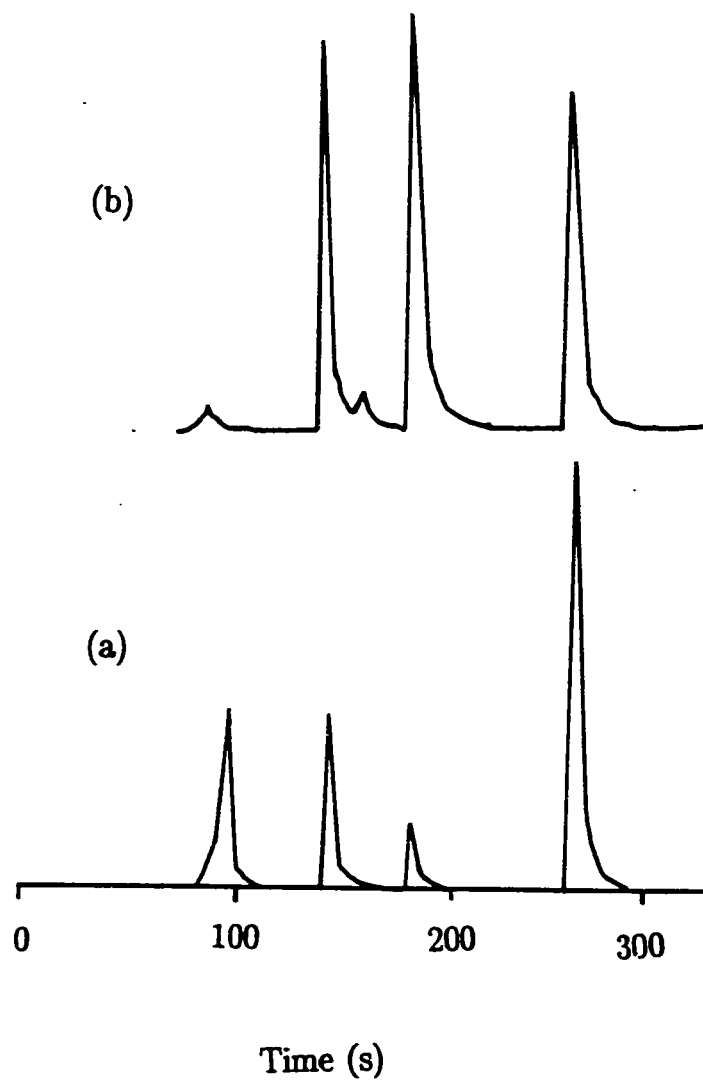
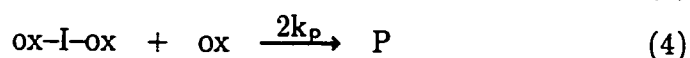
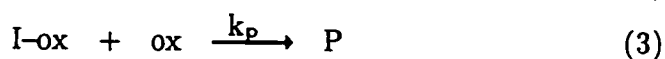
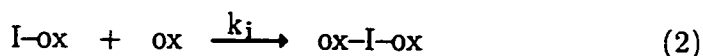
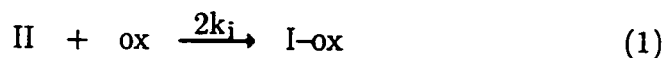


Figure 4.1. HPLC chromatograms of the reaction of 2-p-chlorophenyl-2-oxazoline and dinosylate in  $\text{CH}_3\text{CN}$  at  $82^\circ\text{C}$ . (Top) initial mixture, and (Bottom) after 24.5 h.

Kinetics of the Polymerization of 1 with 2.

In order to evaluate rate constants we used the following kinetic scheme:

## Scheme 4.2



where:

ox is 1 (see Scheme 4.1), II is unreacted 2, I-ox is once-reacted dinosylate 2, ox-I-ox is twice reacted 2, and P is any polymeric salt, containing more than one ox units per reacted-end of 2.

Equations (1)–(4) are based on the following model. Initiation occurs when ox attacks either end of II (effective rate constant  $2k_i$ ) to make I-ox, or the unreacted end of I-ox (rate constant  $k_i$ ) to make ox-I-ox. Propagation happens when more ox attacks the reacted end of I-ox (rate constant  $k_p$ ), or either end of ox-I-ox (rate constant  $2k_p$ ) to produce polymer P. We also assume that  $k_p$  is independent of the number of monomer units already reacted.

The kinetic equations corresponding to equations (1) to (4) are written as follows:

$$-d[\text{II}]/dt = 2k_i[\text{II}][\text{ox}] \quad (5)$$

$$-d[\text{ox}]/dt = 2k_i[\text{II}][\text{ox}] + k_i[\text{I-ox}][\text{ox}] + k_p[\text{I-ox}][\text{ox}] + 2k_p[\text{ox-I-ox}][\text{ox}] \quad (6)$$

Now, let  $\alpha$  denote the fraction of unreacted nosylate ends at time  $t$ . The chance of finding an unreacted end is defined as  $\alpha$ . This is equivalent to saying that the chance of finding a reacted end is  $(1-\alpha)$ . The concentrations of II, I-ox, and ox-I-ox can be expressed in terms of  $\alpha$ , with the assumption that the chance of reacting one end is independent of whether or not the other end has reacted. Thus, the chance of finding two unreacted ends (II) is equal to the product of the probabilities of each end being unreacted, i.e.  $\alpha^2$ . Hence, [II] at  $t$  is  $\alpha^2[\text{II}]_0$ ,  $[\text{II}]_0$  being the initial dinosylate concentration. Similarly, the chance of finding one reacted and one unreacted end (I-ox) is equal to the product of  $\alpha$  times  $(1-\alpha)$  times 2 because there are two ways that this can happen. Thus, [I-ox] at  $t$  is  $2\alpha(1-\alpha)[\text{II}]_0$ . Consequently we obtain the following set of equations:

$$[\text{II}] = \alpha^2[\text{II}]_0 \quad (7)$$

$$[\text{I-ox}] = 2\alpha(1-\alpha)[\text{II}]_0 \quad (8)$$

$$[\text{ox-I-ox}] = (1-\alpha)^2[\text{II}]_0 \quad (9)$$

By substituting [I-ox], and [ox-I-ox] from equations (7)–(9) into (6) we obtain:

$$-d[\text{ox}]/dt = 2[\text{II}]_0 \cdot (k_i\alpha + k_p(1-\alpha)) \cdot [\text{ox}] \quad (10)$$

by substitution of  $\alpha$  from (7) into (10) we obtain (11):

$$-d[\text{ox}]/dt = 2[\text{II}]_0 \cdot \left[ k_i \sqrt{[\text{II}]/[\text{II}]_0} + k_p \left( 1 - \sqrt{[\text{II}]/[\text{II}]_0} \right) \right] [\text{ox}] \quad (11)$$



Equations (5) and (6) are next transformed to contain experimentally determinable quantities. The concentrations of [ox] and [II] at different times can be derived from the areas,  $A_{ox}$  and  $A_{II}$ , of the unreacted oxazoline and dinosylate peaks from the corresponding HPLC chromatograms, by normalizing to the area of standard  $A_{IS}$ , and to the initial concentrations  $[II]_0$  and  $[ox]_0$ :

$$(A_{II}/A_{IS}) = c_{II}[II] \quad (12)$$

$$(A_{ox}/A_{IS}) = c_{ox}[ox] \quad (13)$$

At time  $t=0$  (12) and (13) become:

$$(A_{II}/A_{IS})_0 = c_{II}[II]_0 \quad (14)$$

$$(A_{ox}/A_{IS})_0 = c_{ox}[ox]_0 \quad (15)$$

Since [IS] is constant,  $c_{II}$  and  $c_{ox}$  are constants that from Beer's Law are equal to the ratios of  $\epsilon_{II}/\epsilon_{IS}$ , and  $\epsilon_{ox}/\epsilon_{IS}$  each divided by [IS], where  $\epsilon_{II}$  and  $\epsilon_{ox}$  are the extinction coefficients of II and IS respectively.

Now let  $(A_{II}/A_{IS})$  and  $(A_{ox}/A_{IS})$  be named  $S_{II}$  and  $S_{ox}$  respectively. We then obtain [II] and [ox] by dividing (12) by (14), and (13) by (15) respectively:

$$[II] = \frac{[II]_0}{S_{II,0}} S_{II} \quad (16)$$

$$[ox] = \frac{[ox]_0}{S_{ox,0}} S_{ox} \quad (17)$$

Equations (5) and (11) now become because of (16) and (17):

$$-\frac{d}{dt}\left(\frac{[II]_0}{S_{II,0}} \cdot S_{II}\right) = 2k_i \frac{[II]_0}{S_{II,0}} \cdot S_{II} \cdot \frac{[ox]_0}{S_{ox,0}} \cdot S_{ox} \quad (18)$$

$$-\frac{d}{dt}\left(\frac{[ox]_0}{S_{ox,0}} \cdot S_{ox}\right) = 2[II]_0 \left[ k_i \sqrt{\frac{S_{II}}{S_{II,0}}} + k_p \left( 1 - \sqrt{\frac{S_{II}}{S_{II,0}}} \right) \right] \cdot \frac{[ox]_0}{S_{ox,0}} \cdot S_{ox} \quad (19)$$

After manipulation, and because initially we have  $2[II]_0 = [ox]_0$ , we therefore get:

$$-\frac{dS_{II}}{dt} = 2 \frac{[ox]_0}{S_{ox,0}} \cdot k_i \cdot S_{II} \cdot S_{ox} \quad (20)$$

$$-\frac{dS_{ox}}{dt} = [ox]_0 \left[ k_i \sqrt{\frac{S_{II}}{S_{II,0}}} + k_p \left( 1 - \sqrt{\frac{S_{II}}{S_{II,0}}} \right) \right] \cdot S_{ox} \quad (21)$$

(20) and (21) comprise a system of coupled first-order differential equations, with (20) being linear and (21) nonlinear. Time,  $t$ , is the independent variable, while  $S_{II}$  and  $S_{ox}$  are the dependent variables.  $k_i$  and  $k_p$  are unknown parameters that we wish to determine by fitting the values of  $S_{II}$  and  $S_{ox}$ , calculated from (20) and (21) at different reaction times, to the corresponding experimental values at the same times. We were unable to find an analytic solution of the system for the  $S_{II}$  and  $S_{ox}$  functions of time. However, we were able to approximate the exact solution using the Runge-Kutta numerical approach<sup>8</sup>.

The Runge-Kutta Method: This is one of the numerical methods by which we can integrate, in tabular form, a given differential equation from the

initial conditions. Thus, let us consider the initial value problem:

$$y' = f(x,y), \quad y(x_0) = y_0 \quad (22)$$

and assume that both  $y$  and  $y'$  are continuous in some rectangle in the  $xy$  plane including the point  $(x_0, y_0)$ . Then, according to a theorem (see reference 8), there exists a unique solution  $y = \varphi(x)$  of the problem in some interval about  $x_0$ , and the value of the exact solution at  $x_n$  is  $\varphi(x_n)$ . Now let  $y_n$  and  $y'_n = f(x_n, y_n)$  denote the approximate values of the exact solution and its derivative at the point  $x_n$ . The Runge-Kutta formula involves a weighed average of values of  $f(x, y)$  taken at different points in the interval  $x_n \leq x \leq x_{n+1}$ . It is given by:

$$y_{n+1} = y_n + \frac{h}{6} (k_{n1} + 2k_{n2} + 2k_{n3} + k_{n4}), \quad (23)$$

where  $h$  is the step size and

$$k_{n1} = f(x_n, y_n) \quad (24a)$$

$$k_{n2} = f\left(x_n + \frac{h}{2}, y_n + \frac{h}{2} k_{n1}\right) \quad (24b)$$

$$k_{n3} = f\left(x_n + \frac{h}{2}, y_n + \frac{h}{2} k_{n2}\right) \quad (24c)$$

$$k_{n4} = f(x_n + h, y_n + h k_{n3}) \quad (24d)$$

To determine  $y_n$  we first determine  $y_1$ , knowing  $y_0$  from the initial condition and  $\varphi'(x_0) = f(x_0, y_0)$  from equation (22). Then, knowing  $y_1$  we determine  $y_2$ , and so on. We chose this particular method because it is very accurate and the local formula errors are very low. Moreover, these calculations can easily be done with a computer.

In our case we can write equations (20) and (21) as

$$x' = f(t, x, y), \quad (25)$$

$$y' = g(t, x, y), \quad (26)$$

where

$$x = S_{II}, \quad y = S_{Ox},$$

$$f = -2 \cdot \frac{[Ox]_0}{S_{Ox,0}} \cdot k_i \cdot S_{II} \cdot S_{Ox}$$

and

$$g = -[Ox]_0 \left[ k_i \cdot \sqrt{\frac{S_{II}}{S_{II,0}}} + k_p \cdot \left( 1 - \sqrt{\frac{S_{II}}{S_{II,0}}} \right) \right] \cdot S_{Ox}$$

We also have the initial conditions ( $t_0 = 0$ )

$$x(t_0) = x_0, \quad y(t_0) = y_0 \quad (27)$$

The functions  $f$  and  $g$  are continuous for times  $t \geq 0$ , hence, according to the Theorem mentioned above<sup>8</sup> there is a unique solution in some interval of the  $t$  axis containing the point  $t_0$ . We wish to determine approximate values  $x_1, x_2, \dots, x_n$  and  $y_1, y_2, \dots, y_n$  of the exact solution  $x = \varphi(t)$ ,  $y = \psi(t)$  at the points  $t_n = nh$ . Equations (23) and (24) are then generalized to give

$$x_{n+1} = x_n + \frac{h}{6} (k_{n1} + 2k_{n2} + 2k_{n3} + k_{n4}), \quad (28a)$$

$$y_{n+1} = y_n + \frac{h}{6} (l_{n1} + 2l_{n2} + 2l_{n3} + l_{n4}), \quad (28b)$$

$$k_{n1} = f(t_n, x_n, y_n) \quad (29a)$$

$$k_{n2} = f\left(t_n + \frac{h}{2}, x_n + \frac{1}{2} k_{n1}, y_n + \frac{1}{2} l_{n1}\right) \quad (29b)$$

$$k_{n3} = f\left(t_n + \frac{h}{2}, x_n + \frac{1}{2} k_{n2}, y_n + \frac{1}{2} l_{n2}\right) \quad (29c)$$

$$k_{n4} = f(t_n + h, x_n + k_{n3}, y_n + l_{n3}) \quad (29d)$$

$$l_{n1} = g(t_n, x_n, y_n) \quad (29e)$$

$$l_{n2} = g(t_n + \frac{h}{2}, x_n + \frac{1}{2} k_{n1}, y_n + \frac{1}{2} l_{n1}) \quad (29f)$$

$$l_{n3} = g(t_n + \frac{h}{2}, x_n + \frac{1}{2} k_{n2}, y_n + \frac{1}{2} l_{n2}) \quad (29g)$$

$$l_{n4} = g(t_n + h, x_n + k_{n3}, y_n + l_{n3}) \quad (29h)$$

#### Fitted values of $k_i$ and $k_p$

We wrote a computer program that found the approximate values of the exact solution  $x = \varphi(t)$ ,  $y = \psi(t)$  at the points  $t_n = nh$  from (28), where  $t_n$  varied from 0 to 73 hours with a step  $h$  of 0.01 hours, using equations (29).

First, initial estimates of  $k_i$  and  $k_p$  were put into the program. The following function was then calculated

$$E = \sum_i (\text{error})^2 = \sum_i (x_{\text{exp}} - x_{\text{calc}})^2 + \sum_i (y_{\text{exp}} - y_{\text{calc}})^2 \quad (30)$$

where  $x_{\text{exp}}$  and  $y_{\text{exp}}$  are the experimental HPLC ratios  $S_{II}$  and  $S_{Ox}$  of aliquots (i) of the reaction mixture taken at a given time, and  $x_{\text{calc}}$  and  $y_{\text{calc}}$  are the approximate values of the exact solutions of the system of equations (25) and (26) at that time. The optimal  $k_i$  and  $k_p$  values were found by minimization of  $E$  from equation (30) using the square-grid approach, as follows. First,  $E_1$  was evaluated by running the program with an initial estimate of  $(k_i, k_p)$ . A square grid of  $(k_i, k_p)$  pairs was then constructed around the initial pair by varying each of the initial  $k_i$  and  $k_p$  by plus and minus 20% of its value. The resulting eight new  $(k_i, k_p)$  pairs were next used to compute the corresponding  $E_2, E_3, \dots, E_9$  values.

The nine errors were then compared to find the minimum value. If the minimum was  $E_1$  the program stopped and  $(k_i, k_p)$  were taken as the best-fit values with a 10% uncertainty. However, if another  $E$  was the minimum then the corresponding  $(k_i, k_p)$  pair was taken as a new grid-center and eight new  $E$ 's were again evaluated. This process iterated until a grid-center  $(k_i, k_p)$  value gave the minimum error. The relatively large 20 % grid-step caused the program to converge to a minimum within relatively few iterations. As soon as we knew  $(k_i, k_p)$  to  $\pm 10\%$ , we used the previous optimized pair as initial input for a new grid size of  $\pm 1\%$  in order to find the new optimum  $(k_i, k_p)$  pair to within 0.5% uncertainty. The program also gave calculated approximate solutions of equations (25) and (26) at different times. The values of  $S_{II}$  and  $S_{ox}$  thus calculated, as well as the experimental  $S_{II}$  and  $S_{ox}$  were transformed into  $[II]$  and  $[ox]$  using equations (16) and (17) respectively.

Figures 4.2, 4.3, and 4.4 show the disappearance of  $[II]$  and  $[ox]$  with time. The points depict the molarities corresponding to the normalized HPLC peak-areas, while the solid and dashed lines show the time dependence of  $[II]$  and  $[ox]$  calculated using the designated  $k_i$  and  $k_p$ . From the data used in Figures 4.2-4.4, we construct Table 4.1 which shows the conversion of  $II$  when over 90% of each oxazoline has reacted was constructed.

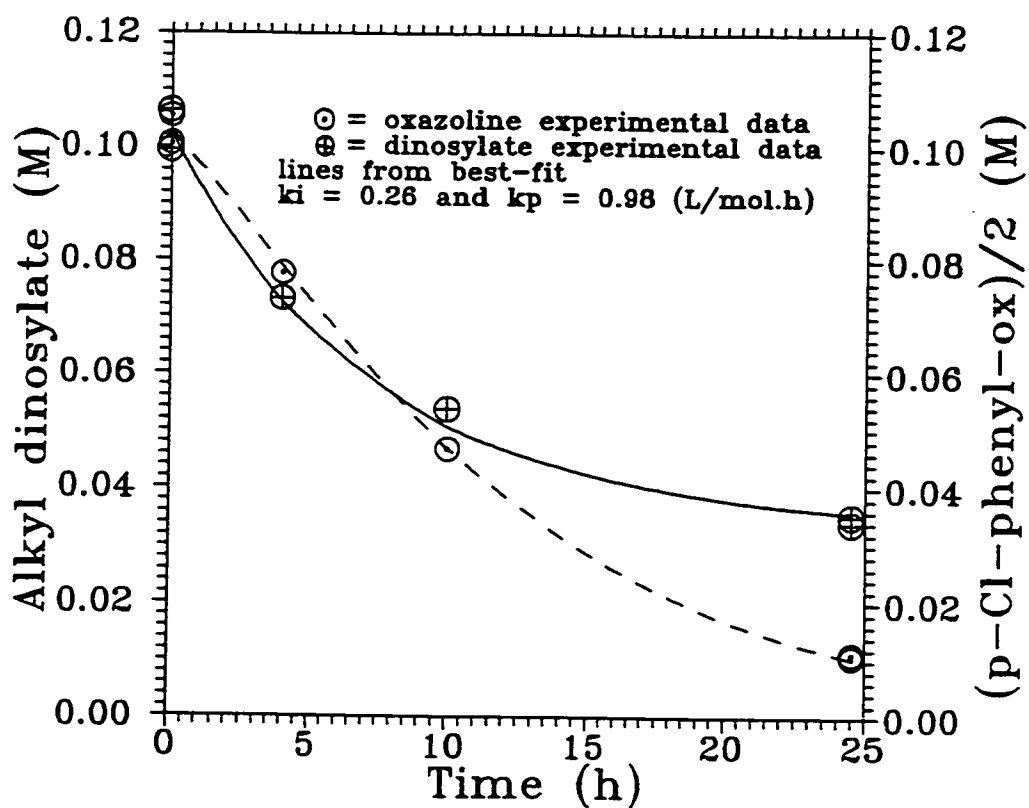


Figure 4.2 Alkyl dinosylate and 2-p-chlorophenyl-2-oxazoline time disappearance from HPLC areas, and numerical analysis.

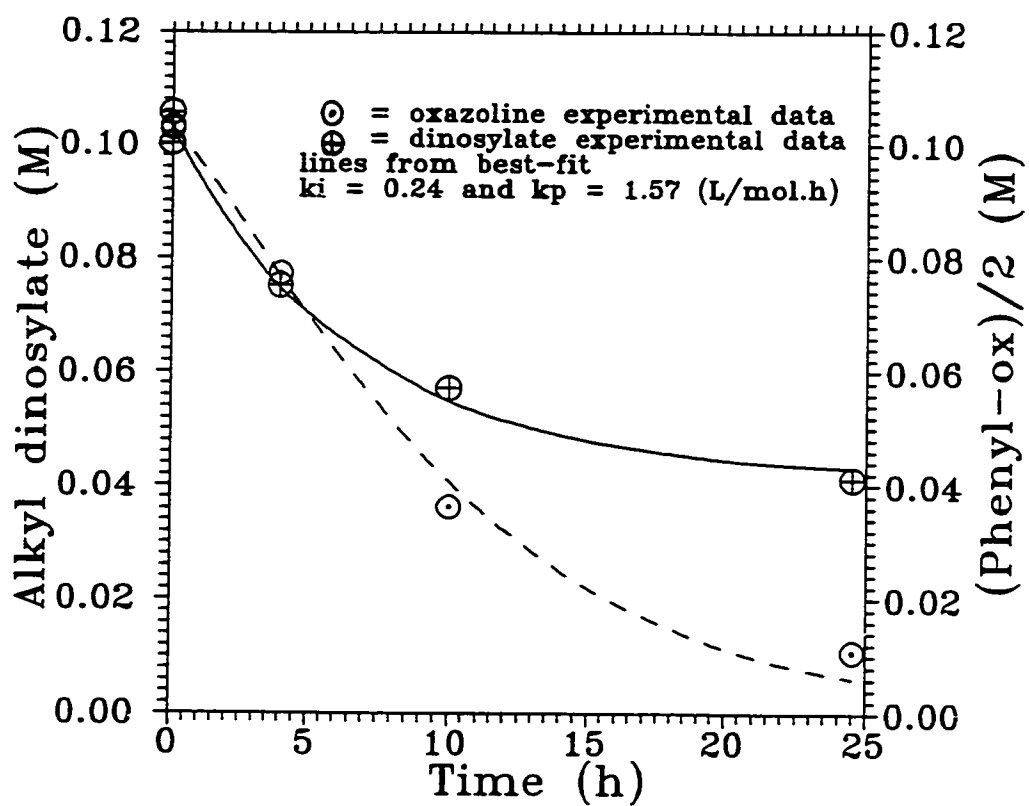


Figure 4.3 Alkyl dinosylate and 2-phenyl-2-oxazoline time disappearance from HPLC areas, and numerical analysis.



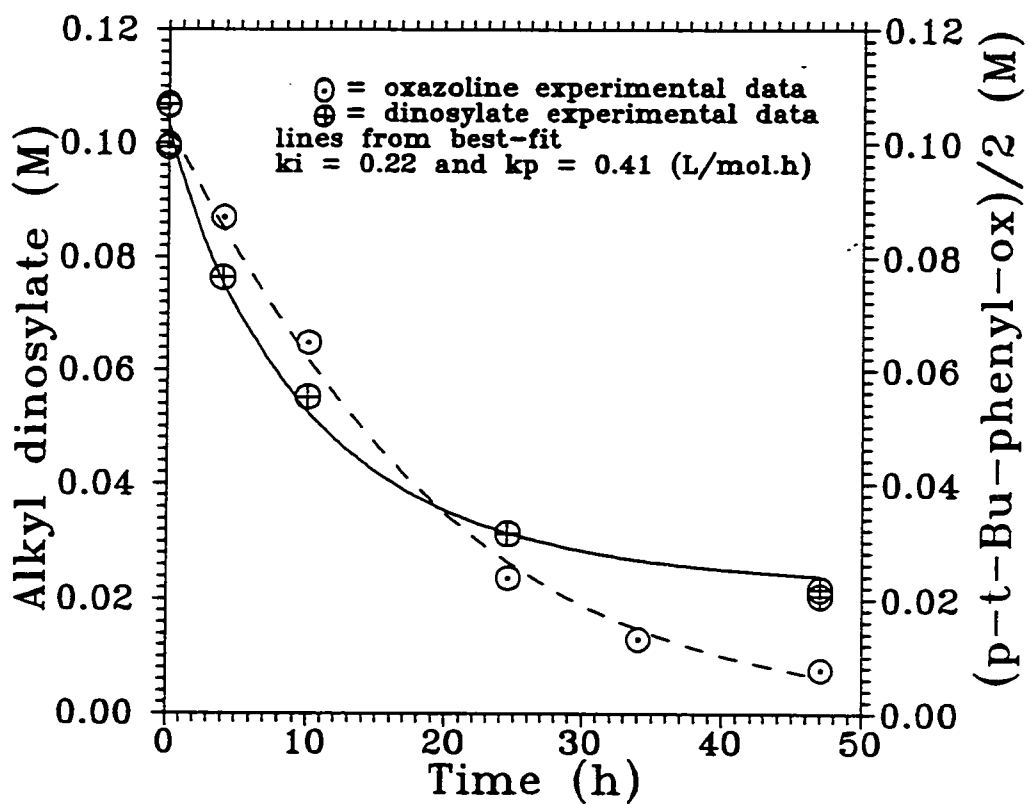


Figure 4.4 Alkyl dinosylate and 2-p-t-butylphenyl-2-oxazoline time disappearance from HPLC areas, and numerical analysis.

Table 4.1 Relative conversions of II and ox after long reaction times (\* 24.5 h, \*\* 47 h).

-X	II (%)	ox (%)
Cl <sup>*</sup>	66 (65)	90 (92)
H <sup>*</sup>	60 (58)	90 (94)
t-Bu <sup>**</sup>	79 (77)	93 (94)

where the numbers in parentheses denote the optimized calculated conversions. Table 4.2 shows the ( $k_i$ ,  $k_p$ ) best-fit values obtained from the numerical analysis of the reaction of II with each of the three oxazolines.

Table 4.2. Best-fit  $k_i$  and  $k_p$  values for three 2-(p-substituted)phenyl-2-oxazolines with an alkyl dioxylate in  $\text{CH}_3\text{CN}$  at 82 °C.

-X	$k_i$ (L/(mol.h))	$k_p$ (L/(mol.h))
Cl	0.26	0.98
H	0.24	1.57
t-Bu	0.22	0.41

Table 4.1 indicates that more than 90% of each of the three oxazolines has reacted at a time when the dinosylate has only partially reacted. Since the initial dinosylate reactive sites and oxazoline concentrations were equivalent, oxazoline conversions higher than that of initiator mean that some ester ends have reacted more than once while others remain unreacted. This is due to  $k_p$  being higher than  $k_i$  for all three cases, as shown in Table 4.2. We believe that the slow initiation is due to steric effects arising from the bulky alkyl core. Thus, this group hinders the attack of monomer on the reactive-ester sites. From electronic reasons alone one expects  $k_i$  to be largest for the oxazoline bearing the electron-donating *t*-butyl substituent, and lowest for the one with the electron-withdrawing chloro- group. However, the three  $k_i$ 's are the same within the experimental error which arises mainly from the determination of the HPLC areas. Thus, as far as alkylation of the oxazolines by the ester is concerned, steric effects of dinosylate prevail over the electronic effects of the *para*-substituent on the phenyl-oxazoline.

Let us now compare the propagation rates,  $k_p$ , of the three oxazolines. These reflect the cationic polymerizability of the oxazolinium salt. If this is determined by the ring-opening reactivity of the oxazolinium ring, then one expects the  $k_p$ 's to follow the order *t*-Bu- < H- < Cl-, since the electron-donating *t*-butyl deactivates the ring towards nucleophilic attack of monomer while the chloro group activates the salt by withdrawing electrons.  $k_p$  of the *t*-butyl-containing oxazoline is indeed much lower than either of the two other oxazolines. However, the order for the other two monomers is the reverse of the expected one, i.e. we find that

$k_p(\text{Cl}^-) < k_p(\text{H}^-)$ . The above orders cannot be explained in terms of electronic effects. However, this may be explained if the ordering of the oxazoline propagation rate constants,  $k_p$ , is governed principally by steric effects, which should decrease in the order  $t\text{-bu}^- > \text{Cl}^- > \text{H}^-$ , as the size of these groups. Future work is needed to test this hypothesis.

#### Conclusions of the core-first method.

From the results of Chapter 3 and 4 we find that high polydispersity polymers result when two- and three- ended nosylate initiators are used to initiate 2-ethyl-2-oxazoline. This arises from slow initiation compared to propagation. A detailed study was done to find out whether it was possible to isolate a two-ended aroyl-2-oxazolinium salt and use it for 2-ethyl-2-oxazoline polymerization. Thus, each of three 2-(p-substituted)phenyl-2-oxazolines was reacted with an equivalent amount of a long alkyl-chain dinosylate ester. We were not able to isolate the bis oxazolinium salt because the oxazoline reacted completely before all the nosylate was consumed. Numerical analysis showed that the rate of initiation is much slower than of propagation for all three oxazolines, and that  $k_i$  is about the same for all three cases, indicating that alkylation of the oxazolines is mainly influenced by the high steric hindrance of the bulky alkyl core of the di-ester.

#### References

1. Saegusa, T.; Ikeda, H.; Fujii, H. *Polymer J.* 1973, 4, 87.
2. Kobayashi, S.; Tokuzawa, T.; Saegusa, T. *Macromolecules* 1982, 15, 707.

3. Seelinger, W.; Aufderhaar, E.; Diepers, W.; Feinauer, R.; Nehring, R.; Thier, W.; Hellmann, H. *Angew. Chem. Internat. Ed.* 1966, 5, 875.
4. Bassiri, T. G.; Levy, A.; Litt, M. H. *J. Polym. Sci., Part B* 1967, 5, 871.
5. Levy, A.; Litt, M. H. *ibid* 1967, 5, 881.
6. Cai, G. F.; Litt, M. H. Article to be published.
7. Riddic, J.; Bunger, W. In *Techniques in Chemistry, Vol. 2*; Weissberger, A., Ed.; Wiley-Interscience: New York, 1970; p 801.
8. Boyce, W. E.; Di Prima, R. C. *Elementary Differential Equations*, 3rd ed.; John Wiley & Sons: New York, 1977; p 336-377.

## Chapter 5

### **Amine End-Capping of Poly(N-benzoyl ethyleneimine): An Arms-First Approach to Star-Block Oxazolines**

a) Introduction

The objective of this work is to find the path to the synthesis of well-defined star-block co-poly(N-acyl or aroylethyleneimine)s. Chapters 3 and 4 of this dissertation dealt with the core-first approach. By this we mean the method where one first grows the arms by polymerizing the first monomer onto a three or more-ended initiator, then obtains the star-block polymer by polymerizing the second monomer onto the oxazolinium chain-ends. Very narrow MWD diblock and triblock polymers were obtained when we used a one-ended initiator, methyl nosylate. However, broad-polydispersity homo- and diblock polymers resulted when we employed two- (and one three-ended) nosylate ester initiators. The broad polydispersities were attributed to a slow initiation step, compared to that of propagation, as demonstrated by studying the kinetics of the reaction of a long-alkyl core dinosylate with each of three p-substituted phenyl-oxazolines.

We therefore decided to examine the arms-first approach to producing well-defined 2-oxazoline star-polymers. This is the generation of a star by terminating the oxazolinium ends of a one-ended polymer chain with a suitable polyfunctional nucleophile. In this chapter we show the synthesis and characterization of polymers made by end-capping living poly(N-benzoylethyleneimine) chains with two primary amines, hexylamine **M**, and hexamethylenediamine **H**, under a variety of synthetic conditions.

A number of studies have recently appeared in the literature involving the termination of living poly(2-oxazoline)s by molecules containing a single





The latter reaction will probably be much slower than that of the primary amine with 1 due to steric hindrance from the attached polymer chain. This work aims at finding the conditions under which a two-ended primary amine can generate a star-shaped molecule by reaction of each end with two living poly(2-oxazoline) chains. In order to successfully make a well-defined star polymer in this fashion we have first to meet two requirements:

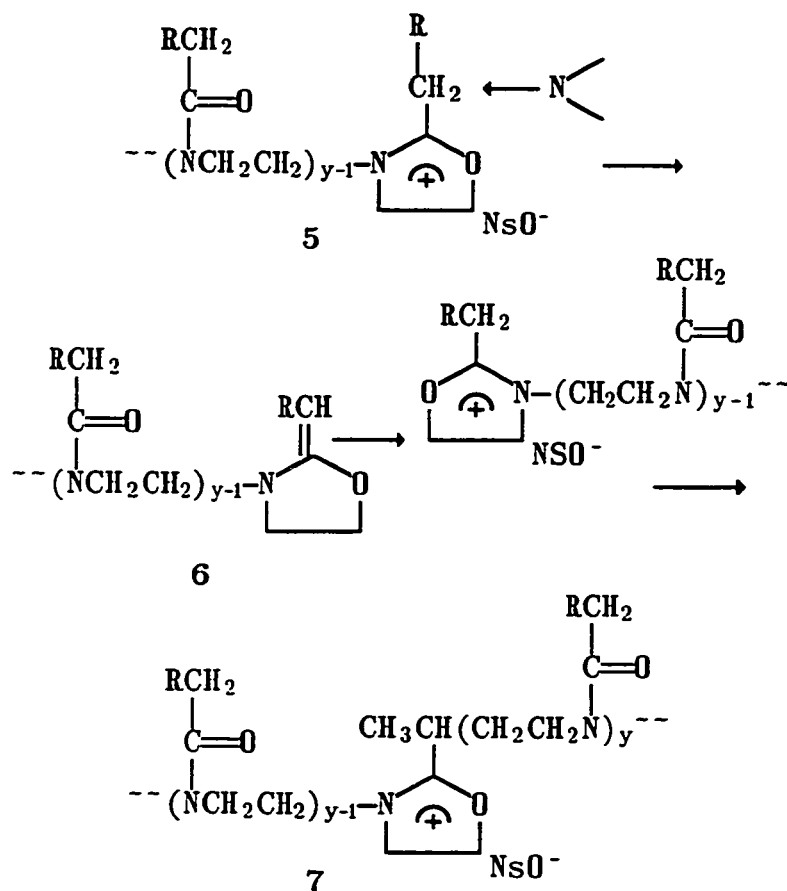
- (1) the polymer chain must have a narrow molecular weight distribution, and contain an oxazolinium-end that can not chain transfer to the amine

and,

- (2) each amine site must be available and react rapidly with a polymer chain only twice.

To meet requirement (1) we will use a good one-ended initiator, for example methyl nosylate. As demonstrated in Chapters 2 and 3 MeONs produces very narrow MWD polymers, showing that it initiates 2-oxazolines very rapidly. In order to avoid chain transfer to amine we will employ an oxazolinium-chain end that does not contain an  $\alpha$ -hydrogen on the 2-substituent. Scheme 5.1 demonstrates the possible adverse reaction sequence in the case of an  $\alpha$ -hydrogen-containing 2-substituent. At high temperatures and long reaction times the amine (most probably the secondary amine containing one polymer chain) might attack and remove the  $\alpha$ -hydrogen from the oxazolinium end. The enamine structure 5 can next repolymerize with another chain to give 6.

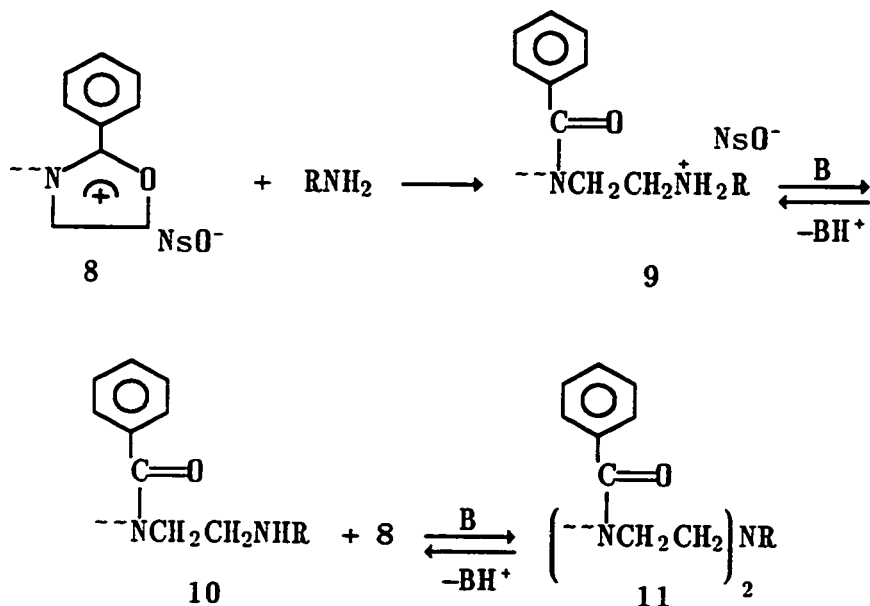
Scheme 5.1



To avoid the previous reactions we use a monomer that has an aromatic 2-substituent, or an aliphatic one which does not contain an  $\alpha$ -hydrogen. We chose 2-phenyl-2-oxazoline as a model monomer to investigate the method. However, if a particular application requires star-block polymers that contain an  $\alpha$ -hydrogen substituent on the outside block, we can first synthesize the desired  $\alpha$ -hydrogen substituent-containing block, then react its living end with several equivalents of 2-phenyl-2-oxazoline to generate 2-phenyl-2-oxazolinium-ended polymer. The latter can next react

to generate the star structure without chain transfer to the amine.

To satisfy requirement (2) we need a proton scavenger **B** to neutralize the protonated secondary amine adduct **9**:



where **8** = poly(N-benzoyl ethyleneimine)

**B** is necessary because the protonated amine **9** does not contain a lone pair of electrons on the nitrogen which can allow further reaction with an oxazolinium-end. A suitable proton scavenger is one that is basic enough to remove the proton from **9** but not able to react with **8**. We chose triisobutylamine for **B** because it is basic enough to remove protons, but non-nucleophilic because the lone-pair electron on the nitrogen is inaccessible to the polymer chains, due to strong steric hindrance from the isobutyl groups.

Additionally, to meet requirement (2) we must have an amine that

reacts with two polymer chains. Since we expect the reaction rate of 10 with 8 to be much slower than that of the primary amine with 8, we desire secondary-amine structures that will react rapidly with the oxazolinium ends. The rate of reaction is a function of the structure of the reacting chains, and the basicity of the amine. Aliphatic amines are more basic than aromatics. For example, a study on reactions of living cationic polytetrahydrofuran chains with secondary amines<sup>4</sup> has shown that the reaction rate of poly(THF) with aromatic amines such as diphenylamine or carbazole is much slower than with aliphatics, for example diethylamine. The same study also showed no further reaction to produce quaternary products. By applying these observations to our case, we decided to use a hexyl group connected to the the primary amine. The  $k_b$  of hexamethylenediamine, for example, is  $5 \times 10^{-4}$ . The high basicity should enhance the reactivity of the amine towards attack of polymer chains to the secondary amine 10, and generate the tertiary amine 11.

The organization of this chapter is as follows. First, we show results of synthesis and characterization of homopolymers made by polymerizing 2-phenyl-2-oxazoline (PO) onto methyl nosylate. The polymers are denoted by  $(P)_x$ , where  $x$  is the initial  $[PO]/[I]$  ratio. Next, we describe the reactions of hexylamine  $M$  with living  $(P)_x$  chains at different stoichiometric ratios. Using the same stoichiometric ratio we compare results at two different temperatures, room temperature and  $110^\circ\text{C}$ . The nomenclature used for these reactions is  $P_y/M$ , where  $y$  denotes the mol ratio of the polymer chain-ends to  $M$ . In the next section of this chapter, we show results obtained from the reaction of  $(P)_x$  with

hexamethylenediamine **H** to make 4-star polymers. Reactions of **H** with  $(P)_x$  were carried out in *o*-DCB and *N,N*-dimethylacetamide (DMAc) in the presence of triisobutylamine **B**. GPC is used to follow the disappearance of  $(P)_x$  with time as it reacts with the amine to produce a four-armed star. The stoichiometry of the reactants in these reactions is denoted by  $P_z/H/B_w$ , where  $z$  and  $w$  are the mol ratio of  $(P)_x$  to **H**, and **B** to **H** respectively. **H** can theoretically react up to four times with each  $(P)_x$  because it contains two primary amine groups, each reacting twice. To determine the number of polymer chains that react per **H** we carry out reactions using three stoichiometries:  $z < 4$  (deficiency of chains),  $z = 4$  (equivalence between amine and chains), and  $z > 4$  (excess of chains). The products of these reactions are then compared with the reaction product using a stoichiometry of  $z = 2.1$ . The polymers of this chapter are characterized mainly by GPC using linear monodisperse poly(*N*-benzoyl ethyleneimine) standards. Additional characterization of hexylamine-treated polymers by  $^1\text{H}$  NMR, and positive-ion Time-of-Flight Secondary Ion Mass Spectroscopy (TOF-SIMS) is given in Appendix B.  $^1\text{H}$  NMR,  $^{13}\text{C}$  NMR, and TOF-SIMS spectra of hexamethylenediamine structures are given in Appendix C.

### b) Experimental

Materials: Benzoyl chloride, ethanolamine, methyl nosylate, hexylamine, hexamethelenediamine, and DMAc were purchased from Aldrich. Triisobutylamine (reported purity over 98% ) was purchased from Fluka. o-DCB, MeOH, EtOH, diethyl ether, CHCl<sub>3</sub>, acetone, and THF were purchased from Fisher. An anion exchange resin was purchased from Biorad (AG 1-X8). This was a styrenic type (quaternary ammonium sites), and had medium pore sizes, 500-100 mesh. Its chemical effectiveness per mass unit of resin was 3.2 meq/g dry or 1.4 meq per ml of resin bed. The resin was cleaned by rinsing with 3N HCl, and stored in the chloride form.

Instrumentation: GPC samples were analyzed with a Waters Chromatograph, equipped with two GPC columns connected in series, as described in Chapter 2. THF eluted the columns at 1 mL/min, and samples were detected by RI and UV after passing through the columns, as described earlier. 200 MHz <sup>1</sup>H NMR spectra were taken on a Varian XL-200 FT-NMR spectrometer. 400 MHz <sup>1</sup>H NMR spectra, as well as the <sup>13</sup>C NMR spectrum were taken using a Bruker FT-NMR spectrometer. All NMR spectra were run in CDCl<sub>3</sub> using TMS as reference. Secondary Ion Time-of-Flight Mass spectra (TOF-SIMS) were run in cooperation with the University of Pittsburgh, and are the result of positive-ion bombardment of the polymer samples. Gas chromatograms were taken on a computerized Perkin-Elmer Model 8500 Gas Chromatograph, equipped with a Flame

Ionization Detector (FID). Samples were vaporized at 100°C at the injection port; they were then separated by passing through a hydrophobic 6 ft x 1/8 in column (Model 370-OV-17), which was heated with a 30°C/min ramping temperature starting at 100°C and ending at 250°C. The separated samples were then detected by the FID, and computer-analyzed to give integrated areas.

o-Dichlorobenzene: About 500 mL of o-DCB were stirred overnight with P<sub>2</sub>O<sub>5</sub> in a flask that was connected to a spinning band distillation column (see Chapter 2) to remove water. A forerun was then removed at the receiver port, after heating the flask under positive pressure nitrogen flow, and about 50 mL pure o-DCB (bp 179°C) was collected in a distillation receiver (see Figure 2.2b); the receiver's stopcock was then closed, and the unit was transferred and connected to the high-vacuum.

N,N-Dimethylacetamide: 500 mL DMAc was first distilled, and a middle boiling point (159.5°C) fraction of about 250 mL was collected. This was stirred overnight with CaH<sub>2</sub> to remove water and connected to the spinning-band distillation column. About 50 mL of the middle bp fraction (164.5–165°C) of pure DMAc was collected in a distillation receiver (see Figure 2.2, Chapter 2), and transferred to the vacuum rack.

2-Phenyl-2-oxazoline, (PO): PO was synthesized according to the literature<sup>5</sup>; the experimental procedure is described in Chapter 4. The purity of the solid crystalline PO was over 99.9% by GC.

Hexylamine, M: 98% M was stirred with Na/benzophenone in a flask which was connected to the high vacuum by an adapter, shown in Figure 2.2b of Chapter 2. The deep blue-colored solution was degassed, and M distilled on the high vacuum system into a storage vessel, which is shown in Figure 2.2a. A sample of M was removed with nitrogen flow by syringe from the flask; analysis by GC and  $^1\text{H}$  NMR showed no impurities.

Hexamethylenediamine (H) stock solutions in o-DCB and DMAc: Stock solutions of H were prepared in the following way: 10–20 g of H was loaded in a flask and attached to the spinning band distillation column. A 10–15 g forerun was removed at  $204^\circ\text{C}$  under nitrogen purge; the receiver flask was removed and a flask graduated in 0.5–mL was connected to the receiver outlet via a joint compatible with that of the outlet. Nitrogen was then directed into the flask through a syringe needle, inserted through a septum that covered the opening of a side-arm on the graduated flask. About 1 mL of H, bp  $204^\circ\text{C}$  was then collected, and the flask was removed and capped with a stopper under a strong flow of nitrogen. The collected mass of H, was found to be .8216 g by weighing the flask before and after transfer. Under nitrogen, a 10–mL syringe was used to remove 7.3 mL of DMAc from a distillation receiver attached to the high-vacuum line. The content of the syringe was then injected into the H-containing flask; the transferred mass was found 6.83 g by weighing the syringe before and after injection. H was then dissolved by shaking, and another syringe was used to transfer the colorless clear solution into a receiver attached on the vacuum rack. The concentration of H was calculated to be 10.74 g /100 g



of solution. A 5.52 g/100 g stock solution of H in o-DCB was prepared in the same way.

Purification:

Great care was taken to purify the polymers that are discussed in this chapter in order to remove salts that resulted during the synthesis, which interfered with GPC analysis and NMR spectral identification of the products. A general purification procedure was therefore developed for the final polymers of the reactions described, as well as for aliquots taken from the corresponding reaction mixtures at different times. The purification method is described in detail in Appendix A.

Kinetics of 2-phenyl-2-oxazoline (PO) polymerization in o-DCB to make (P)<sub>5.7</sub>: 1.6430 g ( $7.564 \times 10^{-3}$  mol) CH<sub>3</sub>ONs was loaded into a polymerization flask (see Figure 2.1 and 2.3) and placed on the vacuum rack. The system was evacuated to  $3 \times 10^{-5}$  torr, after which the vacuum pump was isolated and positive pressure of nitrogen was applied. About 20 mL o-DCB were removed by syringe from a unit on the rack and injected into the polymerization unit. The exact weight of transferred o-DCB was found by difference to be 26.09 g (20.07 mL at 20°C). The solid was dissolved by stirring at room temperature to give a yellowish solution, and cooling water was directed through the unit's condenser. 5.6 mL was then removed from the PO unit on the vacuum rack using a 10-mL syringe, after thawing the PO with a warm (ca. 35°C) water container. The syringe was next weighed and its contents were injected

into the polymerization flask. The delivered PO was found to be 6.30 g ( $4.29 \times 10^{-2}$  mol) by weighing the syringe after delivery. The  $[\text{PO}]/[\text{I}]$  mol ratio was thus 5.7, and  $[\text{I}]$  was 0.277 mol/L. A 0.1 mL aliquot was then removed, and a stirred 108°C oil-bath raised to cover the flask. 0.1 mL aliquots were removed at 17.5, 47.3, 72.5 and 111.7 min, and analyzed by GC within a few minutes after removal from the flask. The chromatograms showed well-separated peaks of o-DCB and unreacted PO, whose areas were obtained by computer-integration. Neither polymer nor methyl nosylate peaks were evident in the GC profiles. Comparison of the GPC chromatogram of the initial mixture with that of the 17.5-min aliquot showed no evidence of methyl nosylate in the latter, confirming its complete consumption by that time. The solution was stirred for a total of 117 min to polymerize all PO; the resulting living polymer was named  $(\text{P})_{5.7}$ .

$\text{P}_{1.0}/\text{M}$  reaction using  $(\text{P})_{5.7}$  in o-DCB at 108 °C: Under stirring, 1.00 mL ( $7.57 \times 10^{-3}$  mol) of distilled M was injected into the  $(\text{P})_{5.7}$  solution using a 1 mL syringe graduated to 0.01 mL. The mol ratio of M to (MeONs) was thus 1.00, and the reaction is hence named  $\text{P}_{1.0}/\text{M}$ . The concentration of  $(\text{P})_{5.7}$  in the solution was 23 g/100 mL. The yellowish clear solution was stirred for a total of 24 h at 108°C. During that period aliquots were removed at 2.1, 11.5, 43.4, 77.9, 115.6, 180.4, 218.0, 667.4, and 1440 min, and analyzed by GC. The 2.1 min did not show a peak due to remaining M, indicating 100% conversion of the latter by that time.

(PO) polymerization in DMAc at 117 and 127 °C to synthesize (P)<sub>20.9</sub> and (P)<sub>49.2</sub>: A procedure similar to the one followed for PO polymerization in o-DCB at 110°C was carried out to find the  $k_p$  of PO in DMAc at 117 and 127°C. Thus 0.0595 g ( $2.739 \times 10^{-4}$  mol) and 0.1478 g ( $6.805 \times 10^{-4}$  mol) of CH<sub>3</sub>ONs were reacted with 1.98 ( $1.35 \times 10^{-2}$  mol) and 2.09 g ( $1.42 \times 10^{-2}$  mol) of PO for [PO]/[I] ratios of 49.2 and 20.9 at 127 and 117°C respectively. The initiator concentrations were 0.0232 and 0.0587 mol/L. Aliquots of the reaction mixture were removed at different times, and analyzed by GC. The solutions were stirred for a total of 10.67 and 8.35 h respectively, at which times the GC aliquots showed over 99.5% conversion of PO. The resulting (P)<sub>20.9</sub> and (P)<sub>50.2</sub> polymers were then precipitated and purified to give white powders according to the method described in Appendix A.

P<sub>1.0</sub>/M reaction using (P)<sub>4.8</sub> in o-DCB at 28 °C, and 117 °C: Living (P)<sub>4.8</sub> polymer was made similarly to the (P)<sub>5.7</sub> mentioned above using the following experimental conditions: 1.6430 g ( $7.5645 \times 10^{-3}$  mol) MeONs was degassed to  $1.0 \times 10^{-5}$  torr, the system was purged with nitrogen and 20.85 mL (27.11 g) of o-DCB was injected to dissolve the solid. 5.37 g ( $3.65 \times 10^{-2}$  mol) of PO was then injected into the solution of MeONs. The total volume was 27.5 mL, [I] was 0.276 mol/L, and the [PO]/[I] ratio was 4.8. A 0.1-mL aliquot was then removed and analyzed by GC and GPC. The mixture was stirred at 110°C for 125 min, and a second 0.1-mL aliquot was removed and analyzed. GC of the latter showed greater than 99% conversion of PO, based on the ratio of the PO and

*o*-DCB peak areas divided by the same ratio in the initial solution. The (P)<sub>4.8</sub> solution was then cooled to room temperature by turning off the heater, and a 1-mL syringe was used to inject 0.98 mL (0.75 g,  $7.41 \times 10^{-3}$  mol) M with stirring. The mol ratio of (MeONs) to M was thus 1.02, and the reaction stoichiometry is therefore named P<sub>1.0</sub>/M. The concentration of (P)<sub>4.8</sub> in the solution was 20 g/100 mL. A thermometer, with graduations every 0.01°C, was immersed in the oil bath to monitor solution temperature before and after injection of the amine. The temperature rose from 28.9°C immediately before injection of M to a maximum of 29.6°C by 10–12 min after injection, then gradually equilibrated to 28.2°C. One mL aliquots were removed from the transparent yellow reaction solution 9, 48, 110, and 753 min after M injection, and analyzed by GC within 5 min of removal from the solution. The 9-min aliquot showed only a minute peak of unreacted M, which was not evident in the profile of the 48-min aliquot. The solution was stirred at 28.2°C for about 22 h; then an 8-mL sample was removed from the reaction mixture, precipitated, and purified, as previously described. The remaining solution was then heated to 117°C, and more aliquots were removed after 10, 40, 80, 120, 225, 303, 720, and 2220 min (37 h) of stirring at 117°C. The solution was then removed from the rack, and the polymer was precipitated and purified, as shown in Appendix A.

P<sub>0.5</sub>/M reaction using (P)<sub>10.2</sub> in *o*-DCB at 110 °C: This reaction was carried out similarly to that of P<sub>1.0</sub>/M using (P)<sub>5.7</sub> in *o*-DCB at 108°C. 0.8240 g ( $3.808 \times 10^{-3}$  mol) of MeONs was evacuated to  $2 \times 10^{-5}$  torr, and

stirred with 5.78 g ( $3.93 \times 10^{-2}$  mol) of PO under nitrogen in 21.2 mL o-DCB at 110°C for 200 min. The [PO]/[I] ratio was thus 10.2, and the initial [I] 0.141 mol/L. To the resulting (P)<sub>10.2</sub> was added 1.00 mL ( $7.57 \times 10^{-3}$  mol) of M. The mol ratio of (MeONs) to M was thus 0.50, and the reaction stoichiometry is named P<sub>0.5</sub>/M. The concentration of (P)<sub>5.7</sub> in the solution was 23 g/100 mL. The resulting clear solution was stirred for a total of 13 h at 110°C. Aliquots were taken just before injection of M, and 3 and 788 min later. GC analysis of the 3-min sample revealed that the ratio of areas of unreacted M and o-DCB was about the same as the corresponding ratio at 788 min. We were not able to obtain the exact ratios because the peak of M was very small compared to that of o-DCB and the two peaks overlapped.

Triisobutylamine, B: This was stirred for 24 h with Na/benzophenone to remove water, then distilled similarly to N,N-dimethylacetamide using a spinning band distillation column operating under nitrogen. A forerun was removed at about 185–190°C, then B was collected at 190°C in a distillation receiver which was next transferred to the vacuum rack (reported bp 189–191°C at 760 torr). A 200 MHz <sup>1</sup>H NMR spectrum of purified B was taken; the peaks were at  $\delta$  0.89 ppm (d, 18H, J = 8, (CH<sub>3</sub>)<sub>2</sub>-CH-),  $\delta$  1.79 ppm (complex, 3H, (CH<sub>3</sub>)<sub>2</sub>-CH-CH<sub>2</sub>-N-), and  $\delta$  2.04 ppm (d, 6H, -CH-CH<sub>2</sub>-N-).

Experiment to test that living (P)<sub>x</sub> chains do not react with B: (P)<sub>5.1</sub> was first made by polymerizing 1.6550 ( $7.620 \times 10^{-3}$  mol) CH<sub>3</sub>ONs and 5.71 g

PO ( $3.89 \times 10^{-2}$  mol) in 20.3 mL *o*-DCB for 52 min at 110°C. 0.92 mL of B was injected into the solution and 0.5 mL of M was injected 66 min later. The obtained polymer was purified according to the method described in Appendix A. A 200 MHz  $^1\text{H}$  NMR spectrum showed no doublet peaks at  $\delta$  0.90 and 2.04 ppm, nor a peak due to  $-\overset{\cdot}{\text{N}}\text{H}(\text{CH}_2)$ , thus showing that B did not react at all with (P)<sub>5.1</sub> during the 66 min before the injection of M.

P<sub>3.5</sub>/H/B<sub>2.0</sub> reaction using (P)<sub>8.6</sub> in *o*-DCB at 121 °C: 1.0340 g ( $4.760 \times 10^{-3}$  mol) of MeONs was evacuated to  $1.0 \times 10^{-5}$  torr, then 16.02 mL of *o*-DCB was injected under nitrogen, and the solid dissolved by stirring at room temperature. 6.04 g ( $4.11 \times 10^{-2}$  mol) of PO was then injected into the stirring solution and polymerized at 121°C for 215 min. The [PO]/[I] ratio was 8.6, and [I] was 0.191 mol/L. A 0.5-mL aliquot of the resulting (P)<sub>8.6</sub> solution was removed, purified, and analyzed by GPC. 0.54 g ( $2.90 \times 10^{-3}$  mol) of B was transferred from a flask containing distilled B into another flask on the rack. To the latter flask was also added 2.97 g of the 5.52 g/100 g stock solution of H in *o*-DCB for a total weight of 3.51 g. 3.27 g of the resulting mixture was then injected into the (P)<sub>8.6</sub> solution. The calculated weight of injected H was 0.153 g ( $1.32 \times 10^{-3}$  mol), and that of B 0.503 g, ( $2.71 \times 10^{-3}$  mol). The total volume of the (P)<sub>8.6</sub> solution was 22.1 mL; thus the 0.5 mL aliquot reduced the prepolymer solution volume by about 2.2%. The stoichiometric ratios of (P)<sub>8.6</sub>, and B, to H were then calculated from the initial initiator concentration, taking into account the removal the (P)<sub>8.6</sub>. Thus,

$P/H = (4.760 \times 10^{-3} \text{ mol}) / (1.32 \times 10^{-3} \text{ mol})(1 - 0.022) = 3.53,$  and  
 $B/H = (2.71 \times 10^{-3} \text{ mol}) / (1.32 \times 10^{-3} \text{ mol})(1 - 0.022) = 2.04.$  From the stoichiometric ratios we thus name the reaction  $P_{3.5}/H/B_{2.0}$ . The total solution volume after injection of H and B was 24.2 mL; hence the polymer concentration was about 24 g/100 mL. Aliquots of the transparent-yellowish solution were removed periodically, purified, and analyzed by GPC. A white cloudy precipitate appeared in the reaction mixture between 2 and 4 hours. The solution was stirred for a total of 40.5 h; then the resulting polymer was precipitated in ethyl ether and purified as described in Appendix A.

$P_{4.0}/H/B_{7.9}$  reaction using  $(P)_{10.5}$  in DMAc at 125 °C: 1.0333 g ( $4.757 \times 10^{-3}$  mol) of methyl nosylate was reacted with 7.32 g ( $4.98 \times 10^{-2}$  mol) of PO in 11.62 g (12.4 mL) DMAc at 125°C for 128 min. The initial [I] was 0.239 mol/L and the [PO]/[I] 10.5. 1.75 g ( $9.44 \times 10^{-3}$  mol) of B was then added to the clear light yellow solution of  $(P)_{10.5}$ , and a 0.5 mL aliquot was removed from the resulting transparent solution. The aliquot turned cloudy upon cooling to room temperature, and separated upon standing into two phases: a small colorless phase on top, and a large light-yellow phase in the bottom. 1.29 g of a 10.74 g/100 g stock solution of H in DMAc was then injected into the stirring solution of  $(P)_{10.5}$  and B. The calculated weight of injected H was 0.1386 g ( $1.192 \times 10^{-3}$  mol). The stoichiometric ratios of  $(P)_{10.5}$  to H and B to H were then calculated from the initial initiator concentration,  $(4.757 \times 10^{-3} \text{ mol}) / (1.192 \times 10^{-3} \text{ mol}) = 4.0,$  and

$(9.44 \times 10^{-3} \text{ mol}) / (1.192 \times 10^{-3} \text{ mol}) = 7.9$  respectively. The nomenclature is thus  $P_{4.0}/H/B_{7.9}$ . The total solution volume was ca. 23.0 mL, and the polymer concentration was about 32 g/100 mL. Aliquots of the solution were removed periodically, purified, and analyzed by GPC. The clear solution was stirred for a total of 96.1 h, while the color gradually turned to dark yellow. Upon cooling to room temperature the solution first turned cloudy and then separated into two phases; a small colorless phase on top, and a large dark yellow lower phase. The relative proportions were similar to those of the initial aliquot of  $(P)_{10.5}$  and B. The  $P_{4.0}/H/B_{7.9}$  mixture was then purified using the standard procedure, Appendix A.

$P_{4.3}/H/B_{8.8}$  reaction using  $(P)_{10.0}$ , and  $P_{2.1}/H/B_{8.4}$  using  $(P)_{10.2}$ , in DMAc at 125 °C: These reactions procedures were similar to that of  $P_{4.0}/H/B_{7.9}$ . The quantities used are summarized in Table 5.1.



Table 5.1. Experimental quantities and conditions of the P<sub>4-3</sub>/H/B<sub>8-8</sub>, and P<sub>2-1</sub>/H/B<sub>8-4</sub> reactions in DMAc at 125 °C.

	P <sub>4-3</sub> /H/B <sub>8-8</sub>	P <sub>2-1</sub> /H/B <sub>8-4</sub>
MeONs	0.7387 g (3.401 x 10 <sup>-3</sup> mol)	0.7381 g (3.3983 x 10 <sup>-3</sup> mol)
DMAc	9.33 g (9.96 mL)	9.32 g (9.95 mL)
PO	4.99 g (3.39 x 10 <sup>-2</sup> mol)	5.09 g (3.46 x 10 <sup>-2</sup> mol)
B	1.29 g (6.96 x 10 <sup>-3</sup> mol)	2.54 g (1.37 x 10 <sup>-2</sup> mol)
H/DMAc	0.86 g	0.19 g
Δt <sub>1</sub>	1.07 h	1.10 h
Δt <sub>2</sub>	92.50 h	92.50

Here Δt<sub>1</sub> and Δt<sub>2</sub> are the the stirring times before and after injection of the H/DMAc solution. H/DMAc denotes a 10.74 g H/100 g stock solution. From the above table we then calculate the parameters, shown in Table 5.2.

Table 5.2. Parameters of the  $P_{4.3}/H/B_{8.8}$ , and  $P_{2.1}/H/B_{8.4}$  reactions in DMAc at 125 °C.

	$P_{4.3}/H/B_{8.8}$	$P_{2.1}/H/B_{8.4}$
$(V_{tot})_1$	9.96 mL	15.19 mL
[I]	0.225 mol/L	0.224 mol/L
[PO]/[I]	9.98	10.19
$(V_{tot})_2$	17.70 mL	20.10 mL
$(P)_x/H$	4.29	2.08
B/H	8.78	8.41
(P)	28 g/100 mL	25 g/100 mL

Here  $(V_{tot})_1$  and  $(V_{tot})_2$  are the solution volumes before and after injection of B and H/DMAc. Both reactions exhibited phase separation after cooling to room temperature, similar to that of  $P_{4.0}/H/B_{7.9}$ .

c) Results and Discussion

Determination of the propagation rate constant  $k_p$  of PO in o-DCB and in DMAc.

In order to synthesize living prepolymer  $(P)_x$  chains and react them with hexylamine M and hexamethylenediamine H we first need to determine the propagation rate constant  $k_p$  of 2-phenyl-2-oxazoline PO in the solvents that we will use, namely o-DCB and DMAc. This helps us to estimate the exact time before amine addition of the  $(P)_x$  solutions, that is after the complete consumption of PO. We therefore followed the disappearance of PO with time using methyl nosylate initiator (I) in both o-DCB and DMAc. Assuming fast initiation, we have equation (1) for the rate of PO disappearance, based on first-order kinetics<sup>6</sup>:

$$-d[PO]/dt = k_p[I][PO] \quad (1)$$

or after integration:

$$-\ln([PO]/[PO]_0) = k_p[I]\Delta t \quad (2)$$

$k_p$  can be found by plotting  $-\ln([PO]/[PO]_0)/[I]$  versus  $\Delta t$ . Since the concentration of solvent in the reaction mixture is constant, we can calculate the conversion of PO at different times by normalizing the GC area of unreacted PO to the area of the solvent, using Equation (3):

$$[PO]/[PO]_0 = \frac{A_{PO}/A_S}{(A_{PO}/A_S)_0} \quad (3)$$

where the numerator denotes the ratio of the area of remaining PO to that of solvent at time t, and the denominator is the corresponding ratio at time 0. Table 5.3 gives the chromatographic data and calculations on the

disappearance of PO with time in o-DCB at 108°C, using the initial [PO]/[I] ratio of 5.7 ([I] = 0.277 mol/L)

Table 5.3: Synthesis of (P)<sub>5-7</sub> in o-DCB at 108 °C using an [I] of 0.277 mol/L

$\Delta t \times 10^{-3}$ (s)	$A_{PO}/A_S$	$[PO]/[PO]_0$	$-\ln([PO] / [PO]_0)/[I]$ ( L/mol )
0	0.1943	1	0
1.050	0.0874	0.4498	2.884
2.838	0.0228	0.1173	7.735
4.350	0.0136	0.0070	9.600
4.350	0.0132	0.0068	9.708

Figure 5.1 shows the plot of  $-\ln([PO]/[PO]_0)/[I]$  from Table 5.1 versus  $\Delta t$ . The 4350 s aliquot was not included in the linear regression because the peak of PO in was much smaller than that of o-DCB and overlapped with the tail of the latter. From equation (2),  $k_p$  is given by the slope of the straight line, 0.0027 L/(mol.s).

Tables 5.4 and 5.5 give the chromatographic data and calculations on the disappearance of PO in DMAc with time, using initial [PO]/[I] ratios of 20.9 and 49.2 at 117 and 127°C respectively.

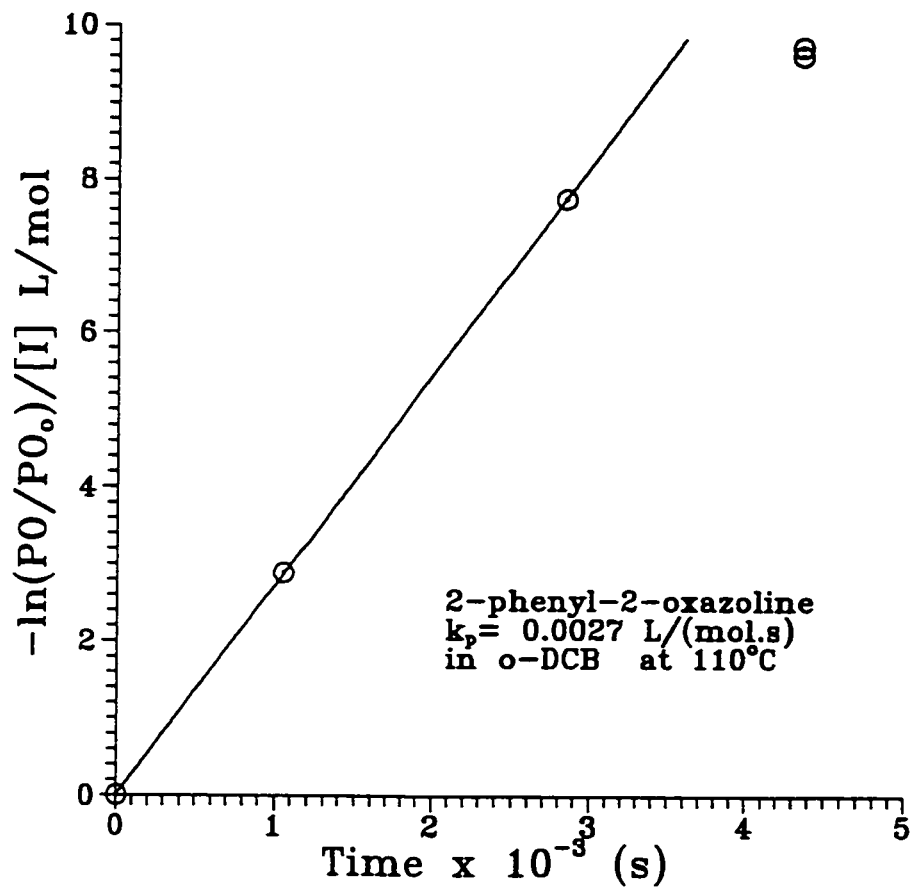


Figure 5.1. First-order plot of remaining 2-phenyl-2-oxazoline vs time at 108 °C in o-dichlorobenzene for 0.277 mol/L of methyl nosylate.

Table 5.4: Synthesis of (P)<sub>20-9</sub> in DMAc at 117 °C using an [I]<sub>0</sub> of 0.0587 mol/L

$\Delta t \times 10^{-3}$ (s)	$A_{PO}/A_S$	$[PO]/[PO]_0 - \ln([PO] / [PO]_0) / [I]$ ( L/mol )	
0	0.3656	1	0
5.700	0.1471	0.4022	15.52
9.360	0.0676	0.1849	28.78
12.720	0.0403	0.1102	37.57
25.200	0.0142	0.0388	55.35

Table 5.5: Synthesis of (P)<sub>49-2</sub> in DMAc at 127 °C using an [I]<sub>0</sub> of 0.0232 mol/L

$\Delta t \times 10^{-3}$ (s)	$A_{PO}/A_S$	$[PO]/[PO]_0 - \ln([PO] / [PO]_0) / [I]$ ( L/mol )	
0	0.3656	1	0
5.820	0.1898	0.4045	39.01
12.660	0.0842	0.1795	74.03
24.900	0.0284	0.0605	120.84

From the slope of the straight lines in Figures 5.2 and 5.3 we obtain  $k_p(117) = 0.0030$  and  $k_p(127) = 0.0060$  L/(mol.s). Matsuda (Reference 6,

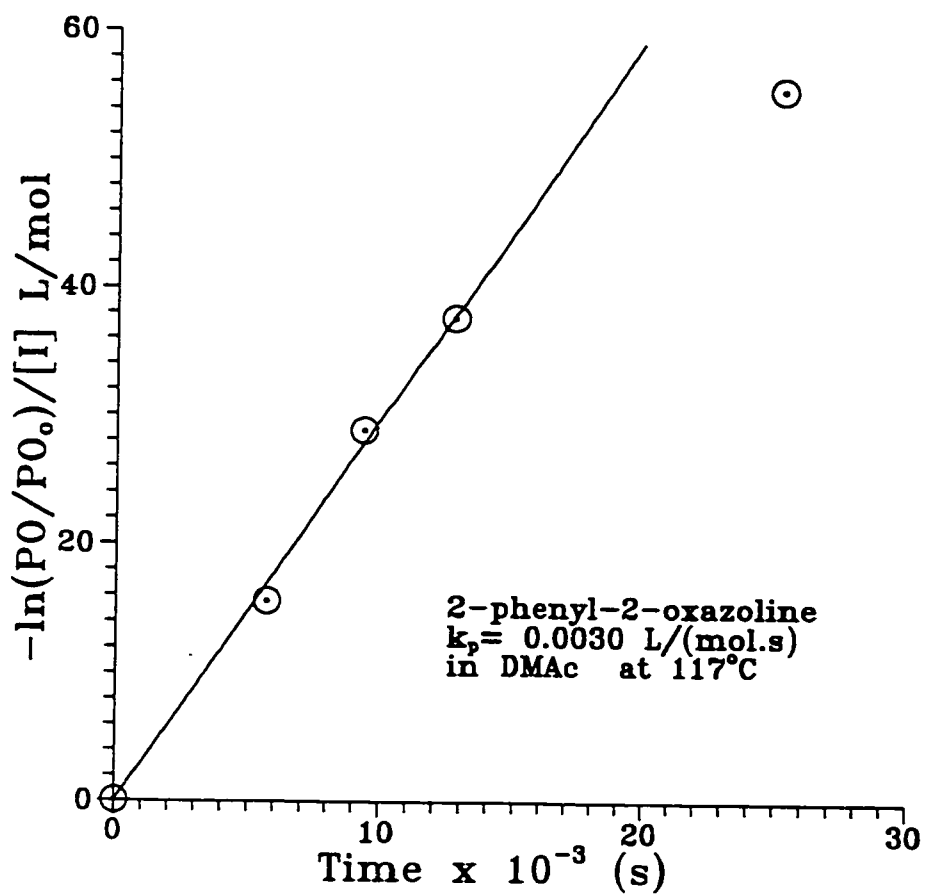


Figure 5.2. First-order plot of remaining 2-phenyl-2-oxazoline vs time at 117 °C in N,N-dimethylacetamide for 0.0587 mol/L of methyl nosylate.

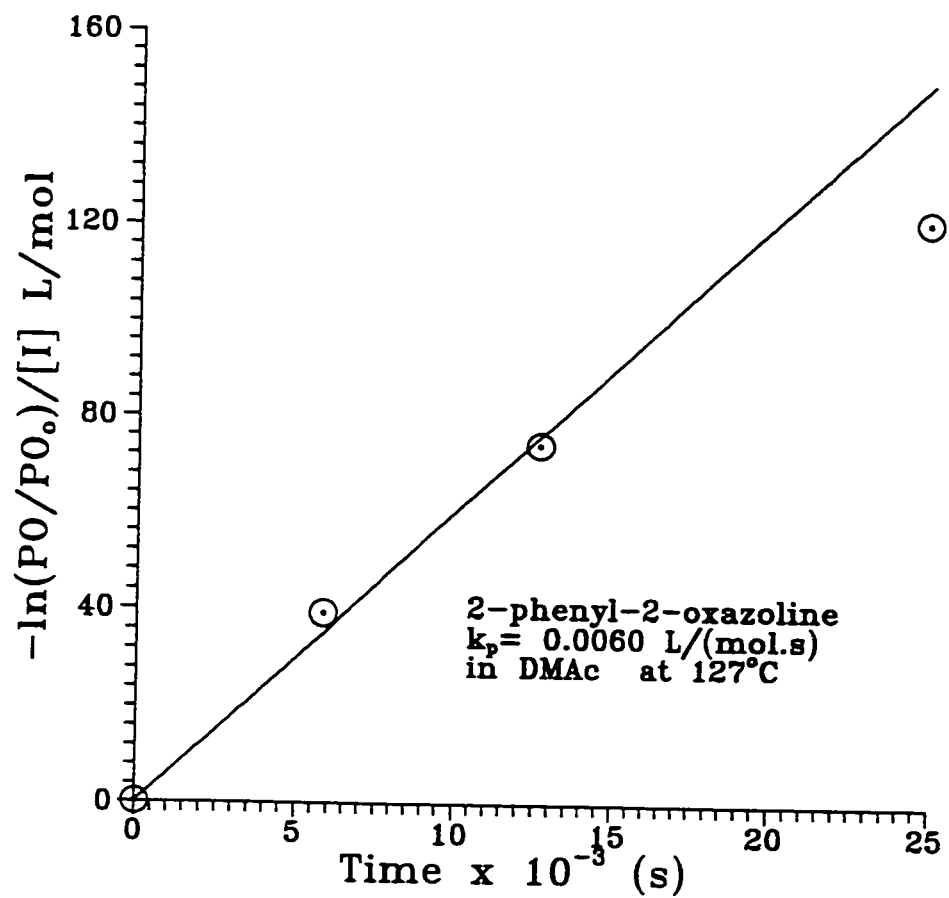


Figure 5.3. First-order plot of remaining 2-phenyl-2-oxazoline vs time at 127 °C in N,N-dimethylacetamide for 0.0232 mol/L of methyl nosylate.

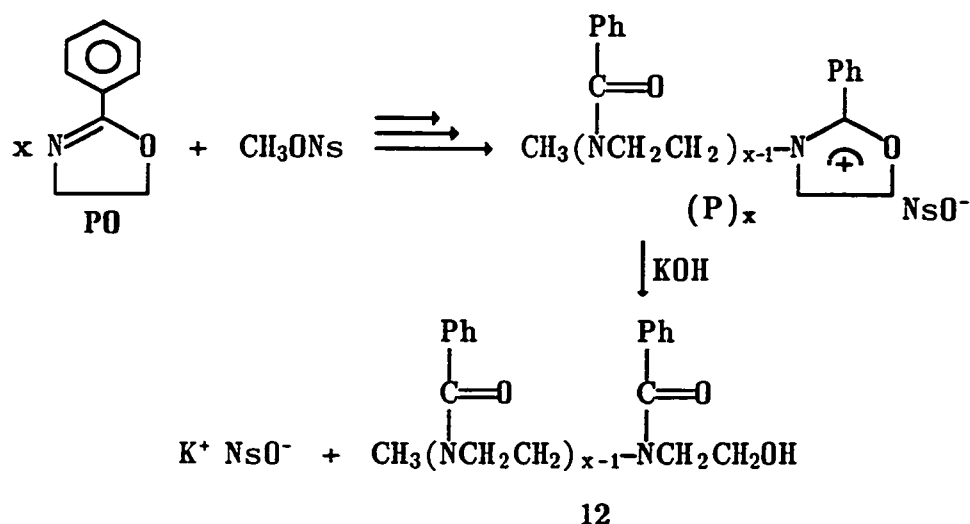


p 102) reports values of  $k_p$  for N-methyl-2-phenyl-2-oxazolinium perchlorate-initiated PO in DMAc of 2.39, 0.690, and 0.250 (L/(mol.min)) at 150, 135, and 120°C respectively. An Arrhenius plot of the above values ( $\ln k_p$  vs  $1/T$ ) gives an activation energy  $E_\alpha$  of 103.5 kJ/mol and an A factor of  $2.271 \times 10^{11}$ . From the relationship  $k_p = A.e^{-E_\alpha/RT}$  we then calculate  $k_p(117) = 0.0031$ , and  $k_p(127) = 0.0069$  L/(mol.s). These values are 3% and 15% higher than our values and should be considered the same within experimental error, due to the small number of points used in our analysis.

For the remaining experiments we calculated the reaction times for 99.5% conversion of PO using the  $k_p$  values obtained from Figures 5.1-5.3.

#### Synthesis and Characterization of (P)<sub>x</sub>

A series of (P)<sub>x</sub> standards was made by polymerizing PO onto methyl nosylate with the corresponding [PO]/[I] ratios x. These polymers were purified by treating with a pH 14 solution of potassium hydroxide in ethanol to neutralize the oxazolinium-nosylate ended polymers, as shown below:



where  $x = 4.8$  (12a),  $10.3$  (12b),  $20.9$  (12c), and  $50.2$  (12d).

Potassium nosylate salt was removed by first treating the polymers with an anion exchange resin; the produced KOH was then removed with a mixed bed resin, as described in Appendix A.

#### Time-of-Flight characterization of the polymers in the (P)<sub>x</sub> series.

Figure 5.4 shows the positive ion Time-of-Flight Secondary Ion Mass (TOF-SIMS) spectrum of 12a. The peak intensities indicate the number of molecules corresponding to the particular mass. On examining the mass spectrum from right to left one notes that there are sets of equidistant peaks, each set separated from the other by a fixed interval. If we compare within the same set the height of each peak to the height of the corresponding peak in the next interval, we observe two distributions of masses. The higher mass peak distribution in each set has its maximum intensity at about 1,500, while the lower mass distribution mass shows a maximum at about 1,800. The intensities of the former distribution are

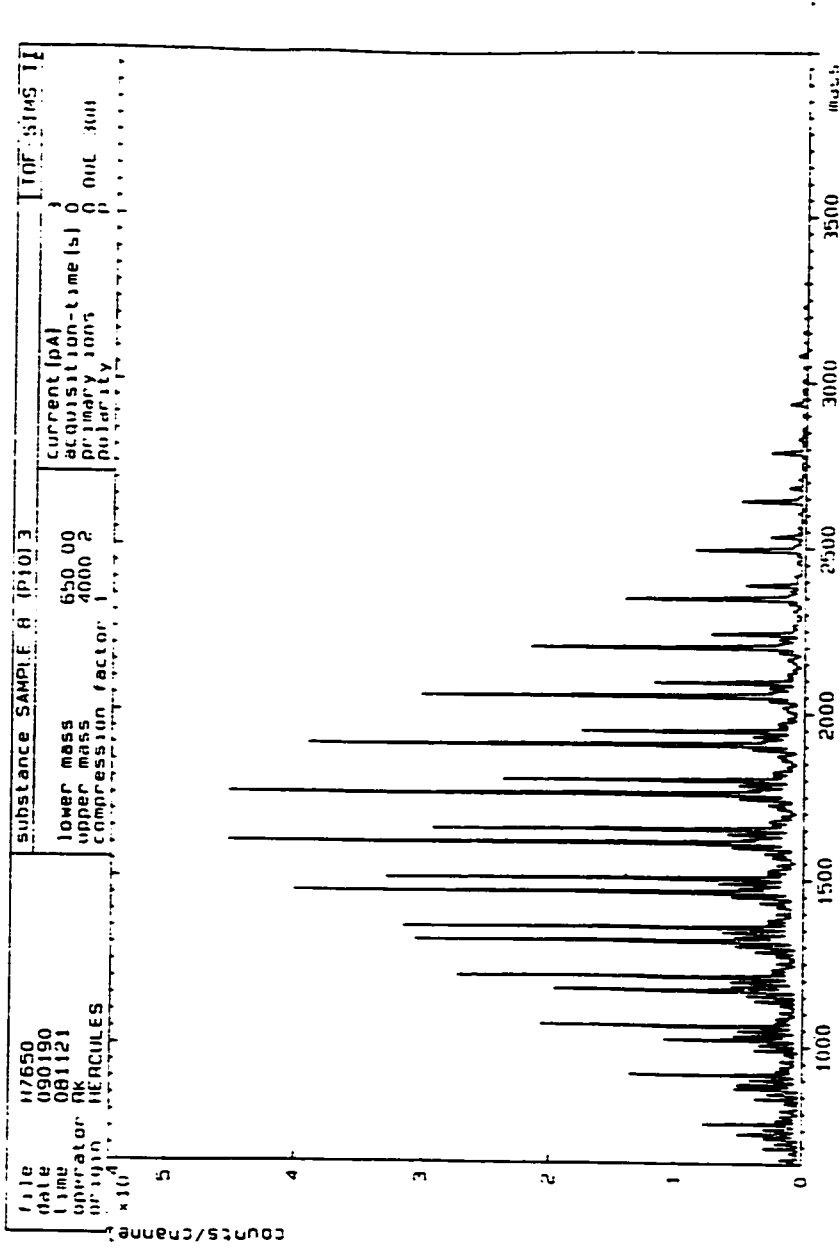


Figure 5.4. TOF-SIMS spectrum of purified (P)<sub>10-3</sub>.

lower than those of the latter at high molecular masses until about 1350, as shown in Figure 5.4.

$(P)_x$  is comprised of a distribution of N-benzoylethyleneimine repeat units. Let  $n$  denote the number of repeat units and  $f(n)$  the corresponding number fraction of molecules in the distribution.  $f(n)$  is equal to the intensity of each peak divided by the total intensity. The mass of each N-benzoylethyleneimine repeat based on the masses of the isotopes  $^1\text{H}$ ,  $^{12}\text{C}$ ,  $^{14}\text{N}$ , and  $^{16}\text{O}$ , plus a small natural abundance of  $^2\text{H}$ ,  $^{13}\text{C}$ ,  $^{15}\text{N}$ , and  $^{17}\text{O}$ , is 147.18. We assign each set of peaks of the TOF-SIMS spectrum of  $(P)_{10-3}$  to the corresponding  $n$  by dividing the particular masses by 147.18, and taking the closest integer value. Table 5.6 shows the peak masses and intensities of each distribution, from Figure 5.5.

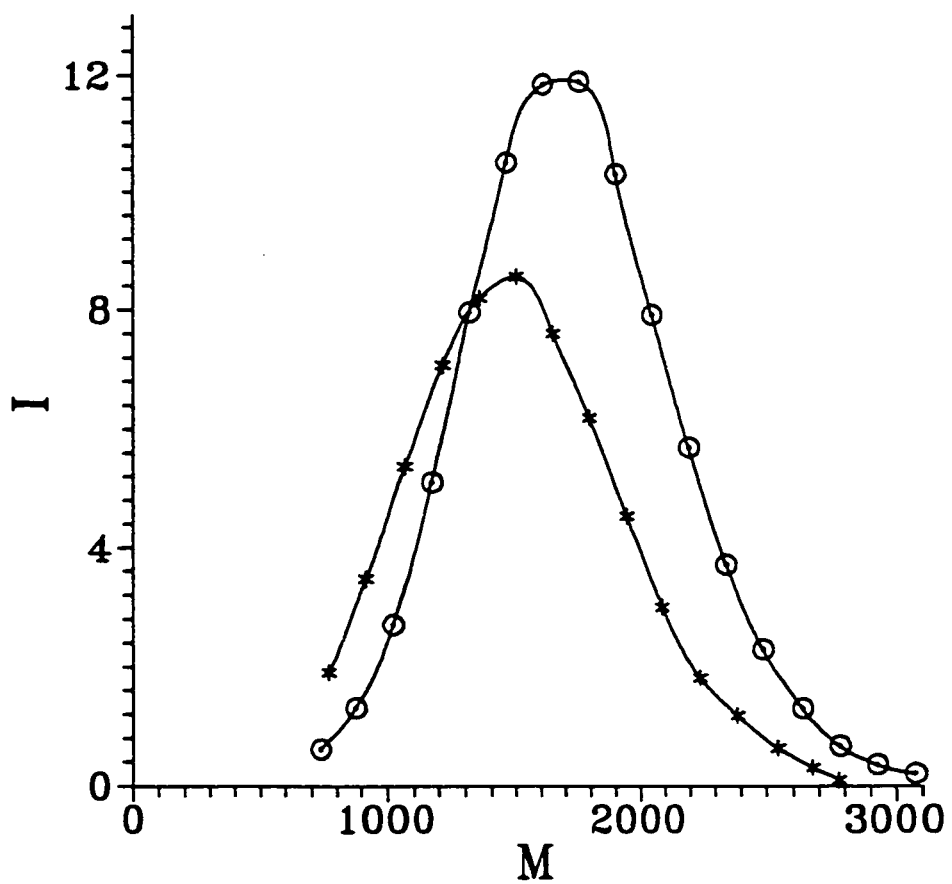
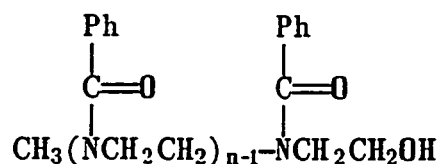


Figure 5.5. Profiles of the mass distributions corresponding to the high- (circles), and low-intensity peaks (stars) of the spectrum of  $(P)_{10-3}$ , shown in Figure 5.4.

Table 5.6. Molecular masses and intensities of the high, and low distributions from the TOF-SIMS spectrum of (P)<sub>10-3</sub> at repeat units n.

n	MW <sub>high</sub>	I <sub>high</sub> (cm)	MW <sub>low</sub>	I <sub>low</sub> (cm)
5	720	0.61	770	1.90
6	880	1.30	920	3.47
7	1020	2.70	1070	5.37
8	1180	5.10	1220	7.07
9	1320	7.95	1360	8.20
10	1470	10.50	1510	8.56
11	1620	11.83	1660	7.60
12	1760	11.88	1800	6.19
13	1910	10.30	1960	4.53
14	2050	7.90	2100	3.00
15	2210	5.68	2260	1.81
16	2350	3.70	2400	1.18
17	2500	2.28	2570	0.63
18	2650	1.29	2700	0.30
19	2790	0.66	2800	0.10
20	2950	0.35		
21	3090	0.20		
$\Sigma(I(n))$		84.23		59.91

Figures 5.6 and 5.7 show plots of  $MW_{\text{high}}$  and  $MW_{\text{low}}$  vs  $n$  respectively. The slopes of the straight lines give the average mass differences between the corresponding peaks of neighboring sets. The  $147.6 \pm .1$  and  $147.3 \pm .2$  values of the distributions of high and low peaks respectively are very close to the 147.18 value of the N-benzoyl ethyleneimine repeat mass and are considered the same within experimental error. From the intercepts of the straight lines of Figures 5.6 and 5.7, we can obtain information on the chemical structure of the chain ends. The  $35.3 \pm 1.2$  intercept of the distribution of low peaks suggests a structure:



This has a molecular mass of  $(147.18)n + 32$ . Therefore these must be considered the unfragmented peaks of the  $(P)_{10-3}$  distribution. The distribution of high peaks gives an intercept of  $-10.4 \pm 0.7$ . Since these peaks are the lower mass peaks of each set they might correspond to fragmentation of the parent chains by the positive-ion beam at the  $\beta$ -carbon bond from the hydroxyl-end. Fragmentation of the  $-\text{CH}_2\text{CH}_2\text{OH}$  gives a mass smaller than that of the parent peak by 44, which is close to the value of  $35 - (-10) = 45$ , calculated from the difference of the two intercepts.

$f(n)$  is calculated by dividing the peak intensities  $I(n)$  by the total intensity  $\sum_{n=0}^{\infty} I(n)$ . The total intensity of the high peaks is found by

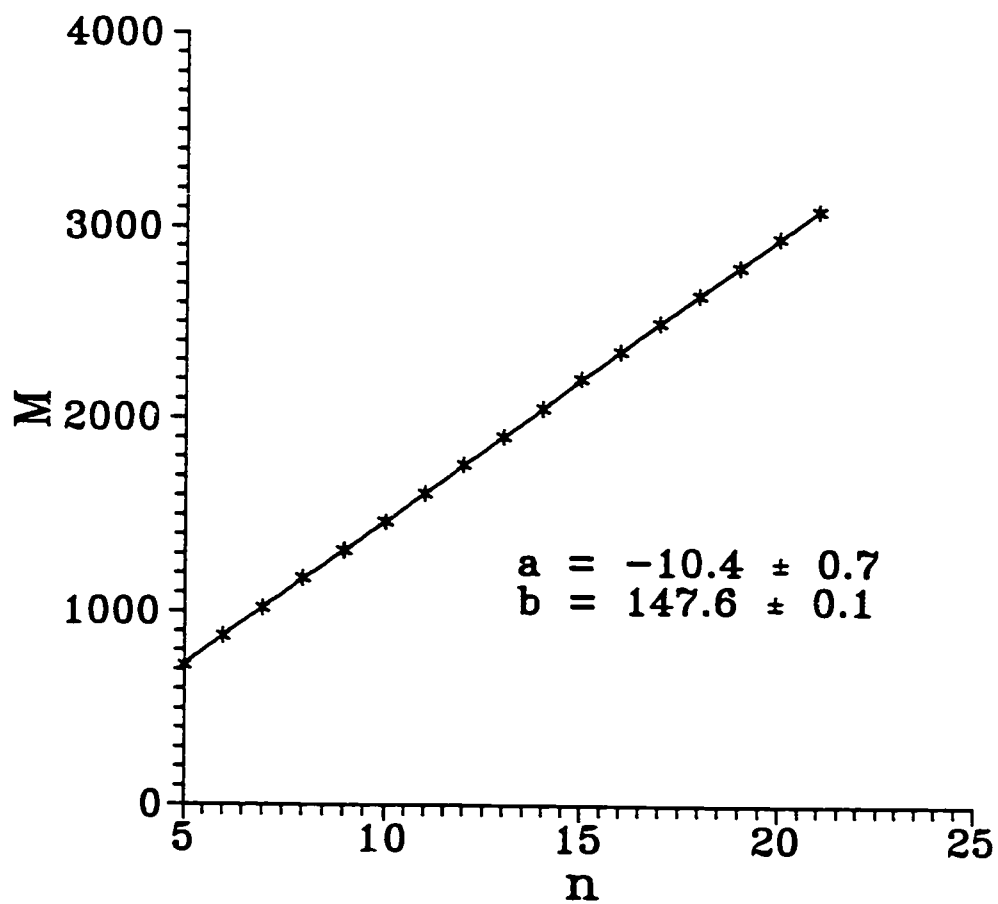


Figure 5.6. Plot of the molecular masses MW of  $(P)_{10-3}$  versus the number of monomer repeat units  $n$  using the profile corresponding to the high peaks, shown in Figure 5.4.



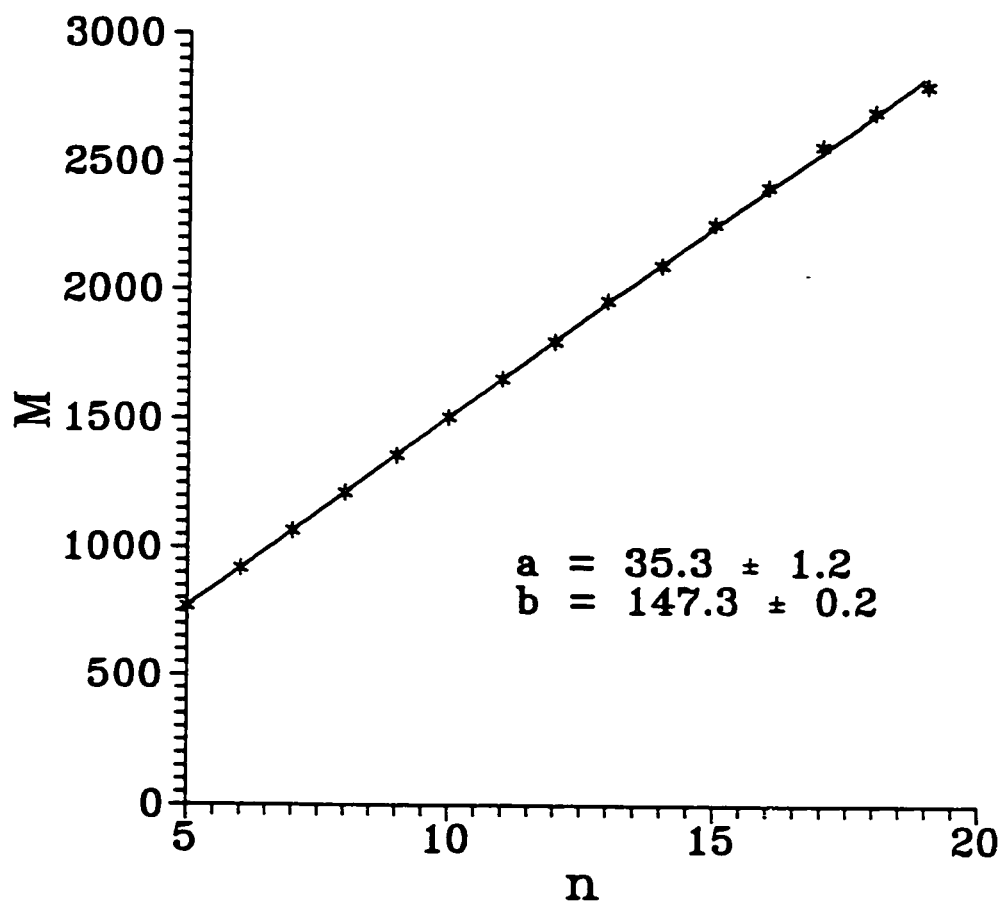


Figure 5.7. Plot of the molecular masses MW of  $(P)_{10-3}$  versus the number of monomer repeat units  $n$  using the profile corresponding to the low peaks, shown in Figure 5.4.

addition of  $\sum_{n=5}^{n=21} I(n) = 84.23$  from the data shown in Table 5.6, to the value of about 0.6, for the total intensity of the fractions corresponding to  $n$  smaller than 5 and  $n$  greater than 21, or  $\sum_{n=0}^{\infty} I(n) = 84.83$ . Also, the total intensity of the low peaks is found by addition of  $\sum_{n=5}^{n=19} I(n) = 59.91$  to an approximate value of about 2.0 for the total intensity of the fractions corresponding to  $n < 5$  and  $n > 19$ , or  $\sum_{n=0}^{\infty} I(n) = 61.91$ . The non-terminating polymerization mechanism of PO in conjunction with instantaneous initiation leads to a Poisson molecular weight distribution<sup>8</sup>. The number fraction  $f(n)$  of the distribution is given by Equation (4):

$$f(n) = \frac{e^{-x} \cdot x^n}{n!} \quad (4)$$

where  $x$  denotes the average number of molecules reacted per initiator molecule. In defining  $x$ , methyl nosylate is counted as  $n = 1$ .  $x$  is equal to the number average degree of polymerization  $\bar{X}_n$ , and is given by the initial  $[PO]/[I]$  ratio. Equation (5) results after rearrangement of (4):

$$\ln[f(n) \cdot n!] = -x + n \cdot \ln x \quad (5)$$

Since  $f(n) = I(n) / \sum_{n=0}^{\infty} I(n)$ , (5) then becomes:

$$\ln[I(n) \cdot n!] - \ln\left(\sum_{n=0}^{\infty} I(n)\right) = -x + n \cdot \ln x \quad (6)$$

The left part of the equation is calculated from the  $I_{\text{high}}$  and  $I_{\text{low}}$  values of Table 5.6, using  $\sum_{n=0}^{\infty} I(n) = 84.83$ , and 61.91, respectively. Figures 5.8 and 5.9 show plots of  $\ln[f(n) \cdot n!]$  vs  $n$ .  $x$  is equal to  $e^a$  and to  $-b$ , where  $a$  and  $b$  are the slope and the intercept respectively of the straight lines, from Equation (5). Table 5.7 shows the results of the linear regression.

Table 5.7. Number average degree of polymerization  $\bar{x}$  from the Poisson function using the high and low peaks of the TOF-SIMS spectrum of (P)<sub>10.3</sub>.

	a	e <sup>a</sup>	b	-b
high	2.453 ± 0.016	11.6 ± 0.2	-11.8 ± 0.1	11.8 ± 0.1
low	2.272 ± 0.012	9.7 ± 0.1	-9.8 ± 0.1	9.8 ± 0.1

The standard error of e<sup>a</sup> is calculated from the law of error propagation<sup>9</sup>:

$$\sigma(e^a) = d(e^a)/da \cdot \sigma(a) = e^a \cdot \sigma(a) \quad (7)$$

Equation (7) can be used with confidence because  $\sigma(a)$  is much less than 10% of a.

From Figures 5.8 and 5.9 it is evident that all points fall on a straight line with a calculated correlation coefficient very close to one. Thus it is concluded that both the high and low-peak profiles are Poisson distributions. The initial [PO]/[I] ratio of 10.3 is very close to the calculated  $\bar{x}$  from the low-peak distribution (9.8 from the intercept, 9.7 from the slope), while  $\bar{x}$  from the high-peak distribution (11.8 from the intercept, 11.6 from the slope) is about 15% higher. From the good fit of the peak intensities to the Poisson function, and the good correlation of the obtained  $\bar{x}$  with the [PO]/[I] ratio, we conclude that (P)<sub>10.3</sub> has a Poisson distribution.

Figure 5.10 shows the TOF-SIMS spectrum of (P)<sub>20.9</sub>. This shows similar patterns of peak sets at higher molecular masses. Below  $n = 18$

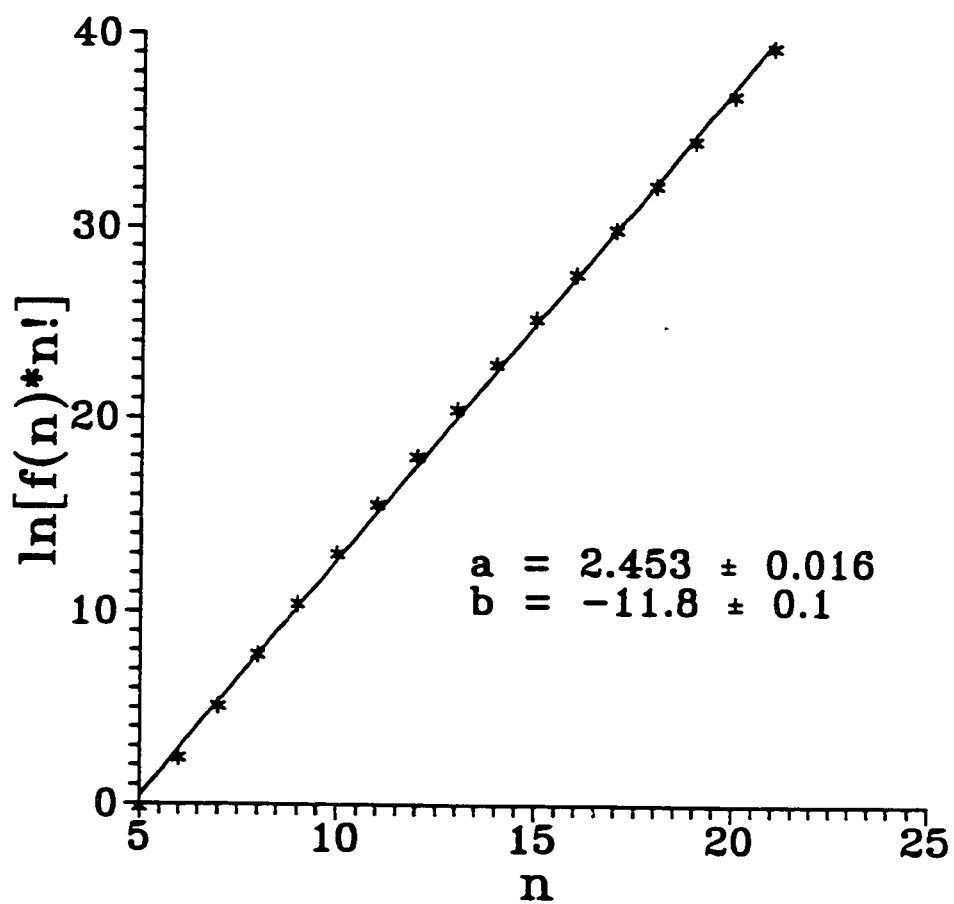


Figure 5.8. Plot of the Poisson function of  $(P)_{10.3}$  using the profile corresponding to the high-intensity peaks, shown in Figure 5.4.

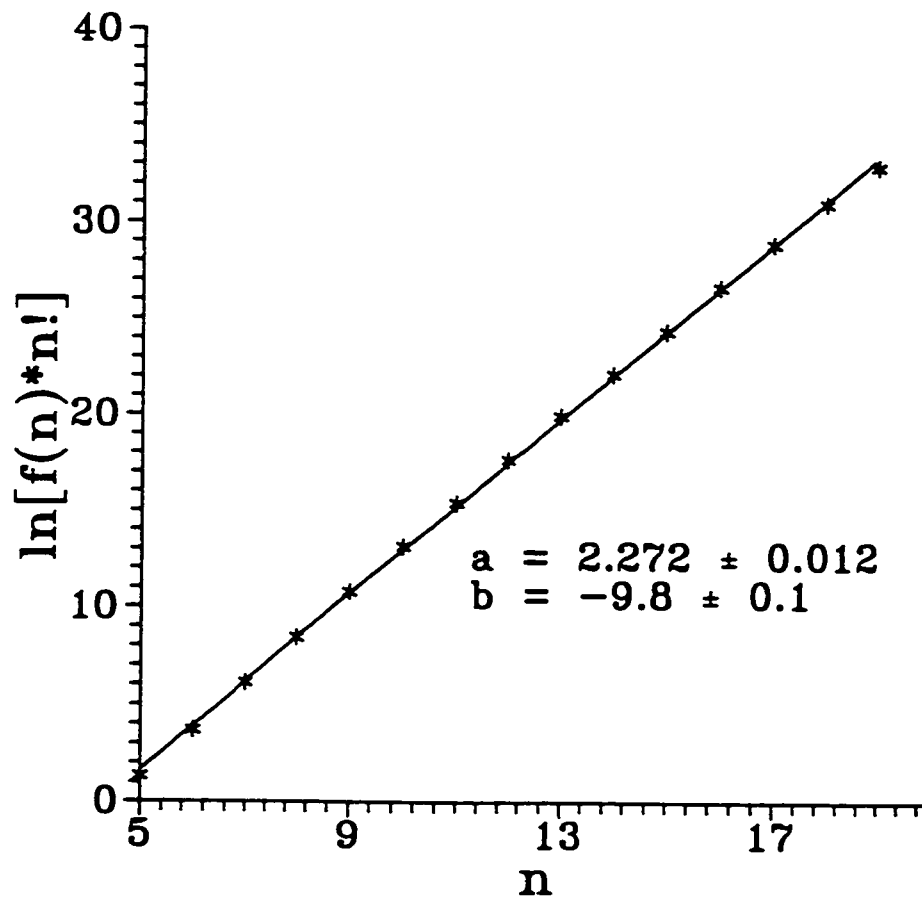


Figure 5.9. Plot of the Poisson function of  $(P)_{10.3}$  using the profile corresponding to the low-intensity peaks, shown in Figure 5.4.

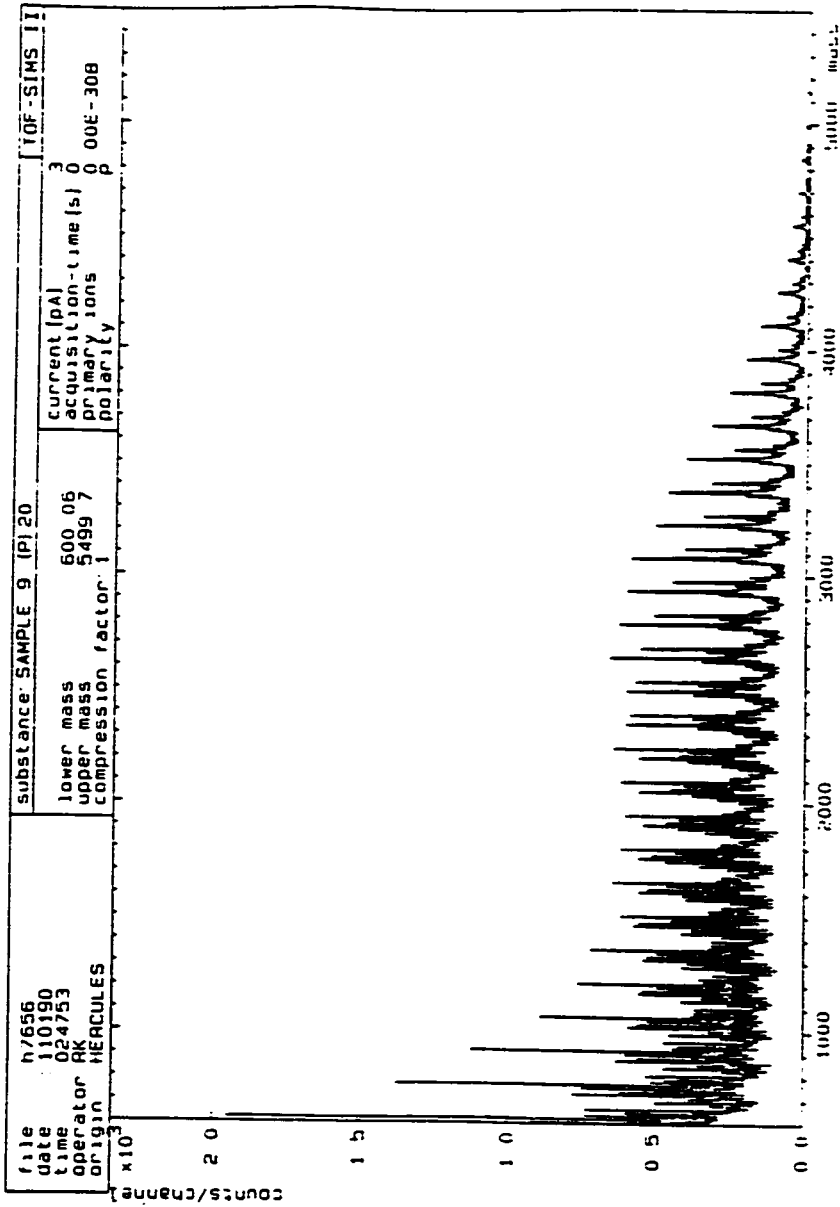


Figure 5.10. TOF-SIMS spectrum of (P)<sub>20-9</sub>.

(2650), however, we notice additional peaks due to complicated fragmentation. In order to calculate the Poisson function we therefore used the peaks for  $n \geq 18$ . Figure 5.11 shows the plot of Equation (6). We only report the slope,  $b = 3.015 \pm 0.005$ , because the intercept shown is derived from an inaccurate estimate of the total intensity,  $\sum_{n=0}^{\infty} I(n)$ , obtained by doubling the measured intensities,  $2 \cdot \sum_{n=18}^{31} I(n)$ . From the relationship  $x = e^b$ , we obtain  $x = 20.4 \pm 0.1$ , which is only 2% smaller than the initial  $[PO]/[I]$  ratio. From the excellent fit of the data points, and the correlation with the feed ratio of 20.9 we conclude that  $(P)_{20.9}$  also has a Poisson MWD.

Figure 5.12 of the TOF-SIMS spectrum of  $(P)_{50.2}$  shows extensive degradation, and we can not distinguish a distribution of peaks centered at 7400 ( $x = 50$ ). Computer analysis of the peak intensities might help understand the fragmentation patterns.

#### GPC characterization of the $(P)_x$ polymer series.

A GPC profile of  $(P)_{10.3}$  is shown in Figure 5.13. The peak width at half-height is 0.92 min and the number average molecular weight is 1,548 using a  $[PO]/[I]$  of 10.3. A narrow MWD polystyrene standard of  $\bar{M}_n$  1800 and polydispersity 1.08 exhibited a peak width of 0.89 min at half-height. Substituting into the relationship shown in Chapter 2:

$$(W_1)^2 / \log d_1 = (W_2)^2 / \log d_2 \quad (8)$$

where  $W_1$  and  $W_2$  are the peak widths of polystyrene standard and polymer at half-height, and  $d_1$  and  $d_2$  their polydispersities ( $\bar{X}_w/\bar{X}_n$ ), we obtain a polydispersity index  $d_2$  of 1.09. The theoretical polydispersity

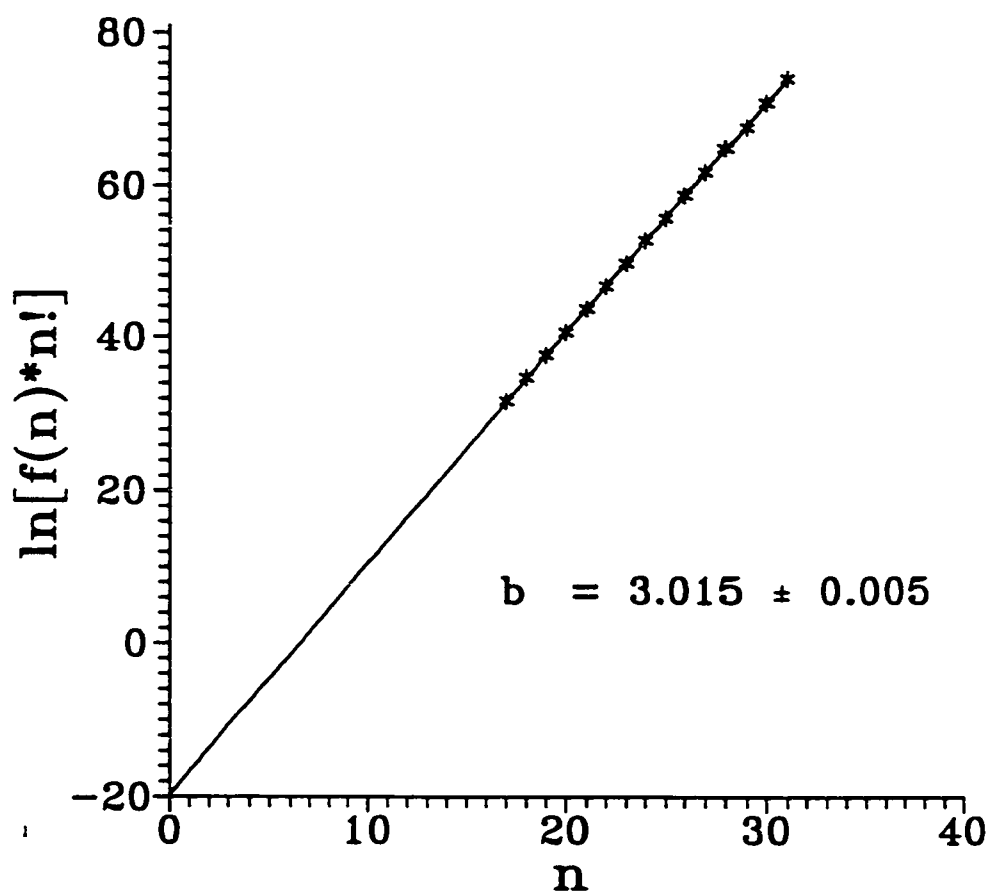


Figure 5.11. Plot of the Poisson function of  $(P)_{20.9}$  using the intensities of the profile corresponding to the high peaks, shown in Figure 5.10.



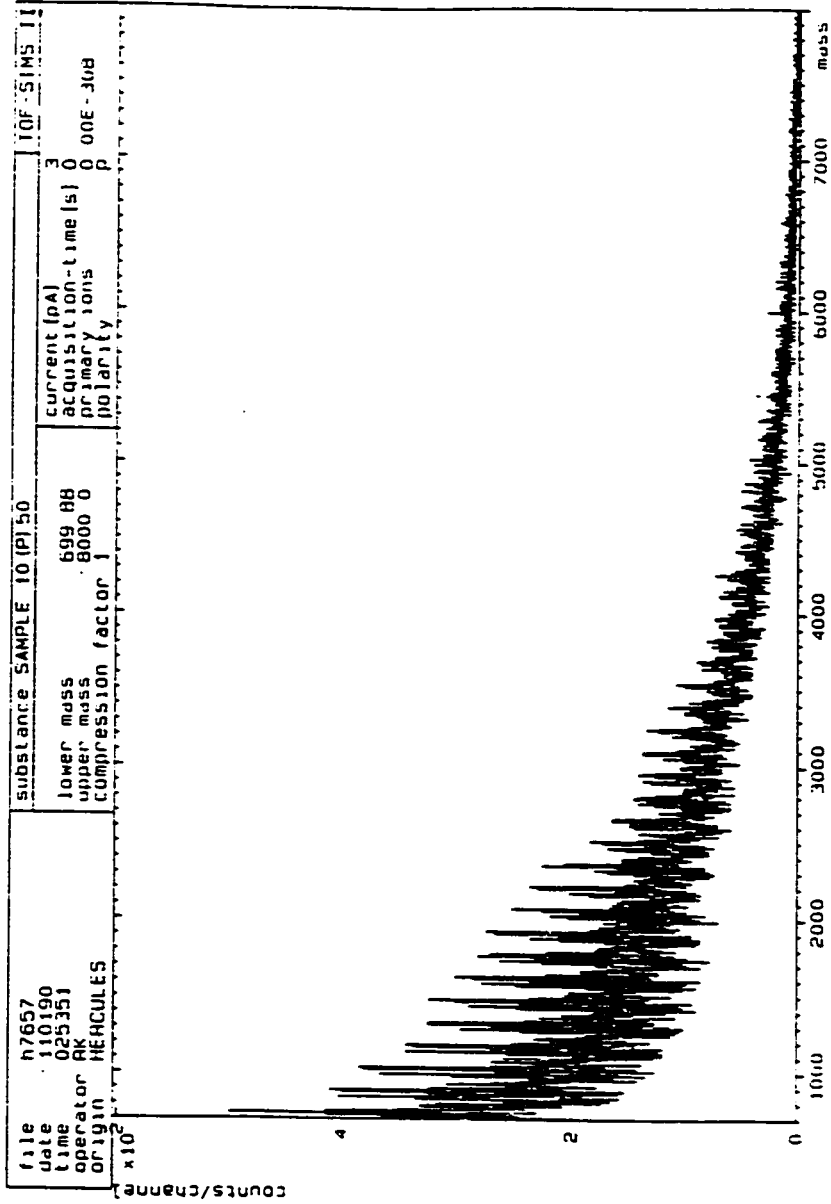


Figure 5.12. TOF-SIMS spectrum of (P)<sub>49-2</sub>.

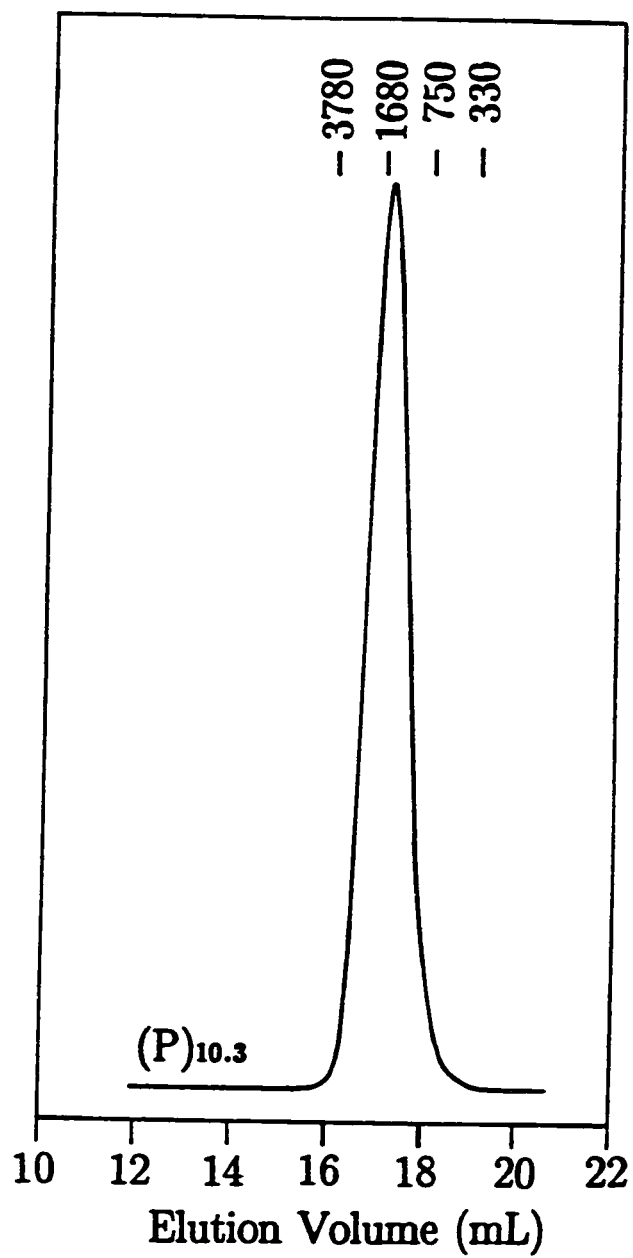


Figure 5.13. GPC-RI profile of purified (P)<sub>10.3</sub>.

based on the Poisson distribution is given by:

$$\bar{X}_w/\bar{X}_n = 1 + 1/\bar{X}_n \quad (9)$$

Thus,  $d_2$  should be equal to  $1 + 1/10.3$ , or, 1.097. The agreement between the theoretical polydispersity and the one obtained from GPC confirms that (P)<sub>10-3</sub> has a Poisson distribution. Table 5.8 shows the polydispersities obtained for (P)<sub>10-3</sub>, (P)<sub>20-9</sub>, and (P)<sub>49-2</sub>.

**Table 5.8. Polydispersities of (P)<sub>x</sub> by comparison to GPC calibration standards, and from the Poisson distribution**

(P) <sub>x</sub>	d (GPC)	d (POISSON)
(P) <sub>10-3</sub>	1.09	1.097
(P) <sub>20-9</sub>	1.10	1.048
(P) <sub>49-2</sub>	1.07	1.020

The GPC profiles of (P)<sub>20-9</sub>, and (P)<sub>49-2</sub> exhibited some tailing on the low molecular weight side which is probably due to remaining salts from purification. This causes an increase in the peak half-widths, which explains the somewhat higher polydispersities measured, compared to those calculated from the Poisson distribution.

The GPC profile of the oligomer (P)<sub>4-8</sub> (see later Figure 5.15) showed the individual peaks of the oligomers with repeat units  $n = 2, 3, 4, 5, 6,$  and 7.

### Peak Position Calibration

The calibration curve for the set of columns described in the experimental section can be established by relating the peak retention volume to molecular weight for a series of narrow-MWD standards. The peak retention volume reflects the size of the macromolecule in solution. The latter is approximated by the radius of gyration ( $R_g$ )<sup>10</sup>. The relationship between  $R_g$  and MW depends on solute/solvent interactions and chemical structures. We therefore used the narrow-MWD polymers of the (P)<sub>x</sub> series to calibrate the GPC columns. This was done to correlate the MW of the amine-treated living chain products with the (P)<sub>x</sub> polymer standards, which have similar chemical structures. Figure 5.14 shows the calibration curve obtained using the peak elution volumes (normalized to the peak retention volume of the internal standard o-DCB) of the polymers (P)<sub>x</sub>, x 2, 3, 4, 5, 6, and 7 (from the polymer (P)<sub>4.8</sub> peaks), 10.3, 20.9, and 49.2. The value of MW used was calculated from  $x \cdot (147) + 32$ , based on structure 12. Such calibration curves were frequently prepared to correct for column deterioration.

### Reactions of poly(N-benzoyl ethyleneimine)s (P)<sub>x</sub> with hexylamine, M.

A series of experiments was carried out in order to understand the mechanism of the reaction between hexylamine M and living poly(N-benzoyl ethyleneimine) chains (P)<sub>x</sub>. Table 5.9 summarizes the reaction conditions of each experiment.

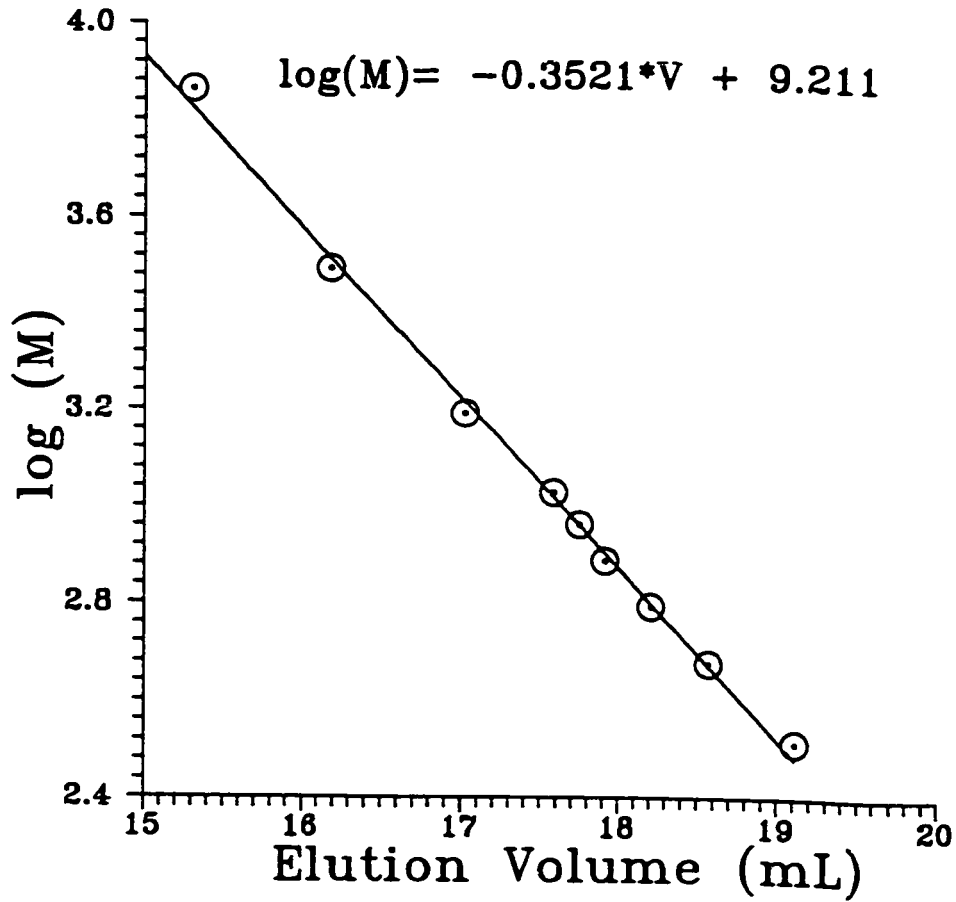
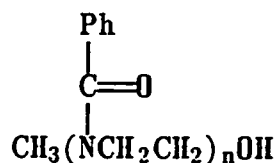


Figure 5.14. GPC calibration curve of  $(P)_x$  polymers made using different  $[PO]/[I]$  ratios.

Table 5.9. Experimental conditions of the reaction between (P)<sub>x</sub> and M in o-DCB.

Exp.	Stoichiometry	T (°C)	$\bar{X}_n$	P <sub>x</sub> (mol/L)
1a	P <sub>1.0</sub> /M	28	4.8	.276
1b	P <sub>1.0</sub> /M	117	4.8	.276
2	P <sub>1.0</sub> /M	108	5.7	.277
3	P <sub>0.5</sub> /M	110	10.2	.131

We conducted experiment (1) to study the effect of temperature. The experiment, using equimolar amounts of (P)<sub>4-8</sub> and M, was carried out in two stages. In the first stage, (1a), the mixture was maintained at 28°C for 22 h; then in the second phase (1b) the temperature was raised to 117°C for another 22 h. Figure 5.15 shows the GPC profiles of the final products of experiments (1a) and (1b) compared to that of (P)<sub>4-8</sub>. (P)<sub>4-8</sub> shows peaks corresponding to n = 2, 3, 4, 5, 6 (maximum), and higher repeats of the structure:



The profile of the final product of (1a) shows the same pattern of oligomer peaks as (P)<sub>4-8</sub> but the elution volume of each peak is slightly lower than

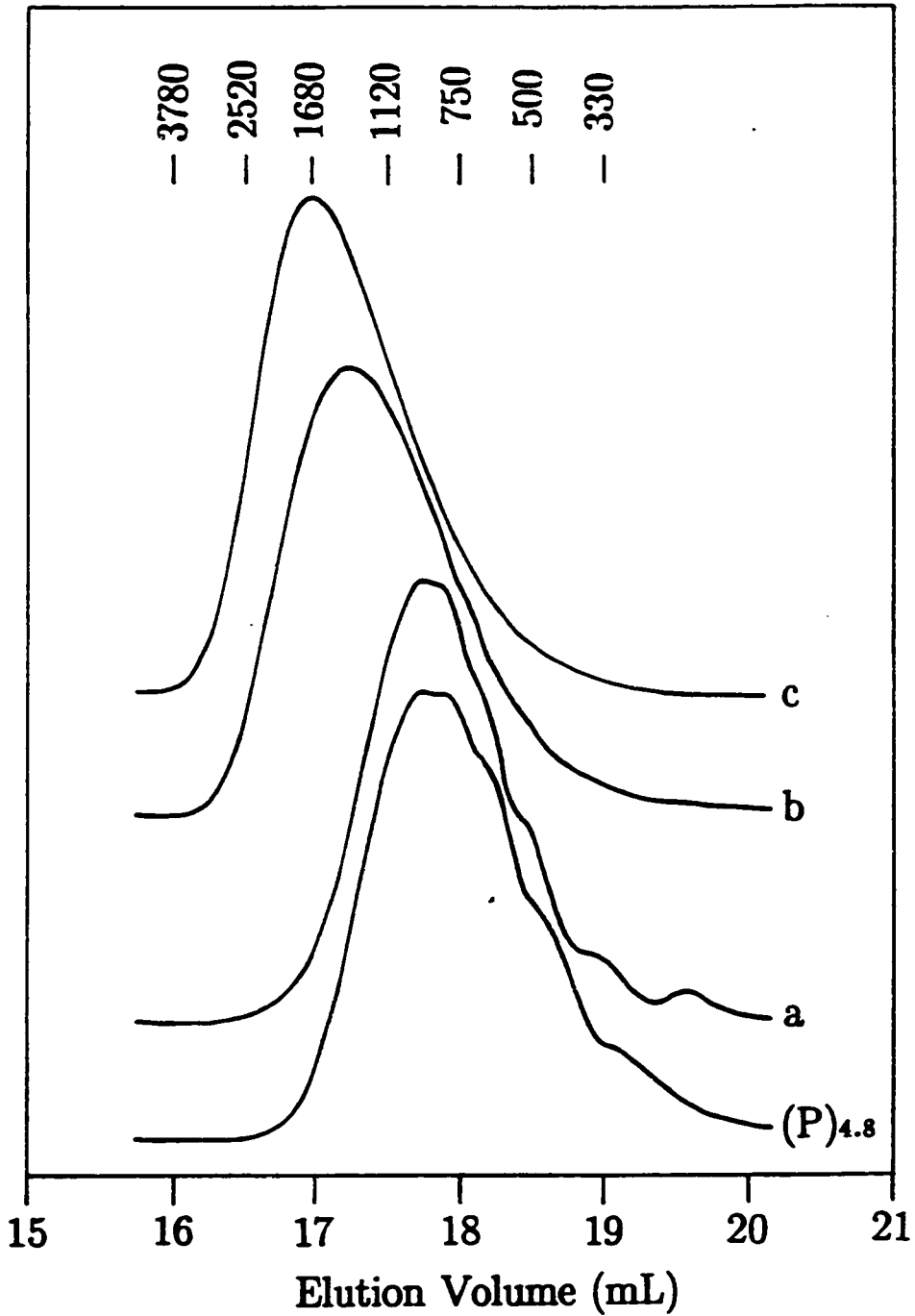


Figure 5.15. GPC-UV profiles of starting polymer,  $(P)_{4.8}$ , and the products of the reactions: (a)  $P_{1.0}/M$  using  $(P)_{4.8}$  at  $28\text{ }^{\circ}\text{C}$ , (b)  $P_{1.0}/M$  using  $(P)_{4.8}$  at  $117\text{ }^{\circ}\text{C}$ , and (c)  $P_{1.0}/M$  using  $(P)_{5.7}$  at  $117\text{ }^{\circ}\text{C}$ .

that of the peak corresponding to the same number of monomer repeats. Additionally, aliquots of the (1a) mixture showed that **M** reacted completely in less than three minutes by GC. Aliquots of the (1b) reaction mixture at different times showed that the distribution of (1a) gradually decreased while a new distribution developed at a lower elution volume. The peak position of the new distribution remained constant with time, and corresponded to a molecular weight of 1487. This value is very close to 1535 which is calculated by adding the MW of **M** (100) to twice the  $\bar{M}_n$  of (P)<sub>4-8</sub>. The distribution of (1a) disappeared almost completely in less than two hours, and the product of (1b) after 37 h is shown in profile b of Figure 5.15.

In experiment (2) we reacted equimolar amounts of **M** and (P)<sub>5-7</sub>, and the mixture was stirred at 108°C for 24 h. GC showed no traces of **M** in the first aliquot after 3 min of injection, as with experiment (1a). GPC showed similar results as with (1b), i.e. a distribution that gradually increased with time while an oligomer distribution at a higher elution volume concurrently decreased in size. The lower-molecular weight oligomer distribution mostly disappeared within ca. 2 h; the product after 24 h is shown in Figure 5.15c. The peak position of the higher-molecular weight distribution corresponded to 1720, compared to a calculated value of 1782 for twice the  $\bar{M}_n$  of (P)<sub>5-7</sub> plus the MW of **M**.

To examine the effect of stoichiometry on the number of (P)<sub>x</sub> that react with **M** we conducted experiment (3). 100% excess of **M** was added to (P)<sub>10-2</sub> (P<sub>0.5</sub>/**M** stoichiometric ratio) and the solution was held at 110°C for 13.1 h. GC chromatograms of the reaction after 3 min and 13.1 h



showed about the same amount of remaining M. The distribution of the final product is shown in Figure 5.16. The profile shows a main peak at position corresponding MW 1559, and a small shoulder of a second distribution on the high molecular weight side of the first peak. The main-peak position corresponds to a molecular weight of 1559, in close-agreement with the 1607 calculated value from addition of 100 to the  $\bar{M}_n$  of (P)<sub>10.2</sub>. We also include the product of experiment (2) in Figure 5.16 in order to compare once- ( $x = 10.2$ ) and twice-reacted polymer ( $x = 5.7$ ). Table 5.10 summarizes the estimations of the molecular weights of the products of experiments (1)–(3) using the peak position calibration curve, and the corresponding calculated molecular weights.

Table 5.10. Molecular weights of hexylamine-treated (P)<sub>x</sub> polymers by comparison to GPC calibration standards, and from the calculated values based on once-, and twice-reacted hexylamine.

Exp.	x	MW (GPC)	$\bar{M}_n$ (Calc)
1b	4.8	1487	1535
2	5.7	1720	1782
3	10.2	1559	1607

The reaction mechanism of M with (P)<sub>x</sub> is shown in Scheme 5.2.

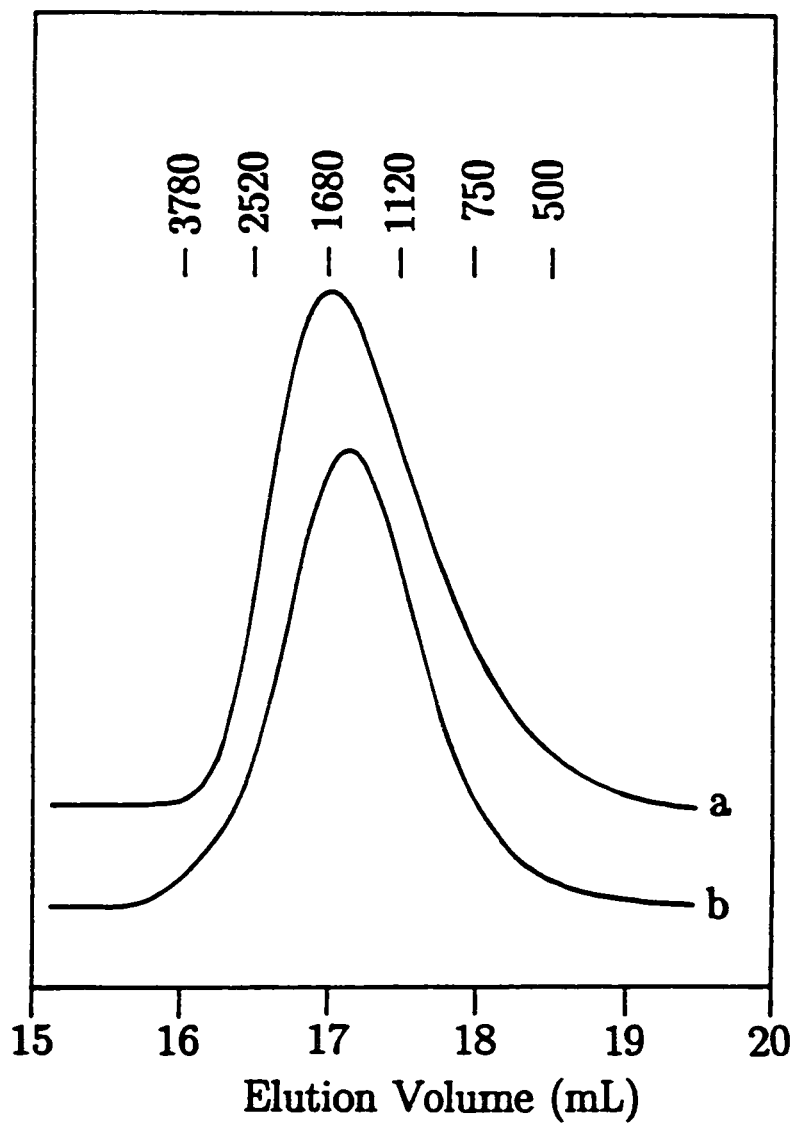


Figure 5.16. Comparison of the GPC-UV profiles of the products of the reactions: (a)  $P_{1.0}/M$  at  $108\text{ }^{\circ}\text{C}$  in *o*-DCB using  $(P)_{5.7}$ , and (b)  $P_{0.5}/M$  at  $110\text{ }^{\circ}\text{C}$  using  $(P)_{10.2}$  in *o*-DCB.



than does  $M$ , as shown from the fact that the final distribution of (3) contains a major peak of once-reacted, and only a very small peak of twice-reacted  $(P)_{10-2}$ .

The conclusion that  $k_1$  is much larger than  $k_3$  was also confirmed from Experiments (1a) and (1b) where we employed equimolar amounts of  $(P)_x$  and  $M$  ( $P_{1.0}/M$ ). GPC of (1a) shows only a slight increase in the peak positions compared to  $(P)_{4-8}$  after 22 h at room temperature, and no indication of twice-reacted material. Additionally,  $M$  disappears in less than three minutes at the same temperature. This indicates that  $M$  is consumed by first reacting with one-half of the polymer chains to generate 13, followed by deprotonation of the latter to produce 14. The much slower reaction of  $(P)_x$  with 14 is demonstrated by the appearance of twice-reacted polymer in the GPC of (1b) only after raising the temperature of (1a) to 117°C, while the profile of (1a) disappears within about 2 h. The increased temperature enhances  $k_3$ , hence allowing the remaining  $(P)_x$  to react with 14 to produce 15. Experiment (2), run at 108°C using equimolar stoichiometry ( $P_{1.0}/M$ ), also confirmed the above mechanism, as shown by the disappearance of  $M$  within 3 min to produce 14, and the slow appearance of twice-reacted polymer 15. The above experiments did not show by GPC a higher MW product, corresponding to three-times reacted amine. Quaternization of 15 by further reaction with  $(P)_x$  cannot occur because of steric hindrance.

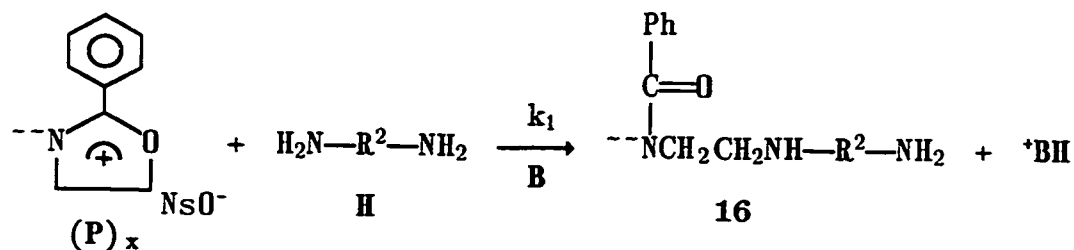
The products of Experiments (1)–(3) were also characterized by  $^1H$  NMR and Time-of-Flight spectroscopy. The details of the structure analysis are given in Appendix B.

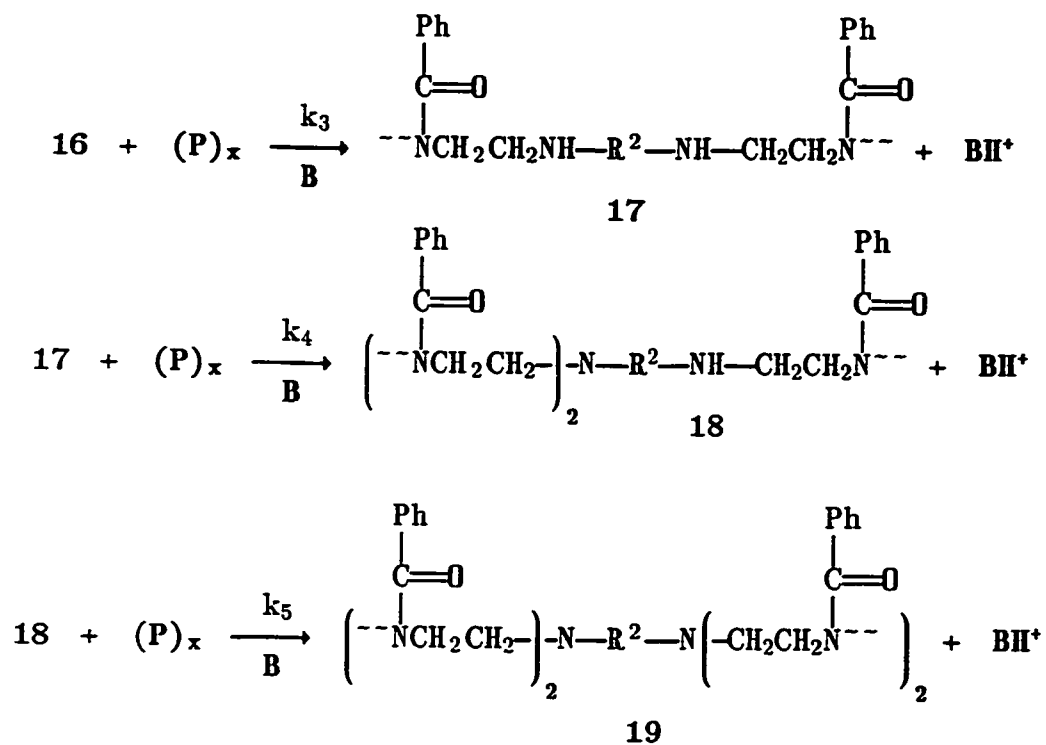
Reactions of living poly(N-benzoylethyleneimine)  $(P)_x$  with hexamethylenediamine H.

This section describes a series of experiments that were done with the goal of obtaining four-star structures via the attachment of four  $(P)_x$  chains to hexamethylenediamine H.

The experiments described in the previous section demonstrated that one can attach two poly(N-benzoylethyleneimine) chains to the amino group of hexylamine (M) (see structure 15, Scheme 5.2) by reacting an equimolar amount of the amine with living prepolymer  $(P)_x$  at high temperatures. One-ended amine M played a dual role in this system, namely it was the anchoring agent, and also the proton scavenger, allowing addition of more  $(P)_x$  to the once-reacted secondary amine 14. In the case of the diamine system of H we employed triisobutylamine B as a proton scavenger. Scheme 5.3 shows the reaction mechanism of  $(P)_x$  addition to H, in the presence of excess B.

Scheme 5.3





where  $\text{R}^2 = -\text{CH}_2(\text{CH}_2)_4\text{CH}_2-$ ,  $\text{B} = ((\text{CH}_3)_2\text{CHCH}_2)_3\text{N}$ , and  $\text{BH}^+ = ((\text{CH}_3)_2\text{CHCH}_2)_3\text{NH}^+ \text{NsO}^-$

The above scheme shows the neutralized amines 16–19. The mixture also contains the protonated ammonium salts of the above amines. The two forms are in equilibria because their protons are being scavenged by B, by H, and by the unreacted end of 16. To drive the equilibria towards the neutral amine forms we employed an excess of B.

Table 5.11 shows the conditions under which the experiments were conducted.

Table 5.11. Experimental conditions of the reaction between  $(P)_x$  and H in o-DCB, and in DMac.

Exp.	Stoichiometry	T ( $^{\circ}$ C)	$\bar{X}_n$	$P_x$ (mol/L)
4 <sup>*</sup>	P <sub>3.5</sub> /H/B <sub>2.0</sub>	121	8.6	.191
5 <sup>**</sup>	P <sub>4.0</sub> /H/B <sub>7.9</sub>	125	10.5	.207
6 <sup>**</sup>	P <sub>4.3</sub> /H/B <sub>8.8</sub>	125	10.0	.192
7 <sup>**</sup>	P <sub>2.1</sub> /H/B <sub>8.4</sub>	125	10.2	.169

\* in o-DCB, and \*\* in DMac.

In Experiment (4) we used a stoichiometry of 3.5 polymer  $(P)_x$  chains per H. This ratio corresponds to a 10% deficiency of chains over the amount required for full reaction of H; since the latter contains two primary amine-groups each of which can react with two chains. The reaction was carried out in o-DCB at 121 $^{\circ}$ C. GPC-UV (at 230 nm) profiles of neutralized aliquots of the reaction mixture at different times are shown in Figure 5.17, and are compared to prepolymer  $(P)_{8.6}$  taken from an aliquot before injection of H (0 h). The peak at about 19.2 mL corresponds to B, which has a weak absorption peak at 224 nm in o-DCB. (This was demonstrated by a separate GPC-UV control experiment). The reaction mixture at 0.5 h shows three peaks at positions 16.3, 17.0, and 17.8 mL corresponding to once-, twice-, and three-times reacted  $(P)_{8.6}$ . In

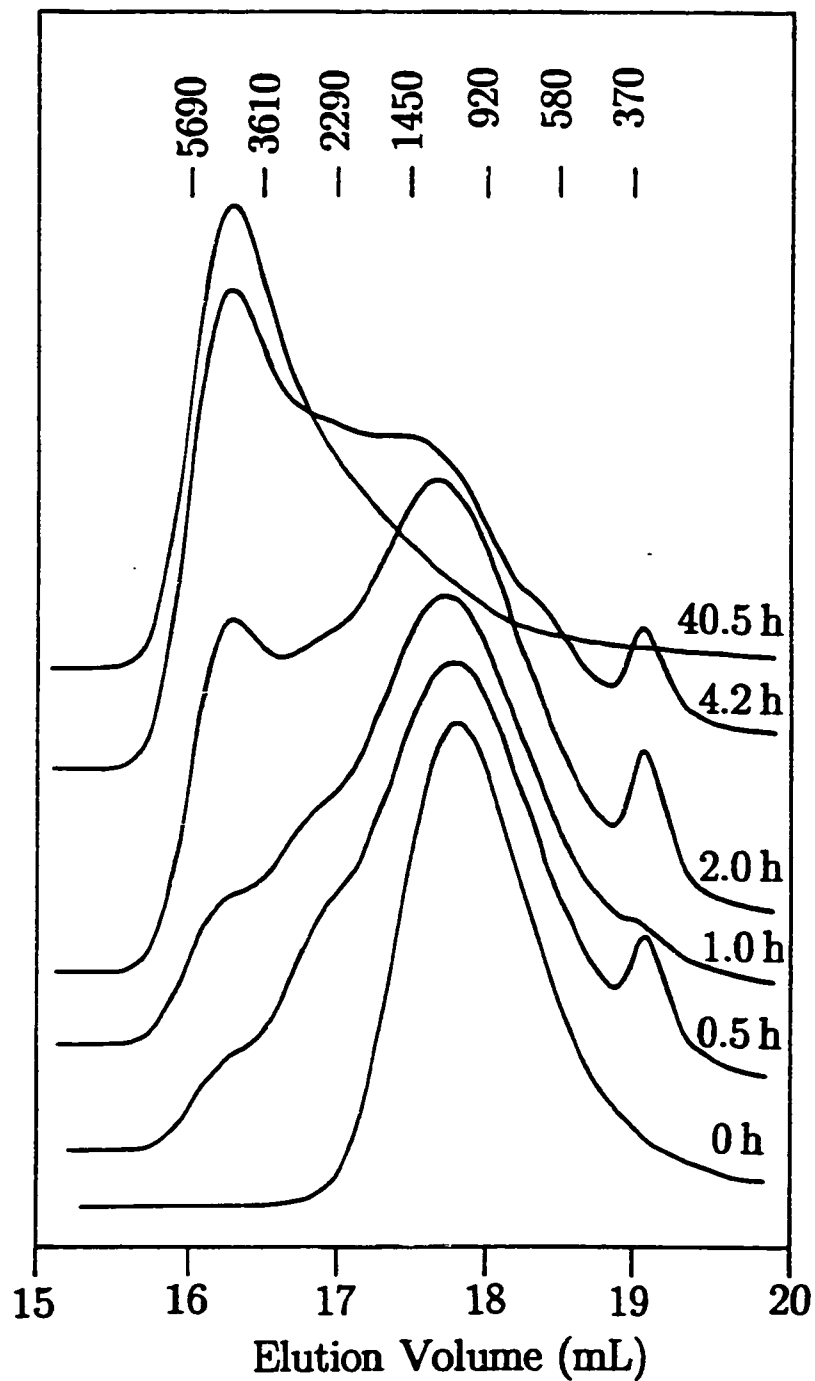


Figure 5.17. GPC-UV profiles of  $P_{3.5}/H/B_{2.0}$  aliquots at different reaction times at 121 °C in *o*-DCB using  $(P)_{8.6}$ .



the case of star structures we cannot use our peak position calibration curve to calculate the exact molecular weights because that curve is based on linear poly(N-benzoyl ethyleneimine) polymers. Linear polymers show a logarithmic relationship between their MW's and their elution volumes. The elution volume is a measure of the size of the molecule, which is approximated by the radius of gyration,  $R_g$ . The latter among other factors depends on the conformation of the molecule. Structures 16 and 17 can be considered linear analogs of  $(P)_x$  with  $\bar{X}_n$  8.6, and  $2 \times 8.6$  respectively and therefore their peak positions can be found from the linear calibration curve. However the branched structures 18 and 19 give a smaller molecular size than that of three- and four-times the  $\bar{X}_n$  of  $(P)_{8.6}$  based on the corresponding linear analogs. Extensive theoretical work appears in the literature relating  $R_g$  of various conformations of star polymers to that of corresponding linear molecules of the same molecular weight<sup>11-13</sup>. However, an exact relationship is not given because the size of the molecule depends on its chemical structure, the specific interactions of the star-branches at the common junction, the particular conformation, the solvent and the temperature. From geometrical considerations the branches of a star can be considered as cutting the surface of a sphere at radius  $r$ . Structures 18, and 19, which have three and four branches respectively, will have similar  $r$  values which in turn leads to similar excluded volumes. Their GPC peak positions will appear close to each other and at the approximate volume corresponding to the linear analog of three times the  $\bar{X}_n$  of the prepolymer reactant. From the above considerations we therefore

assign the peak positions at 17.8 mL to (P)<sub>8.6</sub> and 16, 17.0 mL to 17, and the peak at 16.3 mL to a mixture of 18 and 19. Figure 5.17 shows that the relative proportions of the areas under the three peaks change with time. As the reaction proceeds one notes that the peak at 16.3 mL gradually increases compared to that at 17.0 mL, becomes larger than the latter at 2.0 h and is the major peak at 4.2 h. At 40.5 h the peak at 16.3 mL is the major product, with only traces of the peaks at 17.0 and 17.8 mL remaining. The above time dependence in *o*-DCB shows that  $k_1$  is fast, producing 16 almost instantly. This rate constant should be the same as that of reaction of M with (P)<sub>x</sub> to produce one-ended adduct 14 (see Scheme 5.2). Rate constants  $k_4$  and  $k_5$  are much smaller than  $k_3$ , as shown from the slow generation of 18 and 19. This is because it becomes increasingly difficult for (P)<sub>x</sub> to find the unreacted amine sites of 17 and 18 due to the great steric hindrance created by the presence of the reacted polymer chains. The final polymer must contain on the average 3.5 chains per H core based on the initial stoichiometry. This means that the final polymer should contain a major fraction of four-times reacted 19 and a small amount of the distributions corresponding to once-, twice-, and three-times reacted structures 16, 17, and 18.

In experiment (5) we reacted (P)<sub>10.5</sub> with H in DMAc at 125°C using a 4:1 stoichiometric ratio, the ratio required for reaction of four chains on H. DMAc was used because of its higher polarity than *o*-DCB which solubilized all the produced salts soluble in the reaction mixture. This was desired in order to assure that the protonated ammonium forms of structures 16–18 are in solution and hence are available for exchange and

reaction. Figure 5.18 shows the reaction mixture at different times, 0 h being a sample of  $(P)_{10.5}$  taken before injection of H. As seen, the peak at about 15.9 mL, corresponding to structures 18 and 19 is already the major fraction of the mixture at 1.7 h. At 96.1 h, most of the peak due to  $(P)_{10.5}$  plus 16 has disappeared. From the observed time dependence we can draw the hypothesis that the rate constants  $k_4$  and  $k_5$  are faster in DMAc than in o-DCB. Figure 5.19 shows the profile of the final product, after purification. The major peak is at 15.69 mL corresponding to 19. From the changes in the slope of the profile we assign 18 to 16.09 mL, 17 to 16.36 mL, and the mixture of 16 and unreacted  $(P)_{10.5}$  at 16.72 mL. The above peak positions correspond to 4856, 3511, 2986, and 2106, based on the peak position calibration curve of the linear polymers. Table 5.12 shows the molecular weights of  $(P)_{10.5}$  and 16, 17, 18, and 19 calculated from the  $[PO]/[I]$  ratio, and from the peak positions of Figure 5.19, using the relevant calibration curve of linear standards.

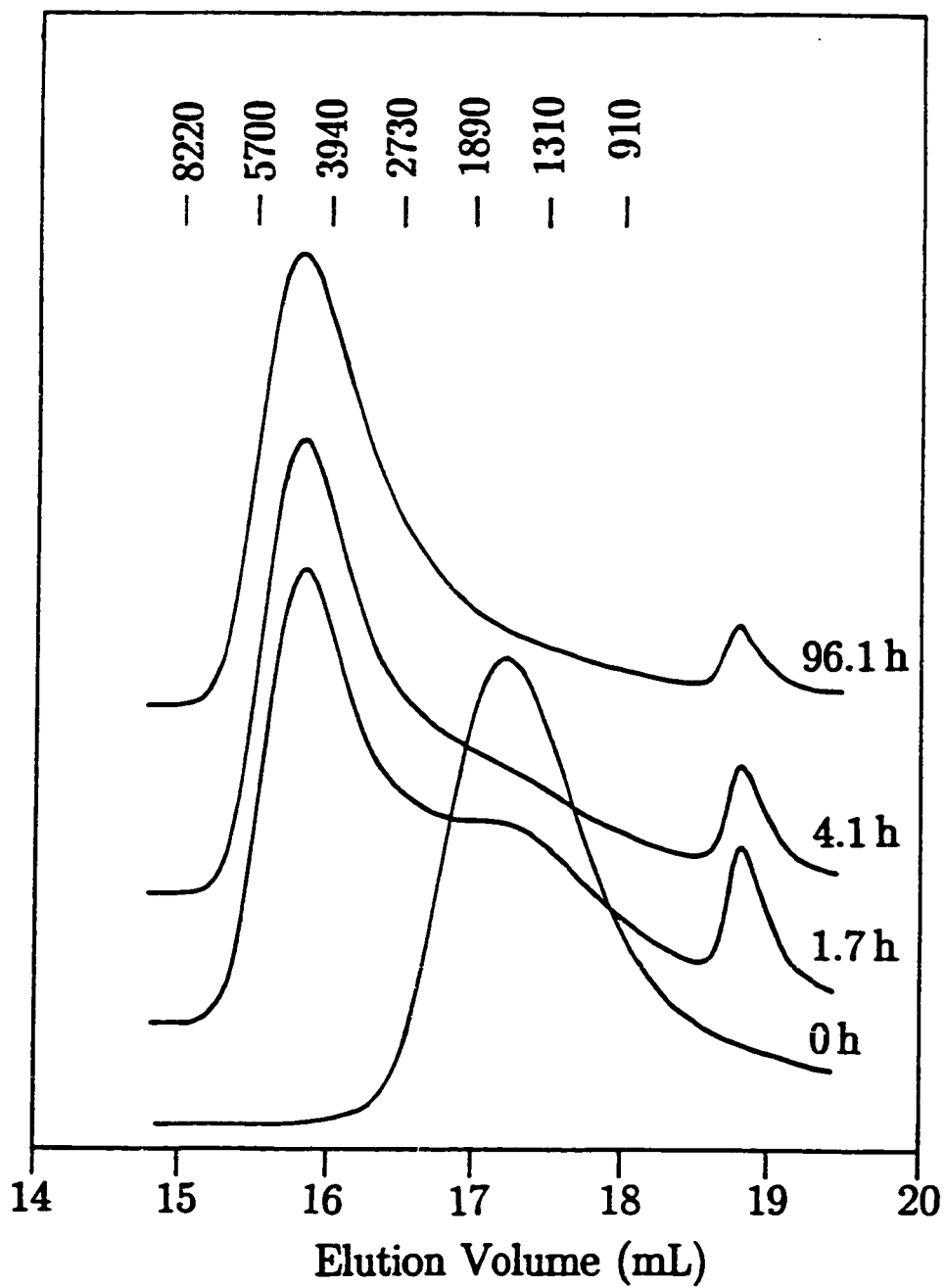


Figure 5.18. GPC-UV profiles at different times of the  $P_{4.0}/H/B_{7.9}$  reaction at  $125\text{ }^{\circ}\text{C}$  in DMAc using  $(P)_{10.5}$ .

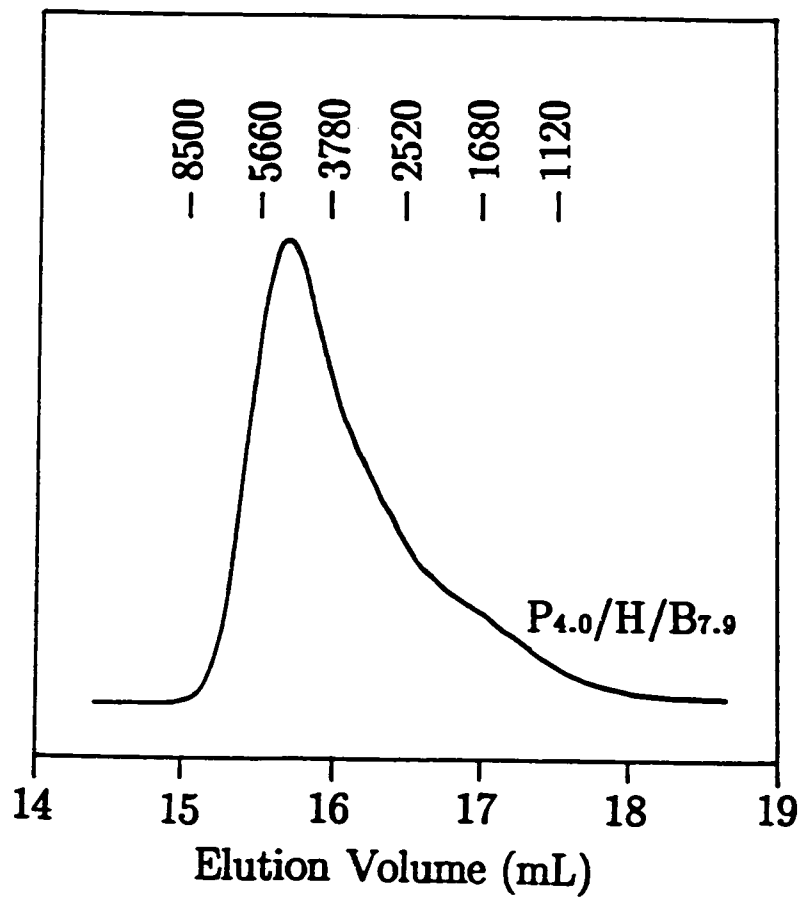


Figure 5.19. GPC-UV profile of the product of the P<sub>4.0</sub>/H/B<sub>7.9</sub> reaction at 125 °C in DMAc using (P)<sub>10.5</sub>.

Table 5.12. Molecular weights of  $(P)_{10-5}$ , and once-, twice-, three-, and four-times reacted H from the calculated  $[PO]/[I]$  ratio, and from the assigned GPC Peak-Positions.

Structure	MW from $[PO]/[I]$	MW (GPC)
$(P)_{10-5}$	1575	
		2106
16	1675	
17	3220	2986
18	4788	3511
19	6346	4856

Table 5.12 shows that the molecular weights that correspond to the peak positions of once- (16), and twice-reacted (17) respectively are close to the ones of linear polymers of the same number of repeat units, whereas for 18 and 19 they are considerably different. This confirms the previous statements on the conformational effects of different number of branches on the molecular size of a star-shaped molecule.

Experiment (5) demonstrated that the final polymer after 96.1 h of reaction of four polymer chains and H consists mainly of the star-four structure 19, and small amounts of structures 16, 17, and 18. In order to show that we can obtain a star-four structure we carried out Experiment (6) in which we started with a stoichiometric ratio of 4.3  $(P)_{10-0}$  per H, i.e.

with about 8% excess of polymer chains compared to the amount required for full reaction of H. The final polymer mixture should therefore consist of 92% star-four 19 and 8% (P)<sub>10-0</sub>. Figure 5.20 shows the reaction mixture at different times, 0 h being a sample of the prepolymer (P)<sub>10-0</sub> taken before injection of H. The relative proportions of the distributions vary with time as with Experiment (5). The peak due to three- and four-times reacted H is distinct even at 0.4 h, and clearly larger than twice-reacted 17. The latter is not evident even at 51.8 h. The final polymer distribution after 92.5 h reaction is shown in Figure 5.21, compared with the products of Experiments (5) and (6). The GPC profile of the P<sub>4.3</sub>/H/B<sub>8.8</sub> product shows a small amount of a peak near the elution volume of prepolymer but it is unclear if there are slope changes corresponding to 17 and 18.

In order to draw conclusions on the relative differences between reaction rates  $k_2$ ,  $k_4$ , and  $k_5$  in DMAc we carried out experiment (7), using an initial stoichiometric ratio of 2.1:1 (P)<sub>10-2</sub> chains to H. If  $k_2$  is much larger than  $k_4$  and  $k_5$  then the final product should consist of twice-reacted structure 17. The distribution of the final product after 92.5 h of reaction is shown in Figure 5.22. The profile consists of a major peak most likely of 18 and significant amounts of peaks due to 16, 17. However, there is a significant amount of trailing at the high elution volumes due to remaining nosylate salts after partial purification, as demonstrated by an <sup>1</sup>H NMR spectrum of the product (see Appendix C). Deconvolution of the peaks might help identify which structure corresponds to the highest molecular weight peak. However, we can draw the conclusion that the rate of

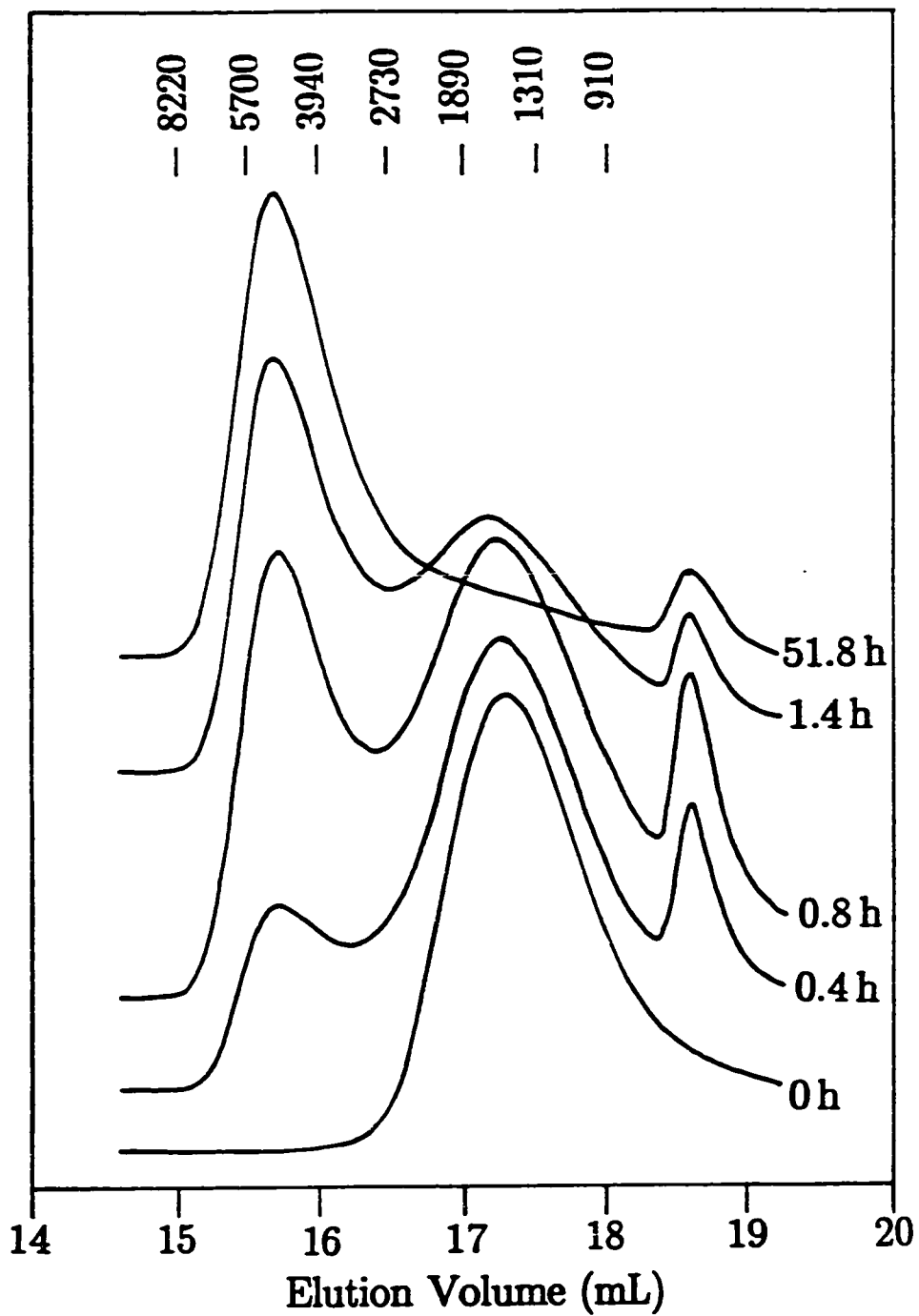


Figure 5.20. GPC-UV profiles at different times of the  $P_{4.3}/H/B_{8.8}$  reaction at 125 °C in DMAc using  $(P)_{10.0}$ .



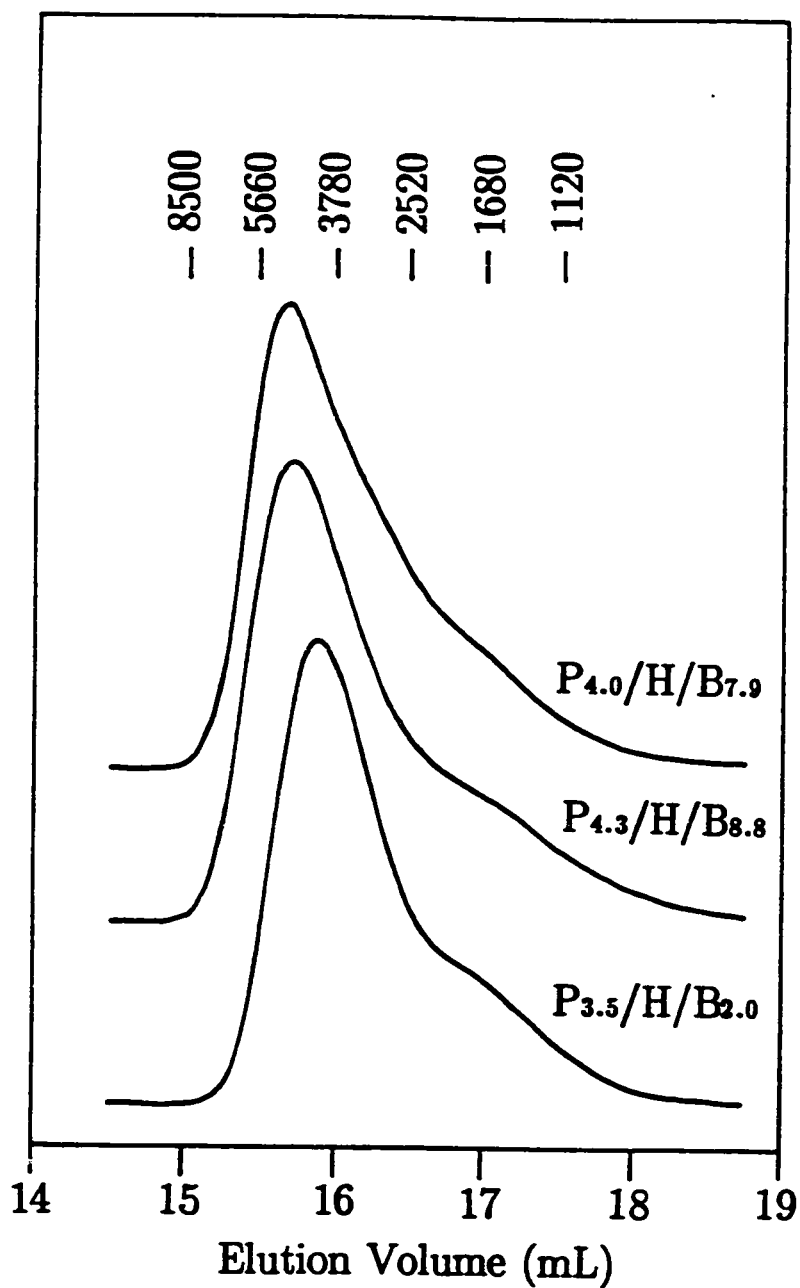


Figure 5.21. Comparison of the GPC-UV profiles of the products of the reactions: P<sub>4.0</sub>/H/B<sub>7.9</sub> using (P)<sub>10.5</sub>, P<sub>4.3</sub>/H/B<sub>8.8</sub> using (P)<sub>10.0</sub>, and P<sub>3.5</sub>/H/B<sub>2.0</sub> using (P)<sub>8.6</sub>.

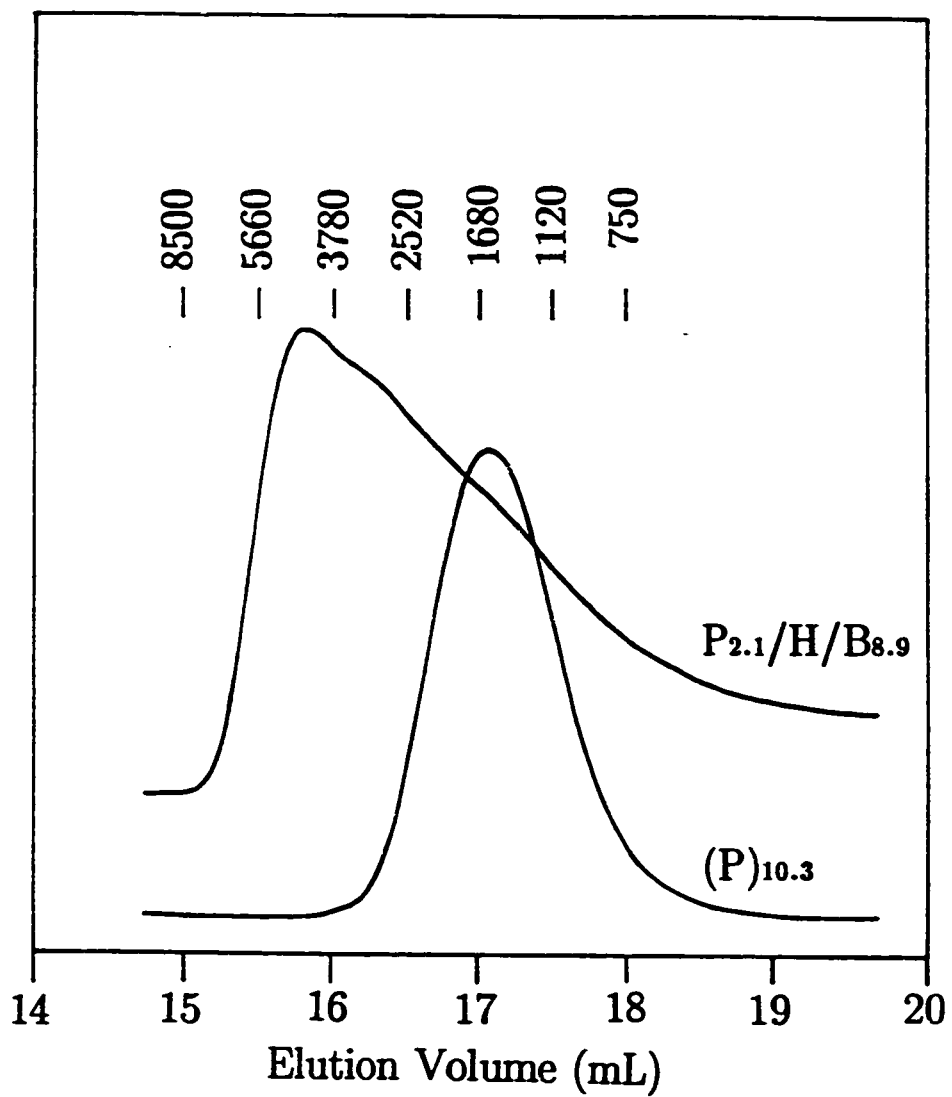


Figure 5.22. GPC-UV profile of the product of the  $P_{2.1}/H/B_{8.4}$  reaction at 125 °C in DMAc.

twice-reaction is significant compared to  $k_1$  and  $k_2$ , since the major peak of the product of (7) has a higher molecular weight than once-reacted 17.

$^1\text{H}$  NMR and TOF-SIMS spectral analysis of the products of hexamethylenediamine-treated poly(N-benzoylethyleneimine)s is given in Appendix C.

#### d) Summary and Conclusions

A study was done on the kinetics of 2-phenyl-2-oxazoline polymerization in o-DCB and DMAc using methyl nosylate initiator. The rate constants of propagation were found to be  $k_p(\text{o-DCB})$  0.0027 at 110°C,  $k_p(\text{DMAc})$  0.0030 at 117°C, and  $k_p(\text{DMAc})$  0.0060 L/(mol.s) at 127°C.

A series of poly(N-benzoylethyleneimine) polymers of the type  $(\text{P})_x$  was synthesized, where  $x$  is the average degree of polymerization. An analysis based on Time-of-Flight Secondary Ion Mass spectra showed that the  $(\text{P})_x$  polymers had Poisson molecular weight distributions. This was also confirmed by gel permeation chromatography.

Living  $(\text{P})_x$  chains were terminated by hexylamine **M** in o-DCB. Equimolar reaction of  $(\text{P})_x$  and **M** produced the once-reacted secondary amine adduct at room temperature within a few minutes. Increasing the temperature to 117°C produced the twice-reacted tertiary amine adduct within two hours. Reaction of an equimolar excess of **M** and  $(\text{P})_x$  at 110°C produced only the once-reacted adduct.

A series of polymers was synthesized by reacting  $(\text{P})_x$  with hexamethylenediamine **H** in the presence of a proton scavenger triisobutylamine at 125°C. The reactions were carried out with four molar

ratios of chains per H: 3.5 (o-DCB), 4.0 (DMAc), 4.3 (DMAc), and 2.1 (DMAc). The products of the first three reactions after long reaction times consisted mainly of three- and four-times reacted adducts and small amounts of once- and twice-reacted ones. The reaction product using the 2.1 stoichiometry after 92.5 hours consisted of a major peak most likely to three-times reacted adduct and significant amounts of once- and twice-reacted ones.

### References

1. Kobayashi, S.; Kaku, M.; Tanabe, T.; Saegusa, T. *Prepr. of the 50th Meeting of the Chemical Society* 1985, 1572.
2. Kobayashi, S.; Kaku, M.; Sawada, S.; Saegusa, T. *Polym. Bull.* 1985, 13, 447.
3. Chujo, Y.; Ihara, E.; Ihara, H.; Saegusa, T. *Macromolecules* 1989, 22, 2040.
4. Hartley, D. B.; Hayes, M. S.; Richards, D. H. *Polymer* 1981, 22, 1081.
5. Seelinger, W.; Aufderhaar, E.; Diepers, W.; Feinauer, R.; Nehring, R.; Thier, W.; Hellmann, H. *Angew. Chem. Internat. Ed.* 1966, 5, 875.
6. Matsuda, T. *Polymerization Reactions of Nitrogen-Containing Heterocyclic Compounds*; Ph. D. thesis; Kyoto University, 1972; p 100.
7. Kagiya, T.; Matsuda, T. *J. Macromol. Chem., A5* 1971, 8, 1265.
8. Flory, P. J. *Principles of Polymer Chemistry*; Cornell University: Ithaca and London, 1969; p 337.
9. Mandel, J. *The Statistical Analysis of Experimental Data*; Dover: New York, 1964; p 74.
10. Yau, W. W.; Kirkland, J. J.; Bly, D. D. *Modern Size-Exclusion Liquid Chromatography*; Wiley and Sons: New York, 1979; p 285.
11. Zimm, B.; Stockmayer, W. J. *Chem. Phys.* 1949, 17, 1301.
12. Vlahos, C. H.; Kosmas, M. K. *Polymer* 1984, 25, 1607.
13. Batoulis, J.; Kremer, K. *Macromolecules* 1989, 22, 4277.

## Appendix A

### Purification Procedure of Poly(N-benzoyl ethyleneimine)s, and their Amine-Terminated Products

The method of purification of the polymers of Chapter 5 was developed from the experiments described below:

Untreated aliquots of the reaction mixtures at different reaction times of both  $(P)_x$  homopolymers, and their amine-treated products, were diluted with THF, and analyzed by GPC. The resulting profiles showed a polymer peak that was skewed towards high elution volumes, with associated strong tailing, which was apparent even several minutes after the elution volume of *o*-DCB. This behavior was quite similar to that exhibited by unpurified  $O_xE_y$  polymers, already discussed in Chapter 2. The GPC column effects exhibited by the polymers also are attributed to compounds containing ionic groups that interact with the column material. This is confirmed by  $^1H$  NMR; precipitated polymers, that were not treated with potassium hydroxide exhibited a pair of doublets at  $\delta$  8.05 –  $\delta$  8.20 ppm, which are assigned to the phenyl protons of nosylate salts. See for example Figures B2, before and B3, after purification respectively. Also, the GPC column effects were greatly reduced when the samples were diluted with more THF, i.e., the polymer peaks became symmetrical and the dragging at high elution volumes was reduced. This indirectly showed the presence of salts because lower concentrations reduce the interactions with polar sites on the column material. The following experiments were then conducted to determine the best procedure to remove all the formed salts in a typical reaction mixture:

- (1) A polymer sample of 2 g in 10 mL *o*-DCB was first precipitated into about 250 mL of vigorously stirred ethyl ether. The resulting powder was suction-filtered, and dissolved in about 10 mL of  $CHCl_3$ . This

solution was then shaken in a separatory funnel with about 50 mL of a 10% aqueous sodium bicarbonate solution, and the organic phase separated. This washing was repeated three times and the organic phase was reprecipitated in ethyl ether; the collected dry sample was dissolved in THF and analyzed by GPC. The salt effects were still evident in the GPC profile, showing incomplete neutralization of the formed cations and the presence of nosylate salts. The polymer sample was then redissolved in MeOH and treated with potassium hydroxide until pH 9–10. After similar work-up, the dried sample still showed the column effect. Another sample of the precipitated polymer was then treated with an excess of 10% potassium hydroxide in MeOH (ca. 5 mL), and the solution was stirred at about 40°C for 5–10 min. The profile of the polymer after work-up now showed a symmetric peak, with some dragging at the low-molecular weight side. Dilution with more THF did not change the position of the main peak. This showed complete neutralization but with some remaining salts.

(2) An anion exchange resin column (AER) was prepared in the following way: A quaternary-ammonium styrenic type AER, packed in 6N aqueous HCl, was rinsed with water until the washings reached pH 7. The chloride anion form of the AER was next changed to the hydroxide form by stirring the bed with a 20% KOH/MeOH solution for about 10 min. The resin was then neutralized by rinsing several times with water until pH 7. The AER was then packed in a glass column (1.3 cm wide and 30 cm high), which ended in a sintered filter above a Teflon<sup>R</sup>-stopcock outlet. The AER column was then rinsed several times with methanol, and a solution of the potassium hydroxide-treated polymer in methanol was

passed through the column. Several column volumes of methanol were then passed through the column, and the clear colorless solutions were collected and rotavaporated to remove the methanol. The resulting fluffy solid was dissolved in  $\text{CHCl}_3$ , reprecipitated into ethyl ether, collected by suction-filtering, and dried in a vacuum oven at 55–60°C and 0.01 torr pressure until constant weight. The yield was about quantitative, except for handling losses. The GPC profile of the resulting sample showed a symmetric peak with no apparent salt-peaks, as shown by the fact that the baseline was steady after the end of the main peak, and at the same level as with the molecular weight side.  $^1\text{H}$  NMR of the polymer sample, after overnight-drying in a vacuum oven at 60°C and 0.01 torr, showed almost no remaining nosylate salt, as shown from the sharp reduction of the intensity of the set of doublets at  $\delta$  8.05 –  $\delta$  8.20 ppm.

(3) 0.2 mL aliquots of the reaction mixtures at different times exhibited similar gpc column effects when subjected to analysis without purification. Due to the small quantity of polymer in the aliquot (about 0.04 g), the purification to remove the salts was done in a small-scale fashion, without precipitation of the polymer. The aliquot from a typical *o*-DCB mixture was diluted with 3 mL of THF. Then about 1 mL of a 10% KOH/EtOH solution was added to the THF solution, and stirred for a short period, with mild heating. A cloudy salt was formed and a small amount of the AER resin, prepared as described above, was added to the slurry in the vial. The vial was then centrifuged at 3200 rpm for 10 min, leaving a clear polymer solution over a compact mixture of the AER resin and a white solid. The GPC profile of the supernatant sample showed a



symmetric polymer peak with, however, a large amount of dragging at the low molecular weight side. To the clear solution was then added a small amount of a mixed-bed resin Amberlite MB-3 (MBR), in order to neutralize the KOH by exchanging the potassium cations with protons to produce water. The GPC profile of this polymer showed no skewing of the main peak, but persistent dragging at high elution times was observed. It is unclear why there were still traces of salts, but to completely remove them we used a special small pore-size filter unit, which would remove fine-particle sized salts, insoluble in the THF solution. Thus, we first tried a 0.45  $\mu\text{m}$  filter, with little improvement in the dragging of the GPC peak. However, after the solution was passed through a Millipore 0.20- $\mu\text{m}$  Millex<sup>R</sup>-FGS polytetrafluoroethylene filter unit the GPC profile showed no effects due to salts. The dragging was no longer apparent, and the polymer peak was symmetric. The polymer peak had the same elution volume and breadth, as measured at half-height, as a treated bulk polymer sample, as described above.

All polymers described in this work were purified according to the following general purification procedure:

- (1) Precipitating the polymer from the reaction mixture into ethyl ether.
- (2) Dissolving the collected powder into MeOH and treating with an excess of KOH/MeOH.
- (3) Passing the methanolic solution through an Anion Exchange Resin.

- (4) Reprecipitating the anion-exchanged polymer solution into ethyl ether.

Aliquots removed from the reaction mixtures at different times were purified from salts in the following fashion:

- (1) Samples of the reaction were diluted with THF to 4 mL in a 5 mL vial.
- (2) An excess of KOH/EtOH was added to the samples until the solution was strongly basic and the solution gently heated for 5 min.
- (3) A small amount of AER was added and after shaking the vials were centrifuged for 10 min at 3200 ppm.
- (4) A small amount of MBR was added to the supernatant clear ethanolic solution transferred to a different vial.
- (5) The clear liquid was passed through a 0.2- $\mu$ m filter unit.

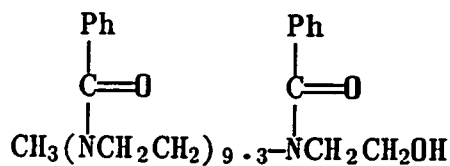
## Appendix B

### <sup>1</sup>H NMR and TOF-SIMS Spectral Analysis of Hexylamine-Treated Poly(N-benzoylethyleneimine)s

The products of the reactions of poly(N-benzoylethyleneimine) (P)<sub>x</sub> polymers and hexylamine M, described in Chapter 5, were analyzed by <sup>1</sup>H NMR (in CDCl<sub>3</sub> using TMS as reference) and TOF-SIMS (by positive-ion bombardment). All structures mentioned in this appendix are numbered in the same way as in the aforementioned chapter.

### <sup>1</sup>H NMR characterization of (P)<sub>10.3</sub>

(P)<sub>10.3</sub> was purified according to the method described in Appendix A, and its 200 MHz <sup>1</sup>H NMR spectrum is shown in Figure B1. We will use this spectrum to compare with spectra of M-treated (P)<sub>x</sub> chains. (P)<sub>10.3</sub> has the following structure 12:



12

The <sup>1</sup>H NMR peak positions are at the following shifts from TMS:

δ 1.91 ppm, δ 2.57 ppm, δ 2.67 ppm, δ 2.82 ppm, δ 3.01 ppm, δ 3.16 ppm, δ 3.45 ppm, δ 3.67 ppm, δ 4.34 ppm (t), δ 7.29 ppm, δ 7.34 ppm (d), δ 7.45 ppm (d, J = 7.6 Hz), δ 8.02 ppm (d, J = 7.6 Hz).

The CH<sub>3</sub>-N- at the beginning of the chain is at δ 3.01 ppm. The -CH<sub>2</sub>OH of the chain end is apparent at 4.34 ppm. -NCH<sub>2</sub>CH<sub>2</sub> protons of the backbone are assigned to the complex structure of multiple peaks between 3 and 4 ppm. This structure consists of a main peak at

$\delta$  3.45 ppm, with two peaks at positions  $\delta$  3.16 ppm and  $\delta$  3.67 ppm. A 50°C  $^1\text{H}$  NMR spectrum of the same sample showed that the complex structure between 3 and 4 ppm collapsed into a single broad peak at 3.45 ppm without peaks on its side. The breadth and position of the latter peak was typical of that due to  $-\overset{|}{\text{N}}\text{CH}_2\text{CH}_2-$  backbone protons of higher molecular weight 2-oxazoline polymers (see for example Figure 3.3, in Chapter 3). The peak at 1.91 ppm might be due to the chain-end  $-\text{OH}$ , since its position shifted downfield when the sample was heated to 50°C. Phenyl ring protons appear as a main peak at  $\delta$  7.34 ppm and a smaller one at  $\delta$  7.29 ppm. The set of doublets at  $\delta$  7.45 ppm and  $\delta$  8.02 ppm is due to a small amount of impurity. There is no evidence of nosylate-anion phenyl protons which appear as a set of doublets at  $\delta$  8.05 ppm and  $\delta$  8.20 ppm, proving that the purification procedure, described in Appendix A, successfully removed all the nosylate salt.

Table B1 shows the  $\bar{X}_n$  of the  $(\text{P})_x$  reactant chains, their stoichiometric ratios with M, and the temperature of each experiment.

Table B1. Parameters of the experiments between  $(\text{P})_x$  and M.

Exp.	Stoichiometry	T(°C)	$\bar{X}_n$
1a	$\text{P}_{1.0}/\text{M}$	28	4.8
1b	$\text{P}_{1.0}/\text{M}$	117	4.8
2	$\text{P}_{1.0}/\text{M}$	108	5.7
3	$\text{P}_{0.5}/\text{M}$	110	10.2



2.82 ppm in Figure B2, due to  $\overset{\cdot}{\text{N}}\text{H}_2\text{CH}_2(\text{CH}_2)_4\text{CH}_3$  (13) has shifted to 2.60 in Figure B3, due to  $\text{NHCH}_2(\text{CH}_2)_4\text{CH}_3$  (14). Thus these facts show that neutralization of 14 has occurred after the purification treatment. Figure B4 shows a 400 MHz  $^1\text{H}$  NMR spectrum of the purified product of (1a). The triplet at 0.81 ppm is assigned to  $\text{N}(\text{CH}_2)_4\text{-CH}_3$  and the complex peak between 1.32 and 1.46 ppm to  $\text{-(CH}_2)_4\text{CH}_3$  of 14. The  $\text{CH}_3\text{N-CH}_2$  due to the beginning of the polymer chain (both 12 and 14) is at 3.00 ppm. A peak at 2.97 ppm might be due to  $\overset{\text{Ph}}{\text{C=O}}\text{-NCH}_2\text{CH}_2\text{NHCH}_2(\text{CH}_2)_4\text{-}$  of 14, however it was not possible to confirm this assignment because the NH- group hydrogen-bonds to  $\text{CDCl}_3$  and it could therefore shift to other regions of the spectrum. The polymer backbone protons are split into many peaks giving a complex structure centered at 3.33 ppm. A small triplet at 4.30 ppm is due to the  $\text{-CH}_2\text{OH}$  at the end of (P)<sub>4-8</sub>. Phenyl ring protons of both (P)<sub>4-8</sub> and 14 appear as a large peak at 7.33 ppm and a smaller one at 7.11.

Figure B5 shows a TOF-SIMS spectrum of purified (1a). On examining the spectrum from right to left, one notices sequences of peaks which are repeated at approximately the molecular mass of the phenyl oxazoline monomer (MW of PO 147.18). The peak sequences consist of a set of three peaks appearing to be part of three respective distributions. The highest molecular mass peak of each set (the first of the three from the right) is part of a distribution with maximum intensity at 758. The calculated  $\bar{M}_n$  of 14 from the Poisson distribution is  $15 + (4.8 \times 147.18) + 100 = 821$ , therefore the highest mass peaks of each set might correspond

to 14, fragmented at the hexyl core. The middle peak of each set shows a distribution with maximum intensity at 690. The calculated  $\bar{M}_n$  for 12 is 738, hence the middle set of peaks might correspond to the unreacted (P)<sub>4-8</sub>.

Experiment 1b: Figure B6 shows a 400 MHz <sup>1</sup>H NMR spectrum of the

purified product of (1b). The  $\begin{matrix} \text{Ph} \\ \text{C}=\text{O} \end{matrix}$   $(-\text{NCH}_2\text{CH}_2)_2\text{NCH}_2(\text{CH}_2)_4-$  appears as a small peak at 2.54 ppm. Two main differences are noted here from the spectrum shown in Figure B4 of (1a): the polymer backbone structure is less split than that of (1a), and the peak at 2.97 ppm assigned to  $\begin{matrix} \text{Ph} \\ \text{C}=\text{O} \end{matrix}$   $-\text{NCH}_2\text{CH}_2\text{NHC}(\text{CH}_2)_4-$  is not evident. We are not certain if this is because the  $\text{NH}-$  has hydrogen-bonded to CDCl<sub>3</sub>, or, because (P)<sub>4-8</sub> has reacted twice with M affording solely 15.

Figure B7 shows the TOF-SIMS spectrum of the purified product of (1b). The highest mass peak of the sequences appears to be part of a distribution with maximum intensity at about 1460. This is close to the calculated  $\bar{M}_n$  of 1542 for the twice-reacted product 15. The other peaks in the sets appear to be fragments that may have resulted from cleavage of the polymer chains at the hexyl group.

Experiment (2): A 400 MHz <sup>1</sup>H NMR spectrum of the product of (2) is shown in Figure B8. The spectrum shows evidence of remaining peaks due to nosylate phenyl protons at 8.06 and 8.19 ppm, thus showing incomplete



neutralization. A small peak appears at about 2.3 ppm which may be due

to  $\begin{array}{c} \text{Ph} \\ \text{C}=\text{O} \\ (-\text{NCH}_2\text{CH}_2)_2\text{N}\text{CH}_2(\text{CH}_2)_4- \end{array}$ . Figure B9 shows the corresponding

TOF-SIMS spectrum of the product of (2). The previously observed peak sequences are not seen here as clearly as in Figures B5 and B7. The highest intensity distribution has a maximum at about 670, which is less than the  $\bar{M}_n$  of 871 for (P)<sub>5.7</sub>. Therefore this set of peaks might be part of a distribution of polymer chains fragmented from twice-reacted 15.

Experiment (3): Figure B10 shows a 400 MHz <sup>1</sup>H NMR spectrum of the purified product of (3). The peak at 2.97 ppm is again apparent, as in the spectrum of Figure B4. This is consistent with the previous assignment to

$\begin{array}{c} \text{Ph} \\ \text{C}=\text{O} \\ -\text{NCH}_2\text{CH}_2\text{N}\text{CH}_2(\text{CH}_2)_4- \end{array}$ . A TOF-SIMS spectrum of (3) is shown in

Figure B11. This shows sequences of sets, each set having multiple peaks. The highest mass peak in each set is part of a distribution with maximum intensity at about 1470, and the second peaks from the right are part of a distribution with maximum at about 1380. The third peaks from the right in each set have the highest intensity and show a maximum at about 1280.

Peak shifts of the <sup>1</sup>H NMR spectra of Experiments (1)–(3) are listed in Table B2. For comparison we have included the shifts of hexylamine M in the first column and those of (P)<sub>10.3</sub> in the second. The sum of areas of the peaks under the indicated regions of the spectra are shown at the bottom of each region; the sums are normalized to the area of the phenyl protons so that the latter have an area of 100.

Table B.1.  $^1\text{H}$  NMR shifts  $\delta$  (ppm), in the area between 0.8–1.5 of hexylamine-treated  $(\text{P})_x$

M	$(\text{P})_{10.3}$ 200	1a 200*	1a 200**	1a 400**	1b 400**	2 400**	3 400**
0.92		0.81	0.86	0.81	0.86	0.81	0.80
1.08							0.86
1.32		1.12	1.23	1.25	1.15	1.13	1.09
1.46		1.45	1.37	1.38	1.49	1.45	1.19
$\Sigma(\text{Areas})$	— 0.0	42.0	40.0	20.5	19.4	23.8	14.2

Table B.1  $^1\text{H}$  NMR shifts  $\delta$  (ppm), in the area between 1.5–4.5 of hexylamine-treated  $(\text{P})_x$

M	$(\text{P})_{10-3}$ 200	1a 200 *	1a 200 **	1a 400 **	1b 400 **	2 400 **	3 400 **
					2.07		
2.57			2.55	2.53	2.54	2.52	
2.67	2.62		2.65	2.63	2.63	2.58	
	2.76						
2.72	2.82	2.60					
			2.93	2.97			2.97
	3.01	3.04	2.98	3.00	2.99	2.99	
				3.08	3.06	3.08	3.09
	3.16			3.17	bump	3.17	3.14
				3.31	3.45		3.45
	3.45	3.48	3.39	3.36	3.41	3.36	3.41
				3.50			
	3.67	3.70	3.61	3.65	3.65	3.61	3.65
	3.88	3.85	3.80	bump	bump	bump	bump
	4.33	4.37	4.33	4.30	4.35	4.33	4.30
$\Sigma(\text{Areas})$	— 94.6	105.6	117.6	84.8	92.9	81.4	86.6

Table B.1 (continued).  $^1\text{H}$  NMR shifts  $\delta$  (ppm), in the area between 7.0–8.5 of hexylamine-treated  $(\text{P})_x$

M	$(\text{P})_{10-3}$ 200	1a 200*	1a 200**	1a 400**	1b 400**	2 400**	3 400**	
	7.13	7.20	7.14	7.11	7.11	7.11	7.11	
	7.34	7.38	7.32	7.33	7.33	7.33	7.33	
$\Sigma(\text{Areas})$	100.0	100.0	100.0	100.0	100.0	100.0	100.0	
8.00								
8.04								
		8.06	8.00	8.05	8.05	8.06	8.05	
		8.22	8.15	8.20	8.20	8.19	8.20	
$\Sigma(\text{Areas})$	—	4.1	16.1	1.6	2.7	1.8	7.1	2.1

\* before purification

\*\* purified

Due to the complexity of the peaks in the area between 2.0 and 3.0 ppm and the overlap with the tail of the backbone protons, we could

not calculate the areas due to  $\begin{array}{c} \text{Ph} \\ \text{C=O} \\ -\text{NCH}_2\text{CH}_2\text{NHCH}_2(\text{CH}_2)_4- \end{array}$  and  $\begin{array}{c} \text{Ph} \\ \text{C=O} \\ (-\text{NCH}_2\text{CH}_2)_2\text{NCH}_2(\text{CH}_2)_4- \end{array}$  and divide by the area of the phenyl protons to obtain the number of chains reacted per M.

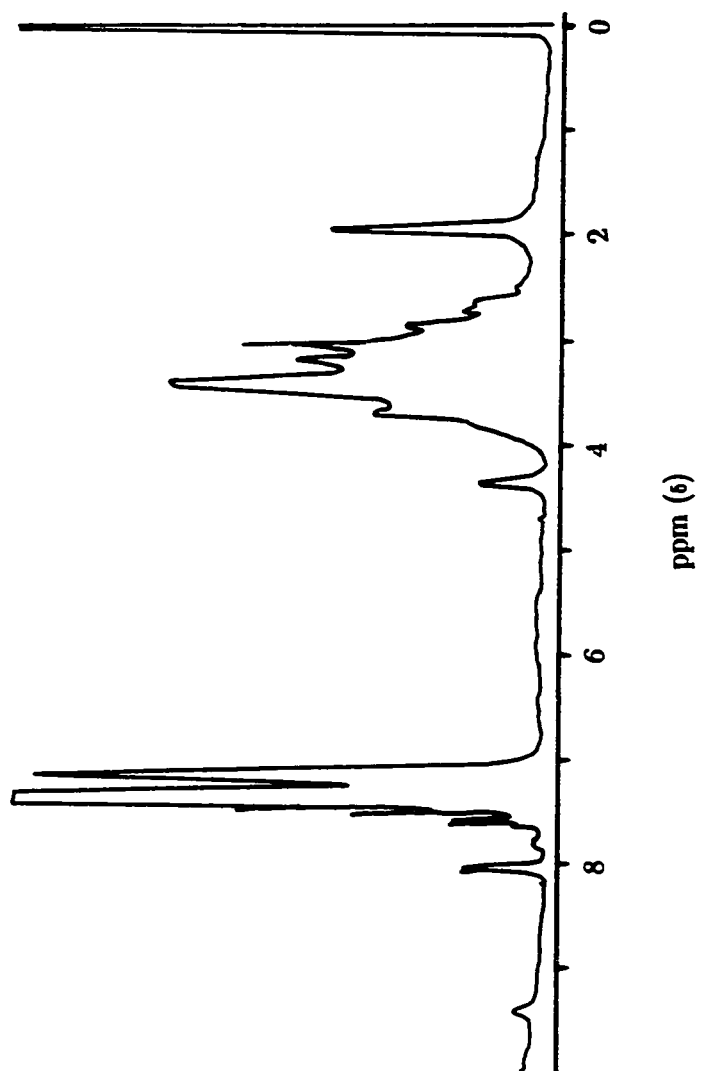


Figure B1. 200 MHz  $^1\text{H}$  NMR spectrum of purified (P)<sub>10-3</sub>.

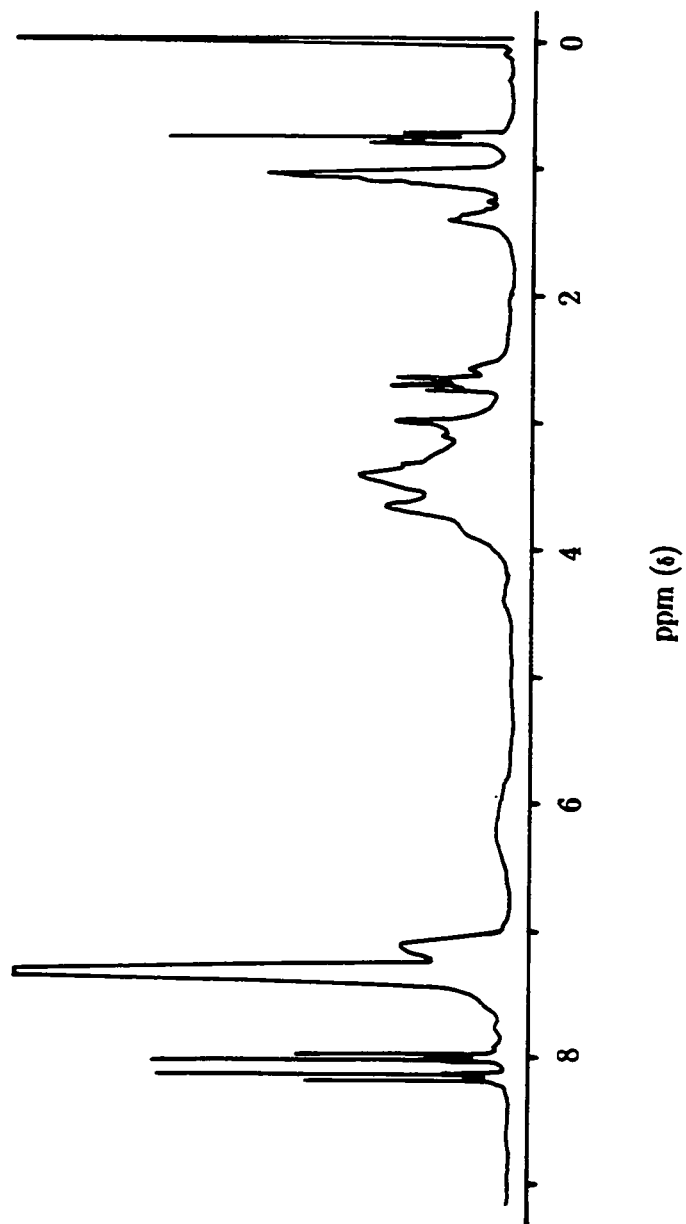


Figure B2. 200 MHz <sup>1</sup>H NMR spectrum of the product of the P<sub>1.0</sub>/M reaction at 28 °C in o-DCB using (P)<sub>4.8</sub>, before purification.

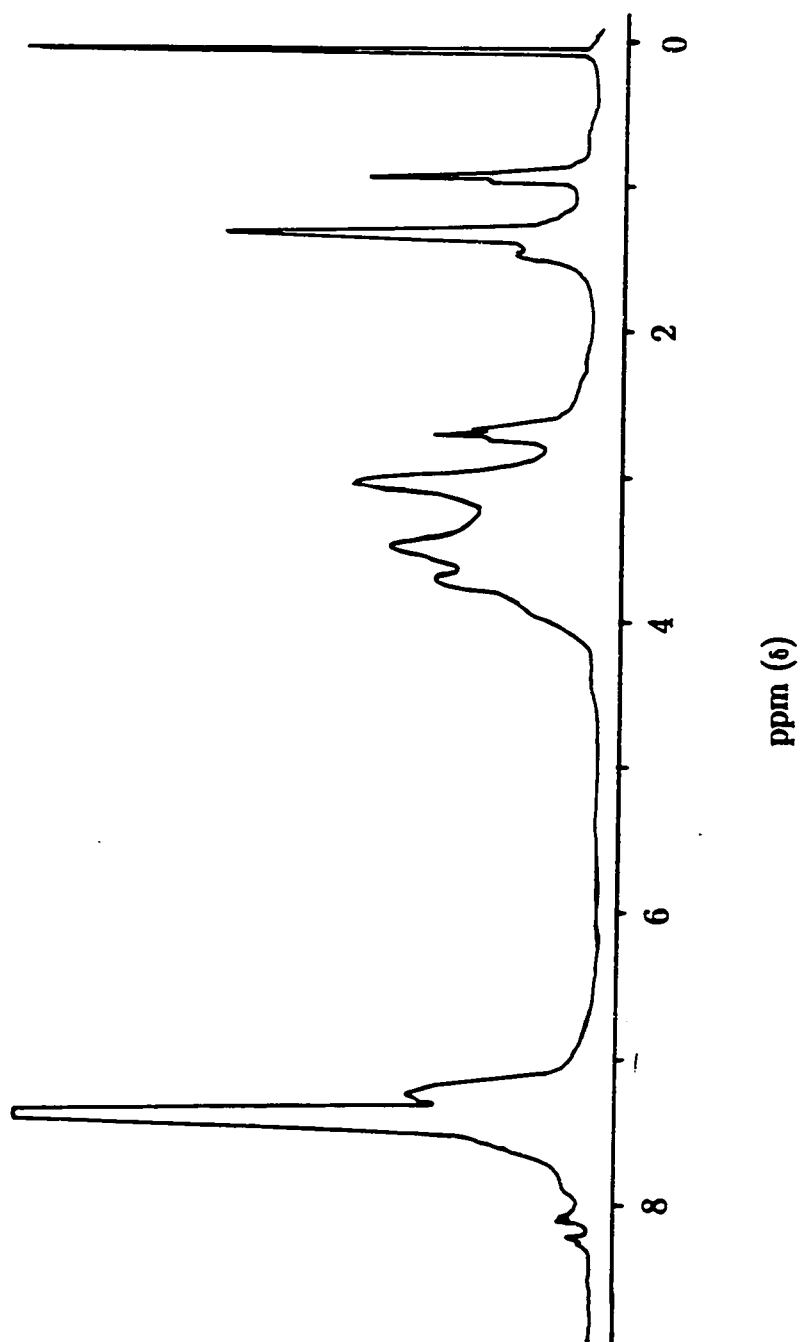


Figure B3. 200 MHz  $^1\text{H}$  NMR spectrum of the purified product of the  $\text{P}_{1-o}/\text{M}$  reaction at 28  $^\circ\text{C}$  in *o*-DCB using  $(\text{P})_{4.8}$ .



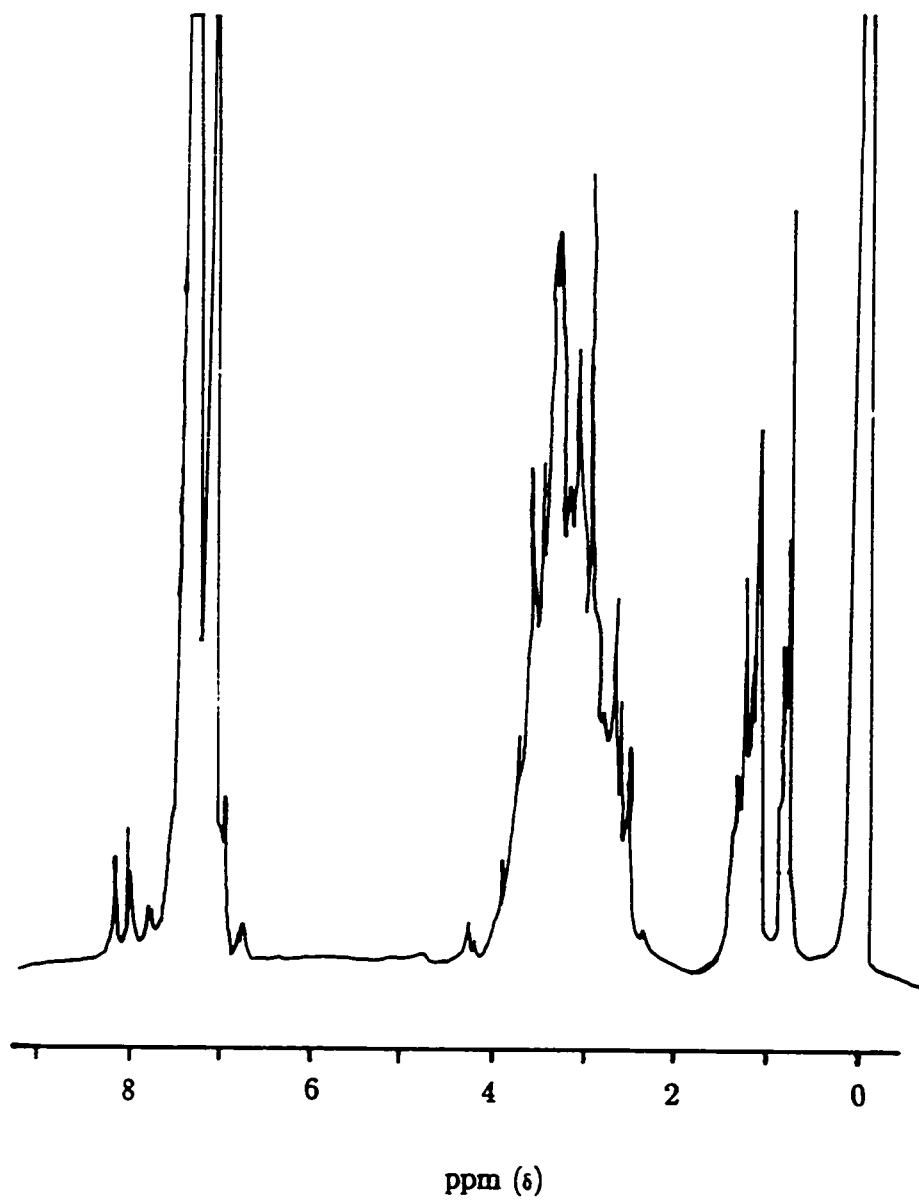


Figure B4. 400 MHz  $^1\text{H}$  NMR spectrum of the product of the  $\text{P}_{1.0}/\text{M}$  reaction at 28  $^{\circ}\text{C}$  in *o*-DCB using  $(\text{P})_{4.8}$ .

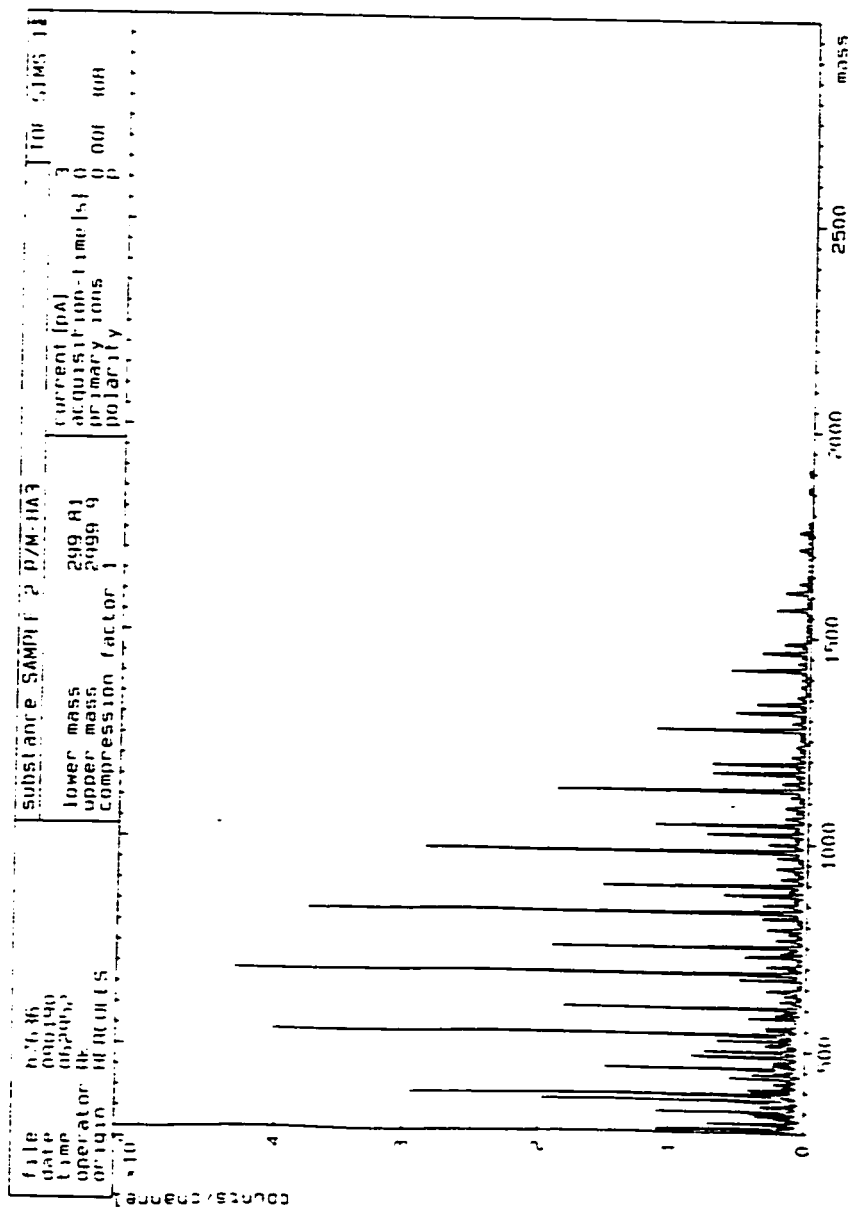


Figure B5. TOF-SIMS spectrum of product of the P<sub>1.0</sub>/M reaction at 28 °C in o-DCB using (P)<sub>4.8</sub>.

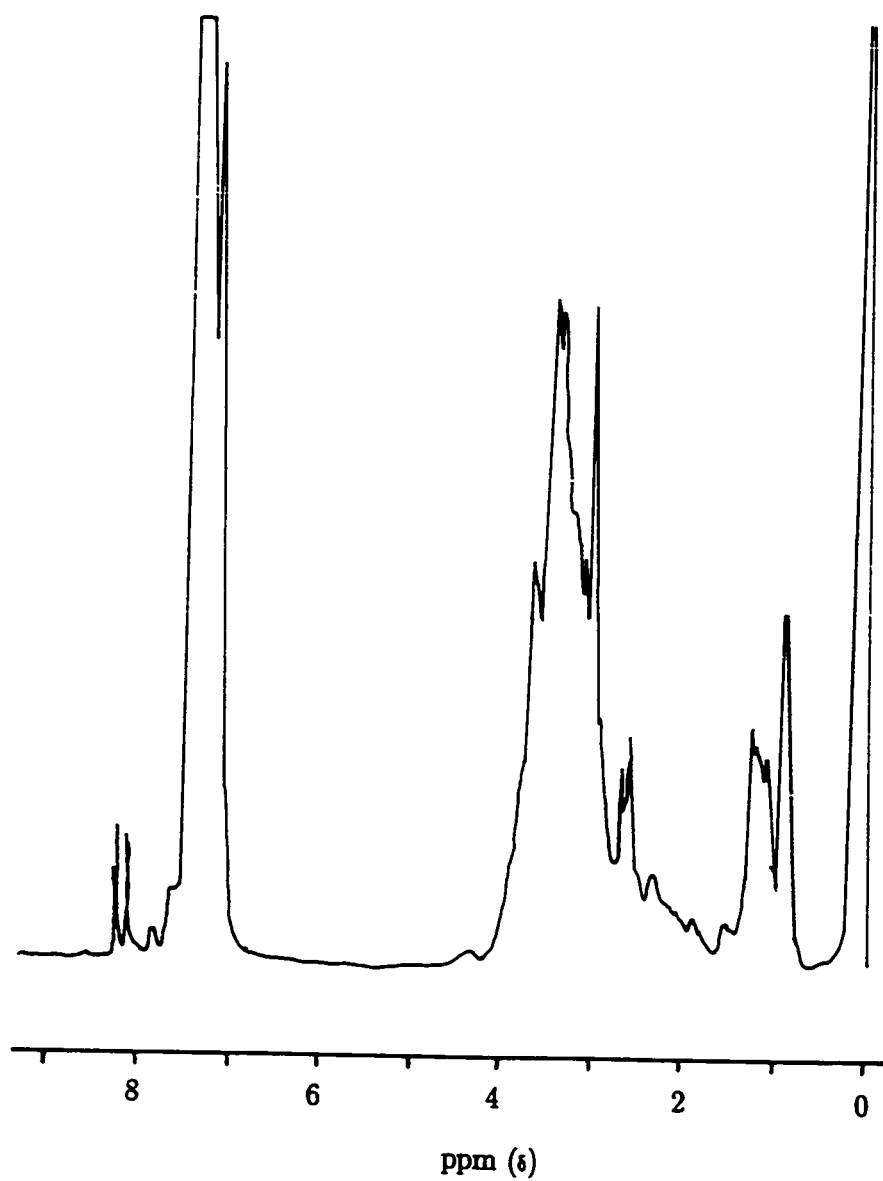


Figure B6. 400 MHz <sup>1</sup>H NMR spectrum of the product of the P<sub>1.0</sub>/M reaction at 117 °C in *o*-DCB using (P)<sub>4.8</sub>.

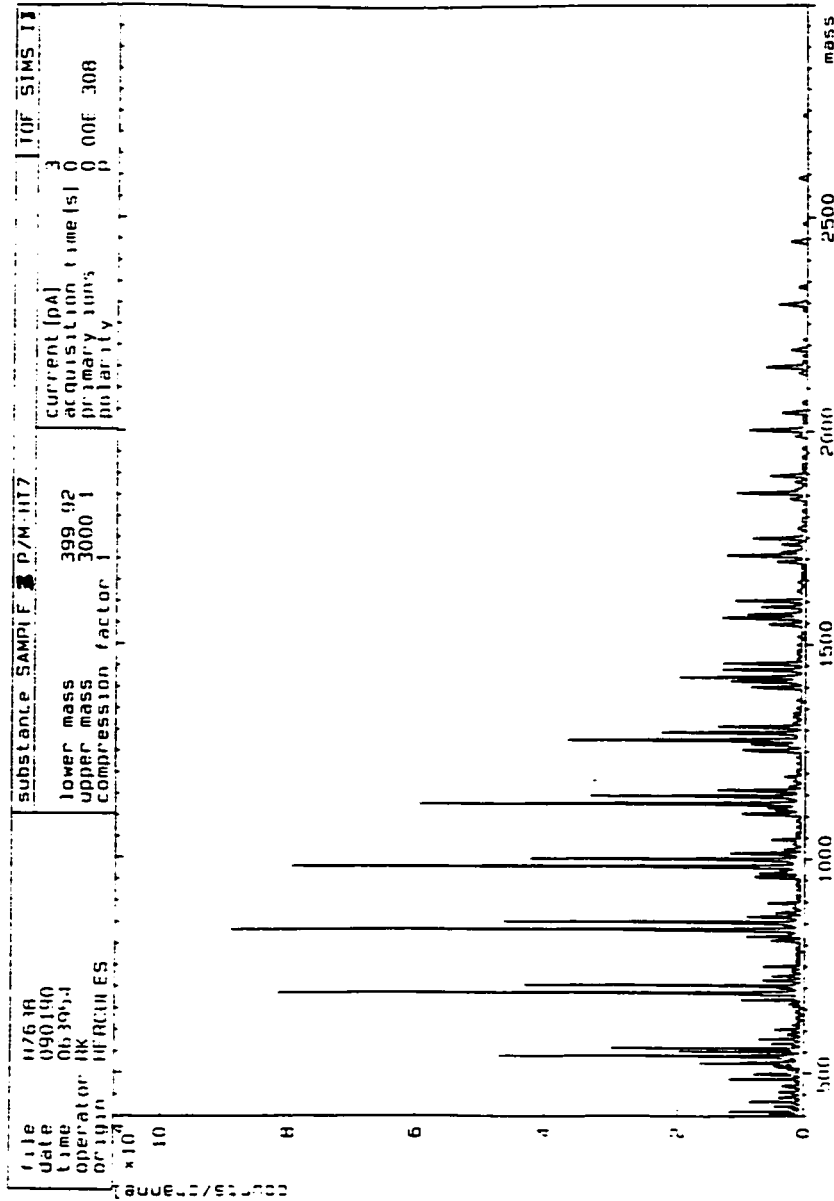


Figure B7. TOF-SIMS spectrum of product of the P<sub>1.0</sub>/M reaction at

117 <sup>13</sup>C in o-DCB using (P)<sub>4.8</sub>.

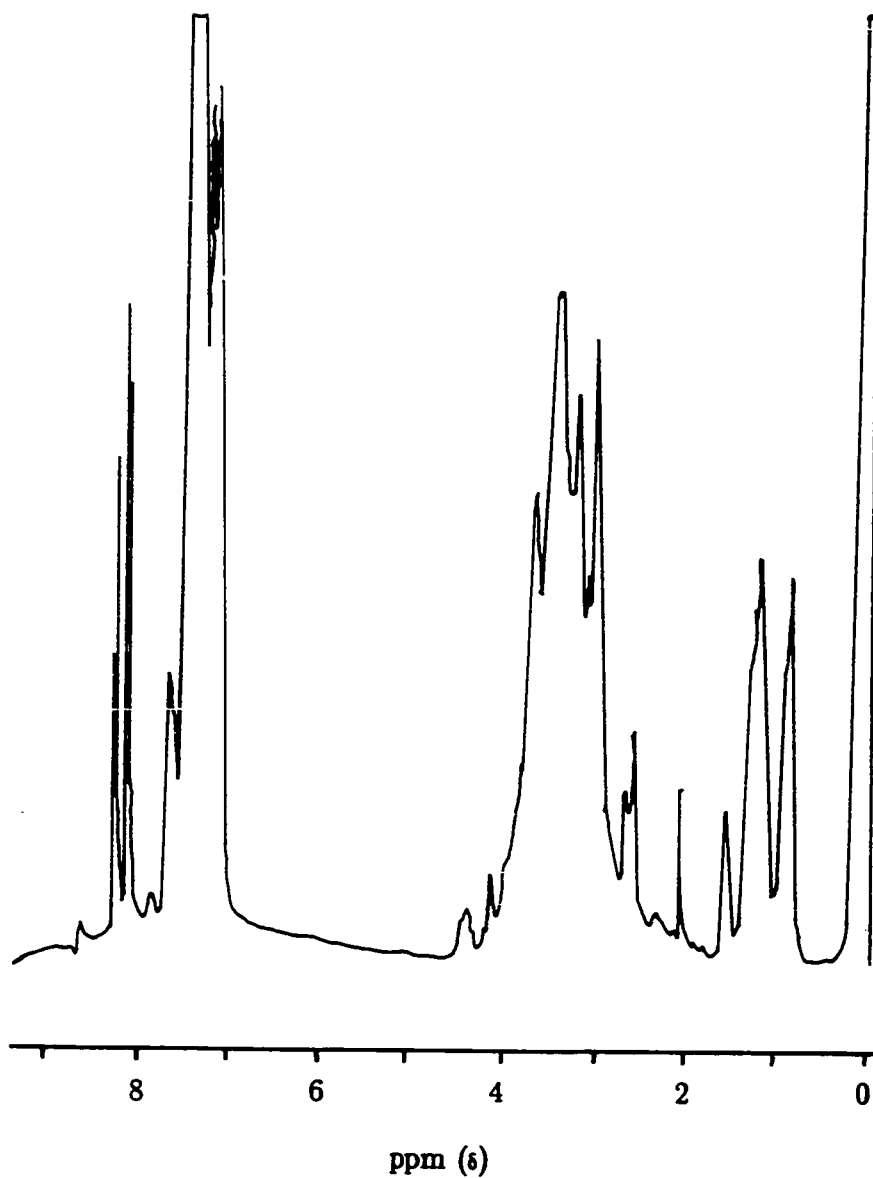


Figure BS. 400 MHz  $^1\text{H}$  NMR spectrum of the product of the  $\text{P}_{1.0}/\text{M}$  reaction at 108  $^\circ\text{C}$  in *o*-DCB using  $(\text{P})_{5.7}$ .



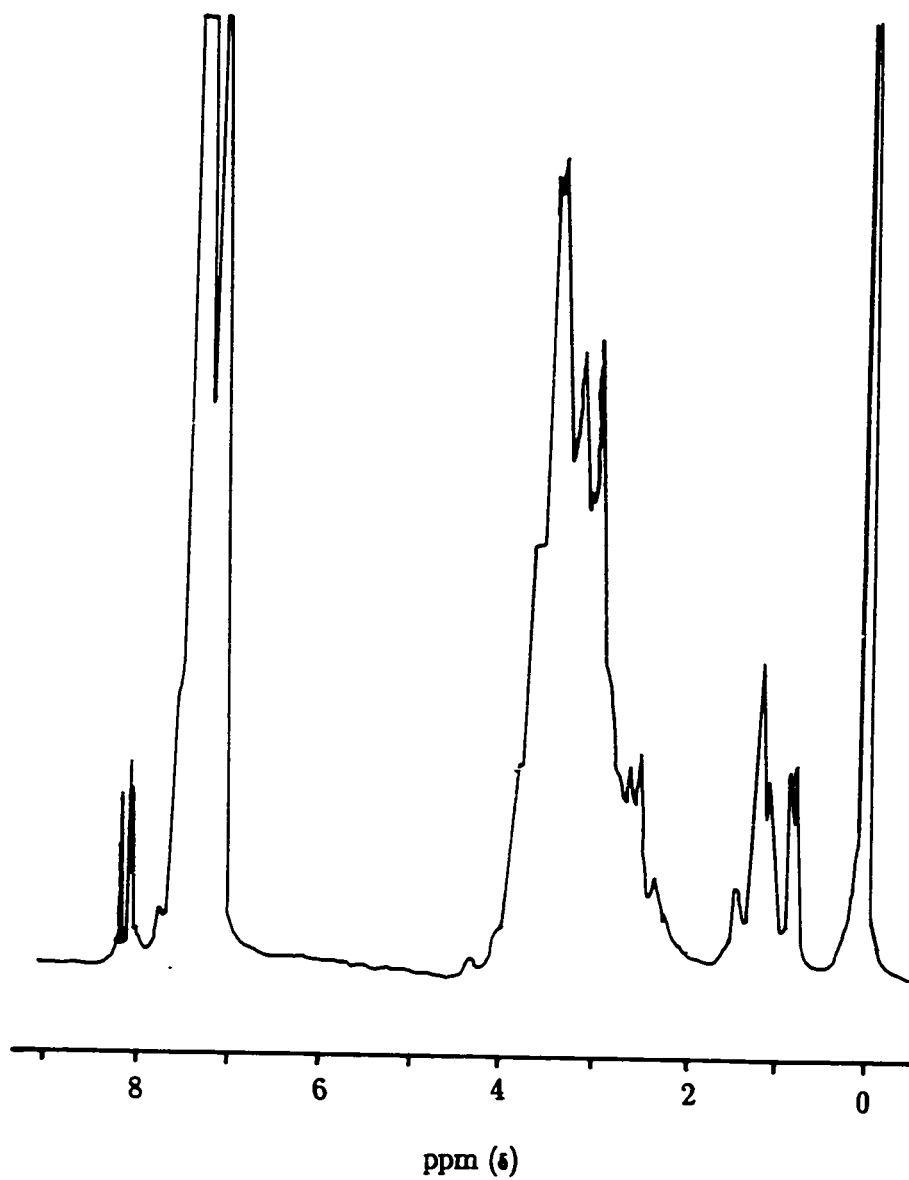


Figure B10. 400 MHz  $^1\text{H}$  NMR spectrum of the product of the  $\text{P}_{0.5}/\text{M}$  reaction at 110  $^{\circ}\text{C}$  in *o*-DCB using  $(\text{P})_{10.2}$ .

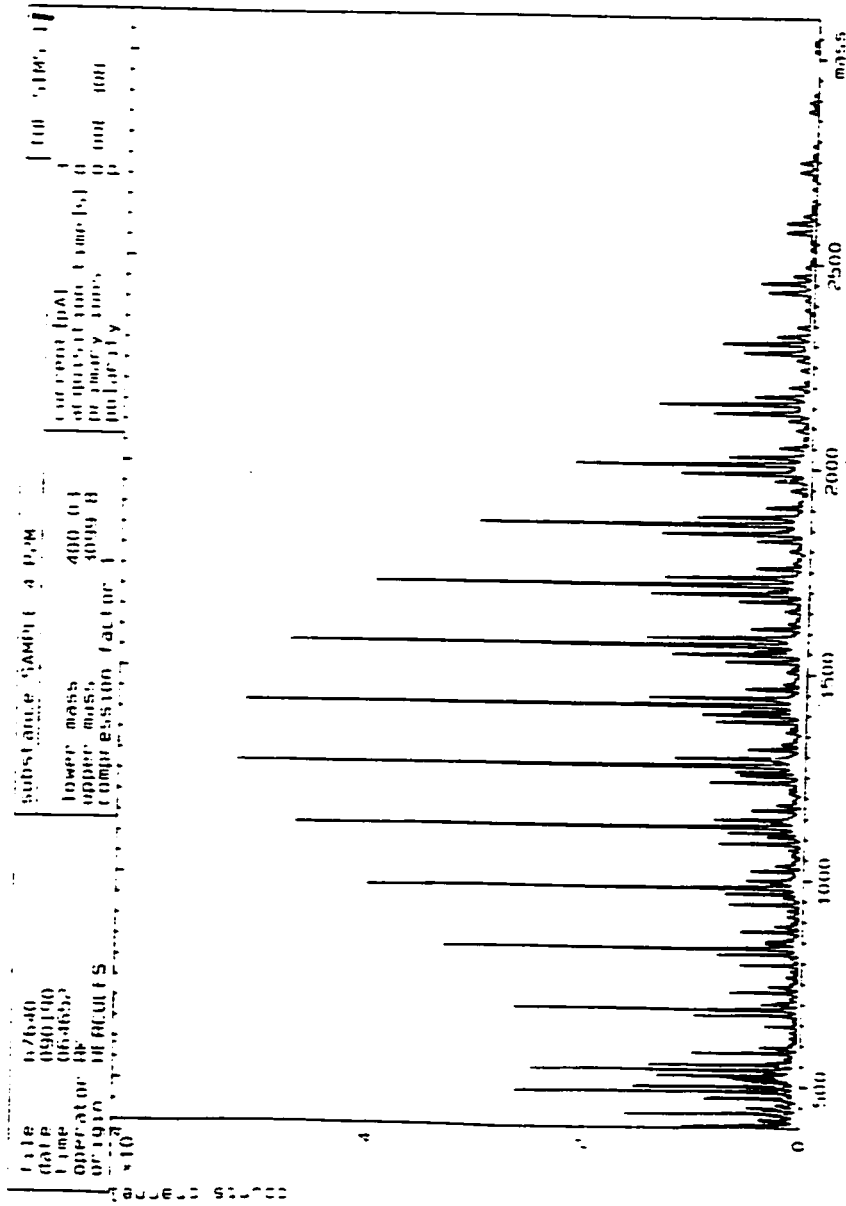


Figure B11. TOF-SIMS spectrum of the product of the P<sub>0.5</sub>/M reaction at 110 °C in o-DCB using (P)<sub>0.2</sub>.



## Appendix C

### <sup>1</sup>H NMR and TOF-SIMS Spectral Analysis of Hexamethylenediamine-Treated Poly(N-benzoyl ethyleneimine)s

This appendix deals with  $^1\text{H}$  NMR (in  $\text{CDCl}_3$  using TMS as reference) and TOF-SIMS (by positive-ion bombardment) analysis of the products resulting from reaction of poly(N-benzoyl ethyleneimine)  $(\text{P})_x$  and hexamethylenediamine **H**, described in Chapter 5. The structures mentioned are numbered in the same way as in Chapter 5.

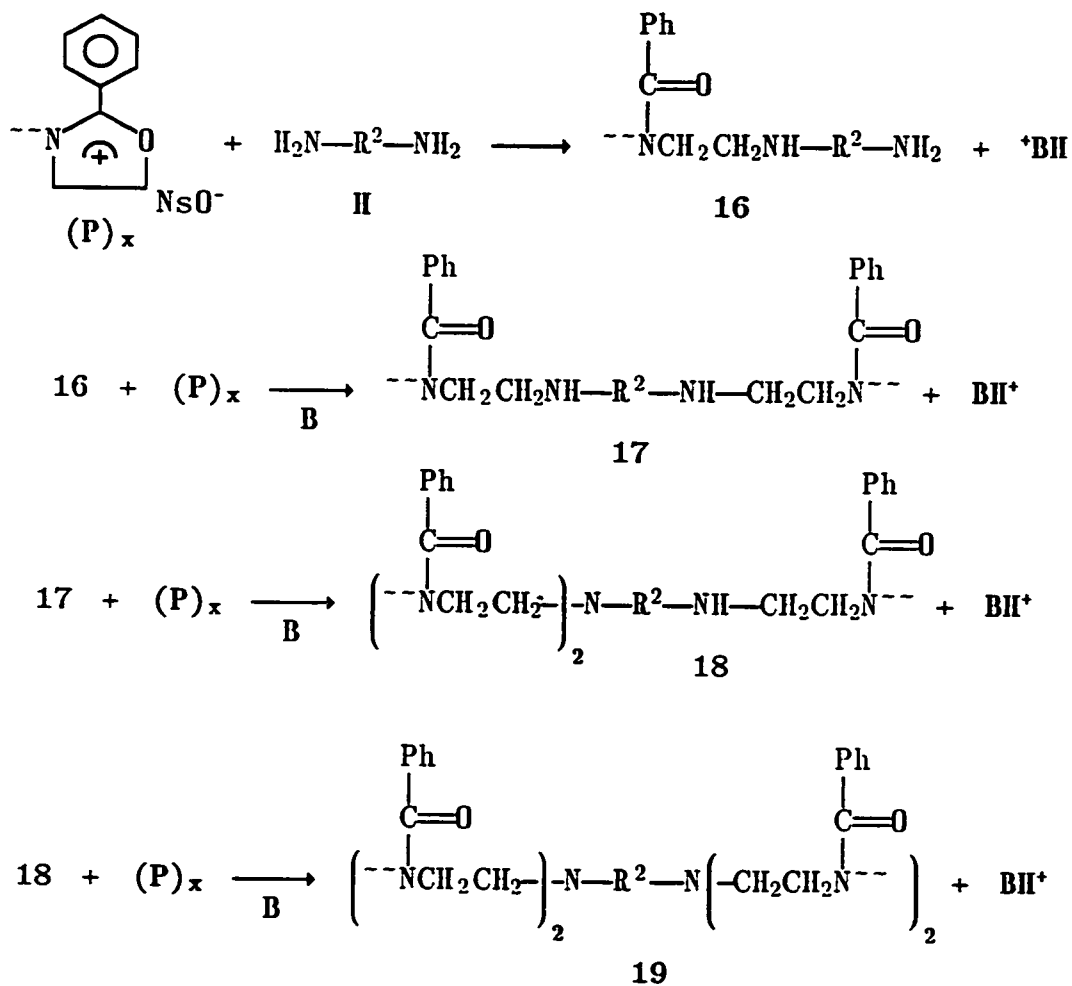
Table C1 shows the experiments carried out by reaction of **H** with living  $(\text{P})_x$  chains.

Table C1. Parameters of the experiments between  $(\text{P})_x$  and **H** in *o*-DCB, and in DMac.

Exp.#	Stoichiometry	$\bar{X}_n$
4	$\text{P}_{3.5}/\text{H}/\text{B}_{2.0}$	8.6
5	$\text{P}_{4.0}/\text{H}/\text{B}_{7.9}$	10.5
6	$\text{P}_{4.3}/\text{H}/\text{B}_{8.8}$	10.0
7	$\text{P}_{2.1}/\text{H}/\text{B}_{8.4}$	10.2

Scheme C1 shows the structures that we will refer to in the following spectral interpretation.

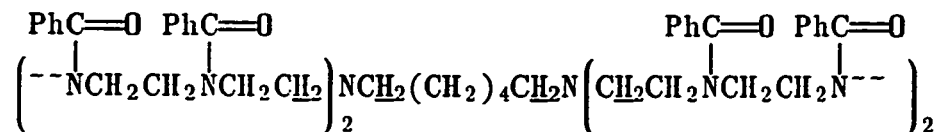
## Scheme C1



where  $\text{R}^2 = \text{---CH}_2(\text{CH}_2)_4\text{CH}_2\text{---}$ ,  $\text{B} = ((\text{CH}_3)_2\text{CHCH}_2)_3\text{N}$ , and  $\text{*BH} = ((\text{CH}_3)_2\text{CHCH}_2)_3\text{NH}^+ \text{NsO}^-$

Experiment (4): Figure C1 shows the 200 MHz  $^1\text{H}$  NMR spectrum of the purified product of Experiment (4). According to the discussion in Chapter 5, the product of this experiment consists mainly of 19

and small amounts of 16, 17, 18 and unreacted (P)<sub>8.6</sub> of structure 12. The methylene protons that surround the nitrogens adjacent to R<sup>2</sup> are shown in 19a:



19a

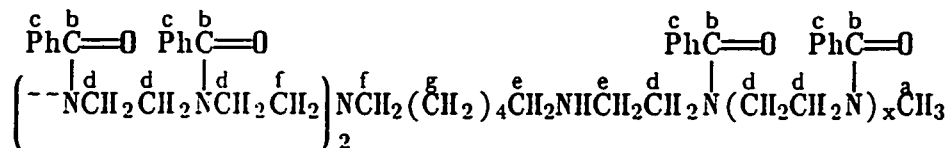
These protons are assigned to a small peak at  $\delta$  2.65 ppm. In order to determine the number of polymer branches attached to R<sup>2</sup> we need to obtain the ratios of the areas due to the phenyl protons ( $\delta$  7.0 and 7.77 ppm). However, we could not obtain their integrated area because they overlapped with the polymer backbone methylene protons, which appear as three broad peaks at  $\delta$  3.18, 3.38, and 3.62 ppm (see Appendix B). The doublets at  $\delta$  0.8 (<sup>1</sup>CH<sub>3</sub>-) and 2.0 ppm (-CH<sub>2</sub>N<sup>2</sup>-) arise from remaining B ((<sup>1</sup>CH<sub>3</sub>)<sub>2</sub>CH(<sup>2</sup>CH<sub>2</sub>)<sub>3</sub>N). The -(CH<sub>2</sub>)<sub>4</sub>- of R<sup>2</sup> appear as a broad peak between  $\delta$  0.62 and 1.53 ppm. There is no evidence of nosylate protons at  $\delta$  8.05 and 8.20 ppm demonstrating complete neutralization of the polymer.

A TOF-SIMS spectrum of the product of (4) is shown in Figure C2. This shows extensive fragmentation evidenced by the multiple peaks in sets of repeated sequences. The peaks of highest intensity appear to be distributed around a maximum of 1050. Since the  $\bar{M}_n$  of (P)<sub>8.6</sub> is about 1300, the highest intensity peaks might be due to cleavage of the polymer

chains from R<sup>2</sup>. Further work is needed to understand the cleavage mechanism.

Experiment (5): Figures C3 and C4 show the 200 MHz <sup>1</sup>H NMR spectra of purified product of (5) at room temperature, and after running the spectrometer at 50°C. The spectrum at room temperature has the same general appearance as that of (4), shown in Figure C1. The impurity due to B is greatly reduced ( $\delta$  0.8 and 2.0 ppm) but there is an impurity due to remaining ethyl ether (from precipitation) at  $\delta$  1.2 and 3.4 ppm. Comparison between Figures C3 and C4 reveals that the complex structure due to polymer backbone protons collapses into a single broad peak at  $\delta$  3.33 ppm.

A 100 MHz <sup>13</sup>C NMR spectrum of the product of (5) in 50% CDCl<sub>3</sub> is shown in Figure C5. This was run without Nuclear Overhauser Effect during the acquisition period in order to obtain quantification of the areas under the carbon peaks. We chose structure 18a to indicate the various carbon shifts ( $\delta$  ppm from TMS):



18a

Table C1 shows the carbon peak assignments of (5) based on Figure C5.

Table C1.  $^{13}\text{C}$  shifts ( $\delta$  ppm) and the corresponding areas of the product of (5).

group	shift	area
a	37.9	2.14
b	171.9	20.55
c	135.5	20.13
c	129.4	59.92
c	128.5	
c	126.2	38.77
d	46.0	20.32
d	40.9	17.01
e	53.9	—
f	52.5	—
g	26.8	—

The average of the areas due to the phenyl carbons (d) is 19.80 per carbon. From the 2.14 for the area of  $\text{N}-\underline{\text{C}}\text{H}_3$  (a), we get a 9.25 ratio of (d)/(a), compared to an initial  $[\text{PO}]/[\text{I}]$  ratio of 10.5. The ratio of 19.80 of the phenyl carbons divided by (1.90/4) of the area due to  $-(\underline{\text{C}}\text{H}_2)_4-$  (g) gives an average ratio of 41.68 carbons per reacted  $\text{R}^2$ . Dividing this value

by the (d)/(a) ratio gives about 4.5 compared to the initial stoichiometry of 4.0. We could not get accurate values for the areas due to (d) and (e) because the areas were very small and overlapped with each other. The peaks at 15.2 and 65.6 are due to remaining ethyl ether, which is also shown in the  $^1\text{H}$  NMR spectra of Figures C4 and C5.

A TOF-SIMS spectrum of the product of (5) is shown in Figure C6. This shows the same pattern of fragmented chains as Figure C2.

Experiment (6): Figure C7 shows a 200 MHz  $^1\text{H}$  NMR spectrum of (6). The spectrum has the same general appearance as that of Experiment (5), except that the peaks due to B are removed. There are impurity peaks at  $\delta$  1.2 and 3.4 ppm due to remaining ethyl ether, and at  $\delta$  5.0 ppm of an unknown compound.

The TOF-SIMS spectrum of (6) shown in Figure C8 shows a high molecular weight fraction extending over 3000; the peaks show low intensity due to extensive fragmentation.

Experiment (7): Figures C9 and C10 show the 200 MHz  $^1\text{H}$  NMR and TOF-SIMS spectra of experiment (7). Figure C9 shows large amount of impurities, as shown by the narrow lines. The peak at about  $\delta$  2.95 ppm may be due to the NH- adjacent to the  $\text{R}^2$  of structure 18, but we could not confirm this because of possible hydrogen-bonding to  $\text{CDCl}_3$ , and the apparent impurities. Figure C10 shows multiple peaks in repeated sequences, the major fraction of which has maximum intensity at about 1600.

From the NMR spectra shown it was not possible to determine the number of polymer branches per  $R^2$  because first the peaks due to the protons adjacent to the anchor  $R^2$  overlapped with the peaks due to the polymer backbone, and second there were impurities present that interfered with the analysis.

More work is needed to understand the results obtained from the TOF-SIMS spectra in order to (1) understand the mechanism of cleavage, and (2) determine the parent distributions of the star polymers by assigning all the peaks over the whole mass spectrum and adding the areas correspondign to each fragment.



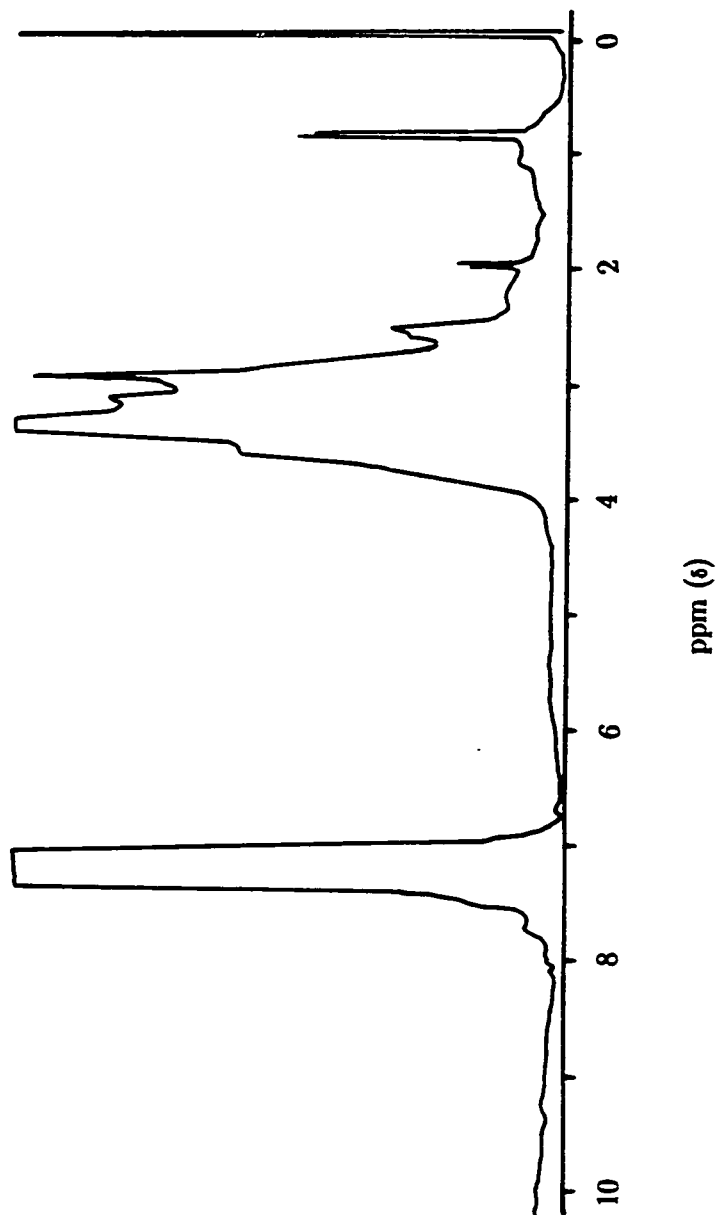


Figure C1. 200 MHz  $^1\text{H}$  NMR spectrum of the product of the  $\text{P}_{3.5}/\text{H}/\text{B}_{2.0}$  reaction at 121  $^\circ\text{C}$  in *o*-DCB using  $(\text{P})_{8.6}$ .

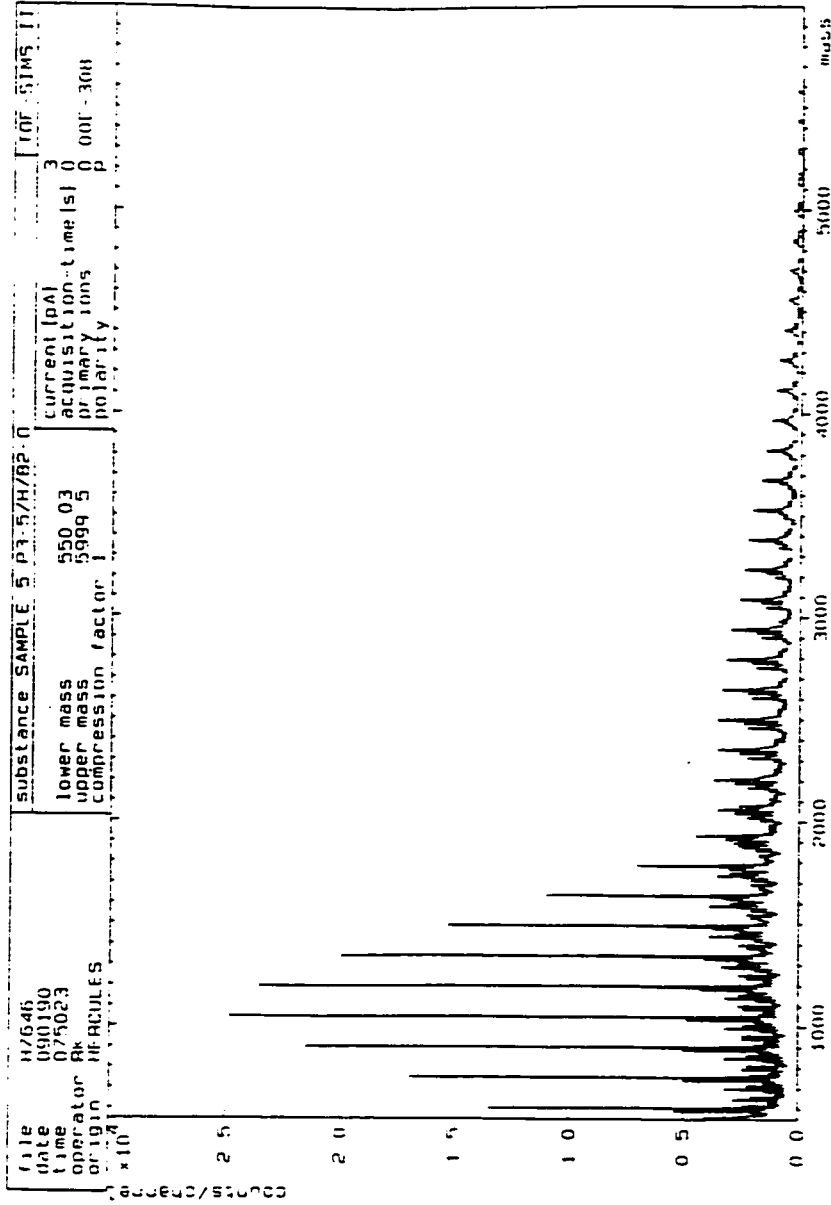


Figure C2. TOF-SIMS spectrum of the product of the P<sub>3-5</sub>/H/B<sub>2-0</sub> reaction at 121 °C in o-DCB using (P)<sub>8-6</sub>.

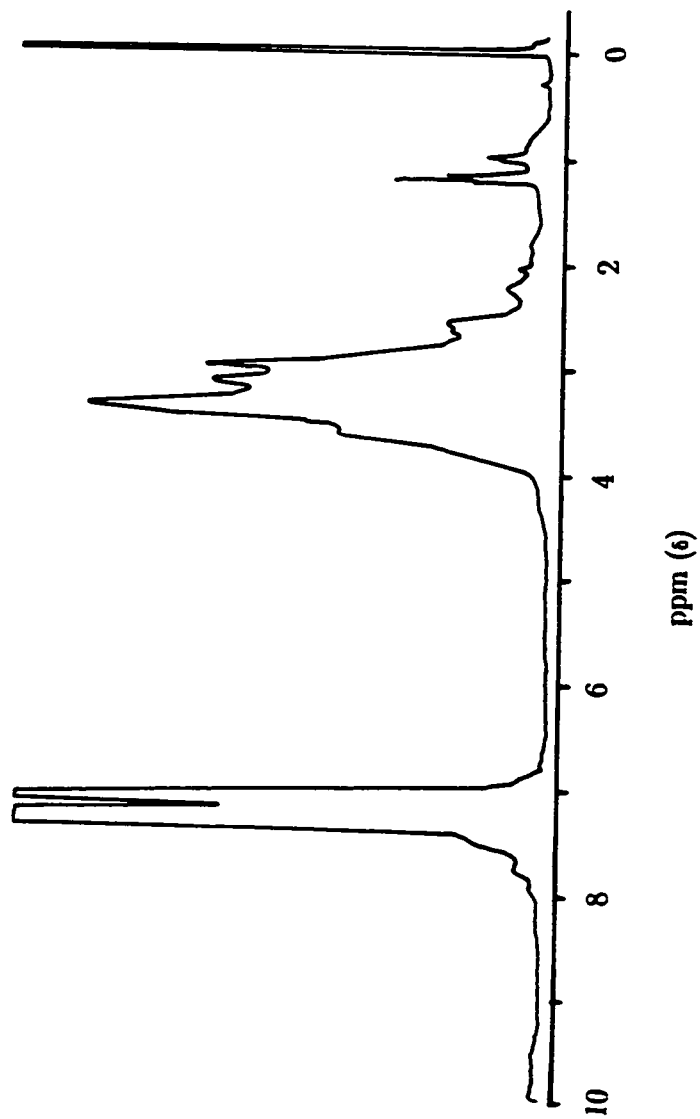


Figure C3. Room temperature 200 MHz  $^1\text{H}$  NMR spectrum of the product of the P<sub>4.0</sub>/II/B<sub>7.9</sub> reaction at 125 °C in DMAc using (P)<sub>10.5</sub>.

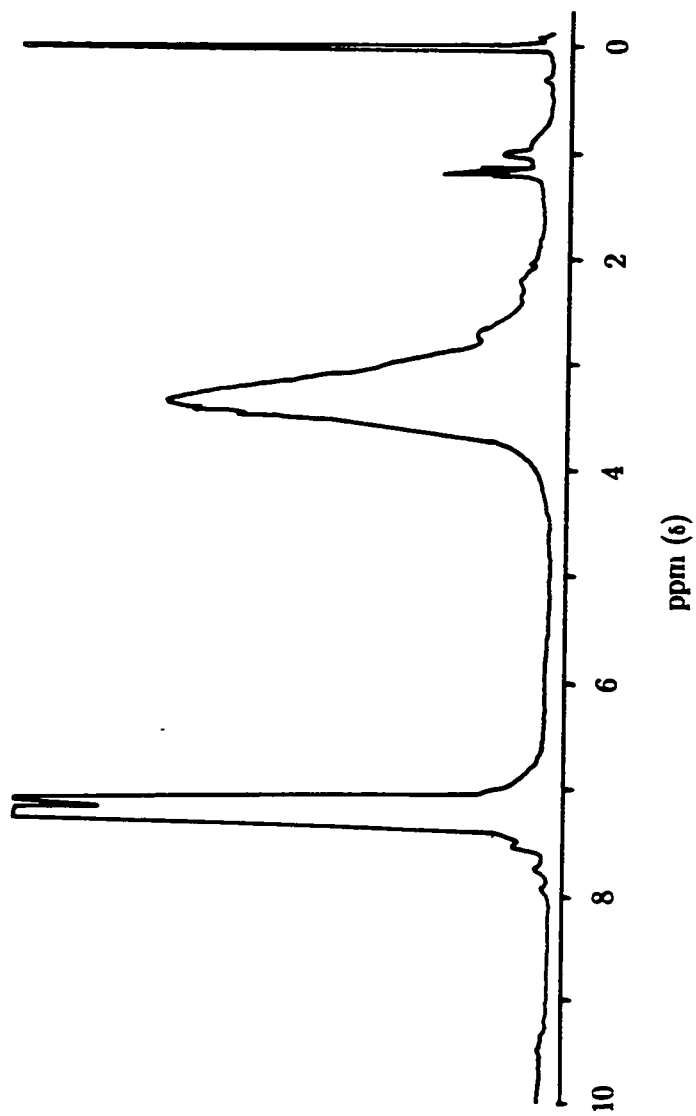


Figure C4. 200 MHz <sup>1</sup>H NMR spectrum taken at 50 °C of the product of the P<sub>4.0</sub>/H/B<sub>7.9</sub> reaction at 125 °C in DMAc using (P)<sub>10.5</sub>.

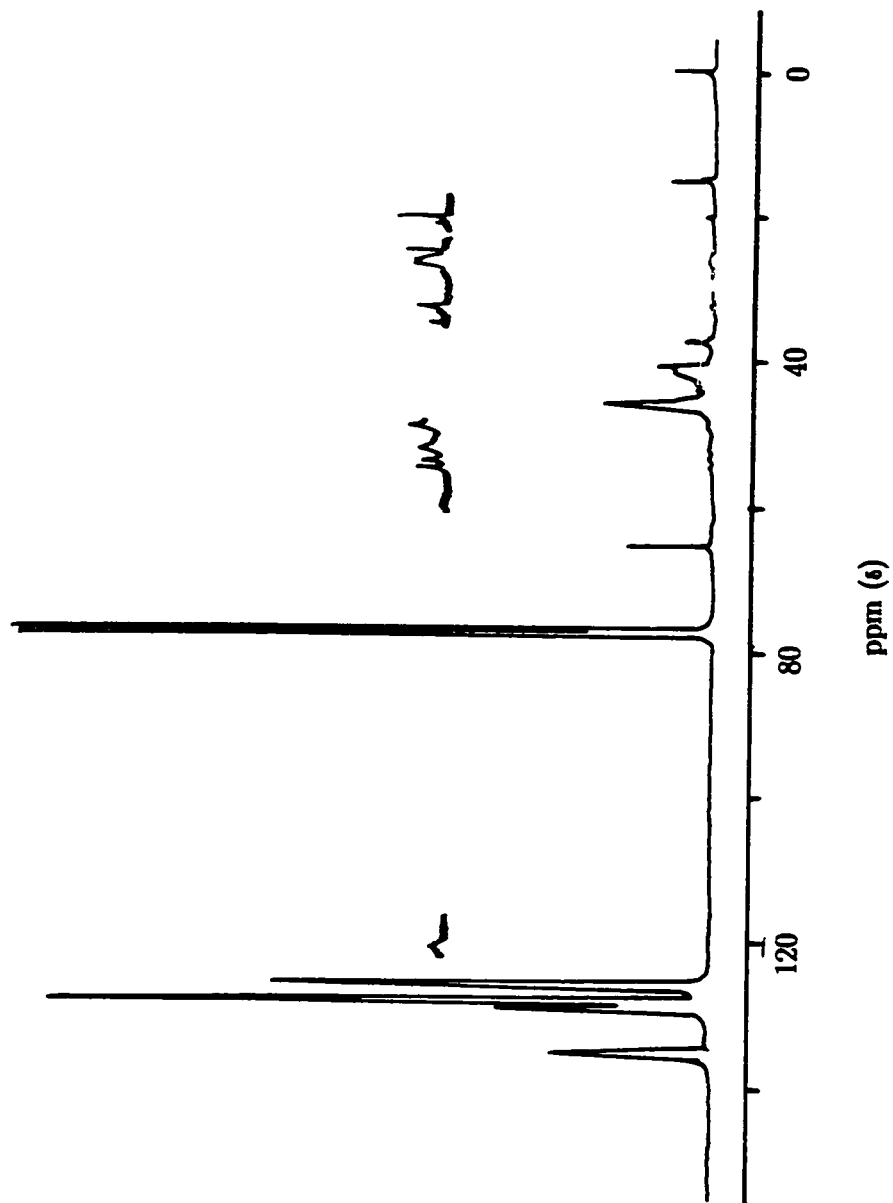


Figure C5. 100 MHz  $^{13}\text{C}$  NMR spectrum of the product of the P4.0/II/B7.9 reaction at 125  $^{\circ}\text{C}$  in DMAc using (P)<sub>10.5</sub>.

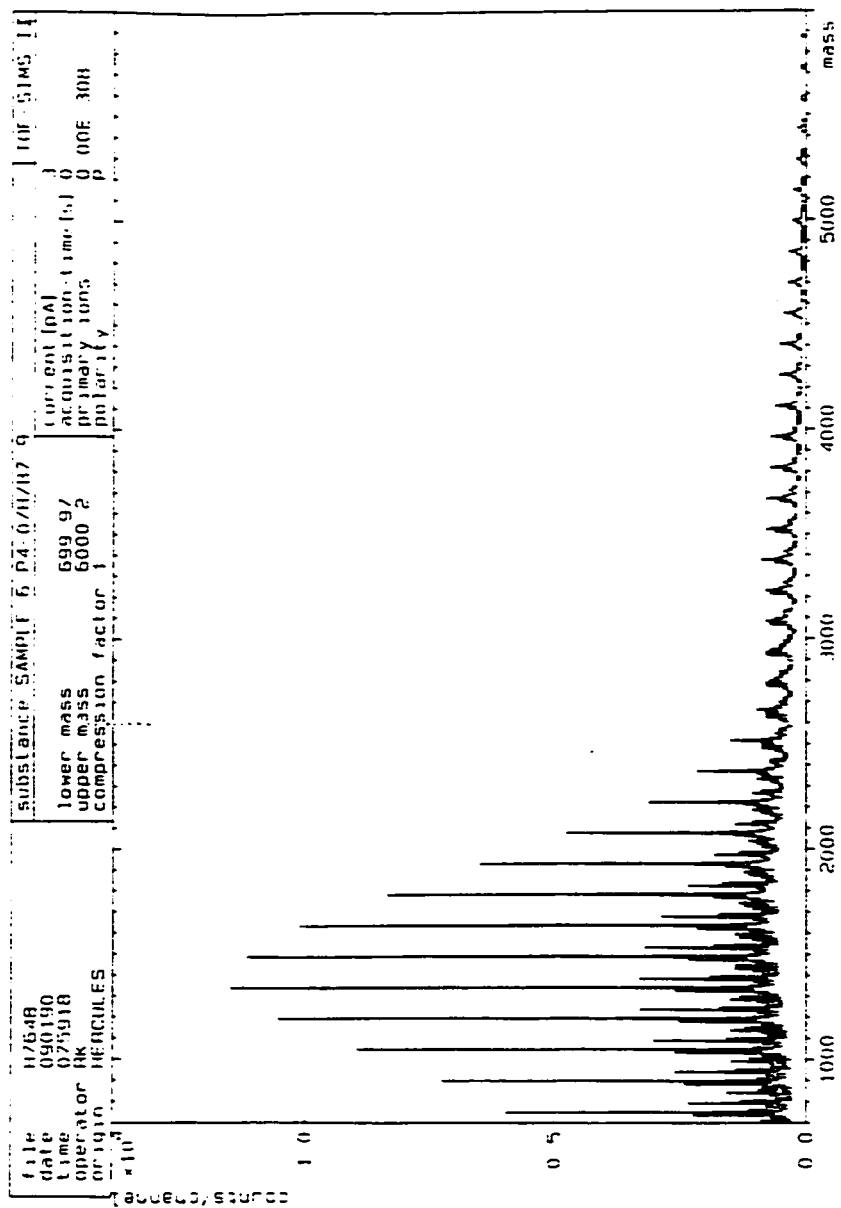


Figure C6. TOF-SIMS spectrum of the product of the P<sub>4-0</sub>/H/B<sub>7-9</sub> reaction at 125 °C in DMAc using (P)<sub>10-5</sub>.

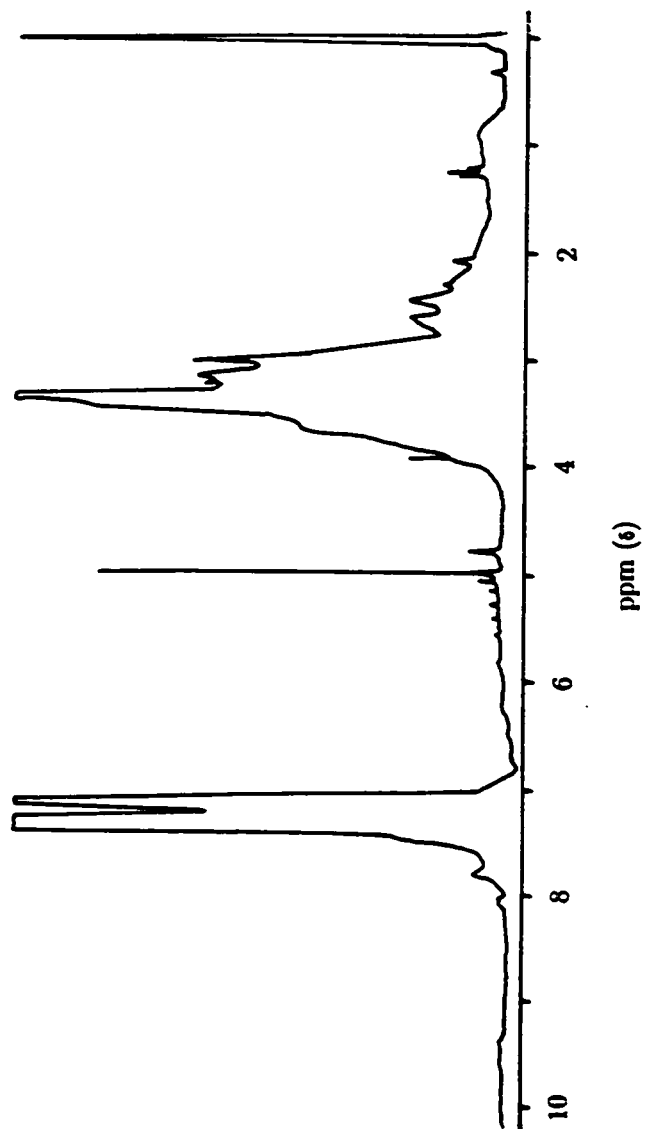


Figure C7. 200 MHz  $^1\text{H}$  NMR spectrum of the product of the P<sub>4.3</sub>/II/B<sub>8.8</sub> reaction at 125 °C in DMAc using (P)<sub>10.0</sub>.

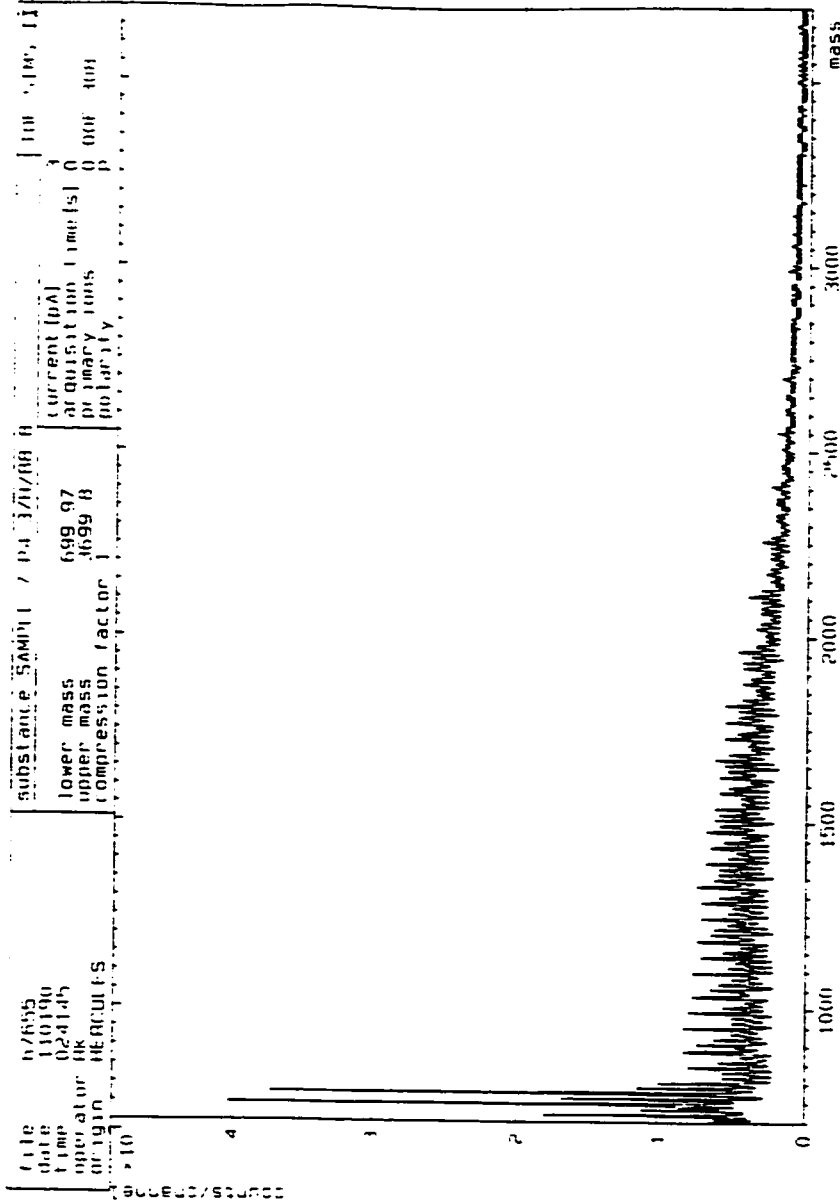


Figure C8. TOF-SIMS spectrum of the product of the P<sub>4.3</sub>/II/B<sub>8.8</sub> reaction at 125 °C in DMAc using (P)<sub>10-0</sub>.



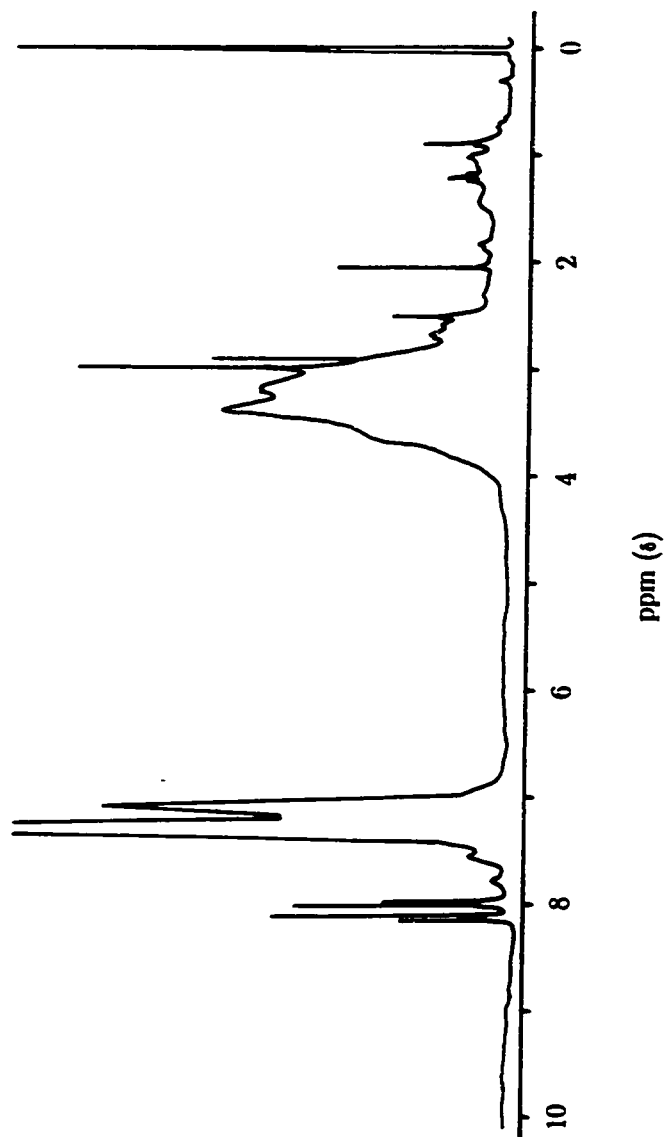


Figure C9. 200 MHz <sup>1</sup>H NMR spectrum of the product of the P<sub>2.1</sub>/H/B<sub>8.4</sub> reaction at 125 °C in DMAc using (P)<sub>10.3</sub>.

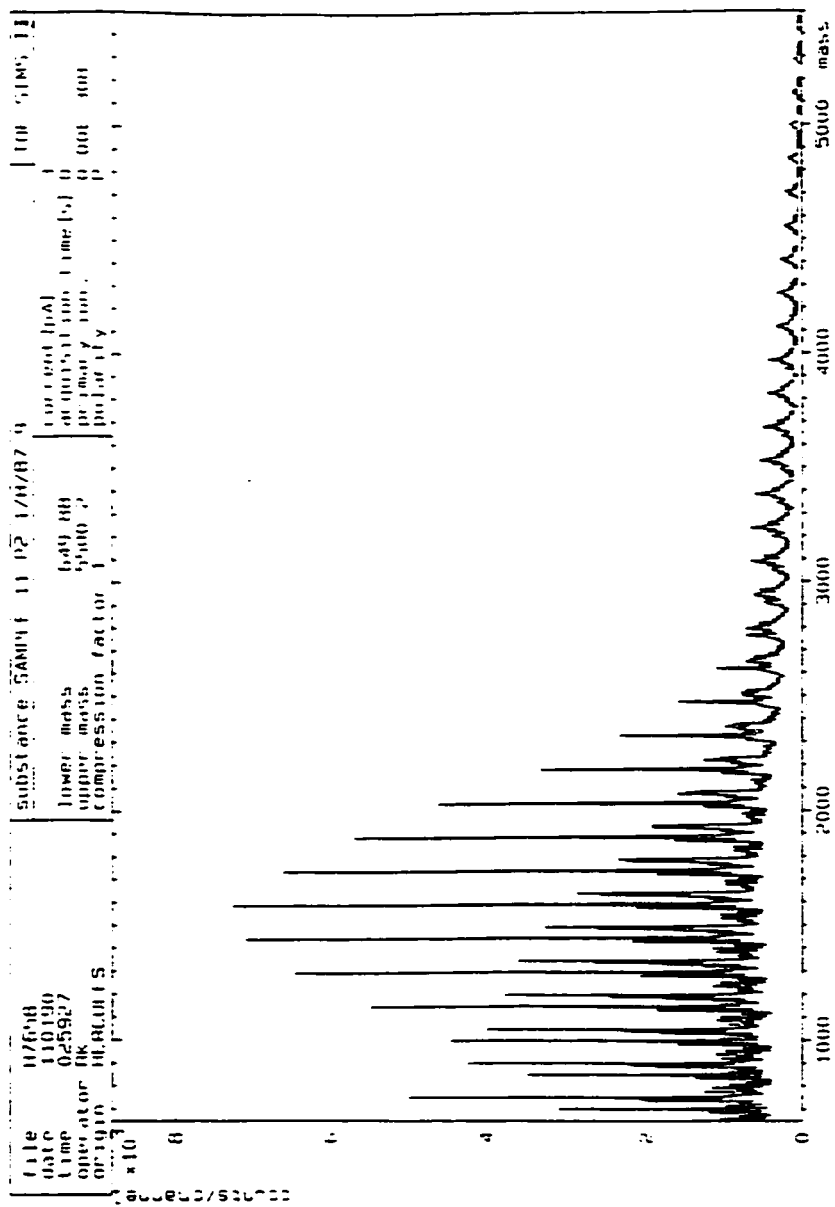


Figure C10. TOF-SIMS spectrum of the product of the P<sub>2.1</sub>/H/B<sub>8.4</sub> reaction at 125 °C in DMAc using (P)<sub>10.3</sub>.

## Bibliography

Chapter 1

1. (a) Riess, G.; Hurtrez, G.; Bahadur, P. In "*Block Copolymers*", *Encyclopedia of Polymer Science and Engineering*, 2nd ed.; John Wiley & Sons: New York, 1985; Vol. 2, pp 324-434. (b) *Dispersion Polymerization in Organic Media*; Barrett, K. E.; John Wiley & Sons: London, 1975. (c) Hancock, R. I. In *Surfactants*; Tadros, Th. F., Ed.; Academic: London, 1984; p 287.
2. Chujo, Y.; Ihara, E.; Ihara, H.; Saegusa, T. *Macromolecules* 1989, 22, 2040.
3. (a) Cai, G.; Litt, M. H. *J. Polym. Sci., Polym. Chem.* 1989, 27, 3603. (b) Cai, G.; Litt, M. H.; Krieger, I. M. In *Contemporary Topics in Polymer Science*; Albertson, B. M., Ed.; Plenum: New York, 1989; Vol. 6, in press.
4. Tadros, T. F.; Vincent, B. *J. Phys. Chem* 1980, 84, 1575.
5. Lin, P.; Clash, C.; Pearce, E. M.; Kwei, T. K. *J. Pol. Sci., Polym. Phys. Ed.* 1988, 26, 603-619.
6. Miyamoto, M.; Sano, Y.; Kobayashi, S.; Saegusa, T. *Eur. Polym. J.* 1983, 19, 955.
7. Szwarc, M. In *Carbonion Living Polymers and Electron Transfer Processes*; John Wiley and Sons: New York, 1968.
8. First reported by: (a) Litt, M. H.; Levy, A., Belgian Patent 666,828, 1965. (b) Kagiya, T.; Narisawa, S.; Manabe, T.; Fukui, K. *J. Polym. Sci., B4* 1966, 441. (c) Tomalia, D. A.; Sheets, D. P. *J. Polym. Sci., A4* 1966, 2253. (d) Also see Reference 15.
9. Litt, M. H.; Rahl, F.; Roldan, L. G. *J. Polym. Sci., Part A-2* 1969, 7, 463-473.
10. (a) Saegusa, T.; Kobayashi, S. *Encyclopedia of Polymer Science and Technology*; John Wiley & Sons: New York, 1976; Suppl. Vol. 1; pp 220-237. (b) Litt, M. H.; Chen, T. T.; Hsieh, B. R. *J. of Polym. Sci., Polym. Chem.* 1986, 24, 3407-3422.
11. Miyamoto, M.; Aoi, K.; Saegusa, T. *Macromolecules* 1989, 22, 3540.
12. Recent reviews and articles therein can be found in: (a) Kobayashi, S.; Saegusa, T. *Encyclopedia of Polymer Science and Engineering*; John Wiley & Sons: New York, 1986; pp 525-537. (b) Kobayashi, S.; Saegusa, T. *Ring-Opening Polymerization*; Elsevier Applied Science: Essex, England, 1984; pp 751-807.
13. Levy, A.; Litt, M. H. *J. Polym. Sci., A1* 1968, 6, 63.

14. Litt, M. H.; Levy, A.; Herz, J. *J. Macromol. Sci. - Chem.*, **A9** 1975, 703.
15. Bassiri, T. G.; Levy, A.; Litt, M. H. *Polym. Lett.* 1967, **5**, 871. See also References 8 (b) and 13.
16. Flory, P. J. *J. Am. Chem. Soc.* 1940, **62**, 1561-1565.
17. Tadros, T. F. In *Polymer Colloids*; Buscall, R.; Corner, T.; Stageman, J. F., Eds.; Elsevier Applied Science: London and New York, 1985; p 107.
18. (a) Sheludko, A. *Proc. Kon. Ned. Akad. Ventensch.* 1962, **B56**, 87 (b) *Adv. Colloid Interface Sci.* 1967, **1**, 391. (c) Scheludko, A.; Maner, E. *Trans. Faraday Soc.* 1968, **64**, 1123.
19. Vrij, A. *Disc. Faraday Soc.* 1966, **42**, 23.
20. Litt, M. H.; Hsieh, B. R.; Krieger, I. M.; Chen, T. T.; Lu, H. L. *J. of Colloid and Int. Sci.* 1987, **115**, 312.
21. Hsieh, B. R.; Litt, M. H.; Demopolis, T. N.; Krieger, I. M. *Polym. Prepr., Am. Chem. Soc. Div. Polym. Chem.* 1986, **27(2)**, 122.
22. Balazs, A. C.; Lewandowski, S. *Macromolecules* 1990, **23**, 839.
23. Gia, H. B.; Jerome, R.; Teyssie, Ph. *Colloid Polym. Sci.* 1979, **257**, 1294.
24. (a) Ahmed, M. G.; Alder, R. W.; James, G. H.; Sinnott, M. L.; Whiting, M. C. *Chem. Commun.* 1968, 1533. (b) Hansen, R. L. *J. Org. Chem.* 1965, **30**, 4322. (c) Streitwieser, Jr. A.; Wilkins, C. L.; Kiehlmann, E. *J. Am. Chem. Soc.* 1968, **90**, 1598.
25. Plumb, J. B.; Atherton, J. H. In *Block Polymers*; Allport, D. C.; Janes, W. H., Eds.; Applied Science: London, 1973.
26. (a) Miyamoto, M.; Naka, K.; Tokumizu, M.; Saegusa, T. *Macromolecules* 1989, **22**, 1604. (b) Kobayashi, S.; Uyama, H.; Higuchi, N.; Saegusa, T. *Macromolecules* 1990, **23**, 54. (c) See also Reference 2.
27. (a) Kobayashi, S.; Saegusa, T. *Macromol. Chem., Suppl.* 1985, **12**, 11-24. (b) Ikeda, I.; Kurushima, Y.; Takashima, H.; Suzuki, K. *Pol. J.* 1988, **20**, 243-250. (c) Shulz, R. C.; Schwarzenbach, E. *Macromol. Chem., Macromol. Symp.* 1988, **13/14**, 495-505.
28. Kobayashi, S.; Kaku, M.; Sawada, S.; Saegusa, T. *Polym. Bull.* 1985, **13**, 447.

29. Swamikannu, A. X. Ph. D. Thesis, Case Western Reserve University, August 1984, p 145.

## Chapter 2

1. Zisman, W. A. In *Relation to the Equilibrium Contact Angle to Liquid and Solid Constitution*; Gould, R. F., Ed.; Advances in Chemistry 43; American Chemical Society: Washington, DC, 1964; p 20.
2. Litt, M. H.; Matsuda, T. In *Advances in Chemistry*; Platzner, N., Ed.; American Chemical Society: Washington, D. C., 1975; ACS Series No. 142; p 320.
3. Litt, M. H.; Herz, J. J. *Colloid Int. Sci.* 1969, 31, 248.
4. Litt, M. H.; Chen, T. T.; Hsieh, B. R. *J. Polym. Sci., Part A, Polym. Chem.* 1986, 24, 3407.
5. Litt, M. H.; Hsieh, B. R.; Krieger, I. M.; Chen, T. T.; Lu, H. L. *J. Colloid Int. Sci.* 1987, 115, 312.
6. Gallant, R. W. *Physical Properties of Hydrocarbons*; Gulf: Houston, 1968.
7. Sanford, R. A.; Kovach, S. M.; Friedman, B. S. *Ind. Eng. Chem.* 1959, 51, 1455.
8. Kovach, S. M.; Friedman, B. S. *J. Am. Chem. Soc.* 1953, 75, 6326.
9. Nightingale, D.; James, J. R. *J. Am. Chem. Soc.* 1944, 66, 154.
10. Hay, A. S.; Blanchard, H. S. *Can. J. Chem.* 1965, 43, 1306.
11. Wiley, R. H.; Bennett, Jr., L. L. *Chem. Rev.* 1949, 44, 447.
12. Matsuda, T. *Polymerization Reactions of Nitrogen-Containing Heterocyclic Compounds*; Ph. D. thesis; Kyoto University, 1972; p 100.
13. Williams, T.; Udagawa, Y.; Keller, A.; Ward, I. M. *J. Polym. Sci., A-2* 1970, 8, 35.
14. Billmeyer, Jr., F. W. *Textbook of Polymer Science, 3rd ed.*; John Wiley and Sons: New York, 1984; p 208.
15. Litt, M. H.; Levy, A.; Herz, J. J. *Macromol. Sci. - Chem.*, A9 1975, 703.

16. Cunliffe, A. V.; Hartley, D. B.; Kingston, S. B.; Richards, D. H.; Thompson, D. *Polymer* 1981, 22, 101.
17. Ambler, M. R. *J. Polym. Sci. (Polym. Lett.)* 1976, 14, 683.
18. Fry, E. M. *J. Org. Chem.* 1950, 15, 802.
19. Goldberg, A. A.; Kelly, W. *J. Chem. Soc.* 1948, 1919.

### Chapter 3

1. Litt, M. H.; Chen, T. T.; Hsieh, B. R. *J. Polym. Sci., Part A, Polym. Chem.* 1986, 24, 3407.
2. Litt, M. H.; Hsieh, B. R.; Krieger, I. M.; Chen, T. T.; Lu, H. L. *J. Colloid Int. Sci.* 1987, 115, 312.
3. Hsieh, B. R.; Litt, M. H.; Demopolis, T. N.; Krieger, I. M. *Polym. Prepr., Am. Chem. Soc. Div. Polym. Chem.* 1986, 27(2), 122.
4. Kobayashi, S.; Igarashi, T.; Moriuchi, Y.; Saegusa, T. *Macromolecules* 1986, 19, 535.
5. Kobayashi, S.; Iijima, S.; Igarashi, T.; Saegusa, T. *Macromolecules* 1987, 20, 1729.
6. (a) Percec, V. *Polym. Bull* 1981, 5, 643. (b) Saegusa, T.; Ikeda, H. *Macromolecules* 1973, 6, 805. (c) Litt, M. H.; Swamikannu, X. In *Ring-Opening Polymerization*; Mc Grath, J. E., Ed.; ACS Symposium Series 286; American Chemical Society: Washington, DC, 1985; p231.
7. Swamikannu, A. X. Ph. D. thesis; Case Western Reserve University; 1984; p 150.
8. Hsieh, B. R.; Litt, M. H. Unpublished work.
9. Cai, G. F.; Litt, M. H. In preparation for publication.

### Chapter 4

1. Saegusa, T.; Ikeda, H.; Fujii, H. *Polymer J.* 1973, 4, 87.
2. Kobayashi, S.; Tokuzawa, T.; Saegusa, T. *Macromolecules* 1982, 15, 707.

3. Seelinger, W.; Aufderhaar, E.; Diepers, W.; Feinauer, R.; Nehring, R.; Thier, W.; Hellmann, H. *Angew. Chem. Internat. Ed.* 1966, 5, 875.
4. Bassiri, T. G.; Levy, A.; Litt, M. H. *J. Polym. Sci., Part B* 1967, 5, 871.
5. Levy, A.; Litt, M. H. *ibid* 1967, 5, 881.
6. Cai, G. F.; Litt, M. H. Article to be published.
7. Riddic, J.; Bunger, W. In *Techniques in Chemistry, Vol. 2*; Weissberger, A., Ed.; Wiley-Interscience: New York, 1970; p 801.
8. Boyce, W. E.; Di Prima, R. C. *Elementary Differential Equations*, 3rd ed.; John Wiley & Sons: New York, 1977; p 336-377.

### Chapter 5

1. Kobayashi, S.; Kaku, M.; Tanabe, T.; Saegusa, T. *Prepr. of the 50th Meeting of the Chemical Society* 1985, 1572.
2. Kobayashi, S.; Kaku, M.; Sawada, S.; Saegusa, T. *Polym. Bull.* 1985, 13, 447.
3. Chujo, Y.; Ihara, E.; Ihara, H.; Saegusa, T. *Macromolecules* 1989, 22, 2040.
4. Hartley, D. B.; Hayes, M. S.; Richards, D. H. *Polymer* 1981, 22, 1081.
5. Seelinger, W.; Aufderhaar, E.; Diepers, W.; Feinauer, R.; Nehring, R.; Thier, W.; Hellmann, H. *Angew. Chem. Internat. Ed.* 1966, 5, 875.
6. Matsuda, T. *Polymerization Reactions of Nitrogen-Containing Heterocyclic Compounds*; Ph. D. thesis; Kyoto University, 1972; p 100.
7. Kagiya, T.; Matsuda, T. *J. Macromol. Chem., A5* 1971, 8, 1265.
8. Flory, P. J. *Principles of Polymer Chemistry*; Cornell University: Ithaca and London, 1969; p 337.
9. Mandel, J. *The Statistical Analysis of Experimental Data*; Dover: New York, 1964; p 74.
10. Yau, W. W.; Kirkland, J. J.; Bly, D. D. *Modern Size-Exclusion Liquid Chromatography*; Wiley and Sons: New York, 1979; p 285.
11. Zimm, B.; Stockmayer, W. J. *Chem. Phys.* 1949, 17, 1301.



12. Vlahos, C. H.; Kosmas, M. K. *Polymer* 1984, 25, 1607.
13. Batoulis, J.; Kremer, K. *Macromolecules* 1989, 22, 4277.